Biological and Medical Physics, Biomedical Engineering

Kazuo Ohki Hidetake Miyata

# Physical Principles of Biomembranes and Cells





# BIOLOGICAL AND MEDICAL PHYSICS, BIOMEDICAL ENGINEERING

The fields of biological and medical physics and biomedical engineering are broad, multidisciplinary and dynamic. They lie at the crossroads of frontier research in physics, biology, chemistry, and medicine. The Biological and Medical Physics, Biomedical Engineering Series is intended to be comprehensive, covering a broad range of topics important to the study of the physical, chemical and biological sciences. Its goal is to provide scientists and engineers with textbooks, monographs, and reference works to address the growing need for information.

Books in the series emphasize established and emergent areas of science including molecular, membrane, and mathematical biophysics; photosynthetic energy harvesting and conversion; information processing; physical principles of genetics; sensory communications; automata networks, neural networks, and cellular automata. Equally important will be coverage of applied aspects of biological and medical physics and biomedical engineering such as molecular electronic components and devices, biosensors, medicine, imaging, physical principles of renewable energy production, advanced prostheses, and environmental control and engineering.

#### Editor-in-Chief:

Elias Greenbaum, Oak Ridge National Laboratory, Oak Ridge, Tennessee, USA

#### Editorial Board:

Masuo Aizawa, Department of Bioengineering, Tokyo Institute of Technology, Yokohama, Japan

Olaf S. Andersen, Department of Physiology, Biophysics and Molecular Medicine, Cornell University, New York, USA

Robert H. Austin, Department of Physics, Princeton University, Princeton, New Jersey, USA

James Barber, Department of Biochemistry, Imperial College of Science, Technology and Medicine, London, England

Howard C. Berg, Department of Molecular and Cellular Biology, Harvard University, Cambridge, Massachusetts, USA

Victor Bloomfield, Department of Biochemistry, University of Minnesota, St. Paul, Minnesota, USA

Robert Callender, Department of Biochemistry, Albert Einstein College of Medicine, Bronx. New York, USA

Steven Chu, Lawrence Berkeley National Laboratory, Berkeley, California, USA

Louis J. DeFelice, Department of Pharmacology, Vanderbilt University, Nashville, Tennessee, USA

Johann Deisenhofer, Howard Hughes Medical Institute, The University of Texas, Dallas, Texas. USA

George Feher, Department of Physics, University of California, San Diego, La Jolla, California, USA

Hans Frauenfelder, Los Alamos National Laboratory, Los Alamos, New Mexico, USA

Ivar Giaever, Rensselaer Polytechnic Institute, Troy, New York, USA

Sol M. Gruner, Cornell University, Ithaca, New York, USA

Judith Herzfeld, Department of Chemistry, Brandeis University, Waltham, Massachusetts, USA

Mark S. Humayun, Doheny Eye Institute, Los Angeles, California, USA Pierre Joliot, Institute de Biologie Physico-Chimique, Fondation Edmond de Rothschild, Paris, France

Lajos Keszthelyi, Institute of Biophysics, Hungarian Academy of Sciences, Szeged, Hungary

Paul W. King, Biosciences Center and Photobiology, National Renewable Energy Laborator, Golden, CO, USA

Robert S. Knox, Department of Physics and Astronomy, University of Rochester, Rochester, New York, USA

Gianluca Lazzi, University of Utah, Salt Lake City, UT, USA

Aaron Lewis, Department of Applied Physics, Hebrew University, Jerusalem, Israel

Stuart M. Lindsay, Department of Physics and Astronomy, Arizona State University, Tempe, Arizona, USA

David Mauzerall, Rockefeller University, New York, New York, USA

Eugenie V. Mielczarek, Department of Physics and Astronomy, George Mason University, Fairfax, Virginia, USA

Markolf Niemz, Medical Faculty Mannheim, University of Heidelberg, Mannheim, Germany

V. Adrian Parsegian, Physical Science Laboratory, National Institutes of Health, Bethesda, Maryland, USA

Linda S. Powers, University of Arizona, Tucson, Arizona, USA

Earl W. Prohofsky, Department of Physics, Purdue University, West Lafayette, Indiana, USA

Tatiana K. Rostovtseva, NICHD, National Institutes of Health, Bethesda, Maryland, USA

Andrew Rubin, Department of Biophysics, Moscow State University, Moscow, c.Moscow, Russia

Michael Seibert, National Renewable Energy Laboratory, Golden, Colorado, USA

David Thomas, Department of Biochemistry, University of Minnesota Medical School, Minneapolis, Minnesota, USA

# Physical Principles of Biomembranes and Cells



Kazuo Ohki Department of Physics Tohoku University Sendai, Japan Hidetake Miyata Department of Physics Tohoku University Sendai, Japan

ISSN 1618-7210 ISSN 2197-5647 (electronic) Biological and Medical Physics, Biomedical Engineering ISBN 978-4-431-56839-1 ISBN 978-4-431-56841-4 (eBook) https://doi.org/10.1007/978-4-431-56841-4

Library of Congress Control Number: 2018948364

#### © Springer Japan KK, part of Springer Nature 2018

This work is subject to copyright. All rights are reserved by the Publisher, whether the whole or part of the material is concerned, specifically the rights of translation, reprinting, reuse of illustrations, recitation, broadcasting, reproduction on microfilms or in any other physical way, and transmission or information storage and retrieval, electronic adaptation, computer software, or by similar or dissimilar methodology now known or hereafter developed.

The use of general descriptive names, registered names, trademarks, service marks, etc. in this publication does not imply, even in the absence of a specific statement, that such names are exempt from the relevant protective laws and regulations and therefore free for general use.

The publisher, the authors, and the editors are safe to assume that the advice and information in this book are believed to be true and accurate at the date of publication. Neither the publisher nor the authors or the editors give a warranty, express or implied, with respect to the material contained herein or for any errors or omissions that may have been made. The publisher remains neutral with regard to jurisdictional claims in published maps and institutional affiliations.

#### Printed on acid-free paper

This Springer imprint is published by the registered company Springer Japan KK part of Springer Nature. The registered company address is: Shiroyama Trust Tower, 4-3-1 Toranomon, Minato-ku, Tokyo 105-6005, Japan

#### **Preface**

We, human beings are member of living organisms on the earth and more or less interested in biology. It is important to study and understand living organisms on the earth from physical view point because origin and evolution of them are closely related to physical principle. Energy is a keyword for physical process in chemical and Darwinian evolutions. Energy is required to escape from equilibrium state and maintain stationary state of life. We focus on biomembranes and cells because cells are essential unit of the living organisms and the cell is composed of various biomembranes. The biomembranes play important roles in integrated system of chemical reactions in the cell because the great many chemical reactions are compartmented and regulated by biomembranes in the cell. Structure and various movements of the cell are related with energy-consuming process. The cell is a system of processing information in signaling system. The system is closely related with various functions such as response to hormone or neurotransmitter through receptor and malfunction inducing oncogenesis. There are a number of techniques that have been introduced and further tailored to the studies in this field (e.g., combination of the fluorescence microscopy and optical trapping technique/atomic force microscopy). In this book only the optical trapping technique is explained, because it plays a central role in the study on the function of motor proteins. Readers should refer to a number of excellent reviews for other developments.

In Chap. 7, biological movements and their molecular mechanisms are described. The background of the researches who are interested in the biological motion has become so diverse that it was not possible to cover the whole area by a single author. Hence, basic knowledges about muscle contraction and cell motility are described in this chapter. There are many cell biology books dealing with this topic, but in the author's opinion, the physical aspect of the phenomenon has not been sufficiently described in those publications. Nowadays, more and more cell biological phenomena have been described and analyzed in the methodology and approach, which have been developed in the field of physics and related fields. The author has been interested in the biological motion, in which the alteration of the filamentous structure leads to the cell shape change this type of motion does not depend on the

vi Preface

motor activity. This is a different type of the mechanism of the transduction of chemical energy into the mechanical work than muscle contraction. The former mechanism is as important as the motor-based mechanism, but in Hidetake Miyata's opinion, it not well described in previously published books. Since many more examples of biological motions have been discovered, it is interesting to know how diverse the physical principles governing those motions would be. Thus, some examples are explained in this book, but there are many unresolved questions in this theme, and the study of the physical principle of biological motions will remain as an important issue.

Sendai, Japan

Kazuo Ohki Hidetake Miyata

#### Acknowledgment

Hidetake Miyata would like to express his thanks to Dr. Hirokazu Hotani who introduced him to the filament-based mechanochemical transduction, to late Dr. Kazuhiko Kinosita who taught him how physicist thinks the biological phenomena, and to Dr. Edward D. Korn who took him to the field of cell biology.

### **Contents**

1	Phy	sics in t	he Origin of Life	1
	1.1	Origin	of Life	1
		1.1.1	Chemical Evolution on the Earth	1
		1.1.2	Origin of Catalytic Activity of Enzymes	4
		1.1.3	Development of Genetic Information	
			and RNA World	4
		1.1.4	Evolution as Progress of Energy Metabolic System	6
	1.2	Therm	odynamics of Biological System	9
		1.2.1	Kinetics of Chemical Reaction	9
		1.2.2	Enzyme as Protein Catalyst and Its Kinetics	11
		1.2.3	Change of Free Energy in Chemical Reaction	11
		1.2.4	Coupling Reaction for Synthetic Chemical Reaction	12
		1.2.5	Non-equilibrium Thermodynamics and Living State	12
	1.3	Station	nary State of Living Organism	13
		1.3.1	Stationary State and Principle of Minimum Entropy	
			Production	14
		1.3.2	Nonequilibrium Thermodynamics	15
		1.3.3	Principle of Minimum Entropy Production	16
		1.3.4	Derivation of Generation Rate of Entropy Production	17
	Refe	erences.		17
2	Cell	s and B	iomembranes	19
	2.1	Cells a	and Biomembranes	19
	2.2		odynamics of Lipid Assemblies	20
	2.3		of Lipid Molecule and Structure of Lipid Assembly	22
	2.4		Structure of Biomembrane	23
	2.5		ns and Functions of a Cell	23
	2.6		s a Device of Information Processing	24
	2.7		rane Potential	25

x Contents

	2.8	Patch Clamp Technique and Membrane Potential	_
	D 6	in Single Channel of a Cell	26
	Refe	rences	27
3	Metl	nods for Physical Properties of Biomembranes and Cells	29
	3.1	Application of Physical Method to Study of Structure	
		and Physical Properties of Biomembranes and Cells	29
	3.2	X-ray Crystallography	30
		3.2.1 Principle of X-ray Diffraction	30
	3.3	Electron Microscopy	31
	3.4	Differential Scanning Calorimetry (DSC)	32
	3.5	Measurement of Density, (Dilatometer)	33
	3.6	Magnetic Resonance	34
		3.6.1 Electron Magnetic Resonance (ESR)	34
		3.6.2 Nuclear Magnetic Resonance (NMR)	42
		3.6.3 Magnetic Resonance Imaging (MRI)	43
	3.7	Fluorescence Method	44
		3.7.1 Fluorescence Polarization Anisotropy	45
		3.7.2 Fluorescence Photo-Bleaching Recovery (FPR)	47
		3.7.3 Fluorescence Resonance Energy Transfer (FRET)	48
		3.7.4 Microscopic Imaging of Physical Property	
		of Biomembranes	48
	2.0	3.7.5 Optical Microscopy Using Evanescent-Field	50
	3.8	Positron Emission Tomography (PET)	54
	3.9	Optical trapping	54 57
	3.10	Outlook of Molecular Dynamics	
	Reie	rences	58
1	Stru	cture and Physical Properties of Biomembranes	59
	4.1	Structure of Biomembranes	59
	4.2	Phase Transition of Lipid Bilayer Membranes	61
	4.3	Phase Separation of Lipid Bilayer Membranes	65
	Refe	rences	69
5	Stru	cture and Function of Protein	71
	5.1	History of Protein Study	71
	5.2	Determination of Three-Dimensional Structure of Proteins	72
	5.3	Basic Concept of Enzyme	72
	5.4	Chemical Reaction and Kinetics of Enzyme	72
		5.4.1 Chemical Reaction and Enzyme	72
		5.4.2 Kinetics of Reactions Mediated by Enzyme	74
	5.5	Regulation of Enzyme Activity	75
		5.5.1 Control of Enzyme Amount	75
		5.5.2 Control of Enzyme Activity	75
		5.5.3 Allosteric Regulation of Enzyme Activity	76

Contents xi

	5.6	Interacti	ion Between Protein and Lipid	76
		5.6.1	Peripheral Enzyme and Integral Enzyme	76
		5.6.2	Synthesis of Membrane Protein and Signal Peptide	77
		5.6.3	Study of Interaction in Membrane Model System	78
	Refe	erences		79
6	Phy	sical Pro	perties of Biomembranes and Cellular Functions	81
	6.1	Diffusio	on Controlled Process by Fluidity of Biomembranes	81
	6.2		eparation of Biomembranes and Biological Functions	82
	6.3		Domain of Biomembranes (Lipid Raft)	83
	6.4		sion of Membrane Lipid with Receiving Stimulus	63
	0.4		actions of a Cell	84
	6.5		ayer Forming Lipids and Function of Biomembrane	87
	0.5	6.5.1	Membrane Structure Formed by Non-bilayer Forming	07
		0.5.1	Lipids	87
		6.5.2	Non-bilayer Membrane Structure in Membrane Fusion	88
		6.5.3	Regulation of Biomembrane Formation by Non-bilayer	00
		0.0.0	Structure as Lipid Storeroom in Biomembrane Lipid	90
		6.5.4	Changes of Structure and Physical Property	
			and Biological Function in Biomembranes	90
	Refe	erences		92
7	Mov	ing Life		95
	7.1		gical Movements	96
		7.1.1	Muscle Contraction and Mechano-Enzyme	96
		7.1.2	Muscle Contraction at the Molecular Level	99
		7.1.3	Single-Molecule Measurement for the Motor Function	
			of Myosin	101
	7.2		ar Movements Other Than Muscle Contraction	102
		7.2.1	Three Filament Systems Supporting the Dynamism	
			in the Cell	102
		7.2.2	Non-muscle Myosins and Organelle Transport	103
	7.3			106
		7.3.1	Actin Monomer Structure	106
		7.3.2	Actin Filament Structure	107
	<b>7</b> .4	7.3.3	Actin Polymerization and Depolymerization	109
	7.4		cs of Actin Polymerization	113
	7.5		mill Phenomenon: Actin Polymerization Under	114
	7.6		on-equilibrium Condition	114 116
	7.0	7.6.1	Structure of Microtubule	116
			Microtubule Polymerization and Depolymerization	110
		7.0.2	TYTICTORUDUIC FUTVITICITALIUTI ATIU DEDUTVITICITALIUTI	11/

xii Contents

	7.6.3 Dynamic Instability: Different Behavior of Plus		
	and Minus Ends in Polymerization/Depolymerization		
	Episode of Microtubule	119	
	7.6.4 Catastrophe and Rescue	119	
7.7	Cell Motility	120	
7.8	Extracelluar Matrix and Its Connection to Cytoskeleton		
7.9	Cell Membrane and Membrane Skeleton		
7.10			
	of the Cell	123	
7.11	Actin Stress Fiber and Focal Adhesion	124	
7.12	Actin Filaments in Lamellipodium and Lamella	126	
7.13	Actin Polymerization and Lamellipodial/Filopodial		
	Protrusion	127	
7.14	Actin Turnover in Lamellipodium	128	
7.15	Extracellular Signaling and Regulation of Actin		
	Polymerization	131	
7.16	Actin-Based Biological Movements: Protrusion		
	of Lamellipodium	132	
7.17	Other Motility Based on Actin Polymerization	134	
7.18	Polymerization Force Developed by Lamellipodium	135	
	7.18.1 Keratocyte: Measurement with Atomic Force		
	Microscope	135	
	7.18.2 Fibroblasts: Measurement with Optical Trapping	100	
	Technique	136	
	7.18.3 What Fluctuates?	139	
7.19	Reconstituted Systems to Study the Polymerization-Based	10)	
7.17	Phenomena	140	
	7.19.1 Actin-Liposome System	140	
	7.19.2 Change in Liposome Shape Accompanying Severing	1.0	
	of Actin Filaments	142	
	7.19.3 Liposomes Encapsulating Tubulin	142	
7.20	Mimicking Bacteria Propulsion with Various Reconstituted	172	
7.20	Systems	143	
7.21	Polymerization Force: Theoretical Studies	144	
7.21	7.21.1 Hill's Theory	144	
	7.21.2 Thermal Ratchet Model of Polymerization Force	147	
7.22	The Force Measured in the Keratocyte and a Reconstituted	14/	
1.22	System	149	
7.23	The ATPase Activity of Actin	149	
7.24	The Experimental Evidence of the Polymerization Force	145	
1.24	*	150	
7.25	by a Single Actin Filament	150	
	Generation of the Polymerization Force by Microtubule		
7.26	The Force Exerted by Depolymerization of Microtubule	152 153	
Keter	rences	103	

Contents	xiii
Contents	X111

8	Glo	bal Environment and Biophysics	159
	8.1	Living Organisms on the Earth	159
	8.2	Mechanism of Adaptation to Environment on Gene Level	160
	8.3	Temperature Acclimation of Cells and Physical Properties	
		of Membranes	161
	8.4	Temperature Acclimation of Cells Observed by Phase Transition	
		and Membrane Fluidity	161
	Refe	erences	166
In	dex .		167

# **Chapter 1 Physics in the Origin of Life**



1

**Abstract** Origin of life started from chemical evolution on the earth by using basic atomic elements such as carbon, hydrogen, nitrogen, oxygen and phosphorus. These elements produce basic biomolecules such as glycine, alanine, lactic acid, and pyruvic acid. Hydrogen cyanide and formaldehyde play key role in formation of these biomolecules.

#### 1.1 Origin of Life

#### 1.1.1 Chemical Evolution on the Earth

Chemical evolution on the earth has proceeded in abundant elements of C, O, H, N and P, and they are also abundant in the universe. Elements in a closed system undergo chemical reaction among them, and finally result in equilibrium state as total bond energy A is minimum in the following equation where  $E_i$  and  $n_i$  indicate chemical bond energy and number of chemical bond of species i, respectively under the restriction condition of number of the elements.

$$A \cong \sum_{i} n_i E_i$$

Computer simulation of  $C_2H_{10}NO_8$  system shows significant amount of important biomolecules such as water, carbon dioxide, methane, ammonia, ethane, formic acid, acetic acid, methanol, formaldehyde, ethylene, hydrogen cyanide, methylamine, acetaldehyde, ethanol, acetone, ketene, formamide, glycine, acetylene, lactic acid, acetamide, ethylene glycol, benzene, alanine, furan, pyrole, pyridine, cyanogen, benzoic acid, pyruvic acid, pyrimidine, phenol, xylene, benzaldehyde, naphthalene, anthracene and asphalt [1] (Table 1.1). This result shows that essential biomolecules are produced in equilibrium state of C, H, O and N. Generation of elements are divided into nuclear fusion and supernova explosion by atomic number of iron. Elements until atomic number of iron, 26 are created by nuclear fusion. On the other hand, elements of atomic number over 26 are created in high energy condition such

© Springer Japan KK, part of Springer Nature 2018 K. Ohki, H. Miyata, *Physical Principles of Biomembranes and Cells*, Biological and Medical Physics, Biomedical Engineering, https://doi.org/10.1007/978-4-431-56841-4\_1

Table 1.1 Production of various molecules in equilibrium state					
Equilibrium distribution of molecules in $C_2H_{10}NO_8$ system at 500 °C, 1 atm [mol/total mol of carbon]					
Water 2.24 Carbon dioxide 0.88					

vv ater	2.24	Carbon dioxide	0.88
Nitrogen	0.50	Methane	0.12
Hydrogen	$0.18 \times 10^{-1}$	Ammonia	$0.15 \times 10^{-3}$
Carbon monoxide	$0.54 \times 10^{-4}$	Ethane	$0.34 \times 10^{-7}$
Formic acid	$0.25 \times 10^{-9}$	Acetic acid	$0.25 \times 10^{-9}$
Methanol	$0.73 \times 10^{-11}$	Formaldehyde	$0.13 \times 10^{-11}$
Ethylene	$0.88 \times 10^{-13}$	Hydrogen cyanide	$0.73 \times 10^{-13}$
Methylamine	$0.64 \times 10^{-13}$	Acetaldehyde	$0.81 \times 10^{-14}$
Ethanol	$0.92 \times 10^{-15}$	Acetone	$0.92 \times 10^{-17}$
Ketene	$0.19 \times 10^{-17}$	Methyl ether	$0.30 \times 10^{-19}$
Formamide	$0.24 \times 10^{-20}$	Glycine	$0.48 \times 10^{-21}$
Acetylene	$0.11 \times 10^{-22}$	Lactic acid	$0.20 \times 10^{-23}$
Acetamide	$0.11 \times 10^{-23}$	Ethylene glycol	$0.62 \times 10^{-24}$
Benzene	$0.52 \times 10^{-25}$	Alanine	$0.97 \times 10^{-27}$
Furan	$0.14 \times 10^{-28}$	Pyrole	$0.31 \times 10^{-30}$
Pyridine	$0.16 \times 10^{-30}$	Cyanogen	$0.77 \times 10^{-31}$
Benzoic acid	$0.65 \times 10^{-31}$	Pyruvic acid	$0.31 \times 10^{-31}$
Pyrimidine	$0.13 \times 10^{-31}$	Phenol	$0.12 \times 10^{-35}$
Xylene	$0.13 \times 10^{-31}$	Benzaldehyde	$0.12 \times 10^{-35}$
Naphthalene	<10 <sup>-38</sup>	Anthracene	<10 <sup>-38</sup>
Asphalt	<10 <sup>-38</sup>	Oxygen	<10 <sup>-38</sup>

M.O. Dayhoff, E.R. Lippincott and R.V. Eck: Science 146 (1946), 1461

**Table 1.2** Element composition of human body (dry weight [%]). Atomic number is shown in parenthesis

Element	Element
Carbon (6) 50	Oxygen (8) 20
Hydrogen (1) 10	Nitrogen (7) 8.5
Calcium (14) 4	Phosphorus (15) 2.5
Potassium (19) 1	Sulfur (16) 0.8
Sodium (11) 0.4	Chloride (17) 0.4
Magnesium (12) 0.1	Iron (26) 0.01
Manganese (25) 0.001	Iodine (53)0.00005

D. Webb and W.R. Frearon: Sci. Proc. Roy. Dublin Soc. 21 (1937), 387

Maximum molecular component of human body is water (60 %) There are boron (5), silicon (14), copper (29), cobalt (27), zinc (30) and molybdenum (42) as minor elements in human body

as early process of supernova explosion. There are boron (5), silicon (14), copper (29), cobalt (27), zinc (30) and molybdenum (42), iodine (53) as minor elements in human body (Table 1.2) and copper, cobalt, zinc, molybdenum and iodine play

1.1 Origin of Life 3

**Fig. 1.1** Generation of glycine from formaldehyde and hydrogen cyanide in primitive atmosphere The most simple amino acid, glycine can be synthesized using hydrogen cyanide and hydrogen cyanide which are generated in equilibrium state of C, N, H and O system in aqueous environment

important roles in metal enzymes or hormone. Formaldehyde and hydrogen cyanide could be generated by Lyman alpha ray and lightening, respectively during the long history of the earth. The age of universe is estimated  $138 \times 10^9$  years and the age of the earth is estimated  $45 \times 10^9$  years. It is enough time for chemical evolution on the earth. Formaldehyde and hydrogen cyanide are important basic molecules to produce amino acid, sugar and pyrimidine from following chemical reactions. Glycine, the simplest amino acid could be generated from formaldehyde and hydrogen cyanide in primitive atmosphere by lightening energy (Fig. 1.1). Ribose, a component of nucleotide and sugars could be generated from formaldehyde by chemical reaction known as formose reaction proposed by Alexander Butlerov [2]. Oró and Kimball have proved adenine, a nucleobase is generated from 5 hydrogen cyanide molecules in ammonia water at 100 °C overnight [3]. Adenosine triphosphate (ATP) could be generated from adenine, ribose and phosphate in water by thermal or nuclear fission energy. And TTP, GTP, CTP and UTP could be generated in similar reaction. Under a condition of energy supply, the initial system escapes from equilibrium state and number of biomolecules increases and molecules of higher bond energy are generated. Stanley Miller performed experiment simulating chemical evolution in primitive atmosphere and lightening energy. The atmosphere was composed of H<sub>2</sub>O, CH<sub>4</sub>, NH<sub>3</sub> and H<sub>2</sub> and these molecules represent oxygen, carbon nitrogen and hydrogen, respectively. Glycine, alanine and aspartic acid were identified in this experiment [4]. Alternatively, another energy source of the earth is hydrothermal vent. And recently hydrothermal vent communities of living organisms were found around the vent. These organisms depend on chemosynthetic bacteria for their food. Development of biomolecules by energy supplement results in proto cells with lipid vesicles as envelope of the biomolecules. These proto cells have developed in evolution of energy-usage system.

#### 1.1.2 Origin of Catalytic Activity of Enzymes

Living organisms are essentially systems of chemical reactions catalyzed by enzymes that synthesized in protein synthesis system according with genetic information of cell. In addition to enzymatic function, biological functions of proteins are antibodies of immune systems and receptors of cellular signaling. There are 20 species of amino acids in living organism on the earth. General structure of amino acid is composed of amino moiety, carboxyl moiety and one of 20 different side chains for each amino acid. And these amino acids are classified into basic (histidine, lysine, arginine), acidic and their amide (aspartate, glutamate, asparagine, glutamine), aliphatic (glycine, alanine, valine, leucine, isoleucine), hydroxyl or sulfurcontaining (serine, cysteine, cystine, threonine, methionine), cyclic (proline) and aromatic (phenylalanine, tyrosine, tryptophan) amino acids. And they are polymerized by peptide bond between amino and carboxyl moieties. Gibbs free energy ( $\Delta G$ ) of peptide bond formation is  $\Delta G_0 = 8-20 \text{ kJ/mol} (1.9-4.8 \text{ kcal/mol})$ . For formation of peptides in biosynthesis of protein, amino acid is activated as amino acyl-tRNA. On the other hand, heating of amino acids mixture polymerizes amino acids to result generation of in thermal polymer in vitro. Catalytic function of enzyme is one of important function of proteins which are polymerized structure of amino acids. And the thermal polymer of amino acids and the polymer shows small but significant catalytic activities such as hydrolysis, decarboxylation, aminization, deamination and redox reaction. Acidic, basic, hydroxyl and sulfur-containing amino acids are required for these catalytic activities, and these amino acids are arranged in active site of enzyme (Table 1.3). For example, active site of trypsin is composed of His57, Asp102 and Ser195, and other parts of amino acids play a role of arranging these amino acids in right position of active site. Living organism on the earth is essentially a system of regulated chemical reactions catalyzed by enzymes. Catalytic role is performed by enzyme and its genetic information is stored in nucleic acid (DNA).

#### 1.1.3 Development of Genetic Information and RNA World

There are two types of nucleic acids, deoxyribonucleic acid (DNA) and ribonucleic acid (RNA) which are polymers of nucleotides. Nucleotide is composed of nucleic acid base, sugar (deoxyribose or ribose) and phosphate (mono- di- or tri-phosphate). There are adenine, thymine, guanine and cytosine for DNA, and uridine instead of thymidine for RNA. Nucleotides of triphosphate (ATP, TTP, GTP and CTP) are high energy biomolecules used in cells. Hydrolysis of nucleotide triphosphate releases  $\Delta G_0$ '=-7.3 kcal/mol as Gibbs free energy, and used in various biological functions (Fig. 1.2). So, it is possible for nucleotide triphosphates to polymerize by use of own energy. Watson-Crick base pair is most important rule for gene replication. Double strand of DNA is formed by complementary structure of base pairs between adenine and thymine (A-T) and between guanine and cytosine (G-C) (Fig. 1.3). Two hydrogen bonds connect between adenine and thymine at distance

1.1 Origin of Life 5

<b>Table 1.3</b> Catalytic functi	on of enzyme
-----------------------------------	--------------

Substrate	Active amino acid residue in thermal	Activity [µM/mg/
Substrate	polymer	min]
Hydrolysis		
p-Nitrophenyl acetate	His, Lys, Asp-imide, Glu, Asp, Ser, Tyr	$1.5 \times 10^{-3}$
p-Nitrophenyl phosphate	Baside and neutral amino acids	$2 \times 10^{-3}$
ATP	Zn, Lysine-rich polymer	~10^-4
Decarboxylation		
Glucose, Gluclonic acid	Lys	~10 <sup>-4</sup>
Pyruvic acid	Glu, Thr	~10^-4
Oxaloacetic acid	Lys	0.3
Aminization · deaminati	on	
α-Ketoglutaric acid	Lys, Basic amino acid	$2 \times 10^{-3}$
H2 N-donor:Glutamic		~10^-4
acid		
Redox reaction		
H <sub>2</sub> 0 <sub>2</sub> (catalase)	Hemoproteinoid Phe inhibitor	~10 <sup>-4</sup>
H <sub>2</sub> 0 <sub>2</sub> and H <sub>2</sub> -donor	Lys-rich hemoproteinoid	0.2

Catalytic activity of enzyme functions at active center

Active center of Chymotrypsin (protease) is composed of only three amino acids (Ser-195, His-57 and Asp-102) while molecular weight of the protein is 25,000

Under the involvement of aspartic acid, the nitrogen atom (N) of the histidine takes the proton (H<sup>+</sup>) from hydroxyl group (-OH) of the serine, and a moiety (-O-) which is easy to give the electron is formed

The enzyme forms the route where the electron is easy to move on internal bonds of a molecule rapidly by lowering the activation energy

Fig. 1.2 Molecular structure of Adenosine triphosphate (ATP) ATP is the most important molecule for high energy source of living organisms

of 11.1 Å and bonding energy E=-5.88 kcal/mol, and three hydrogen bonds connect between guanine and cytosine at distance of 10.5 Å and bonding energy E=-19.18 kcal/mol. The ordered structure of DNA double helix formed by hydrogen bonds is disrupted by raising temperature. And lowering temperature makes the single strand to form double helix by complementary base pairs of A-T and G-C. From viewpoint of genetic information development on DNA, Temperature dependent formation and disruption of base pairs makes it possible to polymerization of nucleotides under the reaction mechanism like PCR (polymerase chain reaction)

**Fig. 1.3** Watson-Crick base pair of DNA Watson-Crick base pair is molecular basis for heredity of living organisms

which uses up and down of temperature for base pairs disruption and formation. This type of circumstances may be occurred in sea shore of the primitive Earth.

There is a mutual relationship between DNA and protein because biosynthesis of protein requires genetic information on DNA and enzymes for DNA replication (DNA polymerase. However, in the RNA world catalytic activity of enzyme protein) is substituted by ribozyme. Coupling of amino acid and codon on DNA should be elucidated. In the present living organisms on the earth, the coupling between mRNA (transcripted codon information from DNA) and corresponding amino acid is mediated by aminoacyl-tRNA having anti-codon and corresponding amino acid. This coupling is mediated by amino-acyl tRNA synthetase that recognizes amino acid and corresponding tRNA having anticodon of the amino acid. However, the origin of this system and evolution to amino-acyl tRNA synthetase is still unclear.

#### 1.1.4 Evolution as Progress of Energy Metabolic System

Evolution of metabolic pathway in living organisms on the earth was proposed by Horrowitz from viewpoint of energy usage [5]. In the ocean of primitive earth, there

1.1 Origin of Life 7

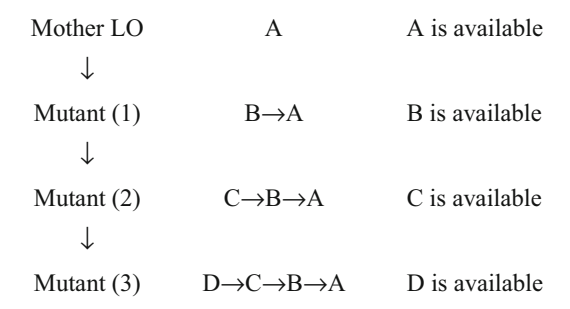


**Fig. 1.4** Evolution of living organism (LO)

Evolution of metabolism caused by change of nutrition source

- (1) Mother species that require organic compound A absolutely as nutrient for living
- (2) When A is exhausted, mutant (1) that obtains enzyme converting B to A propagate by use of B
- (3) Mutant (2) and mutant (3) propagate similarly by use of organic compounds C and D, respectively. The schematic image is made according to his hypothesis of evolution [Horrowitz, N.H.: Proc.NAS USA 31 (1945), 153]

might be various high energy compounds. Primitive cells used some of these compounds as energy source. After the compounds were exhausted by the living organisms, other compounds of similar structure might be new energy source for other living organisms which acquired enzyme for the new compounds by genetic mutation. The living organisms sequentially acquired new mutated enzyme and energy metabolic system extended (Fig. 1.4). Therefore, evolution is essentially progress of energy usage system.

#### 1.1.4.1 Chemoautotroph

Sulfur bacteria are a diverse group of microorganisms capable of metabolizing sulfur and its compounds. These bacteria use hydrogen sulfide ( $H_2S$ ), sulfur, and thiosulfate ( $S_2O_3^{2-}$ ) as energy source and finally oxidized to sulfate ( $SO_4^{2-}$ ) as shown in following equations.

$$H_2S \rightarrow S + 2[H]$$
 Sulfur oxygenase

$$S+O_2+H_2O \rightarrow H_2SO_3$$
  $H_2S_2O_3+H_2SO_3$  sulfurous acid-cytochrome  $C$  reductase  $H_2SO_3+H_2O \rightarrow H_2SO_4+2[H]$ 

Hot water from submarine hydrothermal deposits includes sulfide, and there is ecological system of clubs, clams, asteroids and annelids which eat population of sulfur bacteria for their growth.

#### 1.1.4.2 Photosynthetic Bacteria

In initial stage of evolution such as the mechanism proposed by Horrowitz, exhaustion of an energy source extended metabolic system for new energy source. Solar energy from the sun is non-exhaustion energy on the earth. And photosynthetic bacteria use solar energy for their energy source. Photosynthetic bacteria have two types of metabolic systems. One system synthesizes ATP and another system synthesizes NADPH. ATP and NADPH are major high energy compounds in living organisms (Fig. 1.5). Chemical reaction of ATP $\rightarrow$ ADP+P<sub>i</sub> generates free energy ( $\Delta G_0'=-7.3$  kcal/mol) and redox reaction of NADH $\rightarrow$ NAD<sup>+</sup>+e<sup>-</sup> +H<sup>+</sup> generates redox potential ( $E_0'=-0.32$ V).

These two photosynthetic systems are incorporated into plants as parasite. Thy-lakoids of chloroplast generate NADPH (NADPH is generated instead of NADH in mitochondria) by use of solar energy (Fig. 1.6).

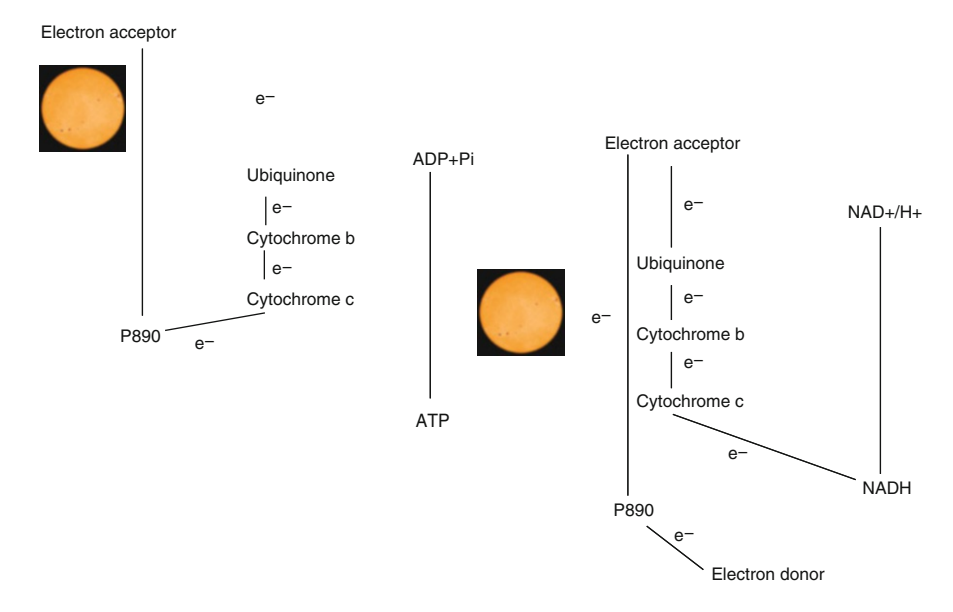


Fig. 1.5 Synthesis of ATP and NADPH in photosynthetic bacteria

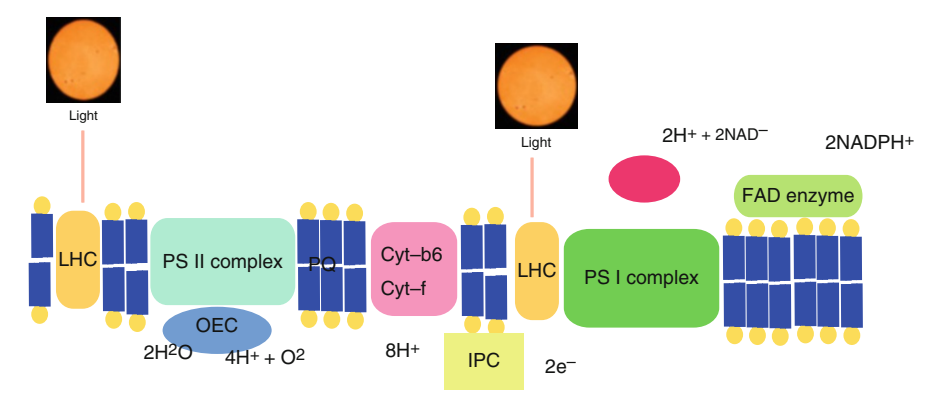


Fig. 1.6 Electron transport system in thylacoid membrane

Water molecule is separated into proton and oxygen molecule by charge separation using solar energy in photosysystem II (PS II) and the proton transferred within thylakoid. The protons generate electrochemical potential for  $H^+$ -ATPase. FADPH<sub>2</sub>+ is generated in FAD enzyme using high energy of electron excited in photosystem I (PS I). These systems in photosynthesis bacteria are integrated in chloroplast. Solar light enters light harvesting complex (LHC)

#### 1.1.4.3 Mitochondria and Ecological System on the Earth

Plant cell has mitochondria in addition to chloroplast. However, animal cell has only mitochondria which use glucose at the first step of metabolic system. And ATP and NADH are generated in inner membrane of mitochondria (Fig. 1.7). In the ecological system on the earth, photosynthetic system of flora and mitochondria of fauna are coupled with mediation of hydrogen oxide (water) (Fig. 1.8).

#### 1.2 Thermodynamics of Biological System

#### 1.2.1 Kinetics of Chemical Reaction

The simplest chemical reaction between reactants A and B and product C is shown as following scheme.

$$A + B \leftarrow \longrightarrow C$$

Rate of association and rate of dissociation are defined as  $v_{+1} = k_{+1}[A][B]$  and  $v_{-1} = k_{-1}[C]$  respectively, where  $k_{+1}$  and  $k_{-1}$  are rate constants.

Using equilibrium condition 
$$v_{+1} = v_{-1}$$
 results in  $v_{+1}/v_{-1} = v_{-1}/v_{[A|[B]} = K_{eq}$ 

 $K_{eq}$  is equilibrium constant. In equilibrium state, association reaction and dissociation reaction are proceeding, and equilibrium constant is obtained as ratio of reactants to products.

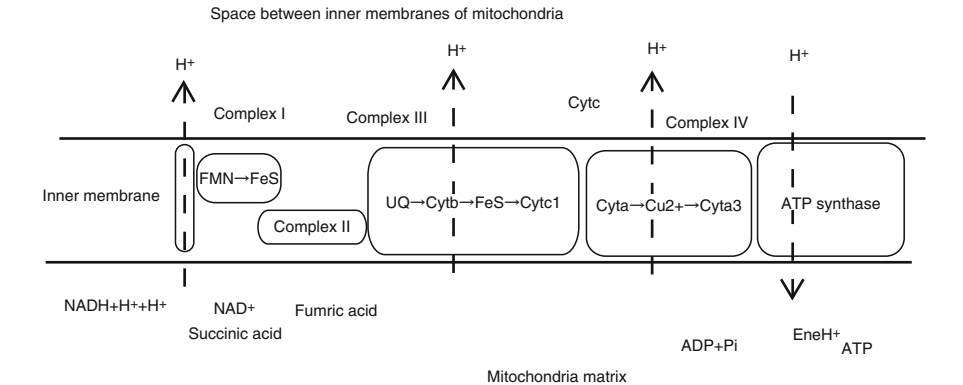


**Fig. 1.7** Electron transport system in mitochondria Energy generated by redox potential (NADH+H $^+$ +2e $^-$ ,  $E'_0$ =-0.315V) is used for transportation of protons from matrix side to space between inner membrane. And electrochemical potential caused by gradient of protons results in synthesis of ATP in ATP synthase

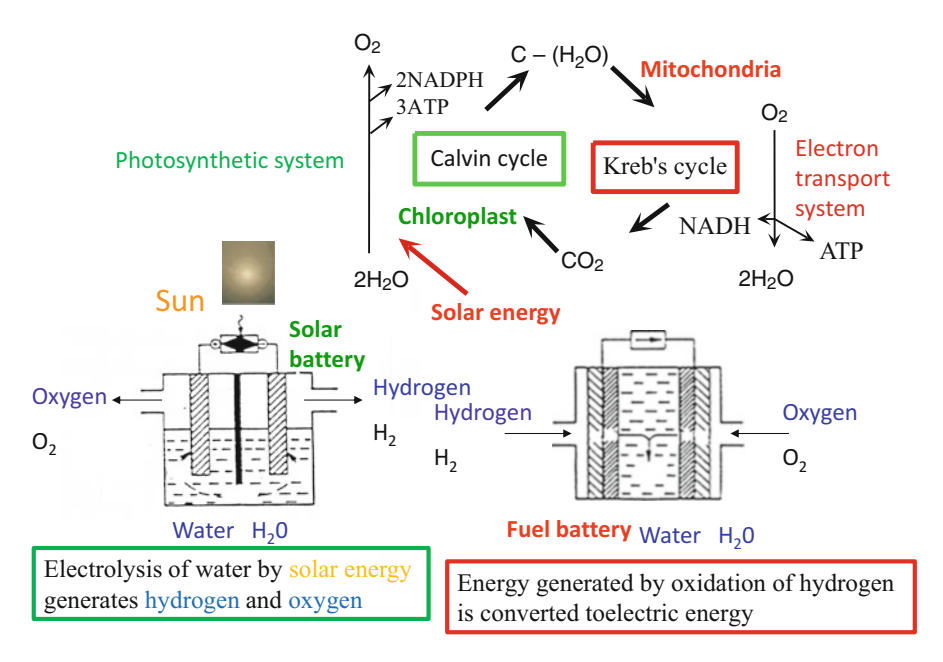


Fig. 1.8 Coupling between flora and fauna similar to electrolysis of water molecules and solar battery

#### 1.2.2 Enzyme as Protein Catalyst and Its Kinetics

Essential unit of living organism is a cell and chemical reactions of its metabolic system is catalyzed by specific enzymes synthesized by use of genetic information of DNA. Chemical reaction mediated by enzymes is shown in following equations where E, S ES and P denote enzyme, substrate, ES complex and product, respectively.

$$E + S \stackrel{\longleftarrow}{\underset{k}{\longleftarrow}} \stackrel{k_{+1}}{\xrightarrow{}} ES \stackrel{k_{+2}}{\xrightarrow{}} E + P$$

Michaelis and Menten assume that E+S and ES are in equilibrium state and then Michaelis constant  $K_m$  becomes  $K_m = \frac{k_{-1}}{k_{++}}$  [6].

Haldane assumes that concentration of ES complex is in stationary state and then Michaelis constant is changed to  $K_m = \frac{k_{-1} + k_{+2}}{k_{+1}}$  in this case [7].

#### 1.2.3 Change of Free Energy in Chemical Reaction

Molecules in isolated system become finally equilibrium state by chemical reaction among them. And the concentration of each molecule is determined by change of Gibb's free energy in the chemical reaction. In a case that reactants A and B make product C, Gibb's energy change is shown in reaction coordinate with activation energy (Fig. 1.9). Ratio of product concentration to reactants concentration is determined by equilibrium constant. Activation energy of chemical reaction is reduced by specific enzyme mediating the reaction in a biological system of cell. Rate of reaction is explained by transition state theory. Temperature dependency of reaction rate, k is shown by following Arrhenius equation.  $k=Ae^{-\frac{Ea}{kT}}$ . A,  $E_{av}$  R and T are frequency actor, activation energy, Gas constant and absolute temperature, respectively. Eyring introduced activated complex as a transition state in his transient theory.

$$A + B \Leftrightarrow (AB) * \rightarrow C$$

In this reaction mechanism, reaction rate v is shown by  $v=k^*[(AB)^*]$ . When equilibrium state between A+B and (AB) \* is assumed, equilibrium constant  $K^*$  is shown by  $K^*=[(AB)^*]/[A][B]$  and finally  $v=k[A][B]=k^*K^*[A][B]$ .

 $\triangle G^* = -RT \ln K^*$  and  $k = k^* exp(-\triangle G/RT) = k^* exp(\triangle S^*/R) exp(-\triangle H^*/RT)$  shows relationship between reaction rate, k and activation energy. The result means that activation energy determines rate of chemical reaction.

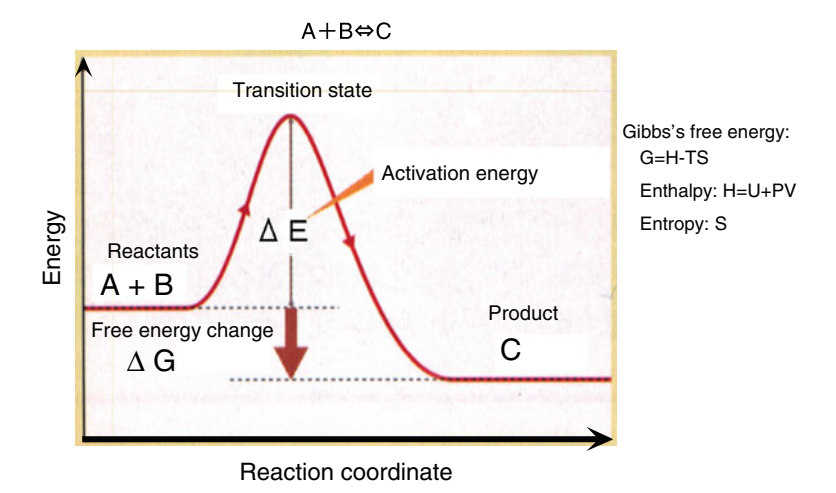


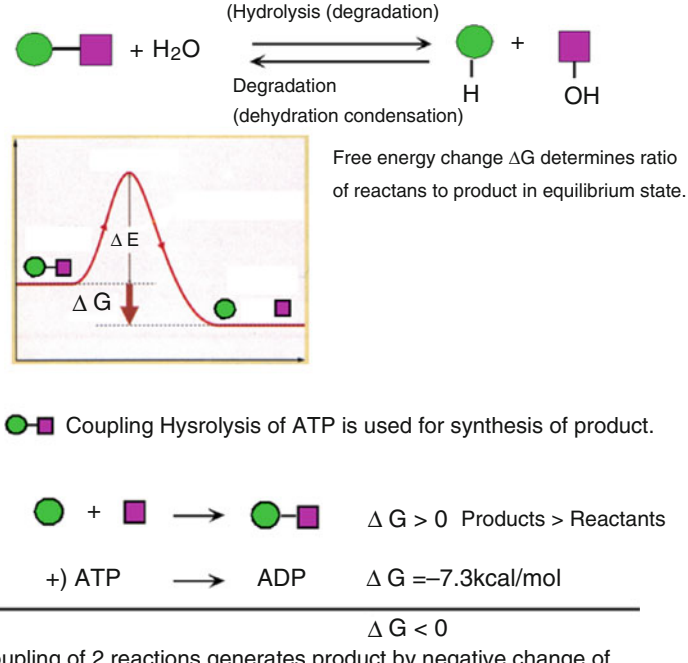
Fig. 1.9 Free energy change of chemical reaction  $\Delta G_o = -RT \ln K_{eq}$  Equilibrium state of chemical reaction Equilibrium constant:  $K_{eq} = [C]/[A][B]$ 

#### 1.2.4 Coupling Reaction for Synthetic Chemical Reaction

Water molecules play key role in chemical reaction of biological system. In most cases, association of molecules occurs as dehydration condensation and dissociation of molecule occurs as hydrolysis. In general, Gibbs's free energy change of association of molecules is positive, and so synthesis of molecule requires supply of energy. Gibb's free energy change of ATP (–7.3 kcal/mol) is used to make the total Gibb's energy change be negative (Fig. 1.10).

#### 1.2.5 Non-equilibrium Thermodynamics and Living State

From physical viewpoint, living state of living organisms is a non-equilibrium state which is different from equilibrium state. For example, *Escherichia coli* cell is composed of carbon  $(5.83 \times 10^9)$ , hydrogen  $(9.83 \times 10^9)$ , oxygen  $(2.67 \times 10^9)$  and nitrogen  $(1.55 \times 10^9)$ . In closed system, these atoms form various molecules and then finally result in equilibrium state where total energy of chemical bonds is in minimum. On the other hand, these atoms are used for synthesizing various biological molecules such as protein, nucleic acid, lipid, sugar and so on. Total bond energy of the biological molecules is higher than the total bond energy of various molecules formed in equilibrium. The difference of total bond energy between molecules in *E. coli* cell and molecules in equilibrium is supplied to maintain living state of *E. coli* cell [8].



Coupling of 2 reactions generates product by negative change of free energy.

**Fig. 1.10** Coupling reactions for biosynthesis in a cell Coupling of 2 reactions generates product by negative change of free energy

#### 1.3 Stationary State of Living Organism

From view point of energetics, formation and maintenance of biological system can be understood by the second law of thermodynamics. Highly ordered biological system is attained in non-equilibrium state. I. Prigogine analyzed the second law of thermodynamics from viewpoints of micro and macro level of biological system, and he concluded that ordered system realized even in non-equilibrium system. This system is in irreversible process and has continuous entropy production, in other word dissipation of free energy [9]. Considering living organisms thermodynamically, if substances and energy do not exchange with those in external environment is assumed (isolated system) in the living organisms irreversible processes such as chemical reaction, diffusion of substances, thermal conduction and so on are proceeding with production of entropy and finally result in equilibrium state where entropy production is zero. However, living organisms exchange substances and energy with external environment (open system) and generate entropy; rate of entropy generation is proportional to difference between non-equilibrium state and equilibrium state. And the non-equilibrium state of living organism is considered approximately as stationary state.

Stationary state is one of non-equilibrium states, and so entropy is generated continuously in biological system. Change of entropy in internal system is represented by  $d_iS>0$ . All state functions do not depend on time in stationary state, and it is formulated by  $\frac{dS}{dt} = \frac{d_eS}{dt} + \frac{d_iS}{dt} = 0$ , where dS and  $d_eS$  represent entropy change of entire system and external environment, respectively. Continuous generation of entropy in biological system is represented by  $\frac{d_iS}{dt} > 0s$ , and so results in  $\frac{d_eS}{dt} < 0$ . This result indicates that negative flow of entropy compensates generation of entropy in biological system for maintaining the stationary state.

Rate of entropy generation is defined as  $\Phi = T \frac{d_i S}{st}$  and then temporal change of  $\Phi$  as  $\frac{d\Phi}{dt}$  is considered. Biological system of open system has an internal term of  $\frac{d\Phi_i}{dt} < 0$  and an external term of  $\frac{d\Phi_c}{dt}$ . Positive or negative sign of the external term is not determined. Living organism is an open system, and flow of entropy is composed of thermal flow and substantial flow. The flow of entropy is shown by  $j_s = \frac{q}{T} + \sum j_i s_i$ .

When there is no thermal flow ( $\mathbf{q}$ =0), flow of entropy generated by substantial flow and results in  $\sum_{i} j_{i} s_{i}$ , < 0. The equation indicates that entropy of imported substances is smaller than entropy of exported substances in stationary state.

## 1.3.1 Stationary State and Principle of Minimum Entropy Production

From viewpoint of natural science, generation and maintenance of energy in biological system should be understood in frame of physics and chemistry. And conversion of energy in biological system is determined by the second law of thermodynamics. Highly ordered biological system is generated in non-equilibrium system. I. Prigogine has analyzed the second law of thermodynamics from micro and macro viewpoint, and he has shown that ordered system is generated in non-equilibrium state. The ordered system is in irreversible process and generates entropy continuously and dissipates free energy. So, this system is called as 'dissipative structure'.

Ecological system on the earth is not in equilibrium system but in 'dissipative structure' like biological system. Reversible process is going with fluctuation in equilibrium state but never escape from equilibrium state. On the other hand, 'dissipative structure' exchanges energy and substances under a condition of non-equilibrium state, and this exchange maintains dissipative structure'. Both equilibrium state and stationary state do not change as time passes. However stationary state produce entropy but equilibrium state does not produce entropy. Stationary state is maintained by some fixed force (independent of time) of external system. However, it is impossible to realize time-independent external system. So stationary state is an ideal state in limited time scale. In other words, stationary state has the minimum production of entropy under limited condition from external

system. Produced entropy flows out and the entropy in the system is kept constant. On contrary, entropy production becomes finally zero in equilibrium state.

#### 1.3.2 Nonequilibrium Thermodynamics

Considering stability and fluctuation of structure in non-equilibrium thermodynamics, P. Glandorff and Ilya Prigosine have studied what living state is thermodynamically [9]. Prigosine received Nobel Prize in chemistry "for his contributions to non-equilibrium thermodynamics, particularly the theory of dissipative structures". He has also proved principle of minimum entropy production in statistical physics. Quasi-static change near equilibrium state was considered in early theory of non-equilibrium thermodynamics, and it only indicated direction of change but did not include temporal factor. Onsegar and Prigogine have developed linear non-equilibrium thermodynamics by introducing assumption of 'local equilibrium' and linear Phenomenological equation which includes flux,  $J_i$  representing temporal change and force,  $X_i$  representing cause of flux.

$$J_i = \sum_j L_{ij} X_j$$

Any Phenomenon can be expressed by the linear phenomenological equation. In the case of Ohm's law of electric resistance, electric current, I and voltage V correspond to flux and force, respectively. In the case of two forces such as Thomson effect,  $Q = \theta \cdot I \cdot \Delta T$ , electric current I and temperature difference  $\Delta T$ correspond to force  $X_1$  and force  $X_2$ , respectively. In other cases of many forces, similar expression of Phenomenological equation is available. Coupling coefficient  $L_{ii}$  is introduced as constant of phenomenological equation. And Onsager could show that the matrix of Phenomenological equation is symmetric, or that  $L_{ii}=L_{ii}$  $(i\neq j)$ . This reciprocal relation between coefficients was proved in process close to equilibrium under condition of micro reversibility. Phenomenological equation is also available for chemical reaction. Flux and force correspond to chemical reaction and affinity (chemical potential difference between before and after the reaction), respectively. However, chemical reaction is scalar, so there is no cross relation with vector of Phenomenological equation. In a case of biological membrane, chemical reaction and substance transport are conjugate, so this non-isotropic system makes possible to use Phenomenological equation. When relation between flux and force is generalized in Phenomenological equation, stationary state is shown as feature that does not change temporally. Prigogine indicates that entropy production by flux is the minimum in stationary state. And he studied non-equilibrium thermodynamics extended to non-linear region.

#### 1.3.3 Principle of Minimum Entropy Production

Main problem of non-equilibrium thermodynamics is to extend method of thermodynamics covering non-linear and unstable phenomenon by start from equilibrium state. Principle of local equilibrium is postulated for this purpose. Considering volume element of small enough but sufficient enormous size for macroscopic nature in non-equilibrium state including irreversible process, there exist state valuables of state function thermodynamics. The state function is as same as that in equilibrium thermodynamics. Principle of local equilibrium implies that effect of collision is dominant to keep thermodynamically. It becomes possible to extend to non-equilibrium state if local entropy is described by same independent valuable. Substances and energies exchange through its surfaces among of each subsystem. And the surface increases at second power while the volume increases at third power as the size of system increases. Therefore, the large system enough to establish condition of statistical independency can be regarded as closed system. And those subsystems are independent from surrounding subsystems. Ergodic hypothesis is available and statistical method can be used in those subsystems.

To introduce 'Principle of minimum entropy production', 'Law of conservation of entropy' is first introduced from 'Principle of local equilibrium'. In General expression of conservation law, specific entropy e is introduced into a. And it becomes equation,  $\frac{d}{dt} = \frac{\partial}{\partial t} + \nu \nabla$ . By coordinates transformation on flow and then use of equation of continuity  $\frac{\partial \rho_a}{\partial t} + \nabla J_s - \varphi_s = 0$ , equation entropy balance,  $\rho \frac{dS}{dt} = \Phi T - \nabla j_s$  in non-equilibrium state is obtained. In general, inner generation rate of entropy production,  $\Phi$  is expressed as  $\Phi = \rho T \frac{dS}{dt} = \sum J_i X_i$  by definition of flux J and force X.

In the presence of n fluxes, some of them are zero in stationary state. When phenomenon equation  $J_i = \sum\limits_j L_{ij} X_j$  is assumed, generation rate of entropy production is expressed as  $\Phi = \sum\limits_i \sum\limits_j L_{ij} X_i X_j$  and derivation of the equation is described in the next section. When forces  $X_1, X_2, \ldots, X_k$  are fixed, condition of  $\Phi$  having maxima or minima is  $\frac{\partial \Phi}{\partial X_i} = 0$   $(i = k+1, \ldots, n)$ . Substituting  $\Phi$  for  $\Phi = \sum\limits_i \sum\limits_j L_{ij}$ 

$$X_i X_j$$
 gives  $\sum_{i=1}^n (L_{ij} + L_{ji}) = 0$   $(i = k+1, ..., n)$ . And  $Ji = 0$  is obtained by using

Onsager reciprocal relations,  $L_{ij} = L_{ji}$   $(i \neq j)$ . The result indicates that forces conjugating the fixed forces remain and other forces become zero. The fixed forces maintain stationary state. In zero-order stationary state, there is no fixed force and all fluxes disappear, and this is equilibrium state. When one of unfixed forces is perturbed, positive flux caused by the force generates negative flux of resistance, and this is an extended Le Chaterier.'s principle. Principle of minimum production of entropy is an important achievement obtained in non-equilibrium thermodynamics. The principle indicates that system selects a path of minimum resistance.

References 17

#### 1.3.4 Derivation of Generation Rate of Entropy Production

Evidence that rate of entropy production is shown as  $\Phi = \sum J_i X_i$  is explained as follows. When general expression of conservation law is converted on flowing coordinate and equation of continuity is used,  $\varphi_s$  becomes internal production rate of entropy. Therefore, equation showing flow of entropy of system in non-equilibrium state,  $\rho_{dt}^{ds} = \frac{\Phi}{T} - \nabla j_s$  is obtained when  $\varphi_s = \frac{\Phi}{T}$ . On the other hand, Gibbs's equation,  $du = Tds - pdV + \sum_i \mu_i dx_i$  is converted to  $\rho_{dt}^{ds} = \frac{\rho}{T} \frac{du}{dt} - \frac{\rho}{T} \sum_i \mu_i \frac{dx_i}{dt}$  by use of  $v = \frac{1}{a}$ .

Following equations of differential of time are replaced in the Gibb's equation.

Internal energy 
$$-\rho \frac{du}{dt} = \sigma : \nabla v - \nabla q - \nabla \sum j_i h_i + \sum j_i x_i$$

$$\text{Pressure } \frac{d\rho}{dt} = -\rho \nabla v$$

$$\text{Mole fraction of component} \quad \rho \frac{dx_i}{dt} = -\nabla j_i + \rho \sum_k \nu'_{ik} \frac{d\zeta_k}{dt}$$

And the equation is classified into 4 terms by use of  $j_s = \frac{q}{T} - \sum j_s i_s$ , and they are viscous flow of unit volume gravity center, chemical reaction in system, diffusion of substance in isothermal system and entropy production rate by heat flow. From comparison of equations, meaning of each term is obtained as follows. Force of velocity gradient of gravity center of part makes flux of stress and static pressure. Force of affinity makes flux of chemical reaction. Force of chemical potential gradient makes flux of diffusion. Force of temperature gradient makes flux of heat flow. These relations are supposed as product of flux and force. Therefore,  $\Phi = \sum J_i X_i$  is obtained.

#### References

- 1. M.O. Dayhoff, E.R. Lippincott, R.V. Eck, Science 146, 1461 (1964)
- 2. A.C. Butlerov, *Comptes Rendus*, vol 53 (1861), p. 145
- 3. J. Oró, A.P. Kimball, Arch. Biochem. Biophys. 96, 293 (1962)
- 4. S.L. Miller, Science 117, 528 (1953)
- 5. N.H. Horrowitz, Proc. NAS 31, 153 (1945)
- 6. L. Michaelis, M. Menten, Biochem. Z. 49, 369 (1913)
- 7. G.E. Briggs, J.B.S. Haldane, Biochem. J. 19, 339 (1925)
- 8. H.J. Morowits, Energy Flow in Biology (Ox Bow Press, Woodbridge, 1979)
- 9. P. Glansdorff, I. Prigogine, *Thermodynamic Theory of Structure, Stability and Fluctuations* (Willey-Interscience, London, 1971)

# Chapter 2 Cells and Biomembranes



**Abstract** Cell is constructed by various membrane structures called biomembrane, and major components of the biomembrane are proteins and lipids. Biomembranes have roles of compartmentation and selective permeation. Most of functions are located on biomembranes. Physical properties such as fluidity, phase transition and phase separation affect and regulate membrane functions. Functional role of cell looks like a device of information processing; cell receives external stimulus by receptor, transduces it and respond to the stimulus properly.

#### 2.1 Cells and Biomembranes

Cell is an essential unit of life in living organisms including animals, plants, fungi and bacteria on the earth. Although there is no strict definition of cell, cells have common properties as follows.

- 1. Separated by envelope
- 2. Maintaining metabolism
- 3. Propagation by replication
- 4. Undergoing Darwinian evolution
- 5. Controlling cellular functions

Cell is composed of various biomembranes, and biomembranes have proteins and lipids as their major components. Water molecules are indispensable for living organisms, which is related to origin of life in ocean and physicochemical process of biomembrane generation. Lipid components of biomembrane are called membrane lipids, and they include phospholipids, glycolipids and sterols. They have amphiphilic property and, molecular shape and structure of assembly are shown in (Fig. 2.1). In aqueous environment, lipid molecules assemble to form lipid bilayer membranes. And proteins which are synthesized according to genetic information are inserted into lipid membranes, and biological functions are added to biomembrane. The cell is constructed by various membrane structures, such as nucleus, mitochondria, endoplasmic reticulum (microsomes), lysosomes Golgi

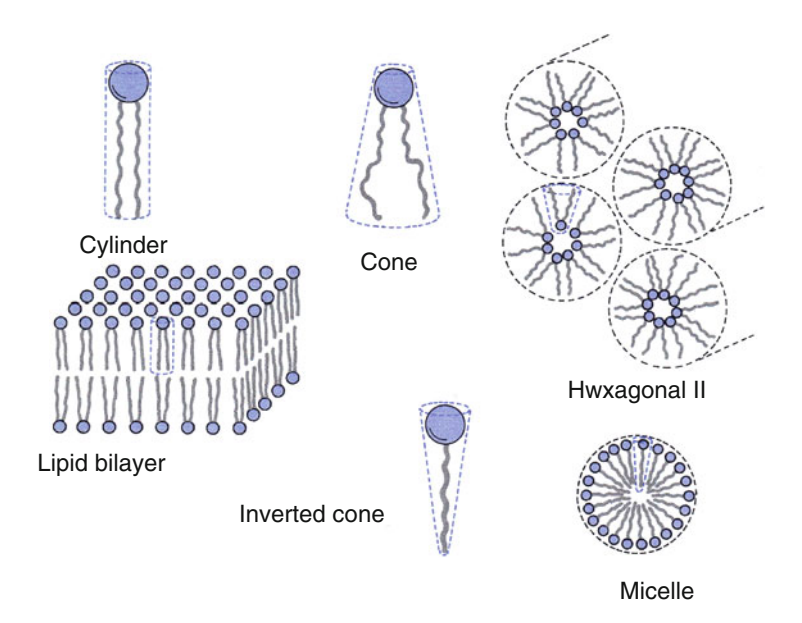


Fig. 2.1 Shape of lipid molecule and structure of lipid assembly Geometrical shape of lipid molecule determines structure of lipid assembly

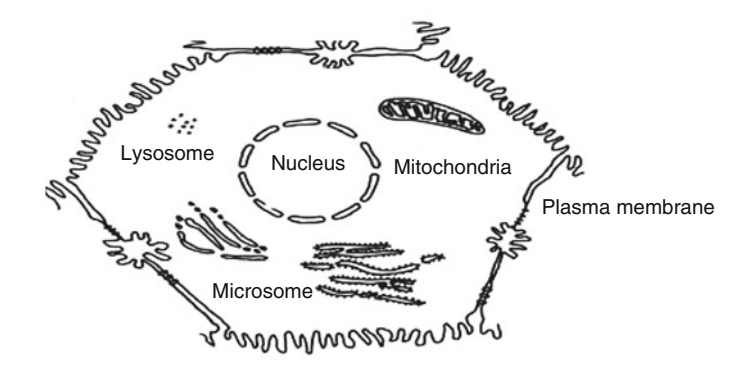
apparatus and plasma membrane (Fig. 2.2). In addition to them plant cells have chloroplasts. There are many chemical reactions catalyzed by enzymes in the cell. Basic functions of biomembranes are compartmentation and selective permeation for those chemical reactions. Water occupies 66% of body weight in a human, and aqueous environment is required even for living organism on land. Biomembranes also provide hydrophobic environment for various functions of biomembranes.

#### 2.2 Thermodynamics of Lipid Assemblies

When lipid molecules are dispersed in water the lipid molecules spontaneously assemble, which is a process of thermodynamics. For this process, chemical potential of one lipid molecule and that of a lipid assembly composed of n lipid molecules are considered as follows. Chemical potential of single lipid molecule in water  $\mu_W$  is represented as follows, where  $\mu_{0W}$ ,  $X_W$  and  $f_W$  are standard chemical potential, mole fraction and activity coefficient of single lipid molecule in water, respectively.

$$\mu_W = \mu_{0W} RT \ln Xw + RT \ln f_W \mu_{0micelle,n}$$

Average chemical potential of a molecule in a micelle as lipid assembly,  $\eta_{micelle,n}$  is represented as follows where  $\mu_{0micelle,n}$  and  $X_n$  are standard chemical potential and mole fraction of a lipid molecule in water, respectively.



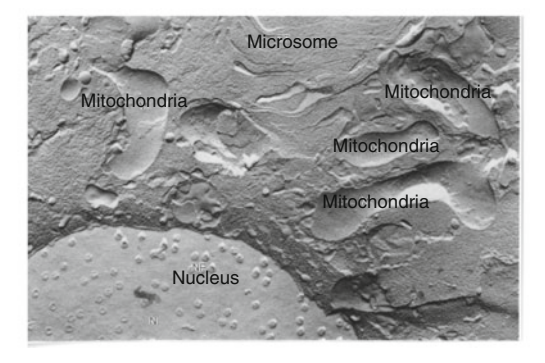


Fig. 2.2 Schematic image and freeze-fractured photo of hepatocyte

$$\mu_{micelle,n} = \mu_{0micelle,n} + \frac{RT}{n} \ln \frac{X_n}{n}$$

Therefore, distribution of assemblies' size can be obtained as a function of  $X_W$  if difference of unitary potential,  $\mu_{0W} - \mu_{0micelle,n}$  and activity coefficient are known. Assuming  $f_W = 1$ ,  $X_N = nX_W \exp\left[-n\frac{\mu_{0micelle,n} - \mu_{0W}}{RT}\right]$  is obtained. There is no formation of lipid assemblies when  $X_W$  is below critical micelle concentration (CMC). When  $X_W$  is above CMC,  $X_W$  is kept constant and additional lipid molecules go to formation of lipid assemblies. Following terms; bulk term (hydrophobic effect), surface term (hydrophobic interaction among hydrocarbons and repulsive interaction among polar heads), curvature term (elastic energy by bending) and packing term (interaction among steric structure of lipid side chains) contribute to difference of unitary potential,  $\mu_{0W} - \mu_{0micelle,n}$ . In these terms, surface term and curvature term reduce  $\mu_{0micelle}$  which become stabilizing force of large assemblies of lipid molecules. Considering formation principle of lipid bilayer membranes from view point of free energies between hydrophobic interaction and repulsive interaction in polarnonpolar interface of lipid assemblies, the free energies are represented by

 $\mu_{n,S}^0 = \gamma (A - A_p) + \frac{C}{A} = \gamma A + \frac{A}{C}$ , where A, A<sub>p</sub>,  $\gamma$  and C are area of one molecule at interface, area of polar group (able to be included in bulk term), density of hydrophobic free energy (3.5 × 10<sup>-20</sup> Jnm<sup>-2</sup>) and constant of repulsive free energy (1.15 × 10<sup>-20</sup> Jnm<sup>2</sup>). Packing constraint is a crucial factor in assembly of lipid molecules in aqueous environment. Area of one lipid molecule in thermodynamic balance is determined as follows. Condition of the minimum interface free energy  $\frac{\partial \mu_{n,S}^0}{\partial A} = 0$ , i.e.  $\mu_{n,S}^0(\min) = 0$  and substituting each value give  $A_0 = \sqrt{\frac{C}{\gamma}} = \sqrt{\frac{1.15 \times 10^{-20} \text{Jnm}^2}{3.5 \times 10^{-20} \text{Jnm}^2}} = 0.57 \text{nm}^2$ . One lipid molecule occupies nearly 0.60 nm<sup>2</sup> in lipid bilayer membranes.

# 2.3 Shape of Lipid Molecule and Structure of Lipid Assembly

Hydration of polar heads of phospholipid molecules makes the lipid molecules disperse in water, and the lipid molecules spontaneously assemble. The process of hydration depends on lipid species. Phosphatidylcholine is easily hydrated, but phosphatidylethanolamine is hardly hydrated, and the hydrations proceeds with main phase transition. Shapes of phosphatidylcholine and phosphatidylethanolamine are cylinder rand inverted cone, respectively. Phosphatidylcholine molecules assemble in planar structure of bilayer, and phosphatidylethanolamine molecules assemble in hexagonal II structure. Relationship between molecular shape and structure of lipid assembly is theoretically explained by Jacob N. Israerachvili [1]. Molecular shape of phospholipid is defined by packing parameter where v,  $A_0$ , l are volume of hydrocarbon chain, area of cross section on interface of water phase and length of hydrocarbon chain, respectively.

$$packing \ parameter = \frac{v}{A_0 l}.$$

Packing parameter <1, packing parameter =1 and packing parameter >1 correspond to cone, cylinder and inverted cone, respectively. From these definitions, a structure of lipid assembly is obtained theoretically by shape of lipid molecule. Volume of the assembly divided by volume of the lipid molecule gives number of constituent lipid molecules, the number must be equal to number that area of the surface divided by area of cross section of lipid in inter phase of water. Using this condition of constraint,  $\frac{43}{3} \left\{ \frac{R^3 - (R - l)^3}{\nu} \right\} = \frac{\pi R^2}{A_0}$  is obtained in a case of outer layer of

bilayer vesicle (liposome). When real values of phospholipid molecule are substituted, possibility of forming assemble structure is obtained.

#### 2.4 Basic Structure of Biomembrane

Cell has various structures such as nucleus, mitochondria, endoplasmic reticulum, lysosome, peroxisome, chloroplast (in plant cell), and plasma membrane in the case of eukaryote. Primary function of biomembrane is compartmentation and selective permeation for chemical reactions and metabolites. Major components of biomembrane are proteins and lipids. Structure of biomembrane has been studied by many researchers, and remarkable model was proposed by Singer and Nicolson as 'fluid mosaic membrane model' in 1972 [2]. They have integrated several studies from different viewpoints and their own experiment using electron microscopy. Those studies are theory of hydrophobic effect of lipids in aqueous environment [3], differential scanning calorimetric study of lipid dispersion [4], X-ray diffraction study of cell membrane [5], Spin labeling study by ESR for lipid bilayer membrane [6, 7], fluorescence microscopic study of antigens on a hybridized cell [8] and freezeetching electron microscopic study of lipid bilayer membrane [9–11]. For folded structure of membrane proteins and even for soluble proteins, degree of hydrophobicity of each amino acid is important, and hydropathy index is useful to consider structure and function of proteins (Fig. 2.3).

#### 2.5 Proteins and Functions of a Cell

Most of functions in a cell are due to proteins, and major functions are catalytic function of enzyme, signaling function of receptor and immune response of antibody. These functions are responsible for amino acid components of protein. 20 species of amino acids play their own role in the function of protein. Acidic amino acid and basic amino acid are associated with electrophilic reaction and nucleophilic reaction of catalytic function of enzyme, and hydrophobicity or hydrophilicity of amino acid is also important for formation of protein structure and interaction with lipid bilayer membrane. Genetic information of amino acid sequence in DNA is transferred to mRNA, and the protein is synthesized in ribosomal system. The genetic information is sufficient for formation of functional structure of protein, and it is proved by an experiment using RNase A [12]. In the experiment, RNase A was denatured by reductive treatment with 2-mercapto-thanol

Chemical structures and hydropathy indexes of amino acids

Methionine (Met, M); 1.9	Serine (Ser, S); -0.8
CH3-S-(CH2)2-CH(NH2)-COOH	HO-CH2-CH(NH2)-COOH
Alanine (Ala, A); 1.8	Threonine (Thr, T); -0.7
CH3-CH(NH2)-COOH	CH3-CH(OH)-CH(NH2)-COOH
Valine (Val, V); 4.2	Tyrosine (Tyr, Y); -1.3
(CH3)2-CH-CH(NH2)-COOH	HO-p-Ph-CH2-CH(NH2)-COOH
Leucine (Leu, L); 3.8	Asparagine (Asn, N); -3.5
(CH3)2-CH-CH2-CH(NH2)-COOH	H2N-CO-CH2-CH(NH2)-COOH
Isoleucine (IIe, I); 4.5	Glutamine (Gln, Q); -3.5
CH3-CH2-CH(CH3)-CH(NH2)-COOH	H2N-CO-(CH2)2-CH(NH2)-COOH
Proline (Pro, P); -1.6	Aspartic acid (Asp, D); -3.5
NH-(CH2)3-CH-COOH	H2N-CO-CH2-CH(NH2)-COOHHOOC-CH2-CH(NH2)-COOH
Phenylalanine (Phe, F); 2.8	Glutamic acid (Glu, E); -3.5
Phenyl-CH2-CH(NH2)-COOH	HOOC-(CH2)2-CH(NH2)-COOH
Tryptophan (Trp, W); -0.9	Lysine (Lys, K); -3.9
Phenyl-NH-CH=C-CH2-CH(NH2)-COOH	H2N-(CH2)4-CH(NH2)-COOH
LL	11214 (0112)4 011(11112) 00011
Cysteine (Cys, C); 2.5	Arginine (Arg, R); -4.5
HS-CH2-CH(NH2)-COOH	HN=C(NH2)-NH-(CH2)3-CH(NH2)-COOH
Glycine (Gly, G); -0.4	Histidine (His, H); -3.2
NH2-CH2-COOH	NH-CH=N-CH=C-CH2-CH(NH2)-COOH

Fig. 2.3 Structure and hydropathy index of amino acids

to dissociate two disulfide bonds of RNase A in 8M urea solution. The denatured RNase A was renatured by oxidative treatment of removing urea by dialysis at pH 8.

#### 2.6 Cell as a Device of Information Processing

A cell receives external stimulus and coverts it to a signal that is available in a signal transducing mechanism in the cell, and the cell shows a cellular function corresponding to the stimulus. So, cell can be considered as an information processing devise. There is a receptor protein on surface of a cell and it receives a ligand (stimulus-molecule) specifically by complementary recognition of molecular

2.7 Membrane Potential 25

structures. The signal from receptor flows through cellular signal transducing system. This system exists in most of cells because neuronal system and hormonal system use receptor on each cell for communication among cells. Hormone as cellular communication signal is secreted by hormone secretory cell and neuro transmitter is secreted by axon terminal and it is received by receptor on a post synaptic cell. Cell membrane (biomembrane) has properties of compartmentation and selective permeation. The selective permeation is due to channel or pump protein. Permeation of specific ion generated concentration difference between inside and outside of membrane, and it triggers action potential of neuron. Pump protein actively transports ions against chemical potential by use of energy. It plays key role for maintaining membrane potential. H<sup>+</sup> ATPase, one of pump proteins generate ATP from ADP and phosphate by rotation of rotator using concentration difference of proton. Molecular structure of a potassium ion channel is obtained by X-ray diffraction study and relationship between selective permeation of K<sup>+</sup> and structure of channel path was elucidated [13].

#### 2.7 Membrane Potential

There are various ions in biological body including cells, and ionic environment is different in both sides of biomembrane. And the difference of ionic concentrations generates membrane potential. Membrane proteins of channel and pump selectively permeate corresponding ions. So, change of membrane potential correlates various biological functions of cells. From view point of physical chemistry, concentration of substance generates chemical potential. In a case that substance is ion, membrane potential is also generated in addition to chemical potential. And electro chemical potential is represented by the following equation.  $\mu_0$ ,  $C_i$ , z, F and  $\varphi$  are standard electrochemical potential, concentration of ion species i, electric charge, Faraday constant and membrane potential, respectively.

$$\mu i = \mu 0 + RT \ln Ci + zF\varphi$$

When there are ions which are unable to permeate membrane in one side of the membrane. Donnan potential is generated in equilibrium state. Donnan equilibrium potential *E* is represented by following equation.

$$E = \varphi out - \varphi in = \frac{RT}{F} \ln \frac{CKin}{CKout} = \frac{RT}{F} \ln \frac{CClout}{CClin}$$

A cell has negatively charged and impermeable proteins inside of it. Considering this case in the presence of permeable ions of K<sup>+</sup> and Cl<sup>-</sup>, the impermeable proteins generate different concentrations of these ions between inside and outside of

membrane. In a condition that K<sup>+</sup> and Cl<sup>-</sup> and the negatively charged proteins 10 mM, 10 mM and 90 mM, respectively, and electrochemical potentials of inside and outside of the cell are equal and electrical neutral, the above equation is obtained.

When temperature is room temperature (25  $^{\circ}\text{C}$ ), Donnan equilibrium potential is – 58 mV.

Donna equilibrium is completed in an excitable membrane of skeletal muscle cell because of high permeability of K<sup>+</sup> and Cl<sup>-</sup>. However, in other cells, Donnan equilibrium is not completed because of low permeability of Cl<sup>-</sup>. And real cells are not in equilibrium state but some ion species permeate membrane. Ion flux is shown as number of ions permeate per unit time and per unit area [mol/cm<sup>2</sup> · sec], and it is proportional to mobility of ion species i u<sub>i</sub>[C/sec · dyn], concentration Ci[mol/cm<sup>3</sup>] and gradient of electrochemical potential  $-\frac{d\mu_i}{dx}[dyn]$ . And this is diffusion potential;  $J_i$  represented by  $J_i = -u_i C_i \frac{d\mu_i}{dx}$ . In the presence of high concentration of NaCl in external cell and low concentration of NaCl in internal cell,  $J_{Na} = J_{Cl}$  under condition of electrical neutrality. In stationary state, integration at membrane thickness=a, results in Nernst equation,  $\varphi_{out} - \varphi_{in} = \frac{RT}{F} \frac{u_{Na} - u_{Cl}}{u_{Na} + u_{Cl}} \ln \frac{[Na]_{out}}{[Na]_{in}}$ .

This equation indicates that diffusion potential is proportional to logarithm ratio of ion concentration outside to that of inside of membrane and mobility.

# 2.8 Patch Clamp Technique and Membrane Potential in Single Channel of a Cell

Membrane potential of biomembrane containing channel proteins is generated by permeation of ions through the channel. Channel proteins distribute on cellular membrane at density of  $10-200/\mu m^2$ . Glass electrode of patch clamp technique is micropipette with open area less than a few $\mu m^2$ . Cell membrane is suctioned into the pipette and removed from the cell membrane. And electrode circuit is constructed with reference electrode. This system has high resistance seal and small noise, and membrane potential of single channel is recorded with small electric current. Using voltage clamp, membrane potential is recorded by compensating current to keep the membrane potential constant. Measurement of membrane potential of single channel shows stochastic behavior. Time lag after stimulation is different for each channel. When the temporal changes of membrane potentials in whole channels on the cell membrane are averaged, the pattern of membrane potential becomes an action potential [14] (Fig. 2.4).

References 27

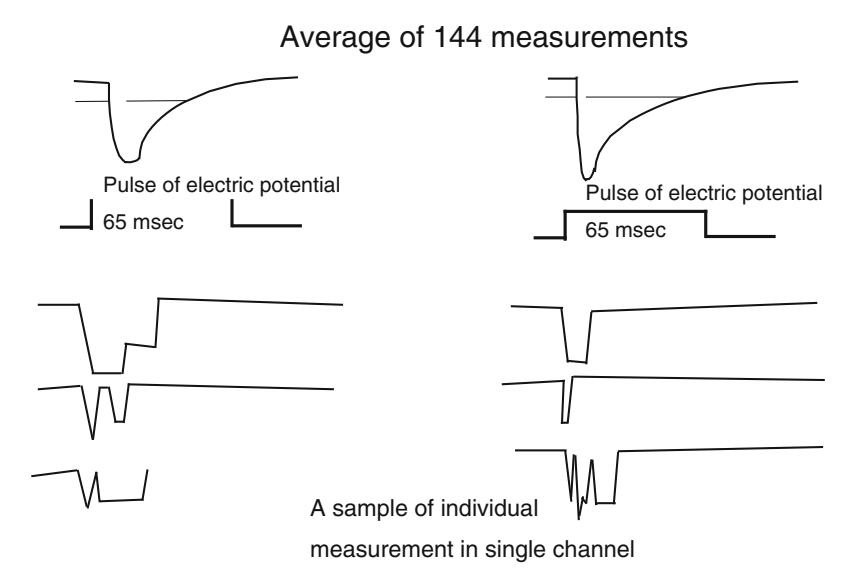


Fig. 2.4 Image of electric potential measurement of single sodium channel Compensated current was measured in fixed electric potential of -110 mV for applied pulse of -50 mV (left) and -30 mV (Right)

#### References

- 1. J.N. Israelachvili, D.J. Mitchell, B.W. Ninham, Biochim. Biophys. Acta 470, 185 (1977)
- 2. S.J. Singer, G.L. Nicolson, Science 175, 720 (1972)
- 3. C. Tanford, *Physical Chemistry of Macromolecules* (Wiley, New York, 1961)
- D.L. Melchior, H.J. Morowitz, J.M. Sturtevant, T.Y. Tsong, Biochim. Biophys. Acta 219, 114 (1970)
- 5. M.H.F. Wilkins, A.E. Blaurock, D.M. Engelman, Nature New Biol. 230, 72 (1971)
- 6. W.L. Hubbell, H.M. McConnell, J. Am. Chem. Soc. 93, 314 (1971)
- 7. R.D. Kornberg, H.M. McConnell, Biochemistry 10, 1111 (1971)
- 8. L.D. Frye, M. Edidin, J. Cell Sci. 7, 319 (1970)
- 9. P. Pinto da Silva, D. Branton, J. Cell Biol. 45, 598 (1970)
- 10. L.A. Staehelin, J. Ultrastructure Res 22, 326 (1968)
- 11. D.W. Deamer, R. Leonard, A. Tardieu, D. Branton, Biochim. Biophys. Acta 219, 47 (1970)
- 12. C.B. Anfinsen, Science 181, 23 (1973)
- 13. Y. Zhou, J.H. Morais-Cabral, A. Kaufman, R. MacKinnon, Nature 414(6859), 43 (2001)
- 14. J. Patlack, R. Horn, Gen. Physiol. **79**, 333 (1982)

# Chapter 3 Methods for Physical Properties of Biomembranes and Cells



**Abstract** Various methods underlying progress of life science which include biophysics of cell and biomembrane are introduced in this chapter. Measurements of bulk system such as X-ray diffraction, differential scanning calorimetry and optical spectroscopy are changed to observation of specific region by use of imaging technique. Bio-imaging system such as X-ray CT and MRI is developed by need of medical diagnosis.

# 3.1 Application of Physical Method to Study of Structure and Physical Properties of Biomembranes and Cells

Living organism is essentially a system of regulated chemical reactions. The chemical reactions are catalyzed by enzymes (proteins) which are synthesized according to genetic information on DNA. For study of these chemical reactions, chemical approach is suitable and useful. On the other hand, physical approach contributes study of biological phenomena and functions related to structure and physical property. Development of life science is correlated with development of technology as well as other fields of natural science. Molecular recognition such as substrateenzyme, antigen-antibody and ligand-receptor is important mechanism by structural complementarity in biological system. Elucidation of structure of biomolecules and assembly of them is important to understand biological functions. Structure of DNA strand was obtained by X-ray diffraction, and it greatly affected development of life science. Essence of heredity was elucidated at molecular level and molecular biology progressed. Novel methods of scanning tunneling microscopy (STM) and atomic force microscopy (ATM) enable direct observation of molecules. Living organism is also a system of materials and energy as well as system of the regulated chemical reactions. Biomembrane as a key component of cell is an assembly of lipids and

**Electronic Supplementary Material** The online version of this chapter (doi:10.1007/978-4-431-56841-4\_3) contains supplementary material, which is available to authorized users.

proteins in aqueous environment. And lipid molecules assemble to form lipid bilayer membranes and show phenomena of statistical thermodynamics such as phase transition and phase separation. Differential scanning calorimetry observes equilibrium of statistical system, but most functions of living organisms is fulfilled in non-equilibrium state. Dynamics of molecules and biological system are observed by various physical techniques such as ESR, NMR and fluorescence spectroscopy, and some of these techniques are developed to become imaging methods to observe the phenomena directly.

#### 3.2 X-ray Crystallography

The best contribution of X-ray crystallography in life science is elucidation of double strand structure of DNA. Most important functional molecule is protein that is synthesized according to genetic information on DNA. There is a concept, 'function is on structure'. And the first 3dimensional structure of protein was determined by contributions of Max Pertz and John Kendrew using X-ray diffraction of hemoglobin. Incident X-ray beams scatter by electron of each atom. The scattered beam of specific angle is enhanced in regular structure of crystal to give a diffraction pattern. And the diffraction pattern is shown by Brag condition,  $\lambda = 2d \cdot \sin \theta$  where  $d, \lambda$  and  $\theta$  are distance between crystal planes, wavelength of X-ray and incident angle to lattice plane, respectively.

## 3.2.1 Principle of X-ray Diffraction

Resolution of optical microscope is determined by equation of  $d=0.61\frac{\lambda}{N.A.}$ , where d  $\lambda$  and N.A. are minimum distance for distinguishing two points, wavelength of observing light and numerical aperture of objective lens, respectively. This means that observation depends on wavelength of light. X-ray diffraction method using X-ray of 0.1 nm wavelength makes possible to observe smaller structure compared to optical microscope using ~300 nm light. When molecules are arranged regularly in crystal, unit of regular structure in crystal is called unit lattice. Structure of the crystal is composed of unit lattices translated x, y and z directions, resulting in diffraction lattice. Incident X-ray beams are scattered discretely to h, k and 1 of diffracted X-ray in reciprocal lattice space. Structure factor, that is relationship between diffracted X-ray and position coordinate of an atom in the crystal is

shown by equation 
$$F(hkl) = \sum_{j=1}^{N} f_j e^{-2\pi i \left(hx_j + ky_j + lz_j\right)}$$
, where  $x_j$ ,  $y_j$  and  $z_j$ ,  $f_j$  are

coordinates of each atom in jth molecule and atomic scattering factor of jth molecule.

Position of electron is maximum position of electron density in deed. Electron density at position coordinate (x,y,z) in the unit lattice is shown by  $\rho(xyz) = \sum_{i=1}^{h} \sum_{j=1}^{k} \sum_{i=1}^{l} F(hkl)e^{-2\pi i \left(hx_j + ky_j + lz_j\right)}$ . Although structure factor is Fourier

transformation, this equation is inverse Fourier transformation. Only scattering intensity |F(hkl)| is obtained by X-ray diffraction data, and relationship between the scattering intensity and X-ray diffraction is shown by  $F(hkl) = |F(hkl)e|^{-2\pi i \varphi}$ , where  $\varphi$  is phase. To obtain electron density, phase should be known. It is necessary to infer phase in X-ray crystallography. There are direct method and heavy atom replacement method to infer phase of X-ray diffraction.

### 3.3 Electron Microscopy

There are two types of electron microscopes in electron microscopy, and they are transmission electron microscope (TEM) and scanning electron microscope (SEM). Difference between them is TEM observing magnified X-ray permeating specimen and SEM observing the second electron generated by reflected X-ray on surface of specimen (Fig. 3.1). For observation of inner structure of cell membrane ad lipid bilayer membrane, freeze-fractured technique is used for preparation of membrane specimen as a replica (Fig. 3.2).

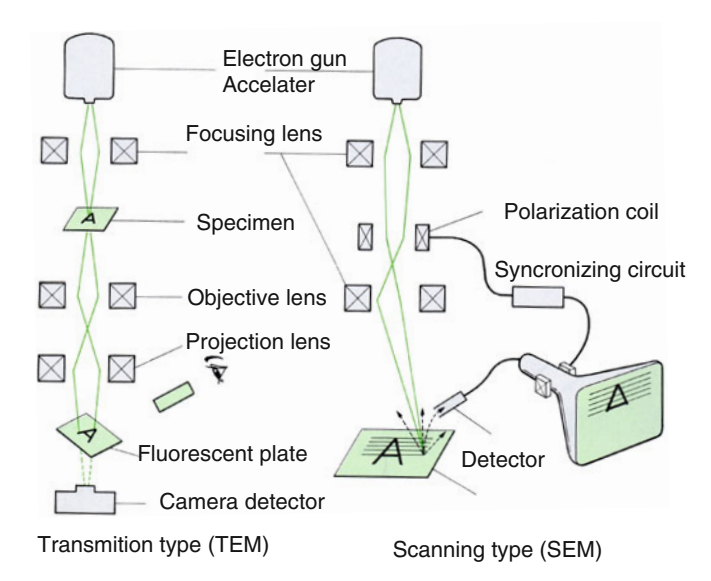


Fig. 3.1 Principles of TEM and SEM observations
Principals for taking magnified image of specimen is illustrated in each electron microscope

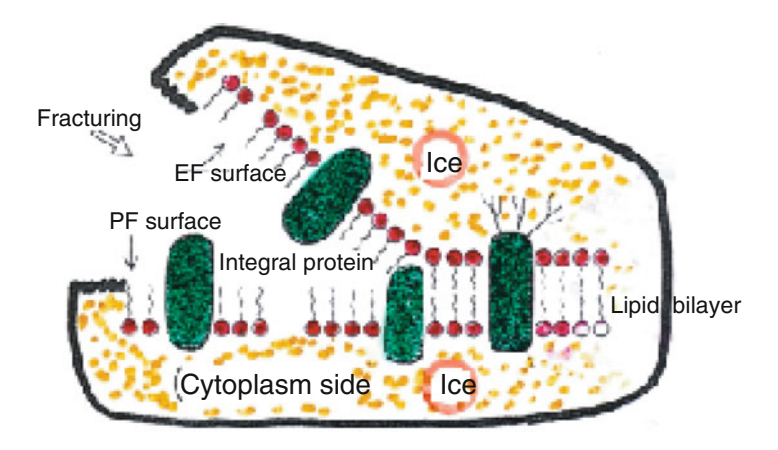


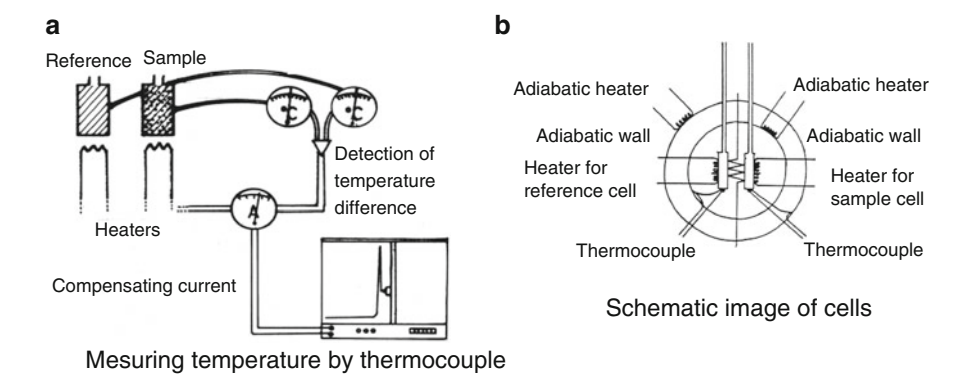
Fig. 3.2 Method of freeze-fractured electron microscopy Process

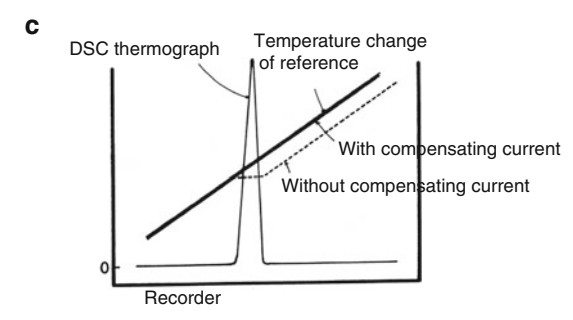
- 1. Specimen(cell, liposome) Freezed at −150 °C
- 2. Fractured at −110°C under high vacuum
- 3. Depositing platinum in oblique angle to make shadow
- 4. Reinforcing by deposition of carbon
- 5. Preparing replica by melting the specimen
- 6. Observation of the replica by electron microscope

## 3.4 Differential Scanning Calorimetry (DSC)

Thermal property is major physical property in biomembrane, and measurement of thermal property provides useful information of structure and physical property of samples. Principle of heat-compensation method for DSC is as follows. When reference and sample are heated by the same electric power, difference of temperature occurs because of difference of specific heat of them. And additional electric power is supplied to keep the same temperature of them, and the electric power is measured as excess specific heat (Fig. 3.3). Thermogram of DSC is shown by the following equation.

 $C_{difference} = C_{sample} - C_{reference} = \left(E_{sample} - E_{reference}\right) \frac{dt}{dT} = E_{difference} \cdot \frac{dt}{dT}$ , where  $\frac{dT}{dt}$  is rate of temperature increase. When the rate is controlled to be constant,  $c_{ifference}$  is proportional to  $E_{difference}$  and measurement of  $c_{difference}$  gives  $c_{difference}$ . Thermal denaturation of protein is observed by DSC measurement. In case of lipid bilayer, lipid assembly in aqueous environment shows phase transition by DSC measurement.





Thermograph (Melting temperature and heating scan)

Fig. 3.3 Principe of DSC measurement

DSC using heat-compensation method has reference and sample cells. When both cells are heated by the same electric power, difference of temperature occurs because of difference of specific heat of them. And additional electric power to keep them in same temperature is measured as excess specific heat

## 3.5 Measurement of Density, (Dilatometer)

Phase transition with structural change is accompanied with change of various physical properties. Change of density is observed by a sophisticated vibration method of Anton Paar DMA/60/602. In the instrument, liquid sample is injected into glass U tube, and frequency of the U tube is measured by digital circuit. Density of the sample is obtained by following equation.

 $T=2\pi\sqrt{\frac{M_0+d\cdot V}{k}}$ , where T, k,  $M_0$ , d and V are frequency of free vibration, spring constant, effective mass of empty U tube, density of sample (liquid or gas) and volume of vibrating region of the U tube (Fig. 3.4). This equation is converted to  $d=\frac{T^2-B}{A}$ , and instrument constants  $A=\frac{4\pi^2V}{k}$  and  $B=\frac{4\pi^2M_0}{k}$  are obtained by measurement of known density of air and water at a certain temperature.

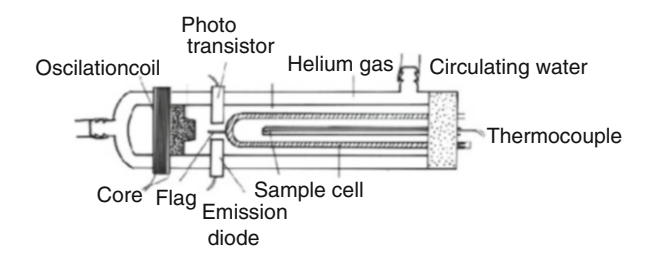


Fig. 3.4 Vibrating dilatometry Anton Paar DMA60/602

Relation between frequency of free vibration and spring constant is shown by  $T=2\pi\sqrt{(Mo+d\cdot V)/k}$  Mo: Effective mass of vacant vibration cell

d: Density of air or water to be measured

V: Volume of vibrating part of cell shown as following equations

d=(T2-B)/A

 $A=4\pi 2V/k$ ,  $B=4\pi 2Mo/k$ 

#### 3.6 Magnetic Resonance

When nuclear spin or electron spin is placed in external magnetic field, magnetic moment generated by its spin interacts with the magnetic field. Classically, compass indicates angular dependent manner in terrestrial magnetism and finally the compass directs north-south direction as the lowest energy state. In a case of nuclear spin and electron spin, their energy states are quantized to discrete energy level. Therefore, electromagnetic wave resonances with energy equal to difference between high-level and low-level energy states, and induces transition between these energy levels. The electromagnetic waves are radio wave and microwave for nuclear magnetic resonance (NMR) and electron magnetic resonance (ESR), respectively.

# 3.6.1 Electron Magnetic Resonance (ESR)

Electron magnetic resonance is also called electron paramagnetic resonance (EPR), and initially used for structural analysis of chemical compounds. Spin labeling method have been developed by use of a unique property of stabilized nitroxide radical as spin probe [1]. Especially, lipid (fatty acid, cholesterol and phospholipid) spin probes are introduced for study of biomembranes and successful results are obtained in measurement of membrane fluidity using order parameter, S [2] and flipflop in lipid bilayer membranes using exchange broadening [3]. The study of membrane fluidity gave an evidence for fluid mosaic model proposed by Singer and Nicolson [4]. Electron rotating with its negative charge generates magnetic moment,  $\mu$ , and the magnetic moment quantized to two states (S=+1/2, antiparallel) and (S=-1/2, parallel) in external magnetic field. An unaired electron takes one of

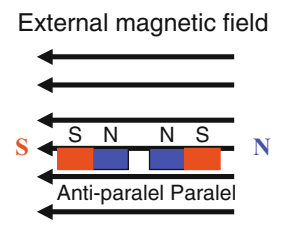


Fig. 3.5 Quantization of spins by external magnetic field Quantum number of electron spin is 1/2 and quantized to anti-parallel or parallel Electron spin is splitted to different energy levels of parallel (-1/2) and anti-parallel (1/2) by Zeeman effect when external magnetic field is applied

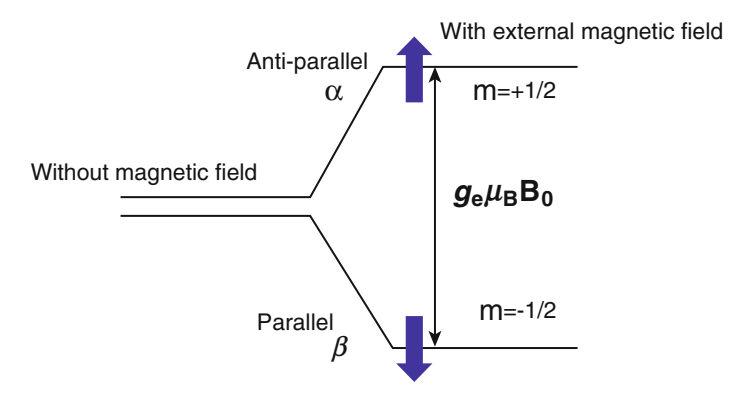


Fig. 3.6 Split of energy level of spin by external magnetic field Electron spin is splitted to different energy levels of parallel (-1/2) and anti-parallel (1/2) by Zeeman effect when external magnetic field is applied

the quantized states by Pauli's exclusion principle (Fig. 3.5). And magnetic moment is shown by  $\mu = -\gamma hS$ , by introducing gyromagnetic ratio  $\gamma$ , g-factor and Bohr magneton  $\beta = \frac{eh}{2mc}$ , and the magnetic moment replaced by  $\mu = -g\beta S$ . And  $Hamiltonian = g\beta H \cdot S_z$  is obtained for along external magnetic field on z-axis. Energy in parallel is shown by  $g\beta \left(-\frac{1}{2}\right) \cdot H$  and in antiparallel is shown by  $g\beta \cdot \left(-\frac{1}{2}\right) \cdot H$  (Fig. 3.6). Difference between these energy levels *i.e.* Zeeman energy is shown by  $\Delta E = g\beta\left(\frac{1}{2}\right)H - g\beta\left(-\frac{1}{2}\right) = g\beta H$ , and electrons distribute these energy levels according to Boltzmann distribution. More electrons distribute in lower level, and radiated microwave  $\Delta E$  to this system in resonance condition of  $h\nu = g\beta H$  makes the electrons in lower level to jump to upper level by absorbing the energy. And simultaneously energy transfer to lower level occurs in relaxation process when applied energy is smaller than certain energy. Difference of electron population is maintained and ESR signal is observed stationary in this condition. Resonance condition is determined by a tensor, g-factor. Value of g-factor for free electron is

g<sub>e</sub>, =2.002319304386. And Magnetic field for resonance is 3400 Gauss (0.34 Tesla) for applied X-band microwave (9.5 GHz). There are two methods for observing ESR signal at resonance condition. One is changing wavelength of microwave at constant magnetic field and another is sweeping magnetic field at constant microwave. Most of ESR machines adopt sweeping magnetic field method.

Stabilized nitroxide radicals are used as spin probes in spin labeling, and electron spin of radical is spitted by hyperfine interaction ( $S \cdot T \cdot I$ ) with quantized nuclear spin of nitrogen atom (I=-1, 0 and +1) (Fig. 3.7). The hyperfine interaction results in three absorption peaks on ESR spectrum, and position of resonance absorption and distance among three absorption lines on ESR spectrum are determined by g-factor and T-tensor, respectively. And there is anisotropy caused by direction of molecular axis because of localization of radical electron on  $\pi$  orbital of nitrogen atom. When z-axis and x-axis are applied to direction of  $\pi$  orbital and direction of N-O bond in molecular axis respectively. Anisotropic ESR spectra are obtained at 9.2 GHz microwave for each direction of applied magnetic field (Fig. 3.8).

#### 3.6.1.1 Order Parameter, S

In spin probes of stearic acid and phosphatidylcholine, z-axis of the nitroxide radicals coincide major axis of the molecules (Fig. 3.9). Molecular motion of these molecules in lipid bilayers of biomembranes appears on ESR spectrum affected by anisotropy of g-factor and T-tensor. When Z-axis of laboratory coordinate (X,Y,Z) is applied to z-axis of molecular coordinate (x, y, z), each direction cosine of Z-axis becomes  $\cos\alpha$ ,  $\cos\beta$  and  $\cos\gamma$ . In this case, ESR spectrum is obtained as time averaged values of g-tensor and T-tensor in transformation from (x, y, z) coordinate system to (X,Y,Z) coordinate system. And relation between these coordinate systems is shown by following equations.

$$g_{ZZ} = \overline{\cos^2 \alpha} g_{xx} + \overline{\cos \beta^2} g_{yy} + \overline{\cos \gamma^2} g_{zz}$$

$$T_{ZZ} = \overline{\cos^2 \alpha} T_{xx} + \overline{\cos^2 \beta} T_{yy} + \overline{\cos \gamma^2} T_{zz}$$

Lipid spin probes in lipid bilayers are arranged their long axis in parallel. Averaged ensemble of the lipid probes indicates an orientated axis toward certain direction. When Z-axis of laboratory  $(X,\,Y,\,Z)$  coordinate system is applied to this direction, time averaged g-tensor and T-tensor for rotational motion around Z-axis becomes constant. Consequently, principle values of these tensors become axial symmetry and principle value parallel to Z-axis, g/ and T/, and perpendicular to Z-axis,  $g\perp$  and  $T\perp$ , respectively are shown by following equations.

$$g// = \overline{\cos^{2}\alpha} \cdot g_{xx} + \overline{\cos^{2}\beta} \cdot g_{yy} + \overline{\cos^{2}\gamma} \cdot g_{zz}$$

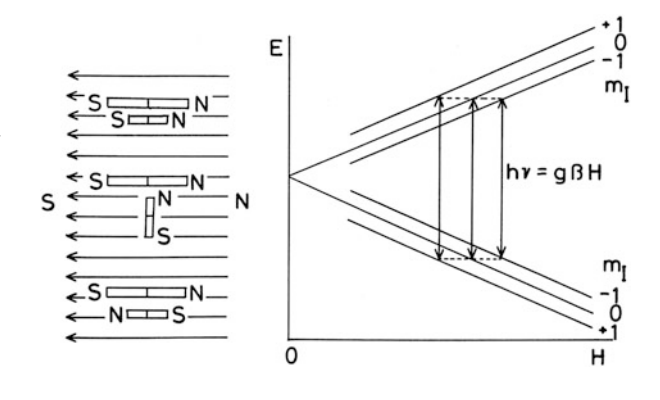
$$T// = \overline{\cos^{2}\alpha} \cdot T_{xx} + \overline{\cos^{2}\beta} \cdot T_{yy} + \overline{\cos^{2}\gamma} \cdot T_{zz}$$

$$g \perp = \overline{(1 - \cos^{2}\alpha)} g_{xx} + \overline{(1 - \cos^{2}\beta)} g_{yy} + \overline{(1 - \cos^{2}\gamma)} g_{zz}$$

$$T \perp = \overline{(1 - \cos^{2}\alpha)} T_{xx} + \overline{(1 - \cos^{2}\beta)} T_{yy} + \overline{(1 - \cos^{2}\gamma)} T_{zz}$$

**Fig. 3.7** Hyperfine interaction of NO Nuclear spins of nitrogen atom (N) have quantum number of +1, 0 and −1, and these spins act as electron spin enhancing, no effect and reducing in magnetic field, respectively Therefore, energy level of electron spin is separated into three levels

Fig. 3.8 ESR spectrum of anisotropic NO radical Position of resonance absorption depends on direction of magnetic field because of anisotropy of g-value, and separated distance depends on anisotropy of T-tensor



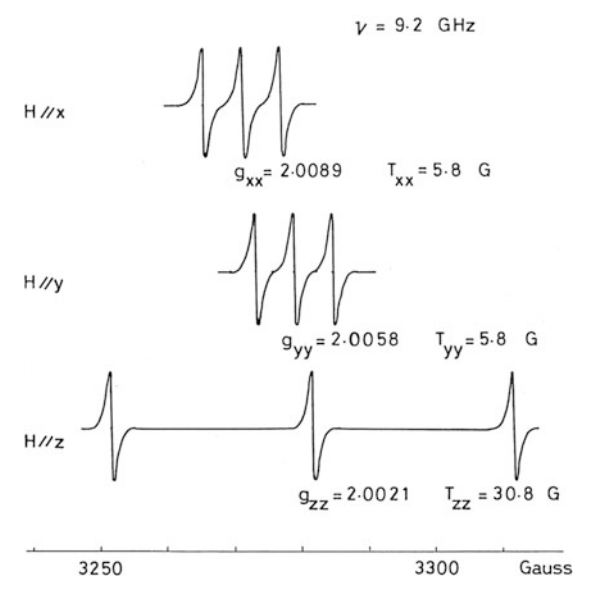


Fig. 3.9 Lipid spin probes

Phosphatidylcholine spin probe

Fig. 3.10 ESR spectrum Values of 2T∥ and 2T⊥ for order parameters of axial symmetric rotation are obtained in ESR spectrum

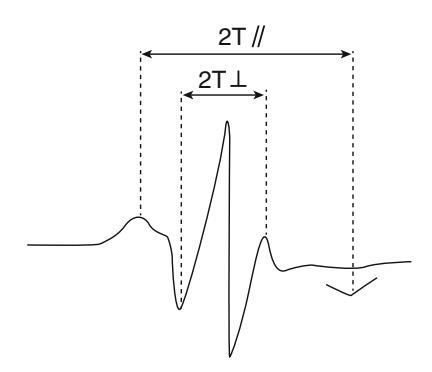


Figure 3.10 shows a typical ESR spectrum of stearic acid spin probe in lipid bilayer membranes. Order parameter,  $S_{zz}$  is defined as following equation by use of  $T_{xx} = T_{yy}$  in a case of nitroxide radical.

$$S_{zz} = \frac{T//-\bot}{T_{zz} - (T_{xx} + T_{yy})} = 3(\cos^2 \gamma) - 1$$

 $S_{zz}$  varies from  $-\frac{1}{2}$  to 1 and the value shows angular range of averaged molecular motion of nitroxide radical. Small value of  $S_{zz}$  shows isotropic motion of nitroxide radical and the motion can be approximated as a motion of sphere (radius =r). And Einstein's relation,  $\tau_C = \frac{4\pi r^3}{kT} \eta$  is applied to this Brownian motion. This equation shows relationship between viscosity  $\eta$  and rotational correlation time  $\tau_C$ . And following equations are derived from theory of line width,  $\Delta H$  of ESR spectrum and the correlation time,  $\tau_C$ .

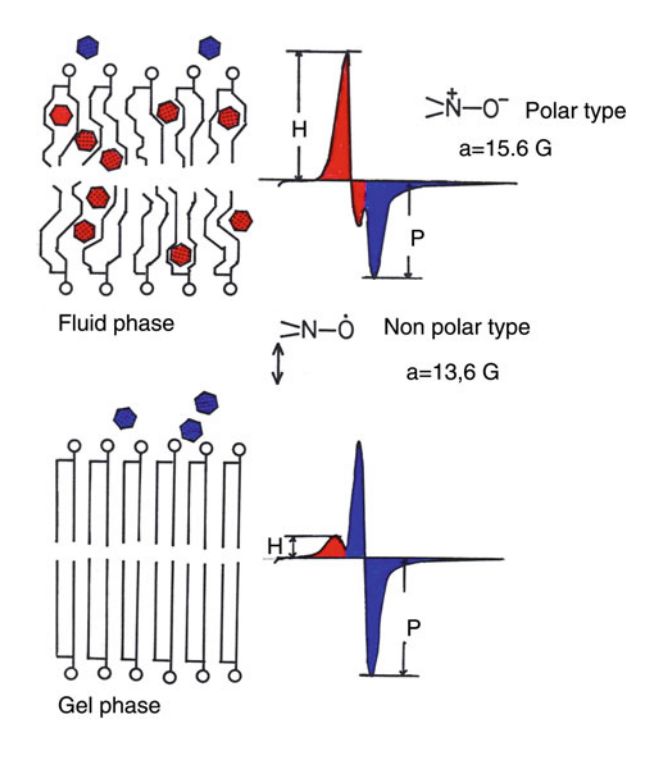
 $\Delta H = \tau_C (A + B \cdot m + C \cdot m^2)$ , where 'm' is quantum number of nucleus, and A, B and C are constant. It becomes possible to obtain viscosity of lipid bilayer membrane and biomembranes by use of spin probe. Real equation to obtain viscosity is  $\tau_C = \left(1 - \frac{h(0)}{h(m)}\right) \frac{3\pi g \beta \Delta H(0)}{h(c_1 m - c_2 m^2)}$  where h(m) are height and width of each peak, respectively.

$$c_1 = \frac{16\pi |\beta| H}{45h} (T_{zz} - T_{xx}) \left( g_{zz} - \frac{g_{xx} + g_{yy}}{2} \right)$$

#### 3.6.1.2 TEMPO Parameter

TEMPO (2,2,6,6,-tetramethylpiperidine-1-oxyl) is small molecular weight and volatile spin probe. When TEMPO is added to biomembranes or dispersion of lipid membranes, the probes are partitioned between aqueous phase and lipid phase of the membranes (Fig. 3.11). Rapid motion of TEMPO averages hyperfine splitting to

Fig. 3.11 TEMPO parameter
Partition of TEMPO spin probes depend on phase structure of lipid bilayer membranes. The probes distribute preferentially in aqueous phase during gel phase, and they distribute preferentially in lipid phase during fluid phase



 $a = \frac{T_{xx} + T_{yx} + T_{zz}}{3}$ . Original value of a in non-polar type is 13.8 G. On the other hand, a vale becomes 15.6 G in aqueous phase because dipolar moment of water molecule changes N-O to polar type. Consequently, separated ESR signal of TEMPO is observed. Partition between aqueous phase and depend on phase transition as well as temperature change. Therefore TEMPO is used to study phase behavior such as phase transition and phase separation [5]. TEMPO parameter depends on polarity around nitroxide radical which generates ESR signal. And measurement of the separated peaks H and P are used to obtain TEMPO parameter. Height of each peak H and P corresponds to content of TEMPO spin probe in hydrophobic environment and polar environment, respectively. Phase behavior of lipid membranes is experimentally realized on change of TEMPO parameter. Partition coefficient of TEMPO spin probe between lipid phase and aqueous phase. The partition coefficient, k is shown in following equation.

$$k = \frac{[C]_{in \ lipid \ bilayef}}{[C]_{in \ aaeous \ phase}}$$

Therefore total TEMPO spin probe in lipid phase= $[C]_{in\ lipid\ phase} \cdot volume$  of lipid phase and total TEMPO spin probe in aqueous phase= $[C]_{in\ aqueous\ phase} \cdot volume$  of aqueous phase.

#### 3.6.1.3 Spin-Spin Exchange Interaction

Effect of spin-pin exchange interaction between different electron spins appears on ESR spectrum as concentration of spin probe in a sample increases. Hamiltonian of this effect is shown by  $J_{ij}S_{ij}$  where  $J_{ij}$  is exchange integration between interacting radicals, i and j [6, 7]. The effect appears in widening of ESR spectrum while effect of the interaction is small. Experimentally, the effect appeared on ESR spectrum is digitalized as a parameter. And relation between spin probe concentration and a parameter is obtained (Fig. 3.12). And relation between distributions of spin probes as ESR spectrum is schematically shown (Fig. 3.13). This technique is used for measurement of lateral diffusion of lipid spin probe in lipid membranes [7] and measurement of phase separation of acidic phospholipid by calcium ions [8]. This technique is also used for measurement of membrane fusion between virus membrane and host cell and membrane fusion of various systems. Decrease of spin-spin exchange is observed in membrane fusion caused by dilution of spin probes. On the other hand, increase of spin-spin exchange is observed in phase separation caused by increase of local concentration of spin probes.

Spin-spin exchange interaction is an effect of quantum mechanics, and overlap of wave function increases or decreases energy of the system Hamiltonian of nitroxide radical in spin labeling method is shown as following equations.

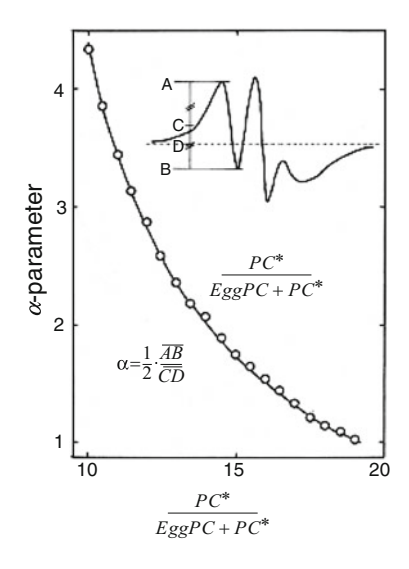
$$H = |\beta|S \cdot g \cdot H_0 + hS \cdot T \cdot I + |-\beta_N|I \cdot g_N \cdot H_0 + H_{exchange} + H_{dipole}$$

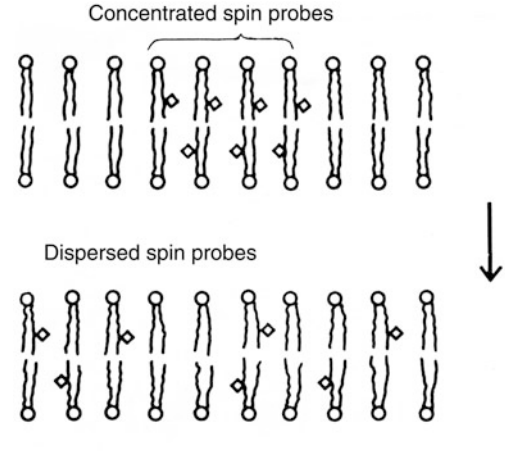
$$(T_{xx}, T_{yy}, T_{zz}) = (5.8, 5.8, 30.8) \text{ Gauss}$$

$$(g_{xx}, g_{yy}, g_{zz}) = (2.0089, 2.0058, 2.0021)$$

In the equation, term of spin-spin exchange interaction is shown as  $H_{exchange} = -2\sum_{i < j} J_{ij} S_i S_j$  where  $J_{ij}$  is exchange integration of interacting unpaired electron i and j. Introducing wave function,  $\Psi_i$  and  $\Psi_j$  for unpaired electrons i and j, respectively, the equation becomes  $J_{ij} = \int \Psi_i(i) \Psi_j(j) \left(\frac{e^2}{r_{ij}}\right) \Psi_i(j) \Psi_j(i) d\tau_i d\tau_j$  where  $I_{ij}$  is distance between i electron and j electron. Line width,  $\Delta \nu_{exchange}$  of ESR spectrum is defined as distance between the maximum and the minimum of first differential of ESR spectrum under condition of exchange broadening. And  $\Delta \nu_{exchange} = 2W_{exchange}$  is obtained. On the other hand,  $\Delta_{exchang} = \frac{(aH)^2}{W_{exchange}}$  is obtained under condition of exchange narrowing. Exchange frequency for fixed radicals is  $W_{exchange} = \nu_{encounter} \cdot p$  where  $\nu_{encounter}$  and p are encounter frequency and probability of exchange for each encounter, respectively. This exchange interaction is used for measurement of lateral diffusion of lipid molecules [6, 7]. The measurement is carried out by use of spin probe of cholesterol analogue (concentration rage

Fig. 3.12 Relation between spin probe concentration and ESR spectrum Liposomes with various ratios of phosphatidylcholine spin probe to egg yolk phosphatidylcholine was prepared, and α-parameter in each ratio was obtained from ESR spectrum measured at 25 °C





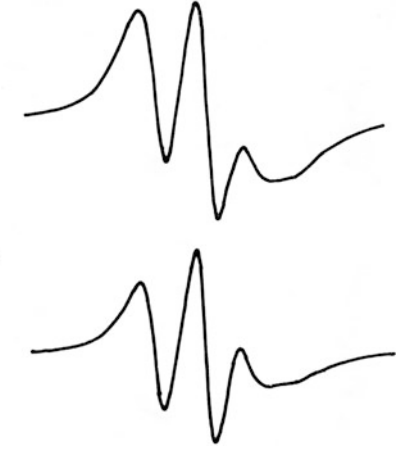


Fig. 3.13 Distribution of spin probes and ESR spectrum ESR spectrum is broadened by spin-spin exchange interaction when local concentration of spin probe is high, and  $\alpha$ -parameter shows smaller value. Therefore,  $\alpha$ -parameter becomes good indication of phase separation and molecular diffusion

from c = 0.01 to c = 0.27) at temperature range from 18 °C to 55 °C in model membranes of dipalmitoylphosphatidylcholine (DPPC). Exchange frequency of spin-spin exchange interaction between androstane spin probes,  $W_{ex}$  is shown as  $W_{ex} = \frac{J}{h}$ . And  $\nu_{encounter} = \frac{\nu_{exchange}}{2p}$  is calculated using  $\nu_{encounter}$  obtained from ESR spectrum. Consequently, diffusion constant,  $D_{diffusion}$  is obtained from following

equation  $\nu_{encounter} = 2d_c \left(\frac{c}{1+c}\right) \frac{1}{F} \frac{D_{diffusion}}{\theta \lambda}$  where  $d_c$ , F,  $\theta$  and  $\lambda$  are effective interaction diameter of radical, area of molecule, geometrical factor and distance of one jump, respectively. In spin labeling method, several types of spin probes are synthesized for each purpose of study [9]. Synthesis method using phospholipase D which can replace polar head of phospholipid is developed for phosphatidylserine and phosphatidic acid spin probes [10].

#### 3.6.2 Nuclear Magnetic Resonance (NMR)

NMR is one of magnetic resonance method as same as ESR. Felix Bloch and Edward M. Purcell and Nicolass Bloembergen independently succeeded in observation of nuclear resonance in solid or liquid molecule in 1945. Theory of NMR can be understood by replacing electron spin with nuclear spin. Atomic nucleus with neither even atomic number nor mass number has non-zero nuclear spin quantum number I and magnetic dipole moment, and it is assumed as a small magnet. Applying external magnetic field, the small magnet shows 2I +1 split of energy levels proportional to strength of the magnetic field by Zeeman Effect. The separated levels have a constant difference of energy. When radiated energy is equal to the difference ( $\Delta E = h\nu$ ), absorption of nuclear magnetic resonance is observed. Actuary, atomic nucleus is in molecular structure and the difference of energy level is affected by chemical environment. The change of resonance condition appears on NMR spectrum, and it is called' chemical shift'. The information of chemical shift gives knowledge of chemical structure of atom. <sup>1</sup>H-NMR for nuclear spin of 1/2 is mostly used and <sup>13</sup> C-NMR is also used for molecules containing carbon atoms because of large chemical shift. <sup>31</sup>P-NMR is used for biomembranes because phospholipid is a major component of biomembranes. In addition, <sup>15</sup>N, <sup>19</sup>F and <sup>29</sup>Si atoms are also used for NMR because these atoms have nuclear spin of 1/2. Development of magnetic resonance technique enables various applications and introduction of superconductive magnet improves resolution of measurement because of increase of magnetic intensity. And it becomes possible to analyze three-dimensional soluble structure of protein by use of double resonance method and Overhauser effect estimation of distance between atoms. MRI (Magnetic Resonance Imaging) using gradient magnetic field is most useful for medical diagnosis becomes popular. Development of FT-NMR plays a significant role for MRI. Pulse of electromagnetic wave is radiated to nuclear spins in constant magnetic field in FT-NMR. The pulse covers a range of wavelength because of the uncertainty principle and nuclear spins having chemical shifts in this range make Larmor precession and generate FID (Free Induction Decay) signals. And these signals are Fourier transformed to NMR spectrum. The time for obtaining the spectrum is short and accumulation of repeated measurements improves S/N ratio.

#### 3.6.3 Magnetic Resonance Imaging (MRI)

Paul C. Lauterbur and Peter Mansfield received Nobel Prize in Physiology or Medicine for discoveries concerning magnetic resonance imaging in 2003, which shows that physics contributes fields of biology and medical science, and a good example of contribution of biophysics to human welfare. MRI method is based on following principle. Water molecules occupy more than 60 % in total weight of the body, and each tissue contains water molecules, i.e. hydrogen atoms. Differences of hydrogen concentration (spin density,  $\rho$ ), spin-lattice relaxation time (T1) and spinspin relaxation time (T2) among tissues of human body. In addition to the differences of these values among the tissues, there is difference of these values between normal tissues and abnormal tissues. MRI uses the differences appeared in the NMR signal and makes image of the NMR signal by use of gradient magnetic field of Lauterbur's idea. Bottomley and his colleagues improved NMR image exceeding X-ray CT image in 1983, and NMR becomes practically realized in clinical application. The difference of relaxation times and positional information obtained from gradient of magnetic field are used for information of imaging in MRI. Gradient of magnetic fields are formed by gradient coils along directions of x-axis, y-axis and z-axis. Frequency of applied pulse of radio wave,  $v_0$  is made resonance under condition of  $\Delta E = h\nu_0 = g_N \beta_N H_0$  and the resonance occurs at position of external magnetic field intensity,  $H_0$ . And so NMR signal and positional information are obtained simultaneously, where  $g_N$  and  $\beta_N$  are g-value and nuclear magneton of atomic nucleus, respectively. On the other hand, values of spin-lattice relaxation time (T1) and spin-spin relaxation time (T2) in relaxation process are used for imaging information. These relaxation times are defined by Bloch's equation as follows. Temporal change of magnetization along z-axis, i.e. spin-lattice relaxation, T1 is relaxation process of spin system to equilibrium magnetization  $M_0$  and diagonal elements of density matrix transfer to Boltzmann distribution, which is shown as following equation.  $\frac{dM_x}{dt} = -\frac{M_z - M_0}{T_1}$ .

Temporal change along x-axis and temporal change along y-axis (spin-spin relaxation time (T2) is process of off-diagonal elements of density matrix transferring to zero which is shown as following equations.

$$\frac{dM_x}{dt} = -\frac{dM_x}{T_2}, -\frac{dM_y}{T_2}$$

Schematic illustration of MRI is shown in Fig. 3.14.

Spin is degree of freedom and atomic nucleus with electric charge generates magnetic moment. Therefore, each spin takes precession around magnetic field  $H_0$  at frequency under condition of  $\nu_o = \frac{\gamma H_0}{2\pi}$ . Magnetic field pulse of Larmor frequency is applied from lateral direction in pulse method. And magnetic field pulse HI of same phase is applied duration time t from x-axis direction in rotating reference frame (  $\nu_o = \frac{\gamma H_0}{2\pi}$ , rotating around z-axis). Direction of magnetic field pulse HI is constant in the rotating reference frame, and spin takes precession at angular velocity of  $\gamma$  HI

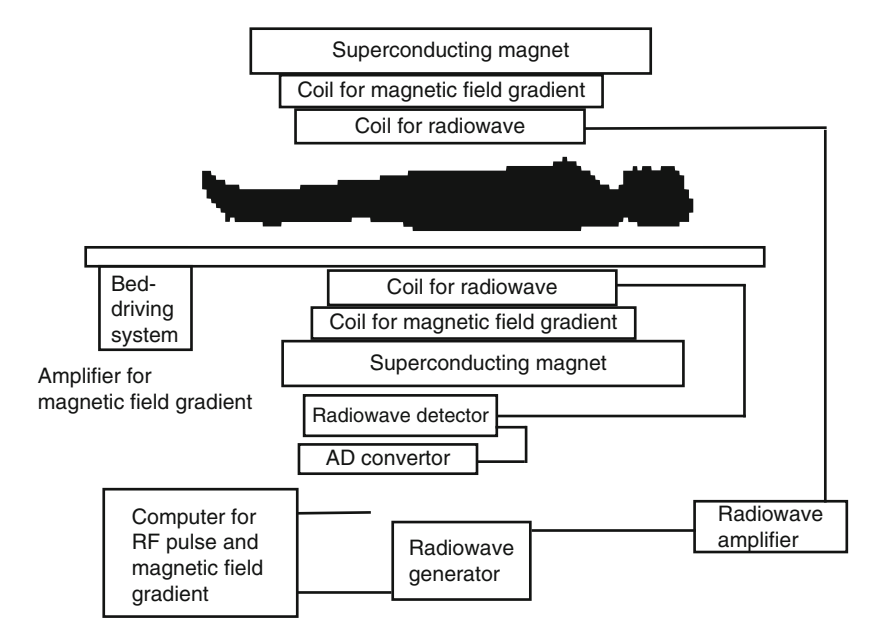


**Fig. 3.14** Schematic illustration of MRI Human body on driving bed is located among superconducting magnet and various coils. Information from various positions in the body are detected as T1 and T2 signals for construction of three-dimensional image

under magnetic field H1. Duration of the pulse is obtained from equation  $\gamma H1t = \frac{\pi}{2}$  to rotate spin 90 degree and duration of the pulse is obtained from equation  $\gamma H1t = \pi$ . Processes of spin-lattice relaxation and spin-spin relaxation are shown in Fig. 3.15.

#### 3.7 Fluorescence Method

Fluorescence is widely used in fluorescence antibody technique in biological science field. Antibody is labeled with fluorescence dye and the labeled antibody binds antigen specifically, and so localization of the molecule can be observed by fluorescence microscope. GFP(Green Fluorescent Protein) gene is cloned from *Aequorea aequorea* by Dr. Osamu Shimomura. The GFP gene is fused with specific gene and expression of the protein and localization can be observed by fluorescence microscope. Fluorescence dye is excited by excitation light, and so its emission can be observed at high sensitivity. Now it becomes possible to observe one molecule of fluorescence dye by reducing back ground light.

3.7 Fluorescence Method 45

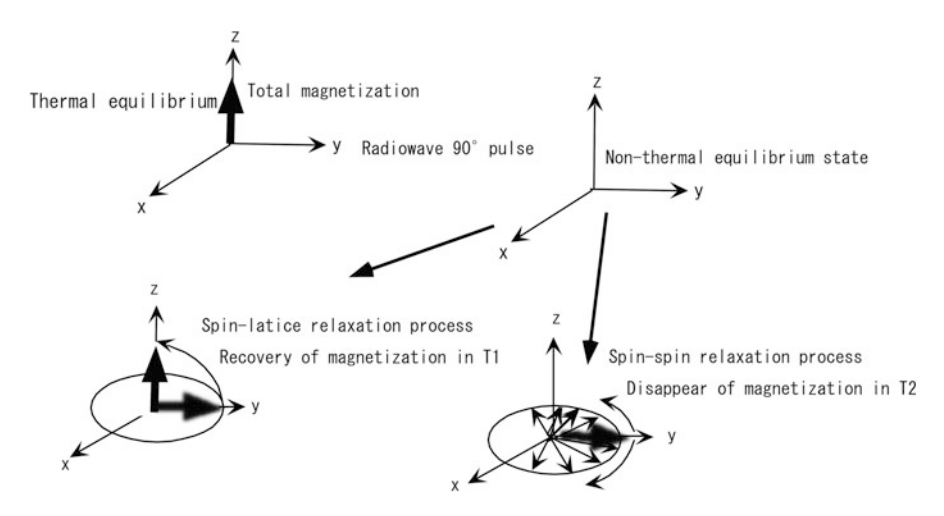


**Fig. 3.15** Processes of spin-lattice relaxation and spin-spin relaxation Spin-lattice relaxation time (T1) and spin-spin relaxation time (T2) are defined by Bloch's equation. Temporal change of magnetization along z-axis, T1 is relaxation process of spin system to equilibrium magnetization M0 and diagonal elements of density matrix transfer to Boltzmann distribution. Each temporal change along x-axis and y-axis (T2) is process of off-diagonal elements of density matrix transferring to zero

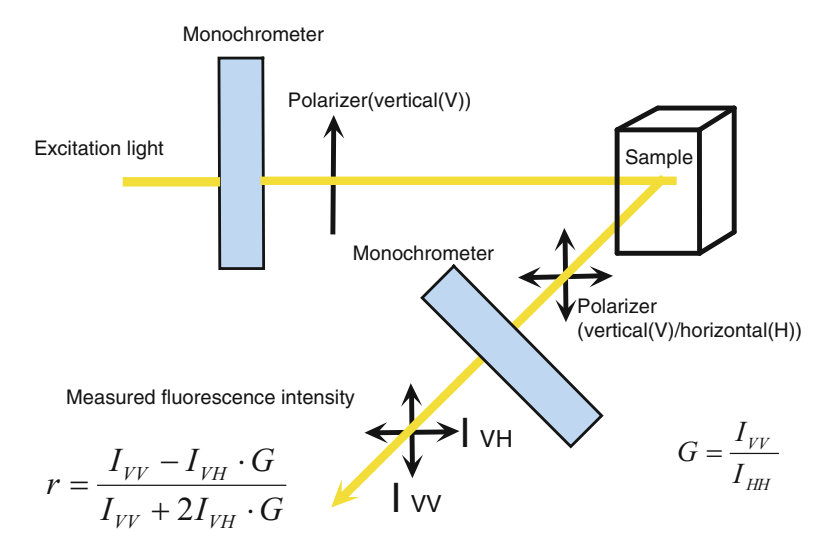
#### 3.7.1 Fluorescence Polarization Anisotropy

Fluorescence polarization anisotropy is a method used for measuring various physical properties in membranes such as phase transition and membrane fluidity (viscosity) in biomembranes and lipid bilayer membranes by fluorescence molecule as a probe. Fluorescence molecule excited by polarized light emits polarized light. Rotational motion of the fluorescence molecule affects direction of the polarized emission light. And the change of emission light is observed by horizontal and vertical polarizer. Fluorescence polarization anisotropy, r is calculated by following equation.

 $r = \frac{I_{VV} - I_{VH} \cdot G}{I_{WV} + 2I_{VH} \cdot G}$ , where  $I_{VV}$  and  $I_{VH}$  are fluorescence intensity of polarized light parallel to incident polarized light and fluorescence intensity of polarized light vertical to incident polarized light, respectively. Correction factor of polarizer for  $I_{HH}$  and  $I_{VV}$ ,  $G = \frac{I_{VV}}{I_{HH}}$  is introduced in the equation (Fig. 3.16).

Quantum yield,  $\phi$  and fluorescence lifetime $\tau$  are defined by rate constants in losing processes of excited energy.

 $\varphi = \frac{k_F + k_{ISC} + k_Q[Q] + k_{ET}}{k_F}$ ,  $\tau = \frac{1}{k_F + k_{ISC} + k_Q[Q] + k_{ET}}$ , where  $k_F$ ,  $k_{IC}$ ,  $k_{ISC}$ ,  $k_Q$  and  $k_{ET}$  are rate constants of fluorescence, internal conversion (S1 $\rightarrow$ ground state), intersystem crossing (S1 $\rightarrow$ triplet state, T), quenching and energy transfer, respectively.



Polarization light ( $(I_{VV})$ ) and fluorescence intensity of horizontal polarized light ( $I_{VH}$ ) are measured. And r is calculated by above equation. G is instrument constant for correction of sensitivity difference between vertical polarized light and horizontal polarized light

Relationship between fluorescence anisotropy, r and rotational correlation time  $\rho$  is shown in Perrin-Weber equation,  $\frac{1}{r} = \frac{1}{r_0\left(1+\frac{3r}{\rho}\right)}$  where  $r_0$ , and  $\rho$  are r values of fluorescence life time and rotational correlation time of molecule at 0 K, respectively. If fluorescence lifetime is obtained by such as pulse excitation method, rotational correlation time  $\rho$  can be calculated using the above equation. By use of Einstein's relationship,  $\rho = \frac{4\pi r^3}{kT}\eta$  where  $\rho$ , r, k, r and r are rotational correlation time, radius of fluorescence probe, Boltzmann constant, absolute temperature and local viscosity, respectively. And local viscosity is obtained by introducing rotational correlation time. Stokes-Einstein equation among diffusion constant, r0, viscosity of solvent, r1 and are rotational correlation time, Boltzmann constant, local viscosity of solvent, absolute temperature and radius of fluorescence probe, respectively. Therefore, diffusion constant of fluorescence probe is obtained in above procedure.

Fluorescence probe DPH (1,6-diphenyl-1,3,5-hexatriene) is widely used for measurement of fluorescence polarization anisotropy (Fig. 3.17).

However, it is not easy to estimate radius of fluorescence probe because its shape affects the molecular structure. Therefore, fluorescence photo-bleaching recovery (FPR) is used for measurement of lateral diffusion of a molecule in membranes.

3.7 Fluorescence Method 47

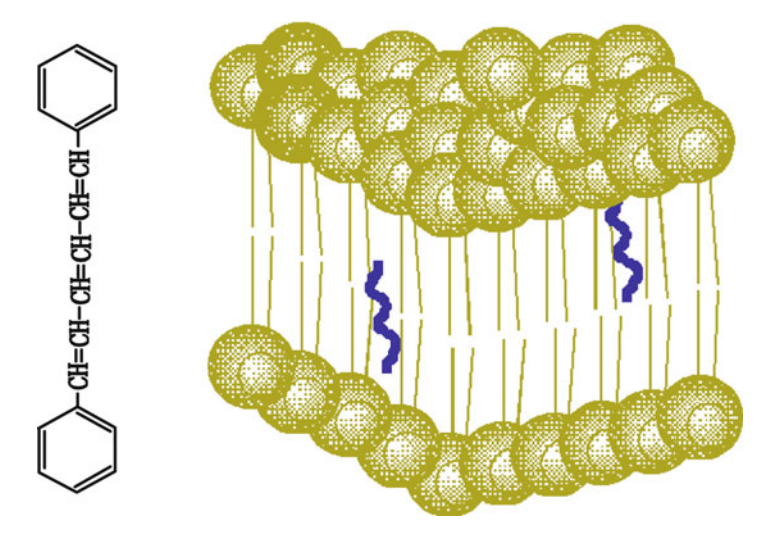


**Fig. 3.17** Structure of DPH and orientation in lipid bilayer membrane DPH (1,6-diphenyl-1,3,5-hexatriene) is located vertically to membrane surface in hydrophobic region of lipid bilayer membrane. Maximum excitation peak is at 359 nm and maximum emission peak is at 426 nm

#### 3.7.2 Fluorescence Photo-Bleaching Recovery (FPR)

Photo-bleaching recovery is developed for method to obtain diffusion constant directly [11]. Molecule labeled with fluorescence dye on cell membrane is observed by fluorescence microscope with weak laser light, and then photo-bleached by strong laser beam. After then the molecules with fluorescence dyes diffusing into the bleached spot from area surround the spot is observed with weak laser light for excitation. Diffusion constant of the molecule labeled with fluorescence dye is obtained by this temporal observation of inlet molecules. Assuming quenching process of fluorescence dye is proportional to rate constant αI(r) of simple non-reversible linear reaction, concentration change of fluorescence dye of unbleached ones under condition of no transportation is shown as  $\frac{dc(r,t)}{dt} = -\alpha I(r)c$ (r,t) where  $\alpha I(r)$ , r and t are intensity of bleaching light at position r, position and time of observation, respectively. Differential equation of one species of molecule transported laterally is shown as  $\frac{\partial c(r,t)}{\partial t} = D\nabla^2 c(r,t) - V_0 \left[ \frac{\partial c(r,t)}{\partial x} \right]$  where D and  $V_0$ are diffusion constant and velocity of homogenous flow of x-direction, respectively. Solution of this differential equation under boundary condition  $c(\infty, t) = C_0$  (homoof fluorescence geneous distribution dye) and initial  $(r,0) = C_0 \exp \left[-\alpha TI(r)\right]$ : is made curve fitting to process of fluorescence recovery to obtain diffusion constant.

#### 3.7.3 Fluorescence Resonance Energy Transfer (FRET)

When there are two species of fluorescence molecules, one molecule (Donor: D\*) emits by excitation and another molecule (Acceptor: A) is excited by accepting the emitted light and then emits fluorescence light. This phenomenon is called fluorescence resonance energy transfer. The donor molecule returns to ground state by releasing energy and the acceptor molecule is raised to excited state. The FRET depends on distance between donor and acceptor and information of inter molecular distance is obtained by FRET. And efficiency of FRET also depends on overlap between emission spectrum of donor and absorption spectrum of acceptor and relative spacial arrangement of emission dipole moment of donor and absorption dipole moment of acceptor. Efficiency of FRET, E is defined as  $E = 1 - \frac{\tau'_D}{\tau_D} = 1 - \frac{F'_D}{F_D} \text{ where } \tau'_D, \ \tau_D, \ F'_D \text{ and FD are fluorescence life time of donor in presence and absence of donor, fluorescence intensity of donor in presence and absence of acceptor, respectively. Dependency of FRET efficiency on distance between donor and accept in the mechanism of dipole-dipole interaction is sown as <math display="block">E = \frac{1}{1+\left(\frac{r}{R_0}\right)^6}, \text{ where } R_0 \text{ is Förster-distance which is obtained by overlap integral of } 1+\left(\frac{r}{R_0}\right)^6, \text{ where } R_0 \text{ is Förster-distance which is obtained by overlap integral of } 1+\left(\frac{r}{R_0}\right)^6$ 

emission spectrum and absorption spectrum, and  $R_0$  is a value at efficiency of 50%.

# 3.7.4 Microscopic Imaging of Physical Property of Biomembranes

Using unique property of environment sensitive fluorescence dye, Laurdan, microscopic imaging system observing physical property of lipid bilayer membranes and biological membranes is developed in the author's laboratory. Cell, an essential unit of life on the earth is compartmented by biomembranes and concerted mechanism generates various biological functions. Therefore, it is required to investigate temporal and spatial change of cellular system of biomembranes to elucidate biological functions of the cell. Method observing real-time image under microscope is widely developed. The author and colleagues have developed real-time microscopic imaging system for physical property of lipid membranes [12]. Environment sensitive fluorescence dye, Laurdan contains lauryl acid in its structure as shown in Fig. 3.18. Laurdan is easily incorporated into lipid membranes and cell membranes by its hydrophobic region. Emission wave length depends on polarity of solvent. Wavelength of emission peak is 440 nm when there is not penetrated water molecules in gel phase of lipid membranes. On the other hand, the emission peak shifts to 490 nm by solvent relaxation when water molecules penetrate in fluid phase. This change is made quantification by GP (Generalized Polarization) value [13]. It is defined as  $GP = \frac{I_{440 \text{ nm}} - I_{490 \text{ nm}}}{I_{440 \text{ nm}} + I_{490 \text{ nm}}}$  where  $I_{440 \text{ nm}}$  and  $I_{490 \text{ nm}}$  are fluorescence intensity at 440 nm

3.7 Fluorescence Method 49

$$(CH_3)_2N$$
 $C - (CH_2)_{10}CH_3$ 

Fig. 3.18 Chemical structure of Laurdan

Environment sensitive fluorescence dye Laurdan (6-dodecanoyl-2-dimethylaminonaphtalene) is synthesized for purpose of charge separation at excited state. And lauric acid is coupled with it for easy partition in lipid membrane

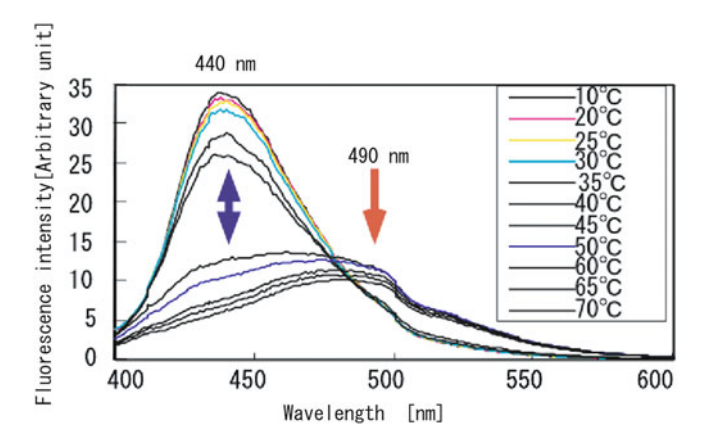
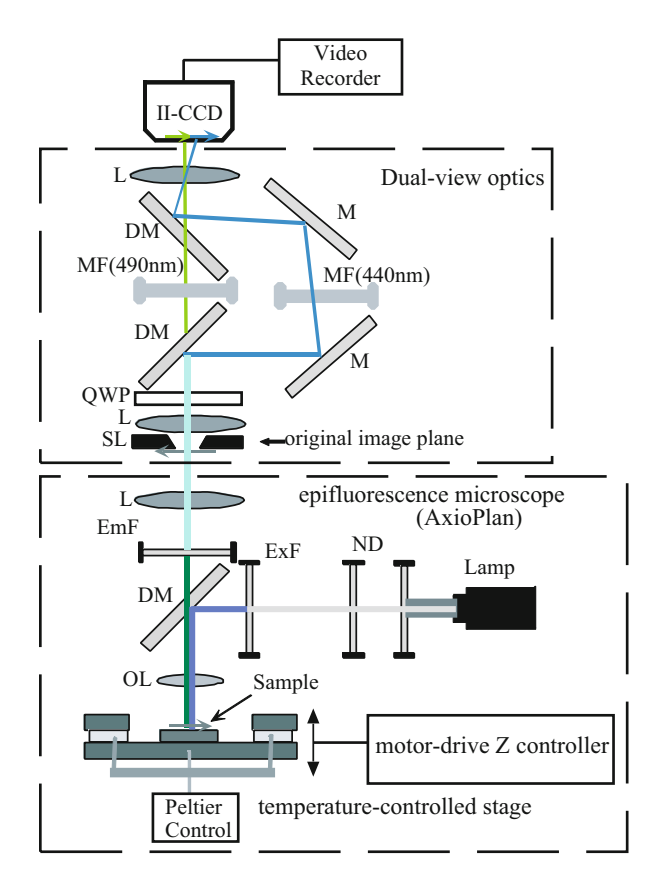


Fig. 3.19 Temperature change of emission spectrum of Laurdan in DPPC membranes DPPC has its phase transition at  $42\,^{\circ}$ C. Wavelength of laurdan shifts from  $440\,\mathrm{nm}$  in gel phase to  $490\,\mathrm{nm}$  in fluid phase because penetrated water molecules in fluid phase make solvent relaxation of emission light

and 490 nm, respectively. Figure 3.19 shows typical change of emission spectrum of Laurdan incorporated in bilayer membranes of dipalmitoylphosphatidylcholine (DPPC) from gel phase to fluid phase. Microscopic imaging of GP value at real time is developed as dual imaging optical unit using dichromic mirror and band pass filters. Fluorescence lights of 440 nm and 490 nm are separated in this optical system and focused on light receiving surface of CCD camera side by side (Fig. 3.20). The 440 nm image and 490 nm images are focused on the light receiving surface of cooled-CCD camera simultaneously, and so time resolution depends on performance of camera. And recorded 440 nm and 490 nm images are superimposed by use of affine transformation and reference image of lattice for calculation of GP value at every pixel of the image. To examine the quality of this instrument, this instrument is applied to observation of G.P. image of a giant liposomes composed of binary mixture of dimyristoylphosphatidylcholine DMPC and dimyristoylphosphatidylethanolamine DMPE (1:1) at video rate. Phase transition temperature of these phospholipids are 23 °C and 49 °C, respectively. And phase separation is clearly shown as the regions of

Fig. 3.20 GP imaging microscopic instrument Microscopic GP image at real time is developed as dual optical unit using dichromic mirror and band pass filters. 440 and 490 nm lights are separated and focused on cooled-CCD camera simultaneously. And recorded 440 nm and 490 nm images are superimposed by use of dynamic affine transformation



different membrane fluidity. Hinge part of high fluidity indicates DMPC rich region and straight part of low fluidity indicates DMPE rich region (Fig. 3.21).

# 3.7.5 Optical Microscopy Using Evanescent-Field

In the preceding sections, methodologies that enable visualization of the physical properties, eg., fluidity of biomembranes are presented. In this section, a method for visualization of the phenomena occurring at the glass-water interface, where cultured cells are bound or molecules in the solution interact with molecules bound to the interface. Figure 3.22a shows the generation of an evanescent wave, a form of near-field illumination. A laser beam which is incident upon the interface of glass and water with the incident angle equal to or larger than the angle called critical angle (~61 degrees), is totally internally reflected, which is accompanied by a generation at

3.7 Fluorescence Method 51

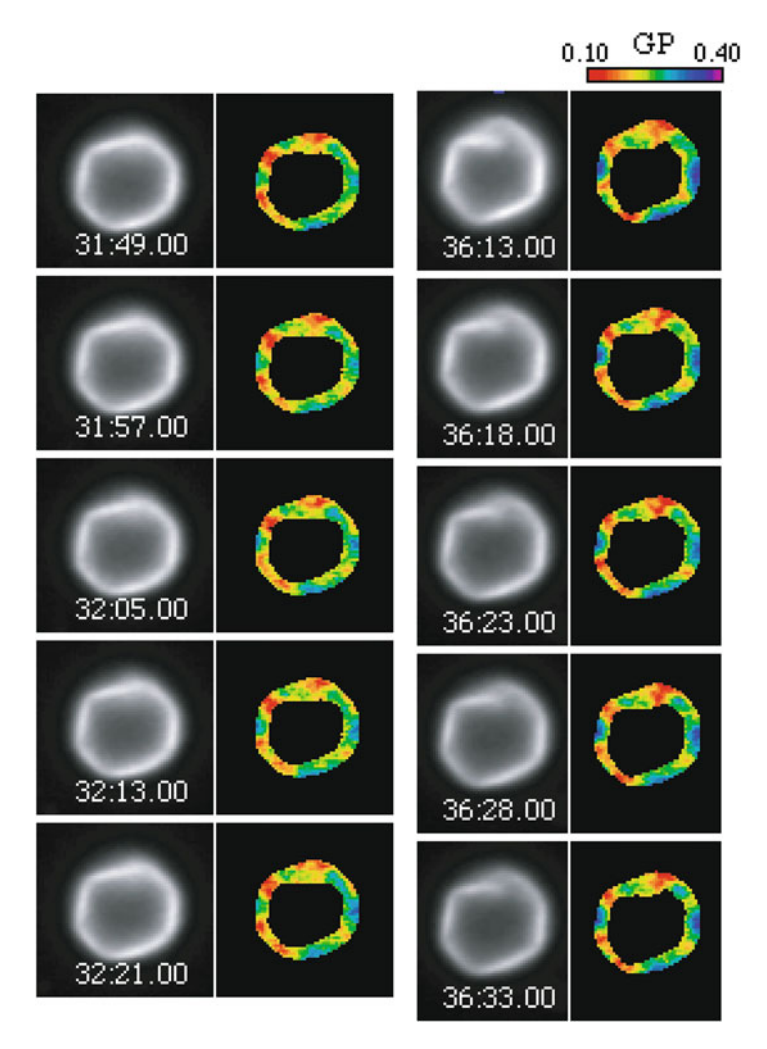


**Fig. 3.21** Real time GP imaging of giant liposome of DMPC/DMPE binary mixture Giant liposome of DMPC/DPPC (1:1) binary mixture was prepared by gentle hydration method in aqueous solution containing 2 mM CaCl<sub>2</sub>. The liposome was observed by GP imaging microscopic instrument in changing temperature

Video is available. (with kind permission of © Kazuo Ohki 2005. All Rights Reserved)

the interface of evanescent wave with the same wavelength as the incident light [14]. The evanescent wave exponentially decays with a characteristic decay length of ~100 nm [15]. Hence, the evanescent wave illuminates the thin region relatively close to the surface, as compared with the epi-illumination, where the light goes deeply into the water phase (Panel b). As a result, the number of fluorophores excited

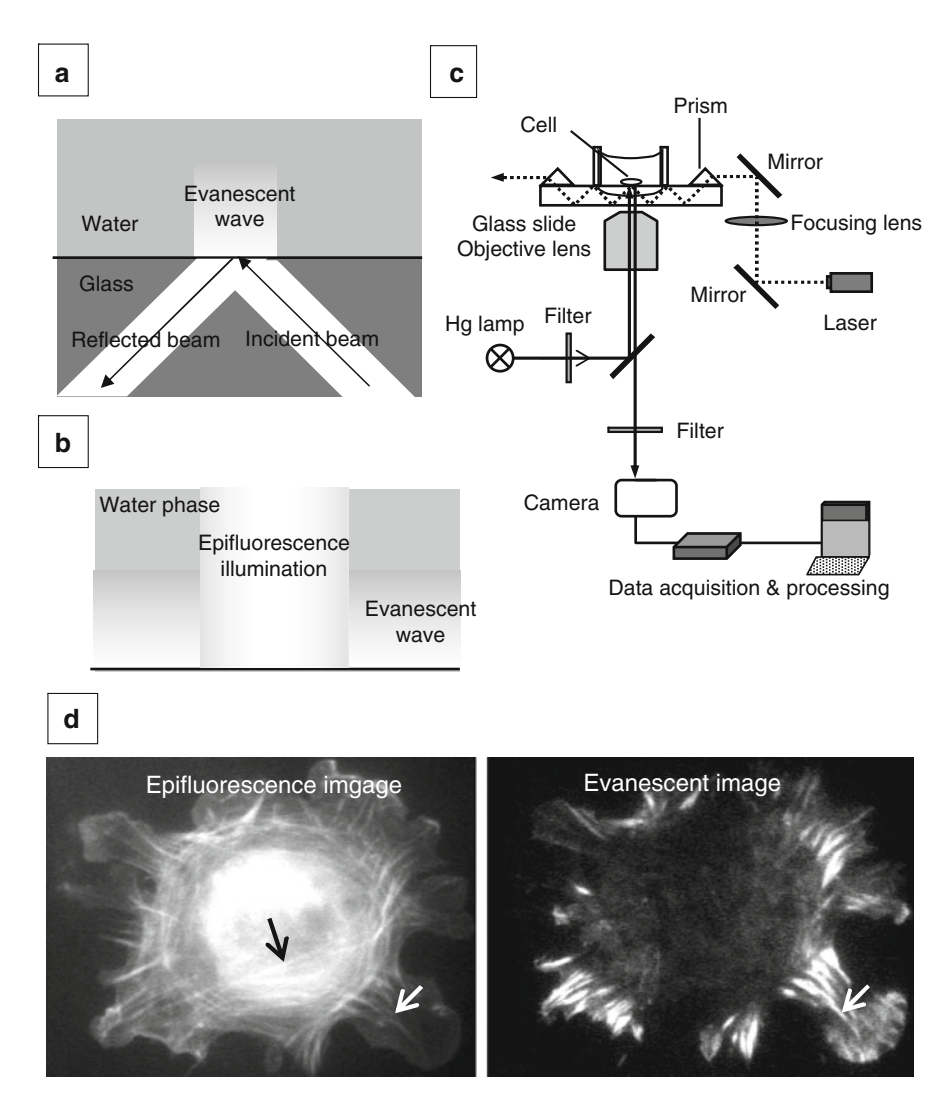


**Fig. 3.22** Panel A, principle of evanescent-wave excitation at the glass-water interface. The laser beam of an appropriate wavelength (eg., 532 nm (green) to excite a fluorophore like rhodamine) is incident on the glass-water interface with the incidence angle equal to or larger than the critical angle (~61 degrees, in the case of glass-water interface), is totally reflected and creates the evanescent wave at the interface. The evanescent wave exponentially decays with the characteristic decay length of ~100 nm. Hence it only excites fluorophores located near the interface and enables the low background fluorescence. Panel B, the feature of the epi-fluorescence excitation is schematically compared with that of the evanescent-wave excitation. As described above, epi-fluorescence illumination penetrates deeply into the water phase whereas the evanescent-wave localizes as a thin layer, in which the intensity exponentially decays. Panel C, an example of the implementation of the evanescent-wave excitation in an inverted epi-fluorescence microscope. A horizontally oriented laser beam is introduced into a coverslip through a rectangular prism. This allows the beam to totally internally reflecting multiple times and the evanescent-wave created

3.7 Fluorescence Method 53

by the evanescent-wave illumination is far less than those excited by the epifluorescence illumination. This and other types of near-field illumination have been proposed [16]. This feature was later combined with high-sensitivity imaging technique to visualize behavior of fluorescently labeled ATP molecules on the myosin molecule attached to glass surface [17]. Figure 3.22c shows an example of the implementation of the evanescent excitation in an inverted epi-fluorescence microscope. The laser beam used for the evanescent excitation is introduced into the coverslip by an optically coupled rectangular prism. The multiple total internal reflections of the laser beam creates evanescent wave at many locations. The cell in the spot can be visualized both in the epifluorescence and evanescent-wave excited fluorescence modes. The left panel of Fig. 3.22d shows an epi-fluorescence image of a cell in which actin filaments were labeled with a fluorophore, rhodamine. A number of actin filaments run within the whole cell body and peripheral membranous protrusion, lamellipodia (black and white arrows). On the other hand, under the evanescent-wave illumination (the right panel of Fig. 3.22d), actin filaments (eg., white arrow pointing as the same filament as in the left panel) in lamellipodia are visible, whereas those in the cell body are visible to a much less extent. This is interpreted as that in the central region of the cell the filaments reside far from the interface, where the evanescent illumination is weak due to the decay. Thus, with the evanescent-wave excitation one can estimate how far the intracellular structure is located from the glass-water interface. A drawback, as compared with the laser scanning confocal microscopy, is the difficulty in the quantitation of the separation. However, in some cases, the separation of the distance between the bottom surface of the cell and the glass surface has been successfully estimated [18, 19]. In these cases, the geometrically simple configuration of the system (eg., the cell adhered to a flat surface) enabled the quantitative estimation of the separation. This method has been also applied to observe the process of exocytosis [20]. Another feature of the evanescent wave is that the polarization of the excitation is uniquely defined. With this feature one can obtain the information about the orientation of the emission dipole of the fluorophore near or at the interface [21, 22].

**Fig. 3.22** (continued) at the position of the cell illuminate the ventral (lower) surface of the cell. The emitted fluorescence is collected by the objective (either water immersion or air) and received by the cooled CCD camera. The acquired image is stored on the computer for later analysis. The same system is also used to perform the epi-fluorescence microscopy. Panel D, comparison of the epi-fluorescence image and the evanescent-wave exited fluorescence image of a cell labeled for actin filaments with rhodamine. The Nd-YAG laser (wavelength = 532 nm) and a mercury-arc lamp (wavelength was selected by an optical filter to be 546 nm) were used as light sources. As described in the text, actin filaments in the cell body are visible by the epi-fluorescence mode (black arrow in the left panel), while the peripheral actin filament bundles (white arrows in both panels) are visible by the evanescent-wave excitation (images taken by Yosuke Senju, Department of Physics, Tohoku University)

### 3.8 Positron Emission Tomography (PET)

Using property of positron, PET is used for medical diagnosis for detecting position of cancer cell on image of human body. Pair annihilation of positron occurs with external electron such as valence electron, conduction electron and so on, and then radiates ray of 2.43 pm as two photons in counter directions each other. Mass of electron and positron is conserved during the pair annihilation and its energy is 511 keV which is rest mass of electron (Fig. 3.23). Water molecules occupy more than 60 % in total weight of human body and pair annihilation occurs between positron and electron of water molecule. PET has detectors arranged on circle for y ray from the pair annihilation. When two detectors detect ray at the same time, position of the pair annihilation is identified as middle point of both detectors (Fig. 3.24). This information is processed by use of computer and reconstituted on three- dimensional image. For medical diagnosis in PET imaging, nucleus of positron release should be generated by synchrotron. Half- life of nucleus releasing positron is order of minutes and synchrotron is located near PET. <sup>11</sup>C, <sup>13</sup>N, 15O and <sup>18</sup>F are used for PET as nucleus species releasing positron, and their half-life time are 20 min, 10 min, 2 min and 110 min, respectively. The process of decay in <sup>11</sup>C is shown as follows. For PET imaging diagnosis of cancer, glucose analogue, <sup>18</sup>Ffluorodeoxy glucose (FDG) is used because cancer cells are very active for cell division and require much energy from glucose. And FDG s gathering around cancer cells are detected by PET and the position is identified in three dimensional image. However, the resolution is about 5 mm because negative factors such as flying distance of positron and angular fluctuation.

# 3.9 Optical trapping

With the progress of biology, a number of techniques have been developed that allow researchers to measure the force developed by the cell and to manipulate cellular objects and even molecules. For this purpose, a glass needle has long been used to measure the forces accompanying the advancement of cells [23] and even single actomyosin motor forces [24]. Atomic-force microscopy was applied to measure the force driving the advancement of keratocyte [25]. All these techniques utilize the precise positioning and optical measurement of the location of needle-like probes with microscope or split photodiode. The range of the force was roughly from 10 nN down to  $10^{-2} \text{ nN}$ . Another technique is the optical trapping. This technique emerged from the technique of manipulation of a single atom by strongly focused laser beams [26, 27]. Later, the possibility was shown to manipulate microscopic objects with a single laser beam [28]. As schematically shown in Fig. 3.25, the forces arise when a pair of rays of the incident light beam is refracted and reflected by the sphere, which has a refractive index higher than the surrounding medium (eg.,

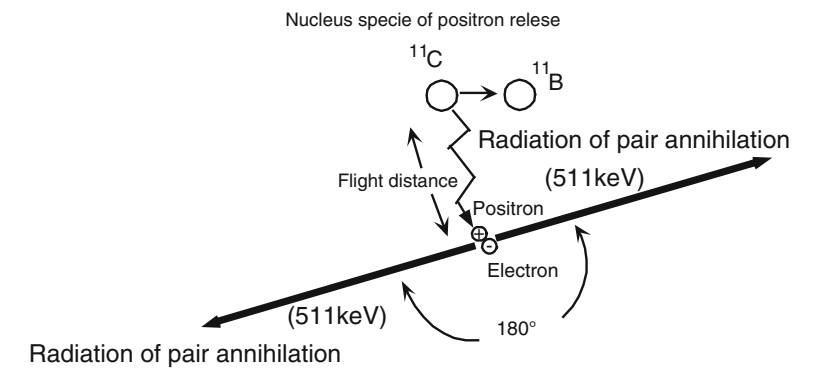


**Fig. 3.23** Process of positron decay and pair annihilation Water molecules occupy more than 60% in total weight of human body and pair annihilation occurs between positron and electron of water molecule

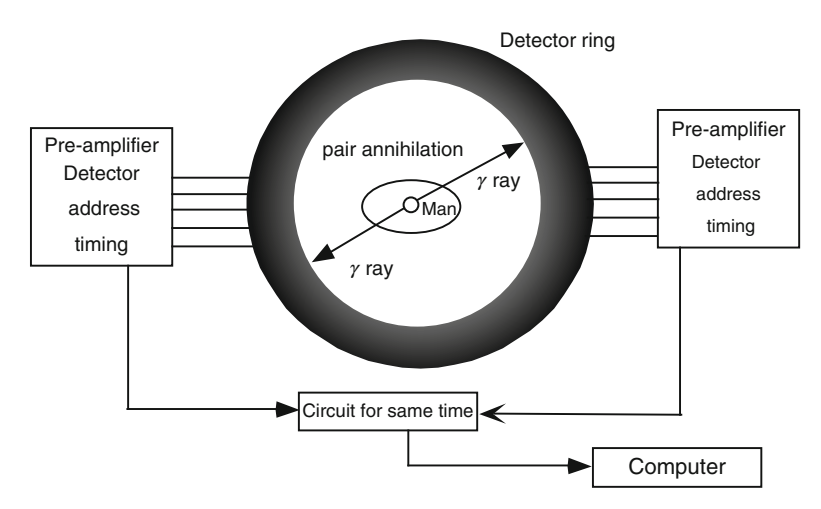


Fig. 3.24 Scheme of PET Human body injected by positron detection nuclide is placed within detector ring. PET has detectors arranged on circle for  $\gamma$ -ray from the pair annihilation. When two detectors detect  $\gamma$ -ray at the same time, and position of the pair annihilation is identified as middle point of both detectors

polystyrene sphere in water) and a diameter much larger than the wavelength of the light beam. The light beam is converged by the lens with high numerical aperture (a microscope objective lens with NA = 1.3 is often used). When the center of the sphere moves on the optical axis off the focal point of the lens, the ray refracted by the sphere will exert a force on the sphere that is toward the focal point; when the center of the sphere becomes off-axis, the force is also directed toward the focal point. Hence, the force exerted by the light beam is a restoring force that pulls the sphere to the focal point; the magnitude of the force is approximately proportional to

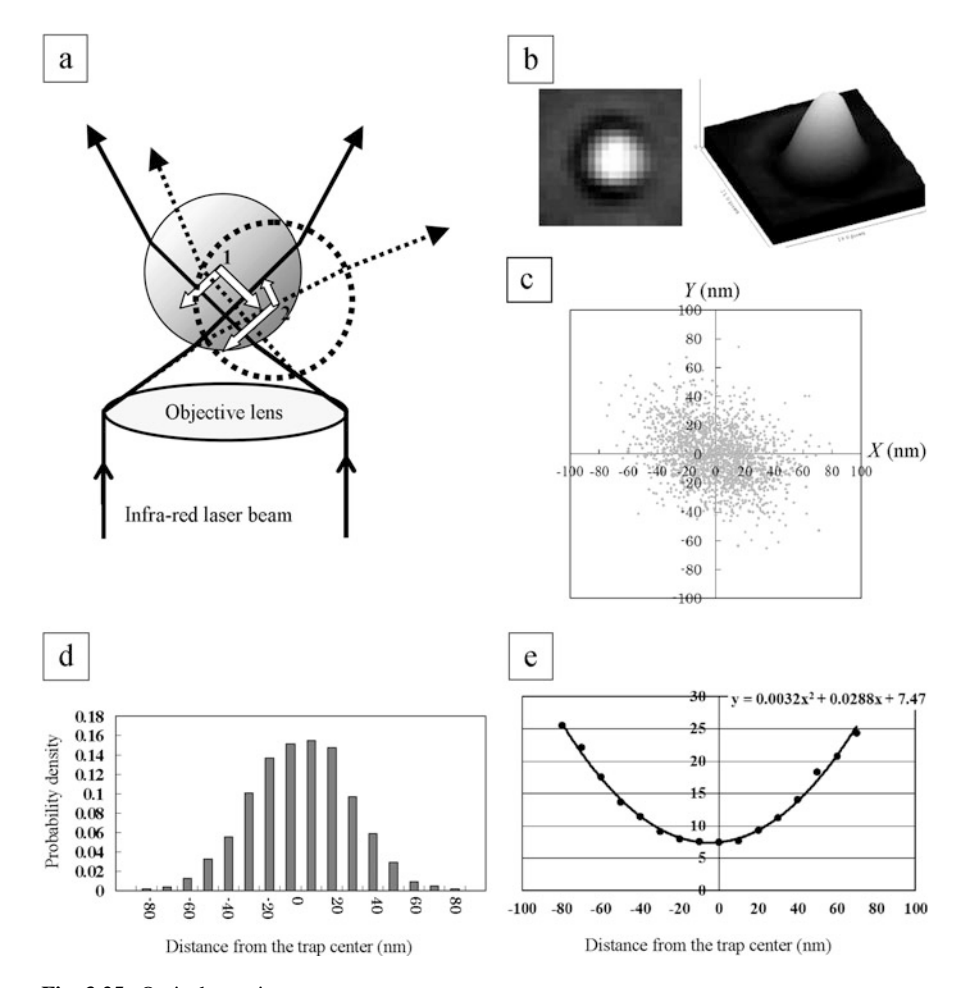


Fig. 3.25 Optical trapping

Panel A, an explanation of the generation of optical force based on the geometrical optics (Ashkin, 1992). When the center of a bead (sufficiently larger than the wavelength of the laser beam and with refractive index larger than the surrounding medium) is on the beam axis (position "1"), the beam is refracted axisymmetrically by the bead. The refraction of the light causes the change in the momentum of the photon by the bead. Hence, the bead will receive recoil from the photon. In this case, all forces from peripheral beams sum up to become a pulling force toward the lens. This force is balanced by the optical pressure from the incident beams. When the bead center is shifted to the position "2", the direction of the refracted beams is changed and as a result, the sum of the force is directed toward the position "1". Thus, the optical trapping exert a restoring force on the trapped object. The amount of the force is proportional to the shift of the bead.

Panel B, left, a phase-contrast image of a 1  $\mu$ m polystyrene bead trapped in the optical trap created by the focused infra-red laser beam (wavelength = 1064 nm); right, a three-dimensional plot of the intensity of the phase-contrast image of the bead. Panel C, X-Y distribution of the bead in the trap potential. Note the axisymmetrical distribution of the bead center. The number of the points that exist between R and  $R + \Delta R$ , where R denotes the distance from the center of the trap and  $\Delta R$  is the increment of R, was counted and was transformed into the probability density distribution,  $\rho(R)$ .

the distance between the bead center and the focal point [28, 29]. Thus, the restoring force, F, has characteristics of a spring: F = kx, where k and x is the stiffness (spring constant) and the amount of the shift of the sphere. Hence, if one can measure k and x, one will know the magnitude of the force exerted on the sphere. Theoretical calculations of the stiffness have been presented [28–31] and an example of the experimental method to estimate the stiffness is given in Fig. 3.25.

With the above feature, the optical trapping technique has been widely used to measure, for example, the force developed by a single motor force or protrusive force of the cell edge (ie., lamellipodium). By utilizing infra-red laser beam, one can manipulate intracellular objects, because the cell membrane is relatively transparent to the infra-red laser beam [32]. Another advantage is that if the light is split by a polarization beam splitter and each light is focused at two different focal points separately, one can hold two objects at each focal point. The ability to separately change the direction of the beam by two independent reflecting mirrors will enable further applications. Some applications of the optical trapping are presented in Chap. 7.

#### 3.10 Outlook of Molecular Dynamics

Nobel Prizes in Chemistry for 2013 were awarded to Martin Karplus, Michael Levitt and Arieh Warshel [33] for the development of multiscale models for complex chemical systems. Chemists used to create models of molecules using plastic balls and sticks. Today, the modelling is carried out in computers. In the 1970s, Martin Karplus, Michael Levitt and Arieh Warshel laid the foundation for the powerful programs that are used to understand and predict chemical processes. Computer models mirroring real life have become crucial for most advances made in chemistry today. For instance, in simulations of how a drug couples to its target protein in the body, the computer performs quantum theoretical calculations on those atoms in the target protein that interact with the drug. Today the computer is just as important a tool for chemists as the test tube. Simulations are so realistic that they predict the outcome of traditional experiments.

Fig. 3.25 (continued) Panel D, an example of the plot of  $\rho(R)$ . Panel E, the potential of the trap and the trap stiffness deduced from  $\rho(R)$ , assuming that the density distribution obeyed the Boltzmann distribution. In fact, the potential was approximated with quadratic function of R (x in the figure), which implied the force exerted on the trapped bead was indeed spring-like (force is calculated from the product of the stiffness of the trap and R). In this instance the stiffness was deduced to be  $\sim 0.01$  pN/nm

#### References

- 1. S. Ohnishi, H.M. McConnell, J. Am. Chem. Soc. 87, 2292 (1965)
- 2. W.L. Hubbell, H.M. McConnell, J. Am. Chem. Soc. 93, 314 (1971)
- 3. R.D. Kornberg, H.M. McConnell, Biochemistry 10, 1111 (1971)
- 4. S.J. Singer, G.L. Nicolson, Science 175, 720 (1972)
- 5. E.J. Shimshick, H.M. McConnell, Biochemistry 12, 2351 (1973)
- 6. E. Sackmann, E. Trauble, J. Am. Chem. Soc. 94, 4482 (1972)
- 7. P. Devaux, H.M. McConnell, J. Am. Chem. Soc. 94, 4475 (1972)
- 8. S. Ohnishi, T. Ito, Biochemistry 13, 881 (1974)
- 9. J.F.W. Keana, S.B. Keana, D. Beetham, J. Am. Chem. Soc. 89, 3055 (1967)
- 10. P. Jost, L.J. Liibernini, V.C. Herbert, J. Mol. Bio. **59**, 77 (1971)
- 11. D. Axelrod, D.E. Koppel, J. Schlessinger, E. Elson, W.W. Webb, Biophys. J. 16, 1055 (1976)
- 12. T. Ohba, S. Tsuchiya, Kumeta, K. Ohki, Jpn. J. Appl. Phys. 44, 8733 (2005)
- 13. T. Parasassi, G. de Stasio, A. d'Ubaldo, E. Gratton, Biophys. J. 57, 1179 (1990)
- M. Born, E. Wolf, *Principles of Optics*, vol 47, 6th edn. (Cambridge University Press, Cambridge, 1977)
- 15. D. Axelrod, J. Cell Biol. 89, 141 (1981)
- 16. A.L. Stout, D. Axelrod, Appl. Opt. 28, 5237 (1989)
- 17. T. Funatsu, Y. Harada, M. Tokunaga, K. Saito, T. Yanagida, Nature 374, 555 (1995)
- 18. H. Hirata, C.T. Lim, H. Miyata, Cell Commun. Adhes. 9, 17 (2012)
- 19. G.A. Trusky, J.S. Burmeister, E. Grapa, W.M. Reichert, J. Cell Sci. 103, 491 (1992)
- 20. M. Oheim, D. Loerke, D.R.H. Chow, W. Stuhmer, *Philosophical Transactions of the Royal Society of London B*, vol 354 (1999), p. 307
- 21. N.L. Thompson, H.M. McConnell, Biophys. J. 46, 739 (1984)
- 22. D. Gingell, I. Todd, J. Bailey, J. Cell Biol. 100, 1334 (1985)
- 23. T. Oliver, J. Lee, J. Jacobson, K. Semin, Cell Biol. 5, 139 (1994)
- 24. A. Ishijima, T. Doi, K. Sakurada, T. Yanagida, Nature **252**, 301 (1991)
- 25. M. Prass, K. Jacobson, K. Semin, J. Cell Biol. 174, 767 (2006)
- 26. A. Ashkin, Phys. Rev. Lett. 40, 729 (1978)
- 27. K. Svoboda, S.M. Block, Annu. Rev. Biophys. Biomol. Struct. 23, 247 (1994)
- 28. A. Ashkin, Biophys. J. 61, 569 (1992)
- 29. P.J. Walla, Modern Biophysical Chemistry (Wiley-VCH, Weinheim, 2009), pp. 209-216
- 30. R. Gussgard, T. Lindmo, I. Brevik, J. Opt. Soc. Am B. 9, 1922 (1992)
- 31. A. Rohrbach, Phys. Rev. Lett. 95, 168102 (2005)
- 32. A. Ashkin, J.M. Dziedzic, Proc. Natl. Acad. Sci. (USA), vol 86 (1989), p. 7914
- 33. A. Warshel, Angew. Chem. 53, 10020 (2014)

# **Chapter 4 Structure and Physical Properties of Biomembranes**



**Abstract** Biological functions of biomembranes are closely related to their structures and physical properties because most of membrane functions require lipid bilayer membranes. The lipid bilayer membranes are composed of a lot of number of lipid molecules, proteins and other constituents. These molecules make statistical assembly and show phase transition and phase separation. And change of these physical properties including membrane fluidity affect and regulate biological functions of biomembranes.

#### 4.1 Structure of Biomembranes

Cell is an essential unit of life and composed of various biomembranes. Major components of the biomembranes are proteins and lipids. These components were obtained in early study of cells, but structure of the biomembranes was not elucidated long time. Some models of biomembranes were proposed before fluid mosaic model proposed by Singer and Nicolson. The model has shown basic concept of biomembranes which is widely accepted as a standard model of biomembranes [1] (Fig. 4.1). They used preceding studies related to membrane structure in addition to their own freeze- fractured study of red blood cell membranes. The preceding studies are calculation of free energy in theory of hydrophobic effect [2], phase transition of cell membrane and extracted lipids measured by DSC, which shows lipid molecules form statistical assembly in cell membranes [3]. X- ray diffraction pattern of neuron membranes showed structure with 40 angstroms thickness [4]. Axial rotation [5] and flip-flop [6] of lipid spin probes in lipid bilayer membranes were observed by ESR. Using fluorescence antibody and cell fusion by Sendai virus, lateral diffusion of histocompatibility antigens on cell membranes was observed by fluorescence microscope [7]. There are other studies using freeze-fractured electron microscopy [8, 9] and particles in the fractured surface of biomembrane were proved to be proteins [10]. Two types of membrane proteins were introduced in the fluid mosaic membrane model. One is peripheral protein which is defined as protein released from cell membrane by treatment with chelating reagent and increasing ionic intensity because

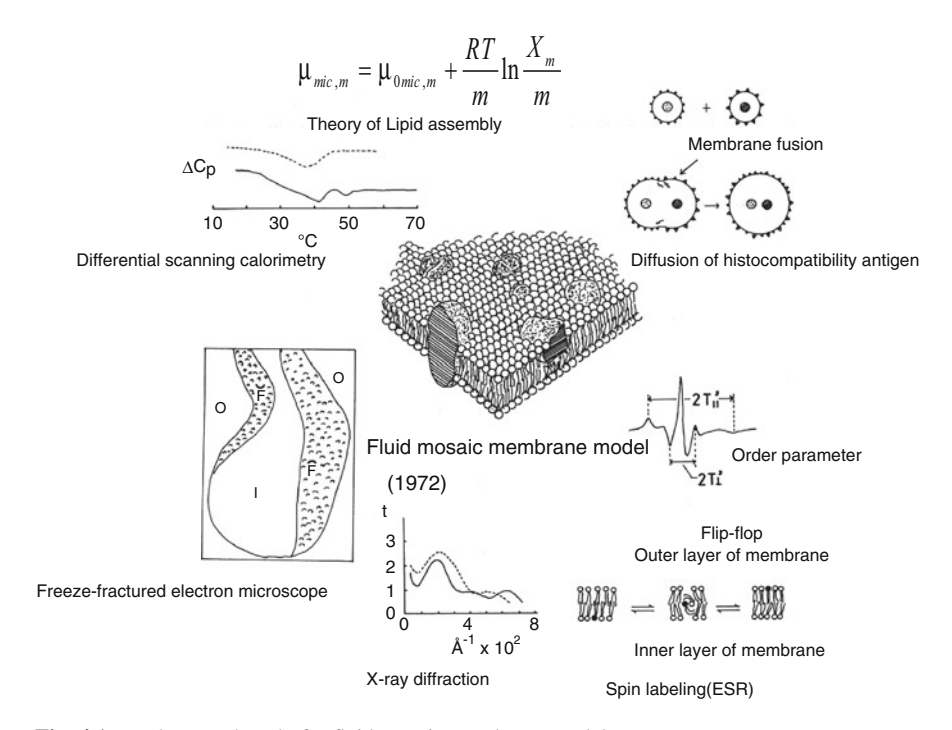
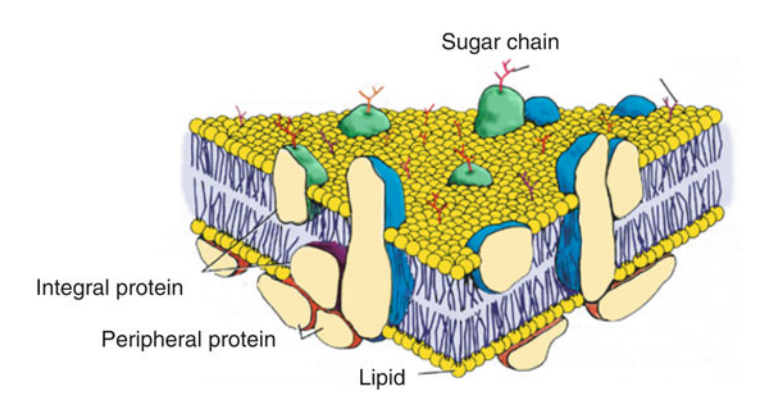


Fig. 4.1 Back ground study for fluid mosaic membrane model



**Fig. 4.2** Scheme of biomembrane Biomembrane is composed of lipid bilayer and two types of proteins such as integral protein and peripheral protein

it is attached to the membrane surface by electrostatic interaction. Another is integral protein which is defined as protein solubilized by detergent such as SDS because it is bound within the membrane by hydrophobic interaction. These types of membrane proteins are included in lipid bilayer membranes which spontaneously assemble in aqueous environment (Fig. 4.2).

#### 4.2 Phase Transition of Lipid Bilayer Membranes

Lipid bilayer membranes are assembly of a lot of number (sufficient for statistical phenomena) of lipid molecules and they show phase transition like first order phase transition and it is an interest research subject from physical viewpoint. From the definition of first order phase transition, Gibbs free energy G for temperature change is continuous under constant condition of pressure and its differential,  $\left(\frac{\partial G}{\partial T}\right)_P$  is discontinuity. So  $\Delta G = 0$  and  $\Delta G = \Delta H = -T_t \Delta S$  becomes latent heat  $\Delta H = T_t \Delta S$ . When 2 phases are independent from each other, Gibbs free energy of these phases are shown as function of temperature, T and pressure, P as follows  $G_1 = f_1(T, P)$ ,  $G_2 = f_2(T, P)$ . In case of fluid phase and gel phase, they become  $G_L = f_L(T, P)$  $P = H_L - TS_L$  and  $G_S = f_S(T, P) = H_S - TS_S$ , and difference of the Gibbs free energy between these phases is shown as  $G_S - G_L = (H_S - H_L) - T(S_S - S_L)$ . Enthalpy in gel phase is smaller than that in fluid phase and entropy in solid phase is smaller than fluid phase because of higher orderliness in gel phase. Therefore, transition from fluid phase to gel phase occurs when a certain temperature, T exists for negative  $(G_S - G_I)$ . This transition reduces the free energy and the transition to gel phase proceeds spontaneously. Temperature,  $T_t$  of first order phase transition is obtained as intersection of Gibbs free energy curves of these phases. DSC measurement of phase transition in biomembranes is focused on lipid membranes. And one component of lipid dispersed in water such as dipalmitoylphosphatidylcholine (DPPC) shows clear phase transitions (Fig. 4.3). DPPC molecules dispersed in water by voltexing form multi-lamellar membranes and they show four phase transitions; sub transition (crystal phase,  $L_c$  to gel phase,  $L_{\beta'}$ ), pre-transition (gel phase to ripple phase) and main transition (ripple phase to fluid phase,  $L_{\alpha}$ ). These phase transitions occur in keeping regular structure of multi-lamellar structure and show characteristic change on X-ray diffraction pattern (Fig. 4.4). Fatty acyl chains of DPPC molecules are arranged all-trans structure in gel phase and some gauche structures appear in fluid phase. This phenomenon is melting of acyl chains of phosphatidylcholine molecules. Structural change of phase transition is observed by freeze-fractured electron microscope as jumbled structured of  $L_{\alpha}$  phase and parallel lines of  $L_{\beta'}$  phase (Fig. 4.5). Phase transition from fluid phase to hexagonal II phase in phosphatidylethanolamine liposomes by lowering temperature. Relaxation process of this phase transition is slow and long time is required to complete the transition. Phase transition of liposomes is also observed as change of density observed by dilatometer (Fig. 4.6). And phase transition from gel phase to fluid phase shows decrease of density of lipid bilayers because of extension of distance between lipid molecules and distance between lamellas. Each lipid molecular species has individual temperature of phase transition. And the temperature depends on length and degree of unsaturation of fatty acyl chains. Phase transition temperature of phosphatidylcholine changes from -7 °C of DLPC to 54 °C of DSPC. However,

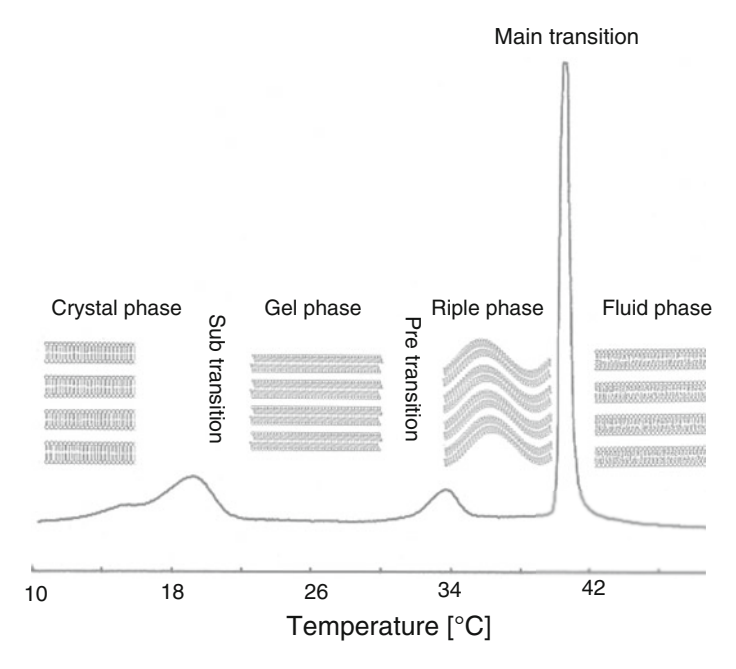
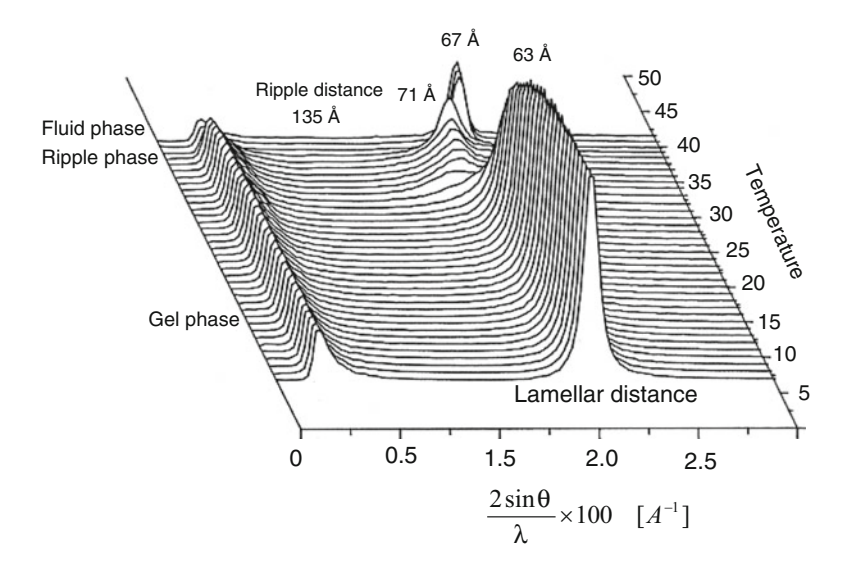


Fig. 4.3 Phase transition of lipid membrane observed by DSC Liposomes of dipalmitoyl phosphatidylcholine (DPPC) were prepared and their thermograph was observed by DSC at scanning rate of  $0.5\,^{\circ}$ C/min



**Fig. 4.4** X-ray diffraction pattern of DPPC multi-lamellar liposomes Multi-lamellar liposomes of dipalmitoyl phosphatidylcholine (DPPC) were prepared and X-ray diffraction patterns at various temperatures were measured by SOR X-ray

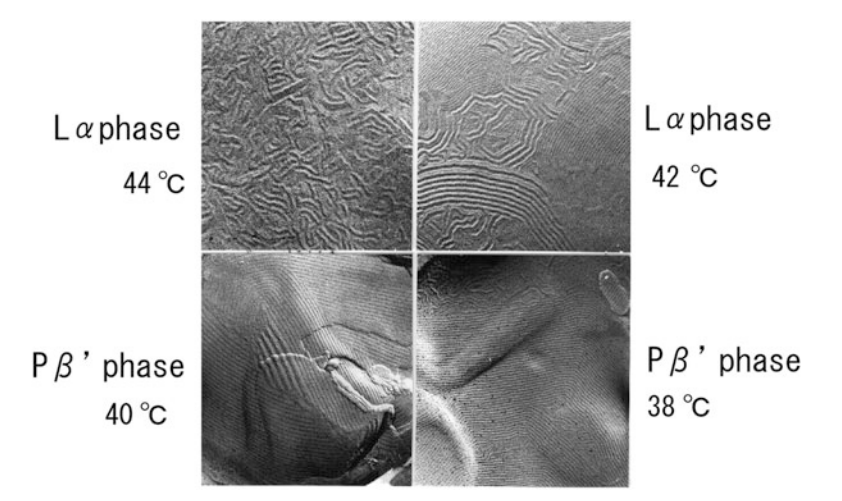
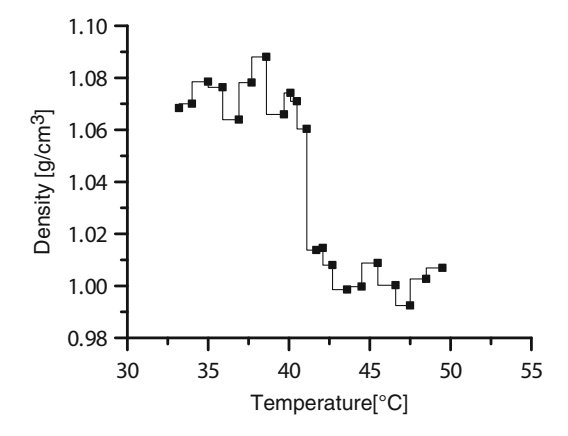


Fig. 4.5 Phase transition of DPPC multi-lamellar liposomes observed by freeze-fractured electron microscope

Multi-lamellar liposomes were prepared and freeze-fractured from different temperatures. The replicas were observed by scanning electron microscope (SEM)

Fig. 4.6 Density change in DPPC multi-lamellar liposomes Multi-lamellar liposomes of dipalmitoyl phosphatidylcholine (DPPC)were prepared and density was measured at various temperatures



phase transition temperature of phosphatidylethanolamine with same fatty acyl chains as phosphatidylcholine is higher because of smaller polar head. DPPC and DPPE have same fatty acyl chains of palmitic acid but phase transition temperatures of DPPC and DPPE are41 °C and 63 °C, respectively. Introduction of *cis* double bond expands distance between phosphatidylcholine molecules because of its kink

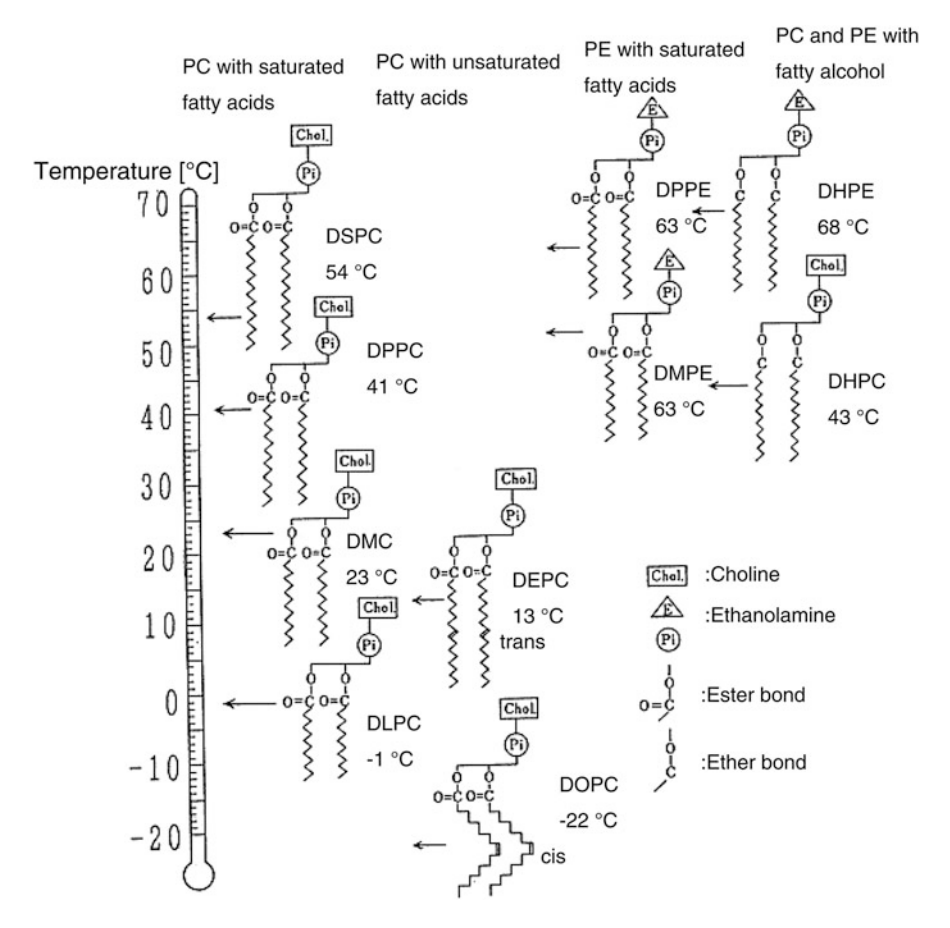


**Fig. 4.7** Structure and phase transition temperature of various phospholipids Schematic images of various phospholipids are shown with their main phase transition temperatures. There are differences of polar head, length of fatty acyl chain and unsaturated bonds among them

structure and reduces Van der Waals force between them. And phase transition temperature 54 °Cof DSPC lowers to -22 °C of DOPC (Fig. 4.7). In thermotropic induction of phase transition, structural parameter of each phase is shown in representative phospholipid, 1,2-palmitoyl-sn-glycero-3-phosphocholine (DPPC) (Table 4.1).

	Crystal phase, L <sub>c</sub>	Gel phase, L <sub>B'</sub>	Ripple phase, P <sub>6</sub>	Fluid phase, L <sub>α</sub>
Area of a lipid measured for parallel	45.8 Å at 0 °C	48.5 Å at 20 °C	г түр	64.3 Å at 50 °C
Cross-sectional area perpendicular to fatty acid	18.9 Å at 4 °C	19.6 Å at 20 °C		
Angle of fatty acid to vertical direction	34.4°	36.3°		
Thickness of lipid bilayer	48.2 Å		48.8 Å	38.3 Å at 50 °C
Repeating distance of multi-layer	39.5 Å at 0 °C	64.0 Å at 20 °C	60.0 Å	60.0 Å at 50 °C
Specific volume	0.906 ml/g	0.939 ml/g		1.011 ml/g at 50 °C
Number of water molecule per lipid	11 at 4 °C	19 at 20 °C		23.0 at 50 °C
between layers	8.6 at 0 °C	17.5 at 20 °C	1	
Volume of lipid in bilayer	1104Å <sup>3</sup> at 0 °C	1144 Å <sup>3</sup> at 20 °C		1232Å <sup>3</sup> at 50 °C

Table 4.1 Structural parameters of lipid bilayer

Structural parameter in each phase of dipalmitoylphosphatidylcholine (DPPC) is listed in the table

## 4.3 Phase Separation of Lipid Bilayer Membranes

Characteristic of phase equilibrium of two components system is shown in temperature-component phase diagram. When two components, A and B are completely miscible in both gel phase and fluid phase, single gel phase exist below solidus curve and single fluid phase exists above solidus curve. Composition in these phases does not depend on temperature but is determined by molar ratio of each component. Phase diagram of ideal solution of two components was obtained by Seltz using graphical method [11]. A. G. Lee obtained phase diagram in non-ideal mixing of two components as follows [12]. In ideal binary system, chemical potential of component A in liquid phase is shown as  $\mu_A^{ideal} = \mu_A^0 + RT \log_e x_A^{liquid}$ , and assuming two components is completely immiscible in solid phase, freezing point is obtained as  $\log_e x_A^{liquid} = \frac{\Delta H_A}{R} \left( \frac{1}{T_A} - \frac{1}{T} \right)$ . On the other hand, Gibbs free energy of chemical potential in non-ideal mixing is shown as  $\mu_A = G + (1 - x_A)$ 

 $\left[\frac{\partial G_E}{\partial x_A}\right] x_B$  and assuming  $G = G_{ideal} + G_E$ ,  $G_E$  becomes excess free energy of mixing. If two components are completely non-mixing, the following equation is obtained.

$$\ln x_A^{liquid} = \frac{\Delta H_A}{R} \left( \frac{1}{T_A} - \frac{1}{T} \right) - \frac{1}{RT} \left[ G_E + \left( 1 - x_A^{liquid} \right) \frac{\partial G_E}{\partial x_A} \right]$$

If mixing is ideal in liquid phase, same mole fraction is realized at different temperature,  $T_{ideal}$  and  $\ln x_A^{liquid} = \frac{\Delta H_A}{R} \left(\frac{1}{T_A} - \frac{1}{T_{ideal}}\right)$  is obtained. From the above two equations,  $\frac{1}{RT} \left[ G_E + \left(1 - x_A^{liquid}\right) \frac{\partial G_E}{\partial X_A} \right] = \frac{\Delta H_A}{R} \left(\frac{1}{T_{ideal}} - \frac{1}{T}\right)$  is obtained. Introducing equation,  $G_{E=\rho_0} x_A^{liquid} x_B^{liquid} = \rho_0 x_A^{liquid} \left(1 - x_A^{liquid}\right)$  as general approximation,  $\rho_0 \left(1 - x_A^{liquid}\right)^2 = \Delta H_A \left(\frac{T}{T_{ideal}} - 1\right)$  is obtained by replacing  $G_E$  in the above equation. This equation enables calculation of phase diagram by considering deviation from ideal state in liquid phase. When mixing is non-ideal in both liquid phase and solid phase, chemical potentials in solid phase and chemical potential in liquid phase are sown as follows respectively.

$$\begin{split} \mu_A^{solid} &= \nu_A^{0,solid} + RT \ln x_A^{solid} + \rho_0^{solid} \left(1 - x_A^{solid}\right)^2 \\ \mu_B^{solid} &= \nu_B^{0,solid} + RT \ln \left(1 - x_A^{solid}\right) + \rho_0^{solid} \left(x_A^{solid}\right)^2 \\ \mu_A^{liquid} &= \nu_A^{0,liquid} + RT \ln x_A^{liquid} + \rho_0^{liquid} \left(1 - x_A^{liquid}\right)^2 \\ \mu_B^{sliquid} &= \nu_B^{0,liquid} + RT \ln \left(1 - x_A^{solid}\right) + \rho_0^{sliquid} \left(x_A^{sliquid}\right)^2 \end{split}$$

The chemical potential of each phase is equal because each phase is in equilibrium state. Therefore, two equations are obtained as follows

$$\begin{split} & \ln \left( \frac{x_A^{liquid}}{x_A^{solid}} \right) + \frac{\rho_0^{liquid} \left( 1 - x_A^{liquid} \right)^2 - \rho_0^{liquid} - \rho_0^{solid} \left( 1 - x_A^{solid} \right)^2}{RT} = \frac{\Delta H_A}{R} \left( \frac{1}{T_A} - \frac{1}{T} \right) \\ & \ln \left( \frac{1 - x_A^{sliquid}}{x_A^{solid}} \right) + \frac{\rho_0^{liquid} \left( x_A^{liquid} \right)^2 - \rho_0^{lsolid} - \rho_0^{solid} \left( x_A^{solid} \right)^2}{RT} = \frac{\Delta H_B}{R} \left( \frac{1}{T_B} - \frac{1}{T} \right) \end{split}$$

Above equations are solved as simultaneous equations by introducing each value of  $T_A$ ,  $T_B$  and  $\rho_{0}$ , and phase diagram is obtained. When excess Gibbs free energy is defined as  $G_E = H_E - TS_E$ ,  $G_E = 0$ ,  $H_E = 0$  and  $S_E = 0$  indicate ideal solution, a thermal solution and regular solution, respectively According to G.M. Wilson's paper [13], ratio of probability finding B molecule to finding A molecule around

A molecule is shown as  $\frac{x_{AB}}{x_{AA}} = \frac{x_B \cdot \exp\left(-\frac{E_{AB}}{RT}\right)}{x_A \exp\left(-\frac{E_{AB}}{RT}\right)} = \frac{x_B}{x_A} \cdot \exp\left(\frac{E_{AB} - E_{AA}}{RT}\right) = \frac{x_B \nu_A}{x_A \nu_B} = F_{AB}$  where  $\nu_A$ and  $\nu_B$  are mole volume of pure A and B, respectively. According to Flory-Huggins's theory of a thermal solution [14], excess free energy is shown as  $G_E$  $=RT\sum_{i}x_{i}\cdot\ln\frac{\varphi_{i}}{x_{i}}$  where  $\varphi_{i}$  and  $x_{i}$  are volume fraction of component i and mole fraction of component i, respectively. Wilson et al. define these mole fractions by use of volume fractions  $f_A$  and  $f_B$ , and finally  $F_{AB} = 2\exp\left(-\frac{\rho_0}{4RT}\right) - 1$  at  $x_A = x_B = 1/2$ because of symmetry of the system. Degree of non-miscibility  $\rho_0$  shows probability that a molecule finds homo molecule or hetero molecule around its self [13]. Phase separation is observed in lipid membranes as correlating phenomenon of phase Dimyristoyliphosphatidylcholine dimyristoylphosphatidylethanolamine (DMPE) have same acyl carbon of myristic acid and their phase transition temperatures are 23 °C and 49 °C, respectively. Binary mixture of DMPC and DMPE shows two separated peaks on DSC thermograph (Fig. 4.8). Phase separation is a separation of regions with different physical properties, therefore the separation is observed by imaging instrument such as GP imaging microscopy. Red hinge-like regions show flexible and DMPC-rich and blue straight regions are rigid and DMPE rich (Fig. 4.9).

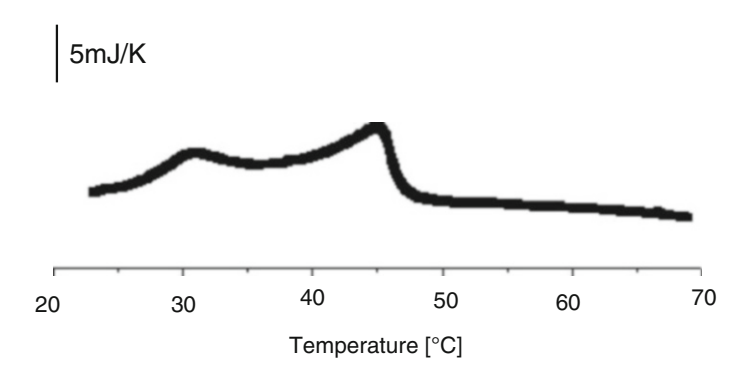


**Fig. 4.8** Phase separation of binary mixture of DMPC and DMPE observed by DSC Liposomes of binary mixture of dipalmitoylphosphatidylcholine (DMPC) and dimyristoylphosphatidylethanolamine (DMPE) were prepare by voltexing in water and its thermograph was measured by DSC

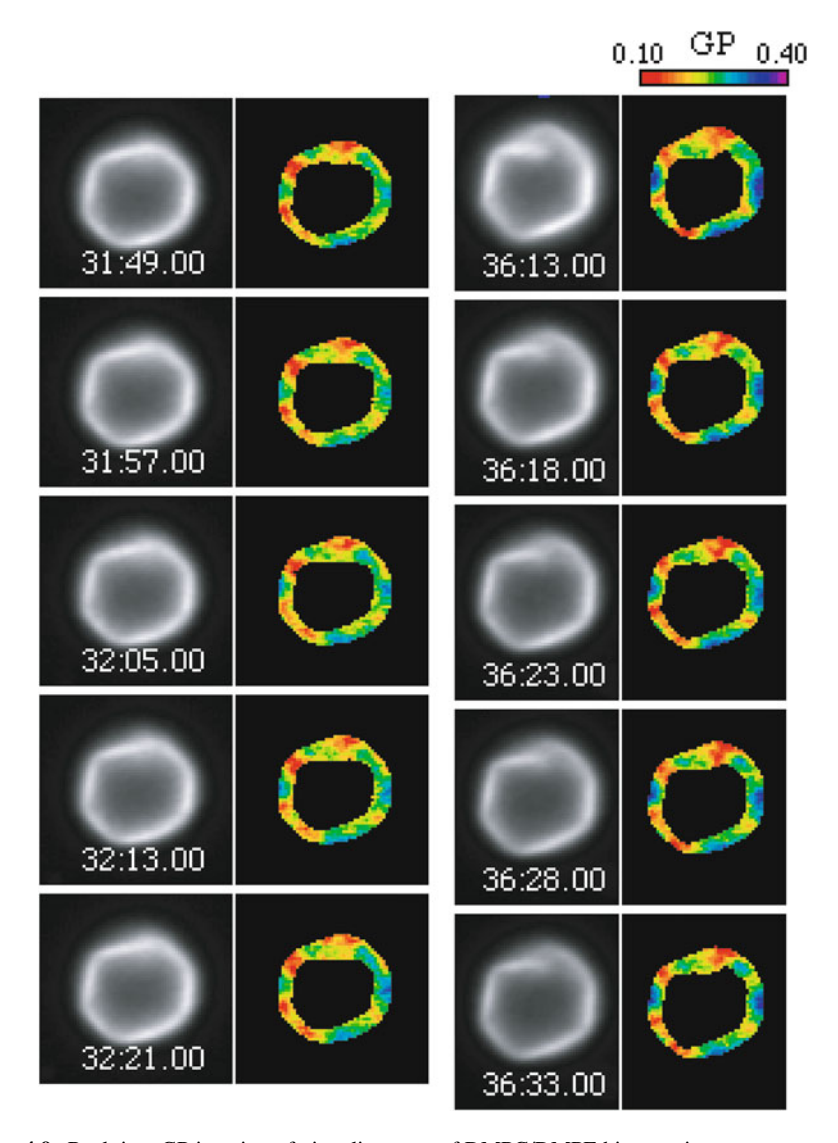


**Fig. 4.9** Real time GP imaging of giant liposome of DMPC/DMPE binary mixture Giant liposome of DMPC/DPPC (1:1) binary mixture was prepared by gentle hydration method in aqueous solution containing 2 mM CaCl2. The liposome was observed by GP imaging microscopic instrument in changing temperature

References 69

### References

- 1. S.J. Singer, G.L. Nicolson, Science 175, 720 (1972)
- 2. C. Tanford in *Physical Chemistry of Macromolecules* (Wiley, New York, 1961)
- D.L. Melchior, H.J. Morowitz, J.M. Sturtevant, T.Y. Tsong, Biochim. Biophys. Acta 219, 114 (1970)
- 4. M.H.F. Wilkins, A.E. Blaurock, D.M. Engelman, Nat. New Biol. 230, 72 (1971)
- 5. W.L. Hubbell, H.M. McConnell, J. Am. Chem. Soc. 93, 314 (1971)
- 6. R.D. Kornberg, H.M. McConnell, Biochemistry 10, 1111 (1971)
- 7. L.D. Frye, M. Edidin, J. Cell Sci. 7, 319 (1970)
- 8. P. Pinto da Silva, D. Branton, J. Cell Biol. 45, 598 (1970)
- 9. L.A. Staehelin, J. Ultrastruct. Res. 22, 326 (1968)
- 10. D.W. Deamer, R. Leonard, A. Tardieu, D. Branton, Biochim. Biophys. Acta 219(47) (1970)
- 11. H. Seltz, J. Am. Chem. Soc. 56, 307 (1934)
- 12. A.G. Lee, Biochim. Biophys. Acta 507, 433 (1978)
- 13. G.M. Wilson, J. Am. Chem. Soc. 86, 127 (1964)
- 14. P. J. Flory, J. Chem. Phys. 10, 51 (1942)

# **Chapter 5 Structure and Function of Protein**



**Abstract** Each protein is synthetized according to its genetic information of amino acid sequence on DNA and the information of amino acid sequence determines three-dimensional structure of the protein. Major functions of proteins are enzyme, receptor and immunological antibody. Enzyme is the most important in them because metabolic system of cell is chemical reactions catalyzed by network of enzymes. Protein kinase and phosphatase is important system to regulate enzyme activity as well as allosteric regulation.

### 5.1 History of Protein Study

Protein as enzyme is most important in chemical reaction system of living organisms. Various chemical reactions become possible even at 37 °C in the presence of enzymes in human beings. Catalytic function of enzyme maintains complex biological functions. 'Enzyme' was named by Buchner for his discovery of catalytic substance in extract from yeast cells in 1897. L. Pauling and R.B. Corey proposed α-helix structure of polypeptide in 1951. F. Sanger determined amino acid sequence of insulin in 1955. D. G. Smyth, W.H. Stein and S. Moore determined amino acid sequence of RNase in 1963. J. Kendrew et al. determined and constructed molecular structure model of myoglobin from sperm of whale using X-ray diffraction in 1962. R. Schwyzen chemically synthesized adrenocorticotropic hormone (ACTH, 39 amino acid residues) and H. Zahn synthesized insulin (51amino acid residues) in 1963. R.B. Merrifield synthesized RNase by solid phase peptide synthesis (124 amino acid residues) in 1969. R.N. Henderson and P.N. Urwin determined structure of membrane protein, bacteriorhodopsin using electron beam diffraction in 1975. K. Itakura et al. biosynthesized somatostatin of E. coli using chemically synthesized DNA in 1977. In membrane proteins, M. Noda et al. determined amino acid sequence of acetylcholine receptor and sodium channel in 1984. S. Yoshikawa et al. crystalized integral membrane protein, cytochrome oxidase and determined its structure by use of X-ray diffraction in 1998. Doyle et al. determined molecular structure of potassium channel by use of X-ray diffraction in 1998.

# **5.2** Determination of Three-Dimensional Structure of Proteins

Nearly one hundred thousand structures of proteins are registered in Protein Data Bank. More than 80% of the three-dimensional structures are determined by X-ray crystallography, and Nuclear Magnetic Resonance (NMR) is used for determination of protein structure in solution. Electron microscope is also used for determination of three-dimensional protein structures. X-ray diffraction method cannot determine position of hydrogen atoms and NMR method determines averaged structures in solution.

### **5.3** Basic Concept of Enzyme

Origin of enzyme is from 'in yeast' because enzyme is found in yeast as substance with catalytic function. Enzyme is protein catalyst which is synthesized by gene expression. Enzyme has substrate specificity and distinguishes optical isomers. There are at least three contact points between enzyme and substrate, which means stereospecificity of enzyme. There is affinity between enzyme and substrate, and inhibitor has affinity proportional to structural similarity to substrate, i.e. binding constant. In a cell, substrate 1 is converted to product 1 (=substrate 2). Substrate 2 is converted to product 2 (=substrate 3). These sequential reactions catalyzed by enzyme forms metabolic pathway. Enzyme is protein, and its catalytic efficiency is more than 10<sup>11</sup> -fold compared to inorganic catalyst. Chemical reactions in cells of human body is proceeded by enzymes even at 37 °C (body temperature). Catalytic function of enzyme is lowering activation energy of chemical reaction. And chemical reaction is conversion of bonding through electron. Lowering of activation energy is realized by overlap of electron orbitals. This is studied in quantum biology, but it is not always easy to analyze complex reactions catalyzed by enzyme.

## 5.4 Chemical Reaction and Kinetics of Enzyme

# 5.4.1 Chemical Reaction and Enzyme

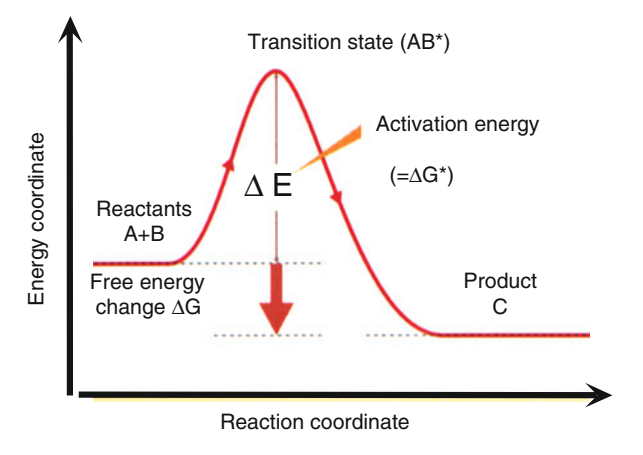
Living organism is system of regulated chemical reactions and enzyme catalyzing chemical reaction should be mentioned for discussion of biological functions. Chemical reaction that molecule A reacts with molecule B and generate molecule C is explained by collision theory.

$$A + B \underset{v_{-1}}{\leftarrow} \underset{v_{+1}}{\rightarrow} C$$

Chemical reaction requires collision of molecules. Frequency of collision is proportional to kinetic energy and molecular concentration. Pair of A and B must overcome activation energy to be converted to C. At molecular level, chemical reaction is reversible, and finally becomes equilibrium state in isolated system (Fig. 5.1). Velocity of association reaction,  $v_{+1}$  and velocity of dissociation reaction, velocity of association and velocity of dissociation are shown as follows.  $v_{+1} = k_{+1}[A][B]$ ,  $v_{-1} = k_{-1}[C]$  where  $k_{+1}$  and  $k_{-1}$  are rate constants. These equations must be verified empirically. And condition of equilibrium becomes  $v_{+1} = v_{-1}$ . And following equations are obtained.

 $k_{+1}[A][B] = k_{-1}[C], \frac{k_{+1}}{k_{-1}} \frac{[C]}{|A||B|} = K_{eq}$  where  $K_{eq}$  is equilibrium constant. Relationship between change of standard free energy and equilibrium constant is shown by following equation  $\Delta G_0 = -RT \cdot \log K_{eq}$ . Temperature dependency of chemical reaction is shown by Arrhenius's equation as follows.  $\frac{d \ln k}{dT} = \frac{E_a}{RT^2}$  or  $k = A \cdot \exp$  $\left(-\frac{E_a}{RT}\right)$  where  $E_a$ , A, R and T are activation energy, frequency factor, gas constant and absolute temperature, respectively. Within narrow region of temperature,  $E_a$  could be considered as constant of approximate activation energy. And this is verified by linear relation of  $\ln k$  vs  $\frac{1}{T}$ . Relationship between reaction velocity and activation energy is explained by Eyring's transition state theory as follows. Active complex, (AB)\* is introduced and reaction mechanism  $A + B \leftrightarrow (AB) * \rightarrow C$  is assumed. As energy decreases simply in process of  $(AB) * \rightarrow C, v = k^*[(AB)*] = k^*K^*[A][B]$  is obtained. Activated complex, (AB)\* is almost equilibrated with 'A + B' and  $\frac{[(AB)^*]}{[A|B]} = K^*$  is obtained. Therefore  $v = k^*[(AB)*] = k^*K^*[A][B]$  is obtained. And rate constant, k becomes  $k = k^*K^*$ . Then  $K^* = \exp\left(-\frac{\Delta G^*}{RT}\right)$  because of  $\Delta G^* = -RT \ln K^*$ , and  $k = k^* \exp\left(-\frac{\Delta G^*}{RT}\right)$  because of  $\Delta G^* = \Delta H^* - T\Delta S^*$ . The equation of rate constant k means product C generated by reaction between A and B depends on the activation energy,  $\Delta G^*$ . Therefore activation energy determines velocity of reaction and role of

Fig. 5.1 Chemical reaction and activation energy Ratio of products to reactants is determined by change of free energy in equilibrium state. And rate of chemical reaction is determined by activation energy. Catalytic effect of enzyme reduces activation energy and accelerates rate of chemical reaction



enzyme protein which lowers activation energy for accelerating chemical reaction. Distribution among A, B and (AB)\* in equilibrium is determined by change of Gibbs free energy and enzyme does not affect the distribution.

### 5.4.2 Kinetics of Reactions Mediated by Enzyme

Michaelis and Menten proposed kinetics to understand enzyme's reaction from experimental result of hydrolysis of sucrose by invertase [1]. Following conditions are described in the kinetics. Reaction velocity is proportional to enzyme concentration at constant substrate concentration. At constant enzyme concentration, reaction velocity is proportional to substrate concentration during low substrate concentration and the velocity is gradually saturated in higher substrate concentration, and to constant velocity. They introduced reaction mechanism by assuming that intermediate complex (ES) is in equilibrium state with enzyme (E) + product (P) and there is no reverse reaction from ES at initial state where rate constant is k.

$$E + S \underset{k_{-1}}{\leftarrow} \underset{k_{+1}}{\rightarrow} ES \underset{k_{+2}}{\rightarrow} E + P$$

From equilibrium condition, Michaelis constant (equilibrium constant) is shown as following equation.

$$\frac{[E][S]}{[ES]} = \frac{k_{-1}}{k_{+1}} = K_m$$

When condition of  $[S] \gg [E]_0$ , substrate concentration can be replaced with equation,  $[S] = [S]_0 - [ES] = [S]_0$ , and Michaelis constant becomes following equation.

 $\frac{[E]_0 - [ES]}{[S]}[ES] = K_m \text{ and this equation is converted to } [ES] = \frac{[E]_0[S]}{K_m + [S]}, \text{ then reaction velocity to generate product is shown as following equation.}$ 

 $v=k_{+2}[ES]=rac{k_{+2}[E]_0[S]}{K_m+[S]}$  And  $v=rac{V_{\max}[S]}{K_m+[S]}$ .  $V_{max}$  is the maximum velocity of the chemical reaction mediated by enzyme showing catalytic efficiency of enzyme. Michaelis constant  $K_m$  shows affinity of enzyme to substrate. Smaller value of  $K_m$  means higher affinity.

On the other hand, Briggs and Haldane assume different condition in reaction mechanism mediated by enzyme. Concentration of intermediate complex is in equilibrium state and there is no reverse reaction from E + P to ES at initial state. And reaction mechanism is shown as following equation [2].

$$E + S \underset{k_{-1}}{\leftarrow} \underset{k_{+1}}{\rightarrow} ES \underset{k_{+3}}{\rightarrow} E + P$$

In this theory of kinetics, stationary state of intermediate complex, [ES] is assumed. Therefore  $k_{+1}[ES] - (k_{-1} + k_{+2})[ES] = 0$  and  $[ES] = \frac{[E]_0}{K_m + [S]}$  is obtained by replaced by  $[E] = [E]_0$ -[ES]. Finally,  $v = k_{+2}[ES] = \frac{k_{+2}[E]_0[S]}{K_m + [S]} = \frac{V_{\text{max}}[S]}{K_m + [S]}$  is obtained.

### 5.5 Regulation of Enzyme Activity

Cell, essential unit of life, provides regulation mechanism to maintain homeostasis. And system of chemical reaction in cell is composed of enormous number of enzymes. Therefore, maintaining homeostasis is mainly due to regulation of enzymes.

### 5.5.1 Control of Enzyme Amount

Amount of enzyme is controlled to keep balance between synthesis and degradation, and control of synthesis is due to operon mechanism. Parade et al. suggested existence of repressor in 1959, and F. Jacob J. Monod proposed operon theory in 1961 [3]. Operon theory was proposed as lactose operon in prokaryote, *E.Coli*. And study of operon is extended to study of promoter including regulation mechanism of eukaryotes. Processing of mRNA is also studied in prokaryotes. On the other hand, regulation by degradation of enzymes is studied for various proteases such as Ca<sup>2+</sup>-dependent protease.

## 5.5.2 Control of Enzyme Activity

There is feedback inhibition that final product in metabolic pathway suppresses an activity of enzyme locating on preceding pathway. There are two types of control mechanism using nucleotide. Nucleotide-1-phosphate is bound on enzyme in bacteria or phosphate moiety is transferred from ATP to OH group of specific amino acid such as serine, threonine and tyrosine in enzyme of eukaryote by protein kinase. And these modifications of enzyme induce conformational change of enzyme and results in regulation of enzyme activity. Regulation by protein kinase is also important mechanism for regulation of functional protein. And the bound phosphate is dissociated by phosphatase to recover the activity to original state. Protein kinase was found by Burnett and Kennedy in 1954. They found protein kinase activity of phosphorylation of casein in rat liver in 1954. There are other protein kinases such as cyclic AMP dependent protein kinase, cyclic GMP dependent protein kinase, Ca<sup>2+</sup> dependent protein kinase and double strand RNA dependent protein kinase.

### 5.5.3 Allosteric Regulation of Enzyme Activity

In allosteric enzyme, there is binding site of activator or inhibitor apart from active site of enzyme. The binding of one of these effectors affect activity of enzyme through conformational change of enzyme. Allosteric enzyme is composed of subunits. Theoretical study of allosteric enzyme was studied in hemoglobin of red blood cell. And two theories were proposed by Monod et al. [4] and Koshland et al. [5], respectively. When activator binds allosteric site apart from catalytic site, substrate binds easier by conformational change of the enzyme. On the other hand, binding of inhibitor on allosteric site makes substrate to be difficult to bind catalytic site. There are relaxing state and taut state in subunits of allosteric protein. R-state is stable when substrate or ligand binds allosteric protein, and T-state is stable during no binding. Monod et al. assume that all subunits change from T-state to R-state cooperatively by binding of substrate. On the other hand, Koshland et al. assume that change from T-state from R-state occurs sequentially for each subunit by binding of substrate. Characteristic of allosteric enzyme is shown by Hill equation. The kinetics equation of allosteric enzyme shows sigmoid curve on graph. Degree of sigmoid curve depends on value of 'n'.

$$v = \frac{V_{\max}[S]^n}{K_m + [S]^n} \quad (n > 1)$$

# 5.6 Interaction Between Protein and Lipid

# 5.6.1 Peripheral Enzyme and Integral Enzyme

Major components of biomembrane are proteins and lipids, and interaction between protein and lipid is a key factor for structural formation, function and regulation of biomembranes. In the fluid mosaic membrane model proposed by Singer and Nicolson [6], membrane proteins are classified into peripheral proteins and integral proteins. The formers are bound by electrostatic interaction and release from the membrane by raising ionic strength. Cytochrome c is an example of peripheral membrane proteins. Calcium ion is an important divalent cation and it crosslinks between anions for binding anionic protein to anionic surface of membrane. These proteins are released from membrane by chelating reagent such as ethylene diamine tetra acetic acid (EDTA). The integral proteins are bound by hydrophobic interaction and solubilized by addition of detergent such as sodium dodecylsulphate (SDS). Cytochrome oxidase of mitochondria inner membrane is an example of integral membrane proteins. ESR measurement using a spin probe, 16-doxylstearic acid has revealed existence of annular lipids interacting with the membrane protein strongly [7]. Assuming size of the protein as parallelepipedon of 52 Å×60 Å, and peripheral

length, 244 angstroms divided by diameter, 4.8 Å of 2 fatty acyl chains gives 47. The result means 47 molecules of phospholipid existing on the first layer around cytochrome c. This estimation shows 0.17 mg of phospholipid for 1 mg of protein, and there is good agreement to experimental result, 0.2 mg of phospholipid. Crystallization was succeeded and detailed information of protein structure was obtained by X-ray diffraction study [8]. This study promotes elucidation of electron transport mechanism to oxygen. Co-crystallization of protein with lipid assembly in cubic phase is applied to bacteriorhodopsin, and relationship between formation of cubic phase and absorption spectrum of bacteriorhodopsin [9]. An idea is proposed that lipids preferring cubic phase (non-bilayer structure) makes lateral pressure and stabilize membrane structure and express function [10]. Interaction between protein (or peptide) and lipid membranes was investigated by DSC measurement. Three types of interactions were appeared on DSC thermographs [11]. First type is water soluble protein bound to surface of lipid membrane by electro static interaction. Second one is hydrophobic protein interacted with lipid membrane by hydrophobic interaction. Third type is medium of the former two types, and interacting lipid membranes electro statically and hydrophobically. Hydrophobic effect between hydrophobic acyl chains and hydrophobic region of protein is major force for constructing biomembrane, and this interaction is studied theoretically by Owicki et al. [12, 13]. This is consideration of effect of protein on physical property of phase transition between gel phase and fluid phase. Using exclusive area of a molecule in gel phase,  $A_s$  and in fluid phase,  $A_f$  order parameter for excusive area of molecule A is defined as follows.  $u \equiv \frac{A_f - A_r}{A_r - A_r}$  And free energy G is obtained as follows from theories of Landau [9] and de Gennes [14].  $G = \frac{T}{2}u^2 - u^3 + \frac{u^4}{2} + \frac{|u|^2}{2}$  where T is phase transition temperature expressed by reduced temperature, set to 1. u is obtained for distribution of proteins in membrane plane by variation method using following equation.  $\iint |u(r), |\Delta u(r)| |dr^2 r = \min$ 

Integration is performed under boundary condition,  $u=u_0$  at interface between lipids and proteins. This means both hydrophobic regions in lipid and protein is adjusted to fit each other. Mouritsen and Bloom considered theoretically in focusing on the adjustment [15]. This is thermodynamical consideration of insertion state of elastic protein into elastic lipid membrane.

# 5.6.2 Synthesis of Membrane Protein and Signal Peptide

Membrane protein is synthesized in rough ribosome and transferred to target site through Golgi apparatus by membrane traffic system. Leader peptide (signal peptide) is firstly biosynthesized in ribosome, and the peptide determines destination of the protein. When leader sequence appears in biosynthesis, signal recognition particle recognizes the sequence and synthesis stops temporally. This complex is

bound by docking protein on ribosome. And stop of synthesis is released. Then the protein is traversed lipid bilayer membrane and leader sequence is cut by signal peptidase and sugar chain is added [16].

### 5.6.3 Study of Interaction in Membrane Model System

Mattress model is proposed in focusing matching between hydrophobic regions of protein and lipid membrane. Supporting experiments for mattress model is shown as follows. Figure 5.2 shows preferential interaction between bee venom, melittin and dimyristoylphosphatidylcholine in membranes prepared by binary mixture of dimyristoylphosphatidylcholine (DMPC) and distearoylphosphatidylcholine (DSPC) by use of DSC. DSC thermograph of the binary mixture shows peak from DMPC rich region and peak from DSPC rich region without melittin. And peak from DMPC rich region is disappeared by addition of 1 mol% melittin. The results indicate that bee venom peptide, melittin composed 26 amino acids including hydrophobic region interact with hydrophobic core in lipid membrane of DMPC rich region of the binary mixture of DMPC and DSPC because size of hydrophobic regions of melittin and DMPC match each other. Figure 5.3 shows reconstruction of

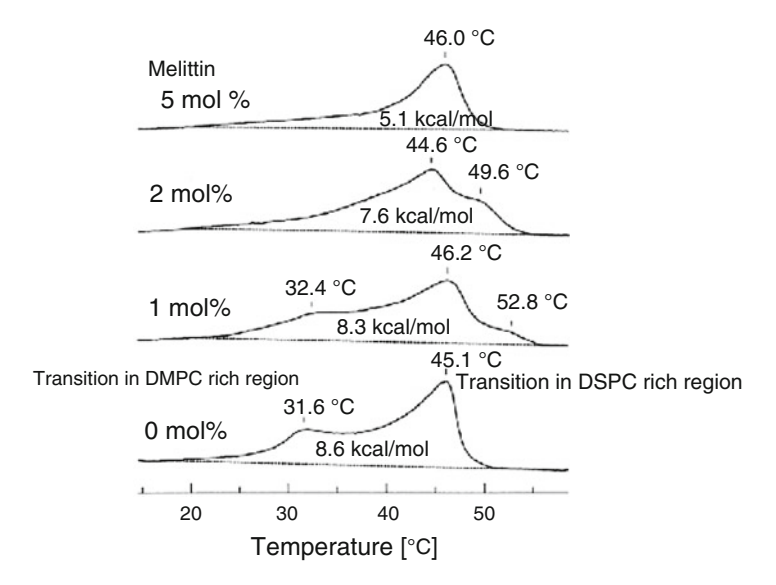


**Fig. 5.2** Preferential interaction of melittin in binary mixture of DMPC/DSPC Liposomes of binary mixtures composed of dimyristoyl phosphaticylcholine (DMPC, C14:0) and distearoyl phosphatidylcholine (DSPC, C18:0) were prepared and thermograph was measured by DSC. Melittin, bee venom peptide preferentially reduced peak from DMPC rich region in concentration dependent manner

References 79

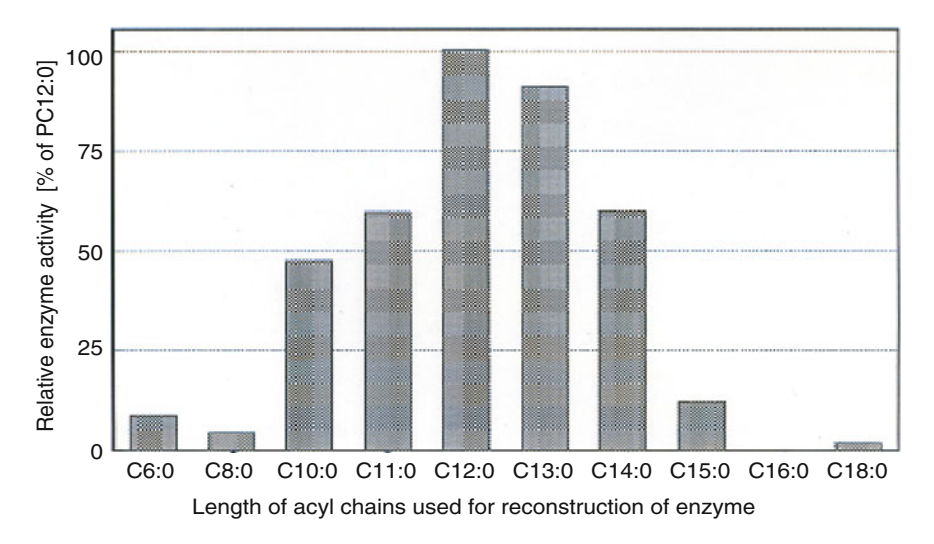


**Fig. 5.3** Enzyme activities of UDP-glucose: ceramide glucose transferase UDP-glucose: ceramide glucose transferase was reconstructed in phosphatidylcholine with different lengths of fatty acyl chains. And the enzyme activity was measured. Optimum length of fatty acyl chain existed for the activity

GDP-glucose: ceramide transferase into different thicknesses of lipid membranes and the enzyme activities of those cases. Different phosphatidylcholines with saturated fatty acyl chains from 15 carbons to 18 carbons are used for different thicknesses of lipid bilayer membranes. And the maximum activity obtained when the enzyme is reconstructed in dimyristoylphosphatidylcholine (12 carbons fatty acid), which means the enzyme takes optimum configuration in interaction with dimyristoylphosphatidylcholine.

### References

- 1. L. Michaelis, M. Menten, Biochem. Z. 49, 333 (1913)
- 2. E. Briggs, J.B.S. Haldane, Biochem. J. 19 (1925), 338(1925)
- 3. Jacob, J. Monod, J. Mol. Biol. 3, 318 (1961)
- 4. J. Monod, J. Wyman, J.P. Changeux, Mol. Biol. 12, 88 (1965)
- 5. D.E. Koshland Jr., G. Nemethy, D. Filmer, Biochemistry 5, 365 (1966)
- 6. S.J. Singer, G.L. Nicolson, Science 175, 720 (1972)
- P.C. Jost, O.H. Griffith, R.A. Capaldi, G. Vanderkooi, Proc. Natl. Acad. Sci. USA 70, 480 (1973)
- 8. T. Tsukihara, T.H. Aoyama, E. Yamaashita, T. Tomizaki, H. Yamaguchi, H.K. Shinzawa-Itoh, R. Nakahima, R. Yaono, S. Yoshikawa, Science **269**, 1069 (1995)
- 9. E.M. Landau, J.P. Rosenbusch, Proc. Natl. Acad. Sci. USA 93, 14532 (1996)
- 10. B. de Kruijff, Nature **386**, 129 (1977)
- 11. R.N. McElhaney, Biochim. Biophys. Acta **864**, 361 (1986)

- 12. J.C. Owicki, M.W. Springgate, H.M. McConnell, Proc. Natl. Acad. Sci. USA 75, 1616 (1978)
- 13. J.C. Owicki, H.M. McConnell, Proc. Natl. Acad. Sci. USA 76, 4750 (1979)
- 14. P.G. de Gennes, *The Physics of Liquid Crystals* (Oxford University Press, Oxford, 1974)
- 15. O.G. Mouritsen, M. Bloom, Biophys. J. 46, 141 (1987)
- 16. P. Walter, R. Gilmore, G. Blobel, Cell 38, 5 (1984)

# Chapter 6 Physical Properties of Biomembranes and Cellular Functions



Abstract Membrane lipids such as phospholipids, glycolipids and sterols form lipid bilayer membranes spontaneously in water, and insertion and binding of proteins result in construction of biomembranes. Membrane proteins are surrounded by lipid molecules, and structure and physical properties of lipid membrane regulate function and activity of protein through interaction between lipids and proteins. Biological functions on biomembranes utilize physical property of lipid bilayer membranes. Molecular collision for chemical reaction is controlled by membrane fluidity which depends on lipid species of different structures such as length and unsaturation. Special regions for signaling system on cell membrane are formed by phase separation. Membrane lipid preferring non -bilayer forming is closely related to membrane fusion.

# **6.1 Diffusion Controlled Process by Fluidity** of Biomembranes

Living organism on the earth is a system of regulated chemical reactions, and collision of molecules is essential for chemical reaction. And diffusion of molecules is major factor for collision frequency. Membrane proteins in biomembranes move in lateral diffusion, and lateral diffusion is measured by such as fluorescence photo bleaching recovery (FPR) [1].

When chemical reaction A + B  $\rightarrow$  C is considered, collision theory requires collision of A molecule and B molecule for chemical reaction of generating product, C. Collision frequency is proportional to kinetic energy and activation energy overcoming energy barrier. And proportional coefficient is shown as where  $k_b$  and [C] are diffusion-controlled bimolecular constant and concentration of molecule, C. All collisions not always proceed to generation of product, C. Therefore, rate constant is shown as  $k_q = \gamma k_b$  where  $\gamma$  is reaction efficiency. And Smolucowski equation is shown as follows.

 $k_b = \frac{9\pi N_A}{100} (R_f + R_q) (D_f + D_q)$  where  $N_A$ ,  $R_f$ ,  $R_q$ ,  $D_f$  and  $D_r$  are Avogadro's number, radius of colliding and collided molecules, diffusion constant of colliding

and collided molecules, respectively. On the other hand, diffusion constant, D is shown by Stokes-Einstein equation as follows.  $D = \frac{kT}{6\pi nR}$  where k and  $\eta$  are Boltzmann constant and solvent viscosity, respectively. Therefore, chemical reaction depends on viscosity of solvent, temperature, size of molecules in addition to concentration of molecules. Biomembrane is dynamic structure and molecular components of it show rotational diffusion and lateral diffusion. Receptor on biomembrane surface binds ligand to make conformational change and diffuses to bind effector protein for transmitting received signal to enzymic signaling system. This diffusion process depends on fluidity (viscosity) of lipid bilayer membrane. And it was shown in adrenalin-induced activation of glycolysis system. In this system, energy supply is promoted through activation of glycolysis when adrenalin receptor binds adrenalin. The complex of adrenalin-adrenalin receptor collides with adenylate cyclase through G-protein. Adenylate cyclase raises level of cyclic AMP (cAMP) in the cell to regulate enzyme activity. Relationship between collision frequency and lateral diffusion rate on biomembranes was analyzed from fluidity change of the biomembranes in reaction system as follows.  $HR + E \xrightarrow[k]{} (HRE) \rightarrow HR$ +E' where HR, E and E' are receptor binding hormone, enzyme and activated enzyme, respectively. HR and E collide with rate constant  $k_b$  in red blood cell of turkey. Membrane fluidity of the blood cells was changed by addition of cis-vaccenic acid. And viscosity at 25 °C was lowered from 6 poise to 4 poise and corresponding diffusion constant of  $\beta$ -adrenalin receptor increased from  $4.0 \times 10^{-11}$  cm<sup>2</sup>/sec to  $9.0 \times 10^{-10}$  cm<sup>2</sup> /sec [2]. Velocity of diffusion-controlled process between substrate and enzyme in stationary state on two-dimensional space is shown as following equation.  $v = \frac{[substrate][enzyme]N_A}{4\pi D_{S,E}} \ln\left(\frac{\pi}{4}[Enzyme]N_A\right)^{\frac{1}{2}\frac{1}{a}}$  where  $N_A$ ,  $D_{S,E}$  and a are Avogadro's number, relative diffusion coefficient and length of active part, respectively. Chemical reaction between substrate and enzyme is bimolecular reaction and velocity is shown as  $v = k_b[E][R_T]$  where [E] and [R\_T] are concentration of adenylate cyclase and whole concentration of receptor, respectively.  $v = k_{observed} = [E]$  is obtained from constant concentration of receptor. And  $v_{observed} = N_A 4\pi R_T \left[ ln\pi \left[ R_T N_A \right]_a^{\frac{1}{2}} \frac{c}{a} \cdot \frac{c}{\eta} \right]$  is obtained from  $D = \frac{kT}{6\pi} = \frac{c}{\eta}$ , therefore specific activity of adenylate cyclase becomes zero at 6.1 poise of membrane viscosity. This result indicates that  $k_{observed}$  depends on  $\eta$  and that the activation of adenylate cyclase is diffusion-controlled process.

# 6.2 Phase Separation of Biomembranes and Biological Functions of Cell

Biomembranes are a key area for biological functions. One of major components of biomembranes, lipid molecules show phase separation correlated with phase transition. Phase transition observed in temperature acclimation of cells regulates function of proteins through varicosity (fluidity) of lipid membranes. On the other hand, it is considered that phase separation affects functions of proteins by making

heterogeneous regions on biomembranes. Phase separation in lipid bilayer membranes was first observed as Ca2<sup>+</sup>-induced phase separation of acidic phospholipid by phospholipid spin probe [3] and then phase separation of acidic phospholipid by basic protein was also observed [4]. Phase separations in lipid bilayer membranes were observed in various systems such as proton-induced phase separation [5], ternary lipid system containing phosphatidic acid [6] and diacylglycerol promoting Ca<sup>2+</sup>-induced phase in lipid bilayers mimicked for cellular signaling [7].

## 6.3 Micro Domain of Biomembranes (Lipid Raft)

Biological functions of biomembranes are directly responsible for proteins, products of genetic information, but interaction between lipids and proteins is essential for the function because most of membrane proteins require lipid for their function. Physical properties of lipid membranes such as membrane fluidity, phase transition and phase separation participate in regulation of the function through interaction between lipid and membrane protein. A cell has various functions in micro regions and the heterogeneous regions of biomembranes play key role for realizing the functions. Membrane fractions insoluble in detergent were found in cell membrane, and they were named lipid rafts from an image of 'raft' in sea of lipid bilayers. Raft is a region, rich in sphingolipids and cholesterol [8] and proteins related to cell signaling were gathered [9] and cholesterol play a key role for formation of liquid-ordered phase [10]. The reported phase separated region of liquid ordered phase [10] is recognized as closely related to formation of raft. Schematic image of lipid raft is shown in Fig. 6.1. In an experiment for examining preferential interaction of cholesterol with various phospholipids, selectivity of cholesterol to various phospholipids was reported as partition coefficient for each phospholipid [11]. Interaction between cholesterol and sphingomyelin was investigated at each atom of these molecules by NMR and specific strong interaction was not found between these molecules

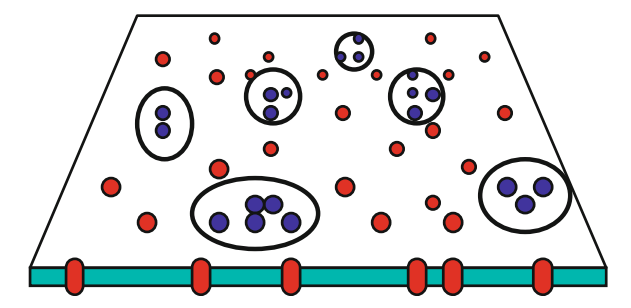


Fig. 6.1 Lipid raft as micro domain in biomembranes

Raft is a micro domain as phase separated liquid-ordered phase composed by interaction of cholesterol with sphingolipids in biomembranes. Proteins related to signaling of cell are assembled in the micro domain. Violet circles of signaling proteins are gathered into large circles of micro domains (raft)

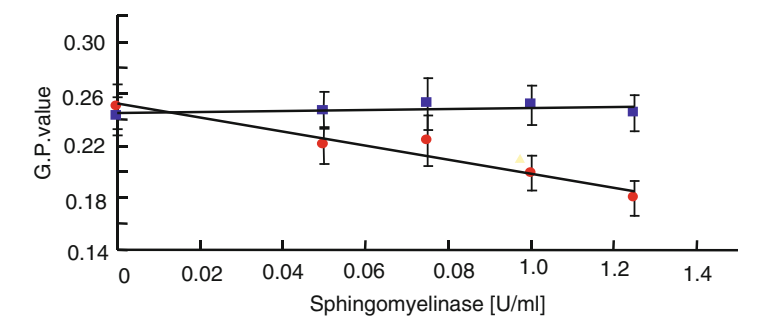


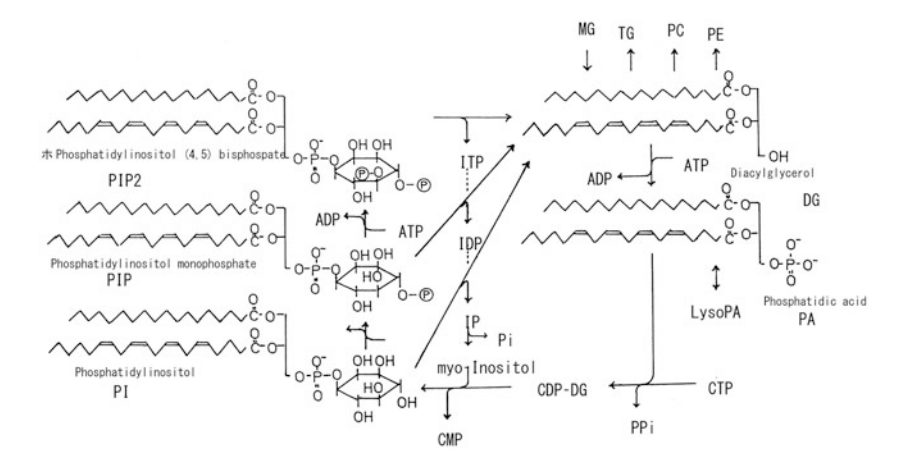
Fig. 6.2 Change of G.P. value by conversion of sphingomyelin to ceramide by sphingomyelinase in living CHO cells

Decrease of G,P, value was observed in sequential treatment of living CHO cells. The cells were treated with 1 mM  $\beta$ -cyclodextrin for 30 min at 37 °C after treatment of various concentrations of sphingomyelinase for 10 min at 37 °C. Decrease of G.P. value in sphingomyelinase concentration dependent manner, which supposed to increase membrane fluidity because of removal of cholesterol from the cell membrane

[12]. On the other hand, preferential interaction between cholesterol and sphingomyelin was investigated in living CHO cells using environment sensitive fluorescence dye, laurdan. Effect of cholesterol on biomembranes is lowering membrane fluidity, which is used for detecting preferential interaction between cholesterol and sphingomyelin. When sphingomyelin molecules in CHO cells were converted to ceramide by sphingomyelinase treatment, G.P. value of laurdan in the cell membranes decreased by successive treatment by  $\beta$ -cyclodextrin. The result suggests that cholesterol molecules removed from cell membranes by β-cyclodextrin because of no specific interaction between cholesterol and ceramide. And The lowering G.P. value was observed in concentration dependent fashion of β-cyclodextrin shown in Fig. 6.2 [13]. The preferential interaction between cholesterol and sphingomyelin was observed in giant liposome of artificial membrane system under G.P. imaging microscopic instrument. Disappearance of micro domain of liquid-ordered phase was observed in this experiment, which also suggested strong interaction between cholesterol and sphingomyelin [14]. Mechanism of gathering specific protein related to signaling into raft is still unclear, and possibility of matching between hydrophobic regions of lipid membrane and membrane protein is examined as a candidate of the gathering mechanism [15].

# 6.4 Conversion of Membrane Lipid with Receiving Stimulus and Functions of a Cell

A lot of number of cells composing multi-cellular organism are concerted by both neural and hormonal control systems to integrate individual living organism. Control factors such as neurotransmitter and hormone are bound by receptor on cell surface, and its stimulus is transferred to each corresponding functional protein through G protein. A series of cellular signaling process is affected by structure and physical property of lipid membrane. Major components of membrane, phospholipids are phosphatidylcholine, phosphatidylethanolamine, phosphatidylserine, phosphatidylinositol, phosphatidic acid. In metabolic pathway of biosynthesis for phospholipids, phosphatidic acid is synthesized from fatty acyl-CoA and glycerol phosphate, and it is converted to diacylglycerol, a start molecule for synthesis of phospholipid. Synthetic reaction is generally chemical reaction with positive change of standard free energy, and nucleotide triphosphate such as ATP, CTP, GTP and UTP is required to couple with synthetic reaction for supplying energy by its hydrolysis of negative change of standard free energy. And nucleotide triphosphate is also used for activation of binding site. In one pathway of phospholipid biosynthesis, diacylglycerol (DG) is activated by CTP and CDP-diacylglycerol is generated. In another pathway, polar base is activated by CTP to generate CDP-polar base and then it binds to diacylglycerol to generate CDP-diacylglycerol. Phosphatidylinositol (PI) is synthesized in former pathway. Phosphatidylcholine (PC) and phosphatidylethanolamine (PE) are synthesized in latter pathway. Phosphatidylserine (PS) is synthesized from PE by exchange reaction with minor change of standard free energy. These biosynthetic pathways are shown in Fig. 6.3). On the other hand, hydrolysis of phospholipids is mediated by phospholipases such as phospholipase A, phospholipase C and phospholipase D. These chemical reactions proceed with negative change of standard free energy. These enzymes are activated when a cell receives stimulus, and rapid conversion of lipid is observed. Phospholipase A releases fatty acid from phospholipid and the released arachidonic acid becomes substrate for generation of prostaglandin, leukotriene, and thromboxane and so on. And these molecules regulate functions of cell. Phospholipase C generates diacylglycerol from phosphatidylinositol as substrate, and the diacylglycerol as second messenger activates protein kinase C. And phospholipase D generates phosphatidic acid from mainly phosphatidylcholine as substrate, and the phosphatidic acid induces proliferation of cell. Regulation of physiological function of cell is performed by transfer of phosphate moiety of ATP to protein, i.e. phosphorylation of protein. Energy of ATP is used in phosphorylation process. For example, some species of protein kinases are activated sequentially in cycle of cell division, and proliferation and differentiation of cell are also regulated by protein kinase. And malfunction of this mechanism is supposed to induce cancer cell from study of oncogene. Malfunction of protein kinase C is a candidate of canceration of cell. Phosphatidylserine, calcium ion and diacylglycerol are required for activation of protein kinase C [16]. Protein kinase C in cytoplasm was bound to plasma membrane when cell received a specific stimulus [17], and calcium ion was required for binding of protein kinase C [18]. Diacylglycerol of neutral lipid generated from negatively charged phosphatidylinositol was supposed to promote calcium ion-induced phase separation of phosphatidylserine in signaling of cell because of the phase separation in signaling -mimicking artificial membrane system [19]. Stimulus received by receptor raised concentration of calcium ion from 0.2 µM to 0.6 µM in liver cell [20], and promotion of phase separation of phosphatidylserine by diacylglycerol was also



Diacylglycerol (DG) and inositol triphosphate (ITP) were generated from phosphatidylinositol bisphosphate (PIP2) in phosphatidylinositol cycle in metabolic conversion of biomembrane lipids. DG activates protein kinase C and ITP releases calcium ions from macrodomes.

**Fig. 6.3** Metabolic conversion of membrane lipids Phosphatidylinositol cycle in a cell is shown. Diacylglycerol (DG) and inositol triphosphate (ITP) are generated from phosphatidylinositol bisphosphate (PIP2) in phosphatidylinositol cycle in metabolic conversion of biomembrane lipids. DG activates protein kinase C and ITP releases calcium ions from microsomes

shown within the concentration change of calcium ion in artificial membrane system. Protein kinase C has hydrophobic region in its structure, but it exists in cytoplasm in resting state, and binds to plasma membrane in calcium concentration dependent manner by stimulation through receptor. Protein kinase C was partially purified from neutrophil of leucocyte and cell membranes of the neutrophil were incubated at various concentrations of calcium ion, and then the membrane fraction and supernatant was separated by centrifugation. And distribution of the protein kinase C was investigated after removal of calcium ions by EDTA and activation by Triton X-100. The result showed that the protein kinase C bound to the cell membranes at a few µM of calcium ion [20]. Relationship between surface pressure of monolayer and binding of protein kinase C to the monolayer was investigated at the presence of calcium ion at various surface pressures. The protein kinase C penetrated the monolayer only in the presence of calcium ion when the surface pressure was more than 26 dyn/cm, but the protein kinase C bound to the monolayer below 26 dyn/cm in the absence of calcium ion. However, the protein kinase C did not bind to the monolayer at concentration of calcium ion more than 43 dyn/cm even in the presence of calcium ion [21]. From the results shown above, electrostatic and hydrophobic interactions for role of protein kinase C in the signaling system are supposed as follows. Base sequence of cDNA including 672 amino acid sequences was elucidated in protein kinase C [22]. Protein kinas C has amino acids sequence of Arg19-Phe-Ala-Arg-Lys-Gly-Ala25-Leu-Arg-Gln-Lys-Asn-Val-His-Glu-Val-Lys-Asn and these amino acids bind to active site of protein kinase C to inhibit its activity as pseudo-substrate [23, 24]. When cell is activated in signaling process, free protein kinase C of inactive form is bound to plasma membrane and then active site of protein kinase C is opened by conformational change of protein kinase C [25]. Calcium ions and phospholipids play important roles in the activating mechanism of protein kinase C. Negatively charged phosphatidylserine is hydrated in aqueous environment. The hydrated water molecule is replaced by calcium ion when calcium ion is added, and surface of phosphatidylserine becomes hydrophobic. This change may be important for interaction between lipid membrane and hydrophobic region of cytosolic protein. In addition, some enzymes such as diacylglycerol kinase, calactin, endonexin, calmcimedin, synexin and calelectin bind membrane in calcium ion dependent manner [26]. Protein kinase C and related protein induced segregation of acidic phospholipid [27, 28]. And using peptide mimicking pseudo-substrate (Acrylodan-labeled MARKS) in binary liposomal system of phosphatidylcholine and NBS-labeled phosphatidylserine, phase separation induced by the peptide was reported [29]. Induction of hexagonal II structure and cubic structure was reported as effects of diacylglycerol on physical property of lipid membranes [30]. From these results, supposed mechanism of lipid second messenger inducing signaling process is shown in Fig. 6.4. And lipid second messenger in signaling system of cell was reviewed by Makowsky and O.M. Rosen [24]. On the other hand, Generation of phosphatidic acids makes possible to translocate calcium ions through lipid membrane as shown in Fig. 6.5 [31].

# 6.5 Non-bilayer Forming Lipids and Function of Biomembrane

Although basic structure of biomembrane is lipid bilayer membrane as assembly of lipid molecules, the lipid membrane shows polymorphism in its structure and physical property. Lipid molecule of cone shape prefers non-bilayer structure such as hexagonal II and lipidic particle. And role of non-bilayer structure on function of biomembrane was studied.

# 6.5.1 Membrane Structure Formed by Non-bilayer Forming Lipids

Basic concept of biomembrane was established by 'fluid mosaic membrane model' proposed by Singer and Nicolson [32], but formation of non-bilayer structure under a condition was observed by <sup>31</sup>P-NMR in 1978 [30], and then observed by freeze-fractured electron microscope [33]. From these results, relationship between non-bilayer forming lipids and non-bilayer structure such as hexagonal II structure

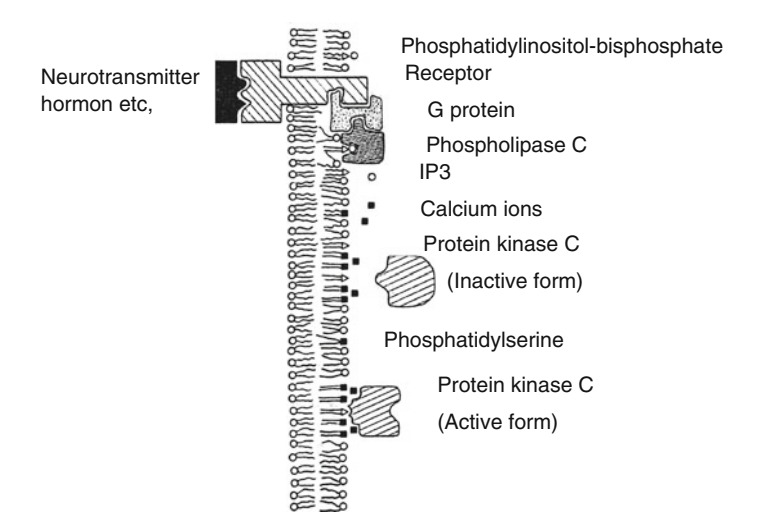


Fig. 6.4 Supposed mechanism of PKC activating cellular signaling Phosphatidylinositol bisphosphate is separated into diacylglycerol and inositol triphosphate by activation of phospholipase C through binding of ligand (such as neurotransmitter and hormone) to receptor. Diacylglycerol promotes phase separation of phosphatidylserine by calcium ions and makes membrane surface hydrophobic. Protein kinase C binds the hydrophobic region of plasma membrane and becomes active conformation

and intra membrane particle was elucidated. Non-bilayer structures are formed by non-bilayer preferring lipids. And Israelachvili *et al.* analyzed thermodynamically relationship between shape of lipid molecule and structure of lipid assembly in aqueous environment [34]. Cylindrical lipids assemble to form lipid bilayer membrane and inverted cone lipids form inverted micelle or hexagonal II structure. These structures are observed by freeze-structured electron microscope as shown in Fig. 6.6.

## 6.5.2 Non-bilayer Membrane Structure in Membrane Fusion

Membrane fusion is important mechanism for change of compartment such as membrane traffic, endocytosis, exocytosis and cell division. Molecular mechanism of membrane fusion was studied in membrane fusion of synapse vesicle in nerve ending. There are specific complexes, t-SNARE and v-SNARE in vesicle membrane and target membrane, respectively. And it is supposed that these complexes change the structure to bind both membranes compactly and result in membrane fusion [35]. Molecular model of region in the membrane fusion was proposed by X-ray diffraction analysis of SNARE complexes [36]. Induction of membrane fusion by close contact was proved by using bee venom, melittin (having positively charged basic amino acids region and hydrophobic amino acids region) in liposomal system

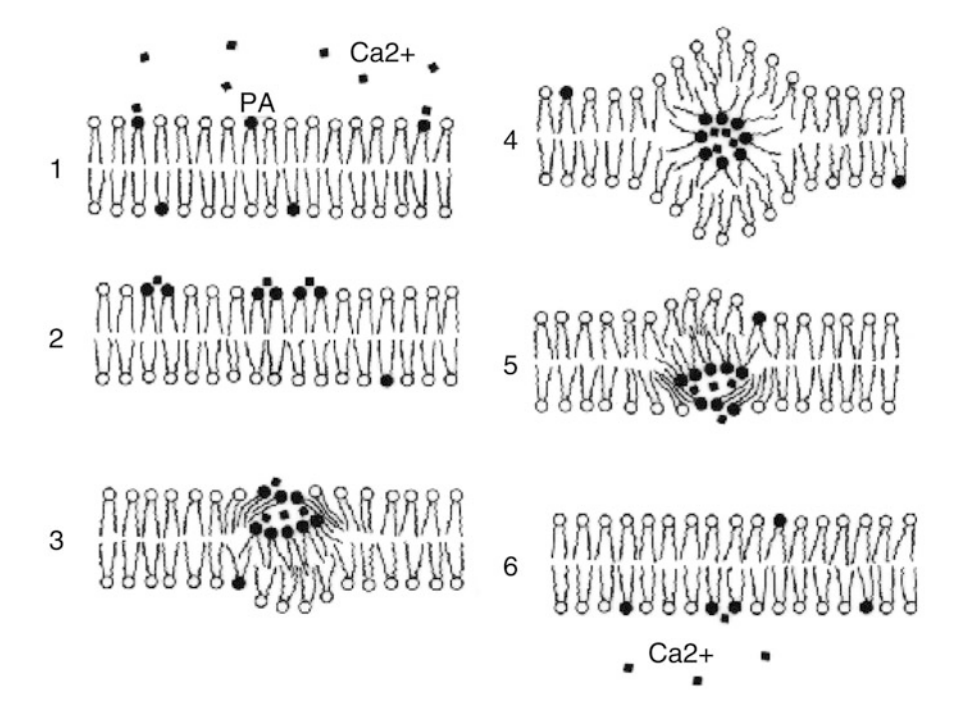


Fig. 6.5 Calcium ionophore function of phosphatidic acid (PA) molecules
(1) Calcium ions bind PA electrostatically. (2) PA is phase separated by replacement of hydration water molecules by calcium ions and the phase separated region becomes hydrophobic
(3) Head of Ca-PA complex is hydrophobic and penetrates hydrophobic center of the membrane
(4) Inverted micelle structure is formed centering calcium ion





**Fig. 6.6** Non-bilayer structures observed by freeze-fractured electron microscope Hexagonal II structure of phosphatidylethanolamine is observed as parallel lines Cardiolipn-Ca2 + complex is observed as arranged lipidic particles

of neutral phospholipid and acidic phospholipid [37]. Inverted micelle was observed in focal fusion point of calcium ion-induced membrane fusion in lipid membrane system including acidic phospholipid [38], and indeed membrane fusion was induced by transition from lamellar phase to hexagonal II phase in membrane system

including non-bilayer preferring lipids [39]. Inverted micelle, a kind of non-bilayer structure was also closely related to membrane fusion [40]. In addition to these results, induction of non-bilayer preferring lipid, diacylglycerol into lipid membrane promoted membrane fusion [41] and also generation of diacylglycerol by catalytic conversion by phospholipase C induced membrane fusion [42]. Calcium ions induce membrane fusion in lipid membrane including negatively charged acidic phospholipids and inverted micelles are involved in this case, and calcium ionophore for calcium ion permeation [31] is supposed to be similar mechanism shown in Fig. 6.5.

# 6.5.3 Regulation of Biomembrane Formation by Non-bilayer Structure as Lipid Storeroom in Biomembrane Lipid

Inner membrane of mitochondria and thylakoid membrane contain much of cardiolipin and phosphatidylglycerol and ratio of proteins to lipids is higher because of electron transfer system. These membranes keep lipid bilayer structure despite higher content of non-bilayer preferring lipids. To keep bilayer membrane structures, excess content of non-bilayer preferring lipids are supposed to be stored as cubic phase or hexagonal II phase induced by calcium ions. These non-bilayer structures function as buffer for lipid supplying store in case of protein degradation or protein assembly [43]. Conversion between lipid bilayer membranes and non-bilayer membrane induced by changes of temperature and lipid composition was demonstrated in a model system composed of mono-methyl phosphatidylethanolamine (DOPE-Me) containing dipalmitoyl glycerol as non-bilayer preferring lipid by use of X-ray diffraction, DSC and freeze-fractured electron microscope [44].

# 6.5.4 Changes of Structure and Physical Property and Biological Function in Biomembranes

Three methyl moieties of phosphatidylcholine are replaced by hydrogen atoms in phosphatidylethanolamine and result in structural change from cylinder to cone. And change of physical property appears in change of phase transition temperature. Phase transition temperature of dimyristoylphosphatidylethanolamine (DMPE) is 27 degrees higher than that of phosphatidylcholine (DMPC). Density of DMPC membrane is 1.13 g/cm³ compared to 1.25 g/cm³ of DMPE membrane in gel phase. These physical properties of DMPE indicate narrower inter molecular distances between DMPE molecules and stronger inter molecular interaction. Therefore, non-bilayer membrane structure is supposed to raise lateral pressure from both sides of membrane protein and to maintain functional structure of the membrane proteins [43]. Indeed, protein translocase of *E. coli* was activated by non-bilayer preferring lipids [45]. Formation of non-bilayer membrane structure is geometrical

effect of molecular shape of lipid and induced by cone type lipid molecule. Lipid bilayer membrane prefers non-bilayer membrane structure when cylinder type lipids of the membrane are converted to cone type lipids, diacylglycerol molecules by phospholipase C because of increase of curvature of the membrane [46]. Phenomenon like endocytosis which was independent of ATP was observed when CHO cells were treated with sphingomyelinase. This phenomenon is supposed that conversion of cylindrical sphingomyelin to cone shape ceramide induces curved plasma membrane to assist endocytosis [47]. Release of cytochrome from mitochondria is observed in apoptosis and related gene tBid is identified for the release. And addition of product from tBid to liposomes including cardiolipin and phosphatidylethanolamine induced increase of membrane permeability, membrane fusion and formation of non-bilayer membrane in correlating with change of membrane curvature [48]. These results imply participation of tBid in formation of non-bilayer membrane structure and permeation of biomolecules through biomembranes. There is standard theory, area-difference elasticity for models in curvature of bilayer membrane spontaneously formed by amphipathic lipid molecules in aqueous environment [49, 50]. Balance between forces acting lipid molecule in lipid bilayer membrane is explained by considering each inter molecular force acting inner and outer layer of bilayer membrane as follows (Fig. 6.7) [51]. Attraction force of inter facial pressure generated from hydrogen bonds between water molecules balances with both of repulsion forces generated from head group pressure and chain pressure. Torque calculated for point of attraction in clockwise  $(21mN \cdot m^{-1} \times 0.5 nm = 10.5pN)$  and torque calculated for point of attraction in anticlockwise  $(14mN \cdot m^{-1})$  $\times$  0.5 nm = 10.5pN) are also balanced. Treatment of polar heads of lipids by phospholipase C or sphingolipase converts to non-bilayer preferring lipid of small polar head and makes the membrane curved by reducing repulsion force between polar heads.

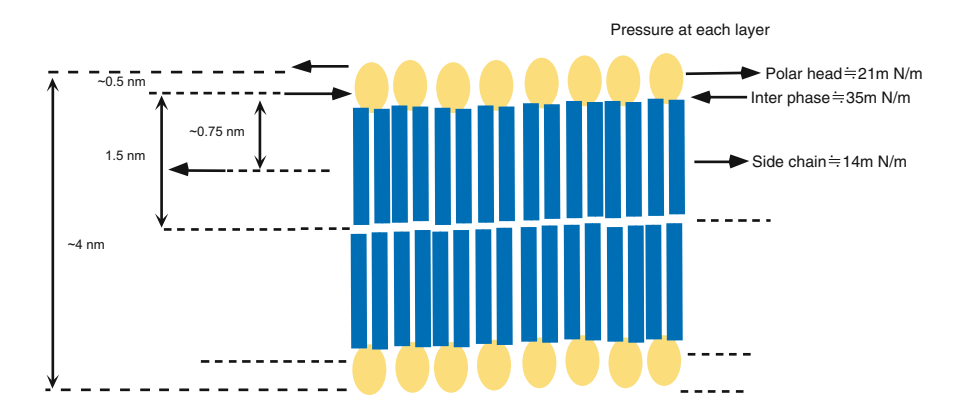


**Fig. 6.7** Curved lipid bilayer membrane and balance of forces Lipid bilayer membrane is planar when repulsion forces of polar head and acyl side chains balanced with attractive force of interphase. Change of pressure induces movement of gravity center and the membrane is curved

### References

- 1. D. Axelrod, D.E. Koppel, J. Schlessinger, E. Elson, W.W. Webb, Biophys. J. 16, 1055 (1976)
- 2. E. Hanski, G. Rimon, A. Levitzki, Biochemistry 18, 846 (1979)
- 3. S. Ohnishi, T. Ito, Biochemistry 13, 88116 (1974)
- 4. J.M. Boggs, D.D. Wood, M.A. Moscarello, D. Papahadjopoulos, Biochemistry 16, 2325 (1977)
- 5. S. Tokutomi, K. Ohki, S. Ohnishi, Biochim. Biophys. Acta 596, 192 (1980)
- 6. K. Ohki, K. Takahashi, S. Kato, A. Maesono, Chem. Phys. Lipids 50, 109 (1989)
- K. Ohki, T. Yamauchi, Y. Banno, Y. Nozawa, Biochem. Biophys. Res. Commun. 100, 321 (1981)
- 8. K. Simons, E. Ikonrn, Nature 387, 569 (1997)
- 9. D.A. Brown, E. London, Annu. Rev. Cell Dev. Biol. 14, 111 (1981)
- 10. J.H. Ipsen, O.G. Mouritsen, Biochim. Biophys. Acta 944, 121 (1988)
- 11. J.R. Silvius, Biochim. Biophys. Acta 1610, 174 (2003)
- 12. W. Guo, V. Kuze, T. Huber, N.H. Afdal, K. Beyer, J.A. Hamilton, Biophys. J. 83, 1465 (2002)
- 13. K. Ohki, J. Phys. Condens. Matter 17, S2957 (2005)
- 14. Y. Taniguchi, T. Ohba, H. Miyata, K. Ohki, Biochm. Biophys. Acta 1758, 145 (2006)
- M.R. de Planque, E. Goormaghtigh, D.V. Greathouse, R.E. Koeppe 2nd, J.A. Kruijtzer, R.M. Liskamp, B. de Kruijff, J. Killian, Biochemistry 40, 5000 (2001)
- 16. A. Kishimoto, Y. Takai, T. Mori, U. Kikkawa, Y. Nishizuka, J. Biol. Chem. 25, 2273 (1983)
- 17. D.S. Drust, T.F.F. Martin, Biochem. Biopys. Res. Commun. **128**, 531 (1985)
- E. Melloni, S. Pontrmoli, M. Michetti, O. Sacco, B. Sparatore, F. Salamino, B.L. Horecker, Proc. Natl. Acad. Sci. USA, vol 82 (1985), p. 6435
- 19. K. Ohki, T. Sekiya, T. Yamauchi, Y. Nozawa, Biochim. Biophys. Acta 693, 341 (1982)
- 20. R. Charest, P.F. Blackmore, B. Berthon, J.H. Exton, J. Biol. Chem. 258, 8769 (1983)
- 21. M.A.D. Bazzi, G.L. Nelsestuen, Biochemistry 27, 6776 (1988)
- P.J. Parker, L. Coussens, N. Totty, L. Rhee, S. Young, E. Chen, S. Stabel, M.D. Waterfield,
   A. Ullrich, Science 233, 853 (1986)
- 23. C. House, B. Kemp, Science 238, 1726 (1987)
- 24. M. Makowske, O.M. Rosen, J. Biol. Chem. 264, 16155 (1989)
- 25. M. Mosior, S. McLaughlin, Biophys. J. 60, 149 (1991)
- 26. F. Sakane, K. Yamada, S. Imai, H. Kanoh, J. Biol. Chem. 266, 7096 (1991)
- 27. C.B. Klee, Biochemistry 27, 6645 (1988)
- 28. M.D. Bazzi, G.L. Nelsestuen, Biochemistry 30, 7961 (1991)
- 29. L. Yang, M. Glaser, Biochemist 34, 1500 (1995)
- 30. P.R. Cullis, B. de Kruijff, Biochim. Biophys. Acta **507**, 207–218 (1978)
- 31. K. Ohki, S. Nagaoka, M. Sogami, Y. Nozawa, Chem. Phys. Lipids 39, 237 (1986)
- 32. S.J. Singer, G.L. Nicolson, Science 175, 720 (1972)
- 33. A.J. Verkleij, C. Mombers, J. Leunissen-Bijvelt, P.H.J.T. Ververgaert, Nature 279, 162 (1978)
- 34. J.N. Israelachvili, D.J. Mitchell, B.W. Ninham, Biochim. Biophys. Acta 470, 185 (1977)
- 35. P. Hanson, R. Roth, H. Morisaki, R. Jahn, J.E. Hauser, et al. Cell **90**, 523–535 (1997)
- 36. R.B. Sutton, D. Fasshause, R. Jahn, A.T. Brunger, Nature 395, 347 (1998)
- 37. Y. Higashino, A. Matsui, K. Ohki, J. Biochem. (Japan) 130, 393 (2001)
- 38. P.M. Frederik, M.C.A. Stuart, A.J. Verkleij, Biochim. Biophys. Acta 979, 275 (1989)
- 39. P.R. Cullis, B. de Kruijff, Biochim. Biophys. Acta **559**(1979), 399 (1979)
- 40. H. Ellens, D.P. Siegel, D. Alford, P.L. Yeagle, L. Boni, L.J. Lis, P.J. Quinn, J. Bentz, Biochemistry 28, 3692 (1989)
- 41. M. Paz Sanchez-Milgalon, F.J. Aranda, J.C. Gomez-Fernandez, Biophys. J. 68, 558 (1995)
- 42. U.-L. Nieva, F.M. Goni, A. Alonso, Biochemistry 28, 7364 (1989)
- 43. G. Garab, K. Lohner, P. Laggner, T. Farkas, Trends Plant Sci. 5, 489 (2000)
- 44. H. Takahashi, M. Watanabe, P.J. Quinn, S. Kato, S. Murayama, K. Ohki, I. Hatta, Biophys. Chem. 77, 37 (1999)
- 45. B. de Kruijff, Nature 386, 129 (1977)

References 93

46. C. Van der Does, J. Swaving, W. van Klompenberg, A.J. Driessen, J. Biol. Chem. 275, 2472 (2000)

- 47. X. Zha, L.M. Pierini, P.L. Leopold, P.J. Skiba, I. Tabas, F.R. Maxfield, J. Cell Biol. 140, 39 (1998)
- 48. R.F. Epand, J.-C. Martinou, M. Fornallaz-Mulhauser, D.W. Hughes, R.M. Epand, J. Biol. Chem. 277, 32632 (2002)
- 49. P.G. de Gennes, *The Physics of Liquid Crystals* (Oxford University Press, London, 1974)
- 50. L. Miao, U. Seifert, M. Wortis, H.G. Dobereiner, Phys. Rev. E 49, 5389 (1997)
- 51. G. Cevec, D. Marsh, *Phospholipid Bilayers* (Wiley, New York, 1987)

# **Chapter 7 Moving Life**



Abstract Previous chapters have dealt with the phenomenon centered on the structure and function of biological membranes. The lipid membrane is an essential structure that guarantees the steady state of the life in the ever-changing environment. Non-stop exchange of matters and information with the environment is a salient feature of the activity of living thing. The previous chapters describe various facts of these aspects. Voluntary movement is another remarkable feature of living things. Thus in Chap. 7, various types of biological motions are described. First, muscle contraction is briefly described, because it is one of the best known and studied example of the motor-based biological motions. Another well-studied example of the motor-based motion is the organelle transport; microscopic observations and analysis of the motion are described as examples. Motors related to the transport motility are briefly described and actin and microtubule tracks are described in some detail. The dynamism of the cell is largely depends on the dynamism of the system of actin filaments, microtubules and intermediate filaments. These filament systems are assembled or disassembled according to the needs of the cell, which is adopted in generating cellular movements. In the case of actin filaments and microtubules the movements such as lamellipodial protrusion, segregation of chromosomes and organelle transport, are driven. For these phenomena polymerization and depolymerization of the subunit of these polymers play essential roles. Thus, the polymerization/depolymerization-driven motions in the cell are one of the main theme of the last half of this chapter.

First, structure of actin monomer and tubulin, actin filament and microtubule are described, and kinetics of polymerization of actin is then explained, because it is necessary to understand the polymerization/depolymerization-driven motions in the cell. Following these sections, overview of the cell motility is given, which is followed by explanation on the actin-related structures in the cell. An important question on the actin-based motility is that if it can really develop the force that leads to the mechanical work such as deformation of the cell membranes in lamellipodial protrusion. Three examples are presented: (1) the measurements done on two types of cells keratocyte, a highly motile cell, and a fibroblast, rather quiescent cell; (2) the reconstituted systems, liposomes encapsulating actin or monomeric unit of microtubule (tubulin); (3) actin-based movement of bacteria. Then, theories that were

96 7 Moving Life

developed on the basis of thermodynamics or on the basis of thermal fluctuation, and the experimental evaluation of the theories are described. In the last section microtubule-based, depolymerization-driven motility is briefly explained.

## 7.1 Biological Movements

### 7.1.1 Muscle Contraction and Mechano-Enzyme

Voluntary movements are remarkable features of life. Most notable biological movement is skeletal muscle contraction (Fig. 7.1). Skeletal muscle is an organ highly specialized for generating force and movement. It is consisted of multinuclear muscle cells, each of which contains a number of contractile units each called sarcomere. Sarcomere is regularly aligned in a muscle cell both in series and parallel. Each sarcomere is consisted of a parallel array of thick, bipolar filaments consisted of myosin and thin actin filaments. The unipolar actin filament is tagged at one end by a structure called Z-line, resulting in the bipolar structure. The thin and the thick filaments overlap each other. Because of the polarities of two filament systems, if individual myosin filaments pull actin filaments, the spacing of the sarcomere is narrowed. This is the essence of muscular contraction. The sarcomere-based highly regular structure in the skeletal muscle makes the fast contraction and the generation of the contractile force possible [1].

Myosin is a hexamer consisted of four small (~20 kDa each) polypeptides and two large (~200 kDa each) polypeptides (Fig. 7.2). The large polypeptides (each called heavy chain) form a globular structure on the side of N-terminus and a long alpha-helix on the side of C-terminus, and the two heavy chains are held together by the coiled-coil structure of the alpha-helical portion. Hence, as a whole, myosin looks like a double-headed snake. This type of myosin is called myosin II. Two small polypeptides (each called light chain) are reversibly bound to individual junctions of globular domain and the helical domain. The bipolar myosin filament is formed as a result of reversible association of the tails of many myosin molecules. Sticking out from the shaft of the filament is the structure called cross-bridge. Cross bridge was first recognized as a structure bridging the myosin filament and actin filament in muscle and is consisted of the head portion of myosin [2, 3]. The head has ability to reversibly bind to actin filament. The head portion binds and hydrolyzes ATP. Myosin is thus an ATP-hydrolyzing enzyme and also produces the contractile force (mechanical work). Hence, myosin is called a mechano-enzyme.

Actin filament is a polymer of a globular protein called G-actin (described in detail in Sect. 7.3). Tropomyosin-troponin complex binds along the filament axis (Fig. 7.3). When Ca<sup>2+</sup> ions are bound to the troponin complex, the position of the tropomyosin shifts on the thin filament and each actin molecule becomes capable of interacting with the myosin heads. As a result of this, the ATP-hydrolyzing activity (ATPase activity) of myosin head is greatly enhanced. The binding of ATP and actin to myosin head is reciprocally coupled. Thus, when ATP is bound to the ATPase site of myosin head, the affinity of the myosin head to actin drastically lowered so that

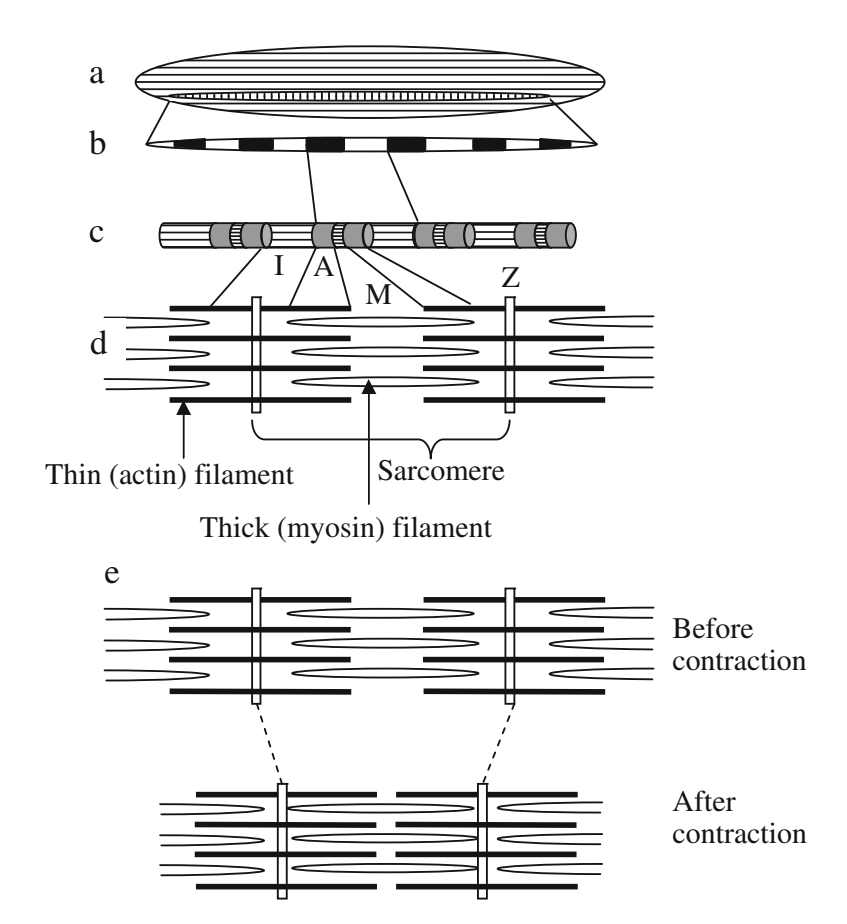


**Fig. 7.1** Highly schematic representation of a muscle and its substructures. Panel a, whole skeletal muscle (long oval); Panel b, a muscle cell (the striated oval); Panel c, myofibril; Panel d, thick filament (myosin filament) and thin filament (actin filament), which are the major constituents of myofibril and regularly arranged in the longitudinal and the vertical direction. The regular overlapping of two filament systems in the sarcomere appears as optically anisotropic and isotropic pattern, which are respectively named anisotropic (A)-band and isotropic (I)-band. M and Z represent M- and Z-line that correspond to the central part of myosin filaments and the structure tagging actin filaments. The anisotropic band is strongly birefringent, because of the overlapping of the two filament systems, while the isotropic band is less isotropic, because there are only actin filaments in this region. Panel e, the overlapping of the thick and thin filaments before (upper panel) and after (lower panel) the contraction; individual filaments do not change their lengths, but the overlapping lengths increase. Binding of Ca<sup>2+</sup> ions to the thin filament through troponintropomyosin complex that are bound to the thin filament switches the thin filament state from the off- to the on. In the on-state myosin becomes able to interact with actin. This greatly accelerates the rate of ATP hydrolysis of by myosin and a contractile force occurs

98 7 Moving Life

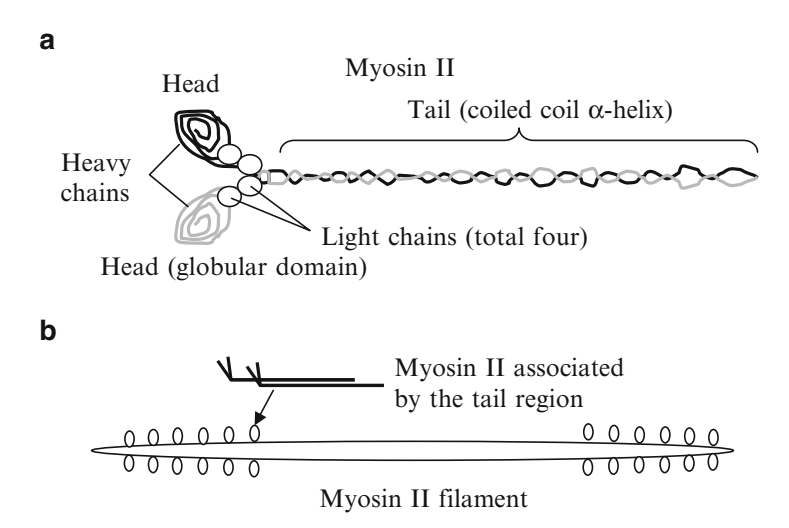


**Fig. 7.2** Subunit structure of a myosin molecule. Panel a, myosin is a hexamer, consisted of four light chains (white ovals) and two heavy chains (black and grey lines). Toward the N-terminus of each heavy chain a globular portion called head is formed; toward the C-terminus of the heavy chain, a long alpha helix is formed. The two alpha-helices from each heavy chain form a coiled-coil structure, which is called tail. This type of myosin is called myosin II. Panel b, myosin molecules associate with each other by the tails to form a bipolar filament. From the surface of the filament the structure called crossbridge (myosin heads) is sticking out. Light chains are bound to heavy chains near the junction of the head and the tail regions

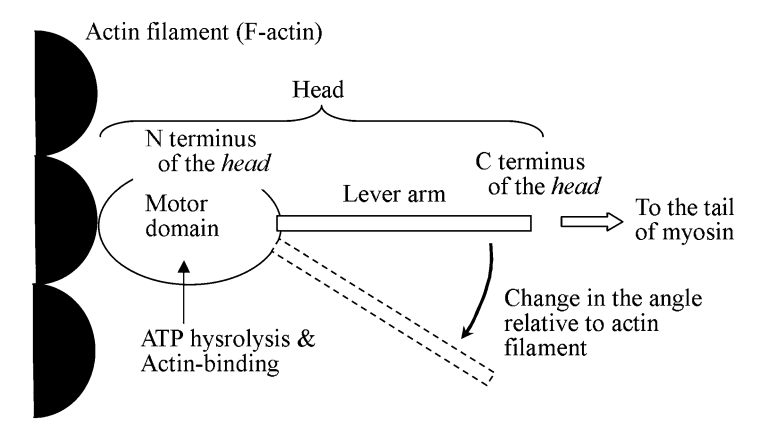
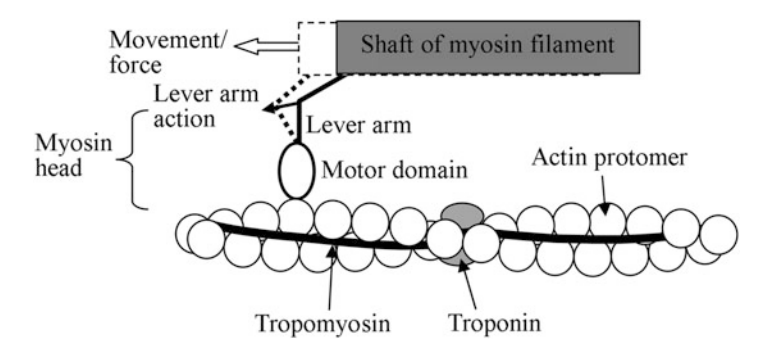


Fig. 7.3 A highly schematic diagram of the myosin head. The head is schematically divided into the motor domain and the alpha-helical lever arm (actual length  $\sim$ 8 nm). The motor domain binds and hydrolyzes ATP and binds to the actin protomer in the actin filament schematically shown on the left. The orientation of the alpha-helical tail changes by  $\sim$ 60° with the progress of ATP hydrolysis on the motor domain; concomitantly, structural change occurs to the motor domain and the affinity of the head to actin protomer increases. The strongest binding occurs when hydrolyzed products (ADP and Pi) dissociate from the ATPase site in the motor domain

the head dissociates from the actin with the rate of ~1000 s<sup>-1</sup>. After ATP is hydrolyzed, the reaction product, inorganic phosphate (Pi) dissociates from the head. As a result, the high affinity of the head to actin is recovered and the head again binds to actin. The rapid dissociation and enhancement of the ATP hydrolyzing activity of myosin head upon its re-binding to actin is necessary for the head to perform the rapid contraction of a skeletal muscle, because during the contraction at the maximum velocity, the time for each head to pass individual actin protomer will be only a few milliseconds. On the other hand, the recovery of the strong affinity of the head to actin with the progress of hydrolysis will be necessary to produce contractile forces of sufficient magnitudes. Thus, the biochemical properties of the skeletal actomyosin seem to be optimized for the contractile property of skeletal muscle.

#### 7.1.2 Muscle Contraction at the Molecular Level

The crystal structure of myosin head [4] revealed distinctive features of the myosin head. The head is divided into two major parts, a long ( $\sim$ 8 Å) alpha helix called "lever-arm", and a globular portion called "motor domain" from which the lever-arm extends. The head includes the N-terminus of the motor domain and the tail domain is closer to the C-terminus (Fig. 7.4). It has been hypothesized that the lever-arm rotates relative to the motor domain with the progress of hydrolysis of ATP (ATP  $\rightarrow$  ADP-Pi  $\rightarrow$  release of Pi  $\rightarrow$  release of ADP) that occurs on the motor domain. Figure 7.5 shows the coupling of ATP hydrolysis of myosin to force generation (conformational change of the head). The myosin head cyclically interacts with actin



**Fig. 7.4** Generation of contractile force by the action of the lever-arm. For simplicity, only one myosin head is drawn. Actin filament is a polymer of monomeric actin (represented with a circle; termed in this chapter actin protomer). Two tropomyosin polymers made by head-to-tail association (thick black lines) are bound to the groove of actin filament. Troponin (grey oval) is constituted of three subunits (not drawn). It binds to tropomyosin to regulate the binding of the myosin heads (motor domain) to actin protomer in Ca<sup>2+</sup> ion-dependent manner

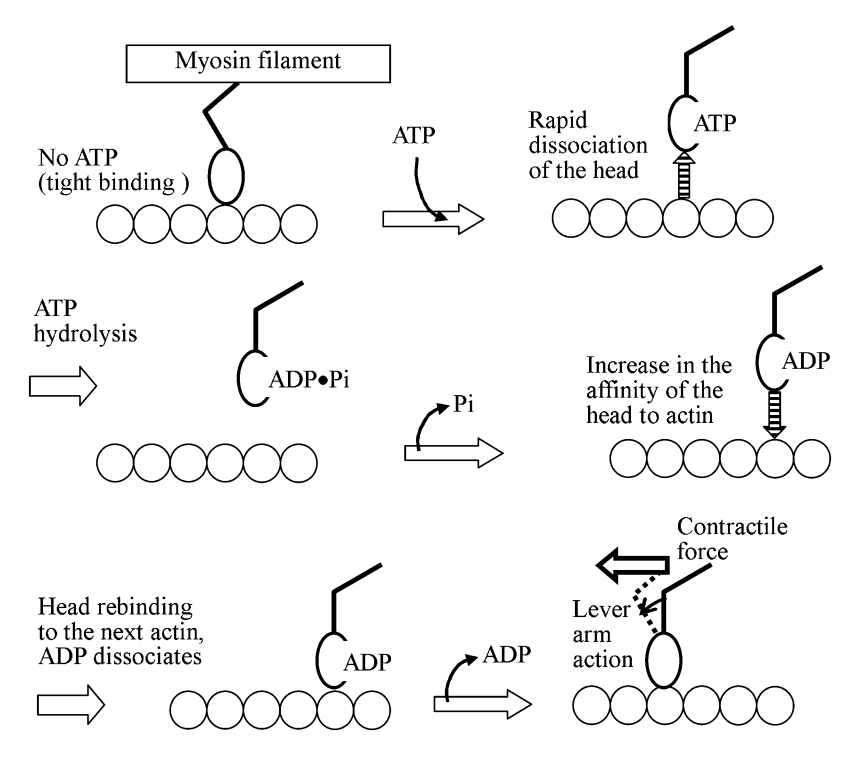


**Fig. 7.5** Coupling of ATP hydrolysis and generation of a contractile force. For simplicity, only one myosin head is drawn and actin filament is represented with a straight chain of circles. The scheme starts from the myosin head tightly bound to actin (top left), which occurs in the absence of ATP. Upon binding of ATP to the head, the affinity between the head and the protomer is greatly reduced and the head rapidly dissociates from the protomer and prepares for the force generation (change in the angle of the lever arm). In the intermediary step of the progress of the hydrolysis of ATP to ADP + Pi, ADP-Pi is bound to the head, which is followed by sequential release of Pi and ADP. Concomitant with these changes, the affinity of the head to actin protomer progressively increases and the strong binding of the head to actin portomer eventually recovers. This process is accompanied by the change in the angle of lever arm occurs, during which the contractile force is generated (power stroke; bottom right)

during its ATPase cycle thereby generating the contractile force (power stroke; [5]). This has been called mechanochemical coupling.

As mentioned above, the motor domain binds to the actin filament. The affinity of the motor domain to actin should be high enough for generation of the force (a few pN, [1]; see next section). Thus, the swinging lever-arm pulls the myosin or myosin filament (Fig. 7.4). It has been suggested that the lever arm action is a result of amplification of more localized change in the intramolecular structure that accompanies the ATP hydrolysis. This is similar to the amplification of a small distortion of the heme in hemoglobin resulting in the relative displacement and rotation of hemoglobin subunits [5].

# 7.1.3 Single-Molecule Measurement for the Motor Function of Myosin

The force generation by myosin has been studied at the level of single molecule under the condition where a load was applied to individual myosin. In one example, a micron-sized plastic bead was attached to one end of actin filament (so-called the barbed end (Sect. 7.3.3.1); Fig. 7.6a; [6]) and the bead was held by an optical trap

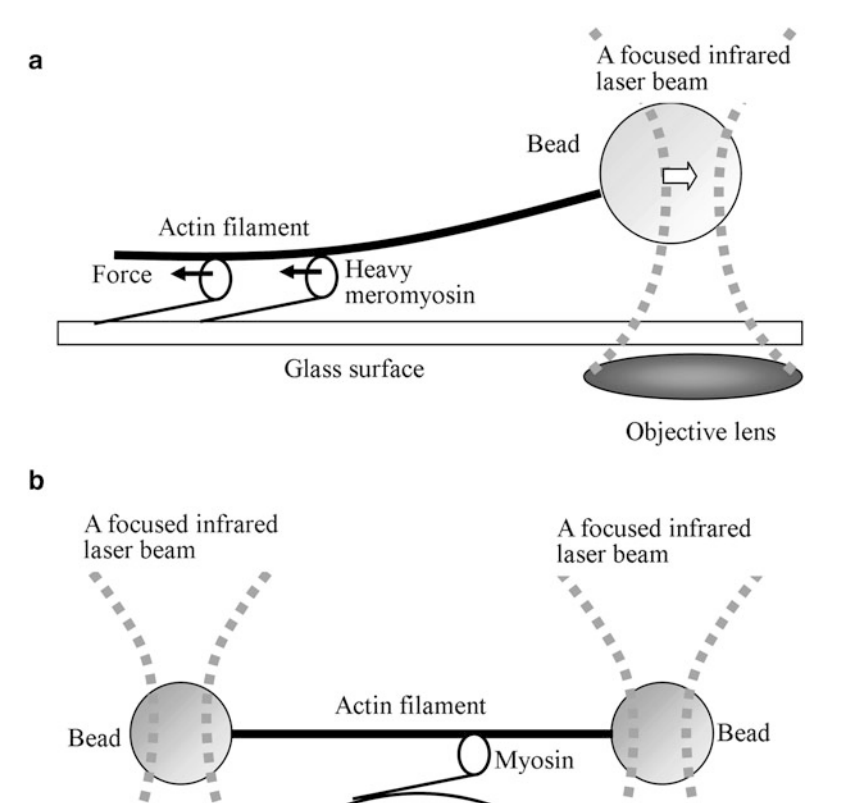


**Fig. 7.6** A highly schematic representation of measurement of the force exerted by myosin. Panel a, heavy meromyosin, prepared as a proteolytic fragment of myosin II, was allowed to sparsely bind to the glass surface, and an actin filament, tethered to a 1 μm plastic bead, was allowed to interact with the surface-bound myosin in the presence of ATP. The bead was trapped by an optical trap (Chap. 3, Sect. 3.8). Intermittent pulling of the bead by heavy meromyosin (only one head is shown for simplicity) against the trap force was observed. Panel b, the force measurement with a different configuration of the optical trap. Here, the double optical trap is created and two beads were held in each trap. The heavy meromyosin bound to the third bead that is bound to the glass surface (not drawn). This configuration allowed the researchers to measure the performance of *a single* myosin molecule, because the actin filament could be kept attached to myosin molecule in the presence of ATP, where the affinity of the head to actin is greatly reduced

Large bead

(see Sect. 3.8 for details), and the filament was allowed to interact with myosin bound to the glass surface. The situation of tug-of-war was established between the trapped bead and the surface-bound myosin molecules, and hence, the displacement of the bead by the pulling action of myosin and the accompanying force could be estimated [7]. Actually, it was difficult to measure the force or movement of a single myosin molecule with this configuration, because in the presence of ATP, the dissociation of the myosin head from the actin filament was unavoidable. Lowering ATP concentration will be required to resolve individual force generation events, because the bimolecular rate constant for the binding of ATP to myosin head is on the order of 10<sup>6</sup> M<sup>-1</sup>s<sup>-1</sup>, and hence, at 1 µM ATP, roughly 1 event of the force generation will be expected [8]. However, the collected data scarcely represented what would be expected form the single event (the displacement of the bead, ~5 nm, which was consistent with the estimation utilizing the result of macroscopic force measurement of skeletal muscle [1] and the value anticipated from the layer arm action); the displacements often exceeded 20 nm. Thus, the possibility of involvement of several consecutive events driven by several heads could not be denied [7]. A similar experiment with different configuration has been performed (Fig. 7.6b; [9]). This configuration allowed the measurement of the single molecule, because the dissociation of the actin filament from the myosin head could be suppressed. The result suggested that the distance over which a single myosin molecule exerted a few piconewton forces on actin filament was about 5 nm.

#### 7.2 Cellular Movements Other Than Muscle Contraction

In the following sections we will describe the movements and dynamics observed in non-muscle cells. Those include the movement of organelles, change in the cell shape and crawling motion of the cell body. The transport of organelles depends on non-muscle type myosin, kinesin or dynein, whereas the contraction of actin filament bundle that occurs in the cell spreading and crawling cell depends on muscle-type myosin, but some movements occur independent of those motor proteins (Sect. 7.17).

# 7.2.1 Three Filament Systems Supporting the Dynamism in the Cell

The cell has intricate filamentous structures: actin filament, microtubule (Fig. 7.7a and b, respectively) and intermediate filaments (not shown). Actin filaments (or F-actin) and microtubules are highly dynamic entities while intermediate filaments are less dynamic: apart from this difference, they are all assembled and disassembled through the process of reversible polymerization of monomeric units and

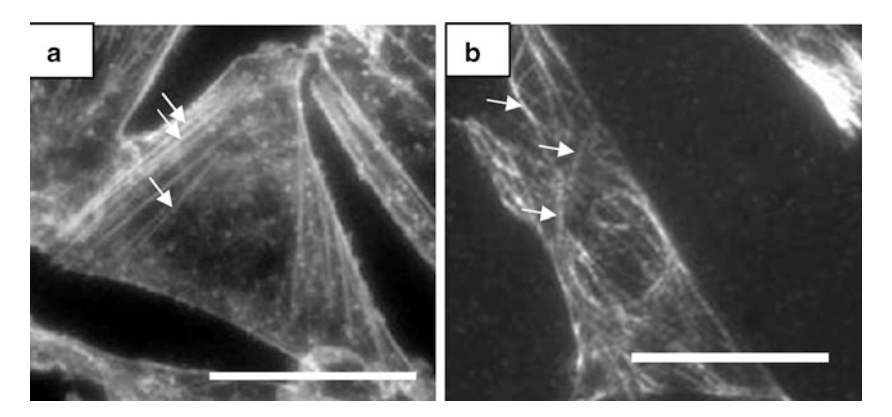


Fig. 7.7 Fluorescence micrographs of actin filament bundles (Panel a, white arrows) and microtubules (Panel b, white arrows) in Chinese hamster ovary cells. For visualization, actin bundles were stained with rhodamine-conjugated phalloidin, a phallotoxin which binds tightly to individual actin filaments and emits fluorescence. For visualization of microtubules, a primary antibody against microtubule was first bound to microtubules, and then, a fluorescence-tagged secondary antibody against the primary antibody was added. As result, fluorescence pattern of microtubules became visible. Under fluorescence microscope, individual actin filaments in the cell cannot be resolved and only bundles are seen. A single microtubule is much thicker than a single actin filament and can be observed under the fluorescence microscope. Microtubules are highly curved, as compared with actin filament bundles. Bars represent 20 µm. (fluorescence micrographs take by Shinji Akiyama, Department of Physics, Tohoku University)

depolymerization of the polymer. As already described, the monomeric unit of actin filament is actin monomer (also called G-actin); in the case of microtubules, tubulin dimers (Sects. 7.3.3 and 7.6.2). Since those filaments are utilized as structural as well as functional components, the reversible nature of the formation of the filamentous structure seems to be quite suitable for the cell to respond to the ever-changing mechanical and/or chemical environment.

The group of intermediate filament system contains several different types of unit (eg., keratin, vimentin or lamin [10]). The intermediate filaments have been shown to cooperate with the above two cytoskeletal system [10–12]. Readers are referred to [13, 14]. Below, we briefly explain non-muscle myosin and from Sect. 7.3., the actin filament and microtubule system in order to understand their cellular functions in detail.

# 7.2.2 Non-muscle Myosins and Organelle Transport

In non-muscle cells, many types of myosin exist. The muscle-type myosin is called myosin II, as mentioned before, because it was discovered *after* the first discovery of a non-muscle myosin (called myosin-I) in *Acanthamoeba* [15]. Myosin I is single-headed, has a short, non-alpha helical tail and does not form a filament. Later, other

Fig. 7.8 Highly schematic representation of various types of muscle and non-muscle myosins. Ovals: myosin motor domain. Motor domains are basically common among different myosins, but shape and lengths of the tails (thick black lines) are highly variable. The diversity of the tails enables myosin to perform their works at many different locations in the cell

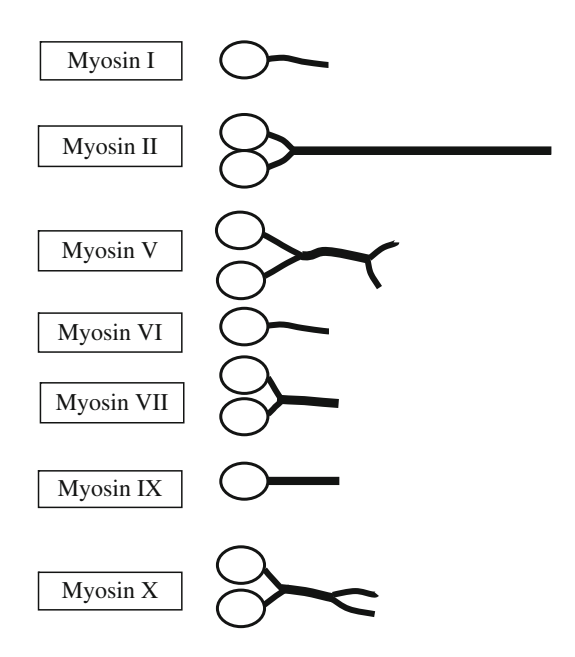


Table 7.1 Various myosins (not exhaustive)

Myosin	Shape (Fig. 7.8)	Localization	Role
I	Single- headed	Microvilli (small, cell-surface projections), lamellipodia	Generation of membrane tension?
П	Two -headed	Muscle Stress fiber	Generation of contractile forces
V	Two- headed	Various organelles, such as mitochondria, filopodia	Organelle transport
VI	Two- headed	Cell-to-cell junction	Formation of cell-cell contact
VII	Two -headed	Cell-to-cell junction	Formation of cell-to-cell junction
IX	Single- headed		Activator of the small GTPase, rho?
X	Two- headed	Lamellipodia, filopodia	Link cytoskeleton and integrin

non-muscle myosins (now called unconventional myosins) were isolated from many organisms and tissues (Fig. 7.8 and Table 7.1). The amino acid sequences of the heads of these non-muscle myosins are more or less similar to that of myosin II, but those of the tails have a wide variation [16]. Some non-muscle type myosins do form a dimer owing to the interaction between their tails, but the filament-forming nature seems to be specific to myosin II.

The non-muscle myosins (eg., myosin V, VI, VII) bind through their tail portion to the cell membrane or organelles. Thus, motor activity of the head portion seems to

be utilized in many different ways depending on the locations where myosin resides. Some myosins drive the movement of organelles on actin filament [17, 18]. The organelle transport is not the only job myosin I does: myosin I is involved in the generation of tension of cell membrane [19].

In addition to the structural role, actin filament and microtubule serve as tracks for the organelle transport with appropriate motors bound to individual organelles. Fig. 7.9a and b shows an example of the intracellular movement of organelles (Shinji Akiyama, Department of Physics, Tohoku University, unpublished data). Myosin

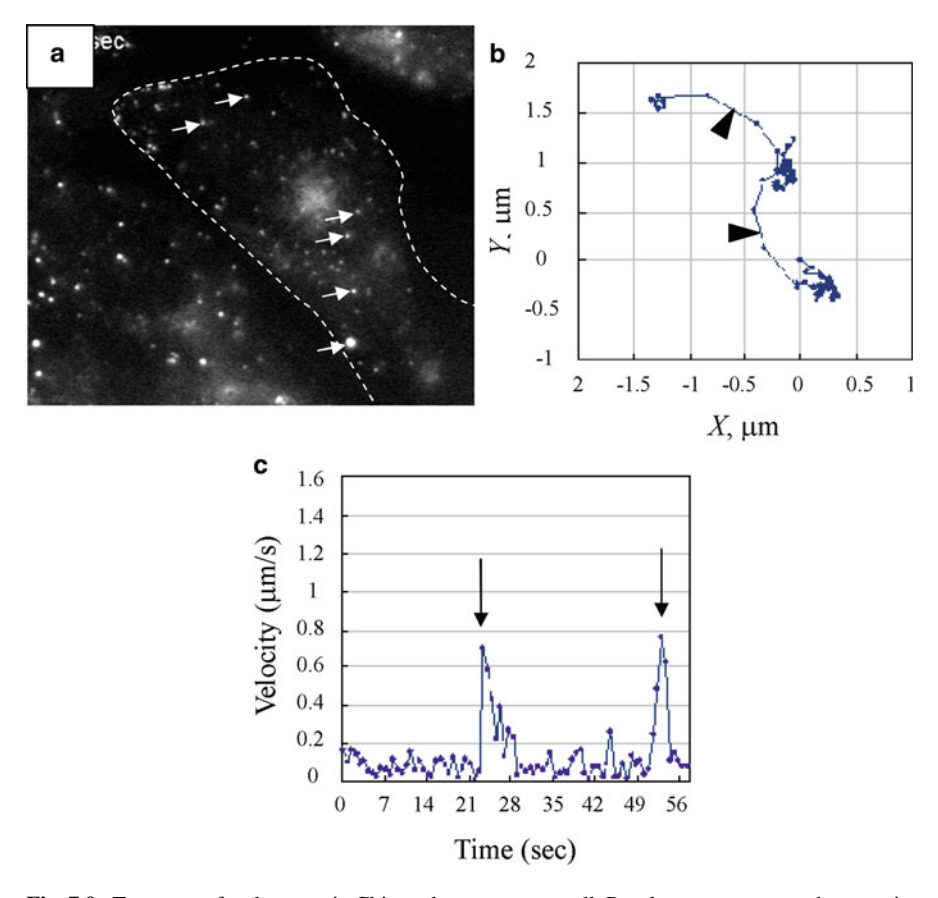


Fig. 7.9 Transport of endosomes in Chinese hamster ovary cell. Panel a, a numerous endosomes in the cell (arrows) labeled with a fluorescent dye, Lucifer yellow. Dotted line indicates the cell periphery. Endosome is formed by endocytosis, an invagination of the cell membrane followed by the closure. The extracellular materials such as the fluorescent dye are encapsulated in the endosome in this process. The endosomes are transported and processed in the cytoplasm. Panel b, an example of the X-Y trace of an endosome indicated with double arrows in Panel a. The movement is a mixture of a long-range, uni-directional motion (arrowheads) and small, less directed motion (arrows). Panel c, the velocity of the endosome along the trajectory. It is apparent that endosomes moved at non-uniform speed. The velocity of the long-rage motion is larger (as fast as  $\sim 1 \mu m/s$ ; downward arrows) than that of the less directed motion ( $\sim 0.1 \mu m/s$ ). (fluorescence micrograph and data obtained by Shinji Akiyama, Department of Physics, Tohoku University)

utilizes an actin filament as the track. Two other motor proteins, kinesin and cytoplasmic dynein [20] utilize a microtubule as the track; the kinesin and cytoplasmic dynein run in the opposite directions. The run length of the organelle on the microtubule track is longer than that on the actin track, and the velocity of the transport on microtubule is generally faster than that on actin filament (as in the example shown in Fig. 7.9c), or in the case of the transport of color pigments in melanocyte [21, 22]). The transport of the color pigment is remarkable, because there is a synergy between the microtubule-based transport and the actin-based transport. Thus, in the dispersion of the pigments in the cell, they are transported first by microtubule system. They are then transported by the actin filament system. The physiological interpretation is that the transport by the actin system will achieve more uniform intracellular distribution of the pigments than microtubule system alone. The kinetics-based mathematical analysis of this interesting phenomenon has been presented [23].

In another example, small membrane vesicle is propelled by the push of polymerizing actin filament, but not by myosin motor [24]. This is considered very similar to the intracellular movements of some bacteria (Sect. 7.17).

#### **7.3** Actin

#### 7.3.1 Actin Monomer Structure

As mentioned in the Sect. 7.2.1, actin takes monomeric or filamentous form. The actin monomer is comprised of a single polypeptide, the primary sequence of which has been determined (375 amino acids; [25]). Its molecular weight is ~42 kDa. The crystal structure of actin monomer that had been complexed with a protein DNase I to prevent polymerization during the crystallization, has been solved. The monomeric actin has been classified as a globular protein; its dimension is  $55 \times 55 \times 35$  Å ([26]; Fig. 7.10). The monomer is consisted of two lobes. In the cleft between two lobes, one nucleotide is bound (ADP when the monomer is incorporated in actin filament and ATP for the monomer in solution with submillimolar ATP). In vivo ATP is thought to be the nucleotide bound to monomeric actin, because the concentration of ATP (Mg-ATP in cytoplasm) exists at a millimolar concentration and is much higher than ADP. In vitro the bound nucleotide forms a complex with one Ca<sup>2+</sup> ion, but this Ca<sup>2+</sup> ion is replaced by an Mg<sup>2+</sup> ion when excess Mg<sup>2+</sup> ions are exogenously added [27]. According to the crystal structure, the nucleotide and the Ca<sup>2+</sup> ion are linked to the protein matrix through a number of hydrogen and electrostatic bonds [28]. The two lobes are further divided into subdomains I to IV. Residues 1-32, 70-144, 338-375 are included in the subdomain I, residues 33-69 in the subdomain II, residues 145-180 and 270-337 in the subdomain III and residues 181-269 in the subdomain IV. This indicates that the polypeptide chain of actin monomer is folded in a complex manner and partially penetrates into other domains.

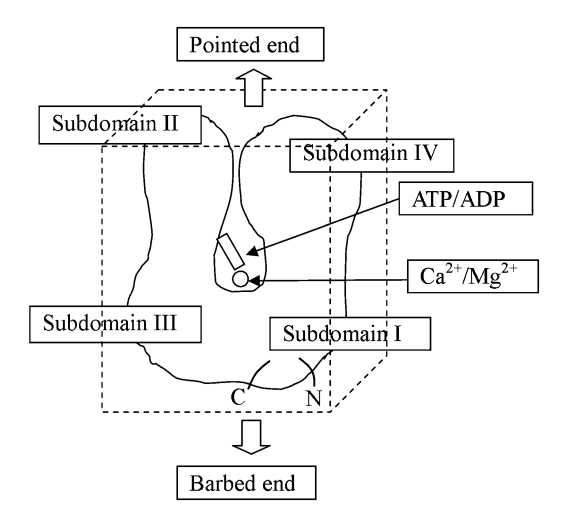


**Fig. 7.10** A highly schematic picture of a monomeric actin. The X-ray crystallography has demonstrated that monomeric actin is roughly divided into two lobes (in the figure represented with two blobs). The lobes are further divided into subdomains I to IV. Located in subdomain I are N and C termini (represented with the labels N and C, respectively). The orientation of the molecule relative to the pointed and the barbed ends (see text and Fig. 7.13) is indicated. The size of the box indicated with dotted lines is roughly  $55(w) \times 55(h) \times 35(d)$  Å

#### 7.3.2 Actin Filament Structure

Actin monomers polymerize to form a long, flexible filament. As mentioned above, we call the actin monomer incorporated in the filament actin "protomer". The actin filament looks like a right-handed, two-start helix according to the electron micrograph (Fig. 7.11a; [29]), but one can trace the individual monomers in the filament along a left-handed, one-start helix [30]: the rise of the one-start helix is 2.75 nm and the monomer makes ~166 degrees rotation around the filament axis: this nearly 180 degrees' rotation of monomer makes the actin filament have the appearance of the right-handed, two-start helix [28]: the pitch of this helix is 72 nm and the interprotomer distance along the filament axis is 5.5 nm. The two ends of filament can be distinguished based on the difference in structural and kinetic properties concerning the binding of the terminal protomers. The two, non-identical ends are named "barbed" and "pointed" ends, according to the polarity as indicated by the bound heavy meromyosin (see below).

The structure of actin filament at the atomic resolution was obtained from the fitting of the filament model constructed from the crystal structure of monomer to an X-ray diagram of actin gel oriented in a glass capillary [31]. The constructed model exhibited that the subdomains had slightly change their positions upon the incorporation of the monomer into the filament. The subdomain II and IV of the last protomer is exposed at the pointed end, while subdomain I and III are exposed at the barbed end (Fig. 7.11b). The cleft between the large and the small domain is

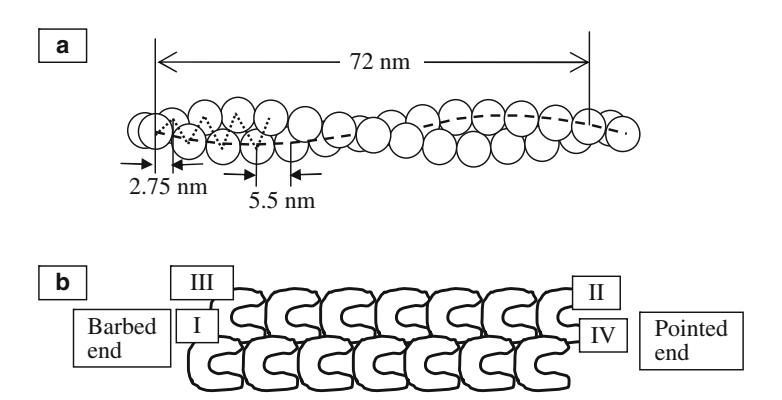
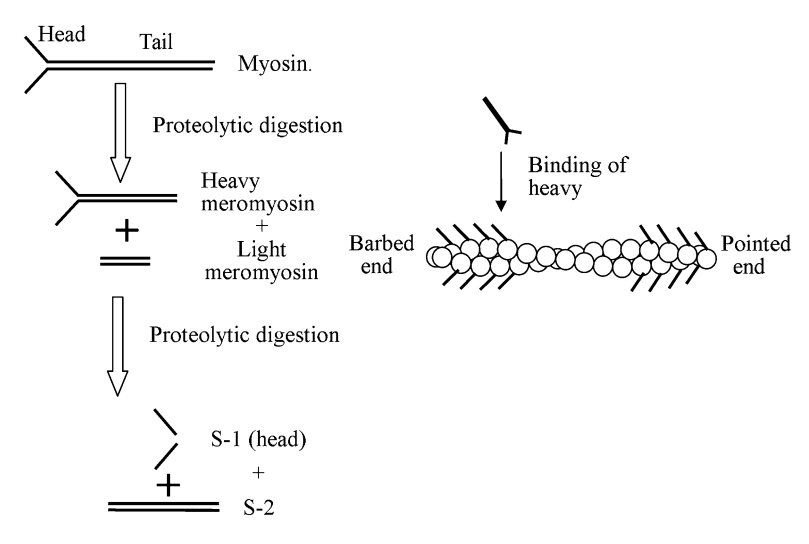


Fig. 7.11 A highly schematic representation of the structure of an actin filament deduced from electron microscopy and the arrangement of individual monomers in the filament. Panel a, the electron micrograph has suggested that the actin protomers in the filament is arranged as a two-start helix (half helix is indicated with dashed line). However, the protomers actually aligned along a one-start helix (the centers of the protomers are traced with a zig-zag dotted line); the  $\sim 166^{\circ}$  turn of a monomer relative to the previous monomer around the filament axis is the reason for the long-pitch helix. The rise of the one-start helix is 2.75 nm; the inter-protomer distance along the filament axis is thus  $\sim 5.5$  nm. In one pitch of the two-start helix ( $\sim 72$  nm) thirteen protomers are included. Panel b, a highly schematic representation of the arrangement of the subdomains in the filament structure; for simplicity, the helical feature is omitted and only the two lobes, each consisted of the subdomain II and III or the subdomain I and IV, are drawn. The barbed and pointed ends can be distinguished by the polarity of bound heavy meromyosin (see text and Fig. 7.12) and are labeled in this figure

narrowed upon polymerization, which will decrease the rate of exchange of the bound nucleotide and the divalent cation. According to the reconstruction [31], subdomain II has been found to move most ( $\sim$ 6 Å) upon incorporation of the monomer into the middle of the filament, and other subdomains move to a lesser extent (1–2 Å).

The presence of the structural polarity was first demonstrated by the binding of heavy meromyosin, a proteolytic fragment derived from myosin, to actin filament in the absence of ATP. The actin filament bound by heavy meromyosin possessed a characteristic appearance called arrowhead structure, according to which the pointed and barbed filament ends were distinguished and were named (Fig. 7.12; [32]). A recent electron microscopic study has shown that the tertiary structure of the terminal monomer of the barbed end is slightly distorted, which may be the basis of the distinction between the two ends [33].

7.3 Actin 109



**Fig. 7.12** The distinction between the two ends of actin filament by labeling actin filament with heavy meromyosin, a proteolytic subfragment of myosin. Myosin is partially digested by a proteolytic enzyme (left); the C-terminus part of the tail is cleaved off, and the heavy meromyosin that includes heads and a short tail is generated. Heavy meromyosin is water-soluble and is convenient for test-tube measurements; heavy meromyosin, like myosin, binds strongly to actin in the absence of ATP, hydrolyzes ATP and the rate of the ATP hydrolysis is accelerated by its binding to actin. Under electron microscope, the actin-bound heavy meromyosin forms a tilted projection, which appears as arrowhead (right). The pointed and the barbed ends are assigned as indicated. The direction of the arrowhead should reflect the difference in the structure of the two ends of an actin filament

### 7.3.3 Actin Polymerization and Depolymerization

#### 7.3.3.1 Methods to Measure Polymerization/Depolymerization

Dynamics of polymerization and depolymerization and its regulation by a number of actin binding proteins are highly important aspects in the dynamical changes of the cell. Therefore, quantitative in vitro measurement of the polymerization/depolymerization kinetics of actin has been developed. In the early stage of the study, the degree of polymerization has been measured by several methods such as flow-induced birefringence of actin filament solution [34] and light scattering at 90 degrees [35, 36]. The drawback of these methods is that they are not sensitive to detect the growth of filament in the initial stage of polymerization, where the length of the filament is < ~0.1  $\mu$ m [35]. Liberation of Pi can be also used as an indicator of the progress of polymerization [37], but the time resolution (at most a few seconds) is low. Thus, one needs methodology with high sensitivity to the growth of the filament and time resolution for the estimation of the kinetic parameters. The most common methodology is based on fluorometry, which is highly sensitive to the filament growth with relatively high time resolution. In these methods, actin monomers are labeled with fluorophores such as pyrene [38],

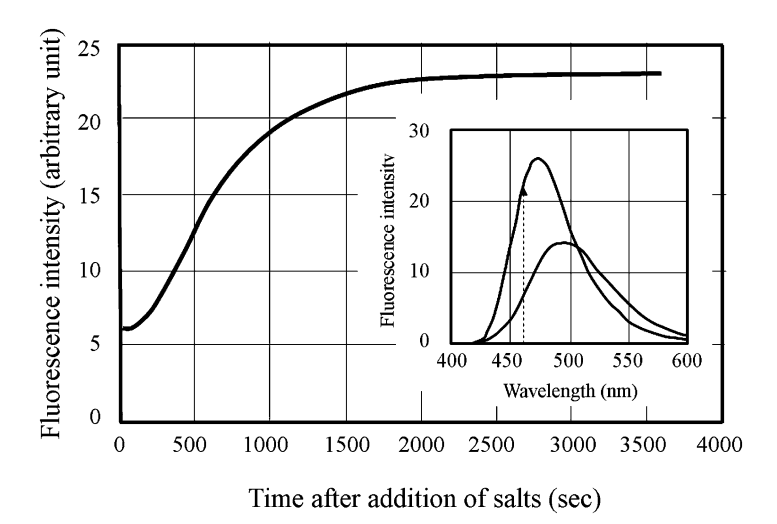


**Fig. 7.13** Polymerization of actin measured with the increase in the fluorescence intensity of prodan. As shown in the *inset*, the emission spectrum of a fluorophore, prodan, bound to the actin actin exhibits a blue shift of the peak and the increase in the quantum yield after the addition of salts (in this case, KCl + MgCl<sub>2</sub>). Thus, the observation at the fixed wavelength (460 nm, dashed arrow in the *inset*) provides the increasing fluorescence signal representing the progress of the polymerization (Miyata, unpublished observation)

rhodamine, [39] or prodan [40]; upon polymerization, those fluorophores are thought to be buried in the interface between adjacent protomers and quantum yield increases several to 10 times. Hence, one can quantify the polymerization kinetics by measuring the increase in the fluorescence intensity (in the case of prodan, the burial of the fluorophore causes the shift of the maximum of emission intensity accompanied by an increase in the quantum yield, both contributing to the increase in the emission intensity; Fig. 7.13).

Electron microscopy has been also employed to measure the polymerization. One may wonder why the technique with rather complex procedure and low time resolution was adopted. However, this technique allowed the investigators to observe individual filaments to analyze the polymerization kinetics at the pointed and the barbed ends separately [41]. To distinguish the barbed end from the pointed end, a nucleus for polymerization was used. The nucleus is prepared by severing the actin filament by sonication and "decorating" (ie., bound) the severed filament with heavy meromyosin to make the "arrowhead" structure (Sect. 7.3.2). The decorated part of the fragment is thicker than the newly elongated filament, which enabled researchers to separately measure the length of the filaments grown from the pointed and the barbed end. The nucleus also serves to facilitate the polymerization by reducing the activation energy required for the spontaneous formation of the polymerization nuclei (see Sect. 7.4). With this technique, it has been shown that the elongation occurred faster at the barbed end. In a later study [42], actin filament bundle isolated from *Limulus* sperm acrosomal process was used, since in the

bundle, which serves as the nuclei, the orientation of actin filaments is uniform. The earliest time point (a few seconds after the start of polymerization) depends on how fast one can prepare the specimen of the electron microscope after mixing the actin monomer with the nuclei. More recently, the technique for observation of single, fluorescently-labeled filaments under fluorescence microscope has been developed, and the rate constant for polymerization/depolymerization kinetics at barbed and pointed ends of the same filament have been separately measured: it turned out that the fast-growing and the slow-growing ends were the barbed and the pointed ends [43]. The rate constants for actin monomer binding ADP, which undergoes reversible polymerization/depolymerization exhibited a remarkable match with those derived from the optical microscopy (see Sect. 7.4).

#### 7.3.3.2 Actin Polymerization and Hydrolysis of ATP

Actin monomer is an ATPase, as mentioned above. It hydrolyzes ATP only once at a rate of ~0.02/sec when it is incorporated into the filament [44]; the product, inorganic phosphate (Pi), dissociates from the filament at ~0.3/s [45]. The other product, ADP, remains bound to the actin protomer; but when the protomer dissociates from actin filament, the ADP bound to the dissociated monomer can readily exchange with ATP in the surrounding medium. If actin monomer loses bound nucleotide, it denatures and becomes polymerization incompetent [46]. Monomer without bound nucleotide is polymerization competent, if a high concentration of sucrose or glycerol is present [46, 47].

In the presence of ATP, the actin monomer and actin filament are in a non-equilibrium steady state because of the ATPase activity of actin (see Sect. 7.5). As mentioned above, the ATP hydrolysis occurs at a finite rate, and hence, if monomer concentration is high, the rate of association of monomer will surpass the rate of ATP hydrolysis, and as a result, several protomers near the barbed end can exist as ATP-bound form [45, 48]. The dissociation of inorganic phosphate from the actin protomer at the filament ends is followed by dissociation of this ADP-binding protomer [43]; in the protomers residing in the middle of the filament, dissociation of inorganic phosphate is 1000 times slower than the filament end [43, 49]. Phosphate binds to actin protomer with a dissociation constant of 1.5 mM [50]. The bound Pi decreases the dissociation rate of the monomer that binds ADP, leading to a decrease in the critical concentration of the barbed and the pointed ends [43, 51]. In in vitro experiment, Pi is often omitted, but in vivo, Pi exists at millimolar concentrations, which will considerably increase the stability of the actin filament against depolymerization [43]. The effect of the type of nucleotide at the ends of the filaments in the nuclei does not seem to be reflected in the elongation rate [42]. This fact simplifies the comparison of the data obtained with the electron microscopy and fluorescence microscopy.

# 7.3.3.3 Structure of the Barbed and the Pointed Ends and Polymerization/Depolymerization

The difference in the polymerization/depolymerization kinetics of actin filament has been interpreted on the basis of the structure of the filament ends [33]. The actin filaments were prepared in the presence of a cap Z protein, which binds to the barbed end of an actin filament and stabilize it against depolymerization. This treatment increases the number of filament with free pointed ends. With this preparation, it was found that at the pointed end, the terminal protomer slightly tilted toward the immediate next protomer and an interaction occurred between two amino-acid loops that extend from each protomer [33]. It has been postulated that this looploop interaction creates a kinetic barrier against the association and the dissociation of the terminal protomer, thereby lowering the rate constants of association and the dissociation. Such strong inter-protomer interaction is not observed at the barbed end, and hence, the rates of dissociation and association of the terminal protomer at the barbed end will be higher than those of the terminal protomer at the pointed end. The slow association of the protomer at the pointed end will lead to the synchronization of ATP hydrolysis with the association of the monomer. On the other hand, as described above, the ATP hydrolysis end lags behind the association of monomer at the barbed, if concentration of monomer is sufficiently high.

#### 7.3.3.4 Actin Polymerization and Metal Ions

In vitro, the purified actin polymerizes in the presence of cations ( $K^+$ ,  $Mg^{2+}$  or  $Ca^{2+}$  ions). As described above, actin monomer possesses one high affinity binding site for  $Mg^{2+}/Ca^{2+}$  ions near the ATP binding site and several binding sites for cations with lower affinity [27]. Upon binding of monovalent cations to these low affinity sites, the electrostatic repulsion between monomers will decrease, facilitating the association of monomer to each other. Divalent cations induce polymerization at much lower concentration than monovalent cations; to polymerize actin, 1 mM Mg $^{2+}$  is sufficient, whereas  $K^+$  ions of tens of mM are required. Under the polymerization condition that is usually adopted in in vitro experiment (a few micromolar of monomer with 1 mM  $Mg^{2+}$  or with 1 mM  $Mg^{2+}$  and 10–100 mM  $K^+$  ions), polymerization occurs on the order of 10 min. Conversely, if monomer concentration is high, even a submillimolar concentration of  $Ca^{2+}$  causes polymerization on a time scale of scores of minutes [36].

### 7.4 Kinetics of Actin Polymerization

The actin polymerization can be regarded as a condensation phenomenon, and it was theorized that the polymerization can be treated as the progress of linear aggregation preceded by the cooperative transition from a small linear precursor to a triple helical aggregate, the nucleus from which the rapid growth of the filament occurs (Fig. 7.14; [52]). As mentioned above, the artificially prepared nuclei will circumvent the initial transition step and only the rapid growth will occur in the presence of nuceli. The measurement of polymerization with pyrene-labeled actin indicated that tetramer prepared by chemically crosslinking monomers serves as a nucleus for polymerization [53].

In the following we describe the actin polymerization with a reversible kinetic model [53, 54]. This treatment does not distinguish the barbed and the pointed end, and hence, it is applicable to the polymerization/depolymerization of actin monomer binding ADP. The "net" rate of actin polymerization *per filament* is expressed as  $k_{\rm on}C - k_{\rm off} = k_{\rm on}(C - k_{\rm off}/k_{\rm on})$ , where  $k_{\rm on}$  (M<sup>-1</sup>s<sup>-1</sup>) and  $k_{\rm off}$  (s<sup>-1</sup>) are the sum of the rate constants of association and dissociation of a monomer to and from the both ends. The quantity, C is the concentration of monomer in solution. When  $C > k_{\rm off}/k_{\rm on}$ , the filament elongates; when  $C < k_{\rm off}/k_{\rm on}$ , the filament shortens at both ends. The value,  $k_{\rm off}/k_{\rm on}$ , is called critical concentration (hereafter, represented with Cc for convenience). In this case, the filament either simultaneously elongates or shrinks at both ends. The existence of Cc implies that an energetic barrier of the transition from linear to helical polymer is reflected in the kinetics of the polymerization.

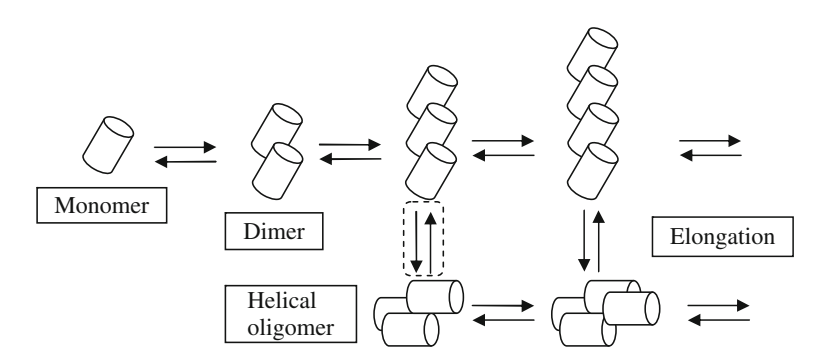


**Fig. 7.14** A proposed model for actin polymerization: condensation-elongation model. The leftmost object represents the actin monomer. In the upper row, growth of linear polymer is represented; in the lower row, helical structure appears after transition of the linear trimer to helical trimer (the step enclosed in the dashed square). The linear-to-helical transition was assumed to be energetically unfavorable. The three-start helical structure has been anticipated from the kinetic study of the polymerization. Free energy change was assumed to be a few kcal/mol. The helical structure is more stable, once formed, because individual monomers interact with two neighbors and the polymer can be more stable than the linear counterpart. (see details for Oosawa and Kasai [52])

We next consider a model in which polymerization and depolymerization rates at barbed and pointed ends are distinguished as  $k_{\rm B}^+$ ,  $k_{\rm B}^-$ ,  $k_{\rm P}^+$ ,  $k_{\rm P}^-$  [55]. The labels represent the association (+) and the dissociation (–) rate constants at the barbed (B) and the pointed (P) ends. The net elongation rate per filament at each end is represented  $k_{\rm B}^+C-k_{\rm B}^-$  and  $k_{\rm P}^+C-k_{\rm P}^-$ . Thus, the critical concentration for the barbed end is  $k_{\rm B}^-/k_{\rm B}^+$  and that for the pointed end is  $k_{\rm P}^-/k_{\rm P}^+$ . The net on-rate is equal to  $(k_{\rm B}^+ + k_{\rm P}^+)C$  and net off rate is equal to  $k_{\rm B}^- + k_{\rm P}^-$ . The elongation or shortening of a filament occurs according to the condition:

$$(k_B^+ + k_P^+) C > (k_B^- + k_P^-) \text{ or } (k_B^+ + k_P^+) C < (k_B^- + k_P^-).$$

Thus, the concentration at which the filament length remains constant is

$$C \equiv (k_{\rm R}^- + k_{\rm P}^-)/(k_{\rm R}^+ + k_{\rm P}^+).$$

At the equilibrium, the detailed balance,  $k_{\rm B}^{-}/k_{\rm B}^{+} = k_{\rm P}^{-}/k_{\rm P}^{+}$  holds and the *C* is equal to the critical concentration at each end;  $C_{\rm C} = k_{\rm B}^{-}/k_{\rm B}^{+} = k_{\rm P}^{-}/k_{\rm P}^{+}$ . In this case also, the filament either elongates or shrinks simultaneously at both ends according to the monomer concentration.

The Cc value depends on the solution condition such as temperature, pH and the type and concentration of cations. It also depends on the type of bound nucleotide (ie., ATP or ADP). The Cc value is estimated from the plot of the amount of polymer or polymerization rate against total actin concentration [43, 52, 56]. The Cc value for actin monomer binding ADP in the presence of 1 mM Mg<sup>2+</sup> and 10 mM K<sup>+</sup> ions has been estimated to be 1.7  $\mu$ M for pointed end and is virtually the same as the value for barbed end (1.9  $\mu$ M) [42]; a direct observation of single filaments revealed that the former value has been estimated to be 1.7  $\mu$ M and the latter to be 1.8  $\mu$ M under similar ionic condition [43]. On the other hand, in the absence of free cations, Cc value is as high as 100  $\mu$ M.

# 7.5 Treadmill Phenomenon: Actin Polymerization Under the Non-equilibrium Condition

As described above, in the presence of ATP, the critical concentration at barbed end ( $Cc_{\rm B}=0.12~\mu{\rm M}$ ) is lower than that at the pointed end ( $Cc_{\rm P}=0.62~\mu{\rm M}$ ); this inequality is due to the ATP hydrolysis by actin protomer [42]. In the steady-state in which the concentration of unpolymerized actin remains unchanged (see the main graph of Fig. 7.13, in which the plateau of the fluorescence is shown); if the ATP concentration is maintained, the critical concentrations at the two ends remain different. This is because of the difference in the kinetic parameters, which yields different ratios of the on-rate to off-rate at each end. As a result, when  $Cc > 0.62~\mu{\rm M}$ , filament elongates at both barbed and pointed ends, whereas  $Cc < 0.12~\mu{\rm M}$ , filament shortens at both ends, but at a concentration between these two limiting values, the

rate of elongation occurring at the pointed end and that of the shortening occurring at the barbed end can be equal. If one assumes that the dissociation occurs with ADP-bound protomer and the association occurs with ATP-bound monomer, this occurs at

$$C_0 = (k_{BD}^- + k_{PD}^-)/(k_{BT}^+ + k_{PT}^+)$$

[55]. Parameter values estimated from the electron microscopy yield 0.58  $\mu$ M for  $C_0$  value. As far as this monomer concentration is maintained, the length of the filament remains constant. The actin monomer at  $C_0$  associates with the barbed end, because  $C_0 > Cc_B$ , and dissociates from the pointed end, because  $C_0 < Cc_P$ . As a result, the distance between the incorporated monomer and the barbed end increases with time; in other words, the monomer "travels" away from the barbed end and eventually "reaches" the pointed end and dissociates. This unidirectional shift in the position of the actin monomer from the barbed end to the pointed end is called "treadmilling" (Fig. 7.15). The kinetical asymmetry of actin polymerization/depolymerization is not merely a test-tube phenomenon, but it is assumed to be a basis for the turnover of actin filament and maintenance of the actin network in lamellipodia. It should be noted, however, that the rate of the treadmilling alone is insufficient to support the lamellipodial protrusion (Sect. 7.14).

It has been suggested that within the filament, the mode of interaction between the ADP-binding and ATP-binding protomers may not be greatly different from that between ATP-binding monomers, because the rate of ATP hydrolysis by the protomer adjacent to the ADP-binding protomer is not more than 10 times faster than the rate by the protomer adjacent to the protomer binding ATP [56]. More recent study has suggested at most several times difference between the association/dissociation kinetic parameters of the ATP-bound actin protomer in the filament polymerized from ATP-bound monomer and those of ADP-Pi-bound protomer in the filament polymerized from ADP-Pi-bound monomer [43]. This implies that the

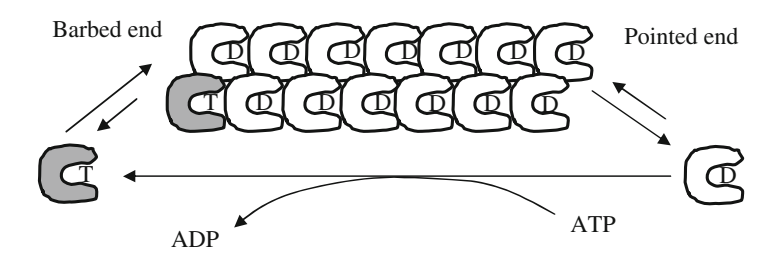


**Fig. 7.15** Treadmilling of actin monomer in an actin filament in the presence of ATP. In the presence of ATP, actin polymerization predominantly occurs at the barbed end, while the depolymerization occurs at the pointed end due to the different critical concentration for each end (see text). At an appropriate monomer concentration, the rates of the polymerization and the depolymerization are balanced, and hence, the length of the filament remains constant. However, at the barbed end, polymerization of the ATP-binding monomer (gray figure) continues, whereas at the pointed end, depolymerization of the ADP-binding protomer occurs. As a result of this, the distance between the barbed end and the terminal protomer initially bound to the barbed end increases with time under the constant length of the filament

structure of the ATP-bound protomer and ADP-Pi-bound protomer are not altogether the same.

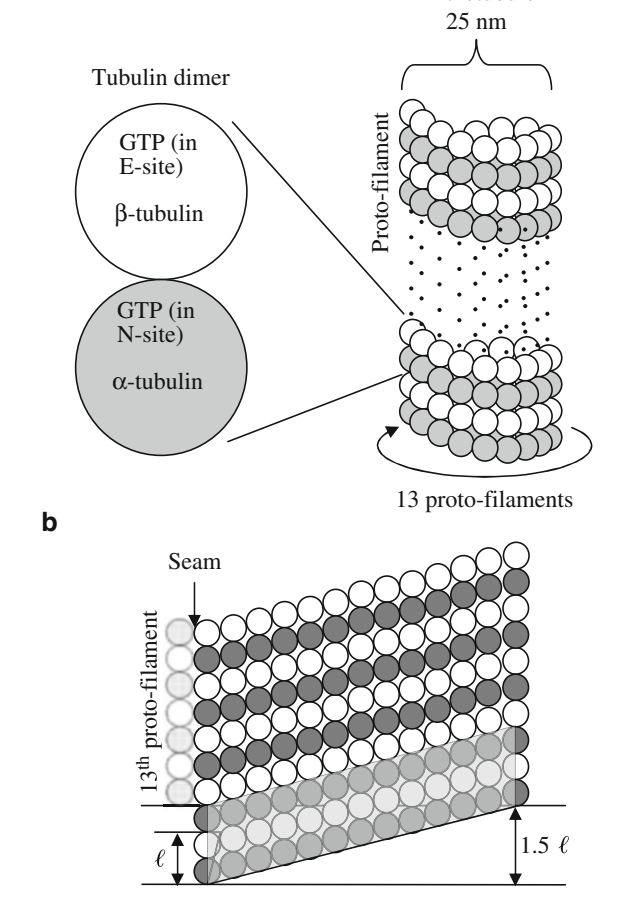
#### 7.6 Microtubule

### 7.6.1 Structure of Microtubule

Microtubule is a hollow cylinder and is much thicker than actin filament (outer diameter:  $\sim$ 25 nm as compared with  $\sim$ 7 nm for an actin filament). A microtubule is consisted of equal number of alpha and beta tubulins: the two types of tubulins are structurally very similar [57] and form a heterodimer that behaves as a unit in the process of binding to and dissociation from the microtubule. The approximate dimension of the heterodimer is 8 nm  $\times$  4.6 nm  $\times$  6.5 nm [58]. As shown in Fig. 7.16a, in a microtubule, the heterodimers make head-to-tail association with

а

**Fig. 7.16** The schematic representation of a structure of a tubulin dimer and a microtubule. Panel a, left, a tubulin dimer (alpha-tubulin is in gray and the betatubulin is in white); right, the dimers form a protofilament and 13 protofilaments are aligned in parallel to form a hollow cylinder. Panel b, The rise of the 3-start helix (the shaded parallelogram) is 1.5 times *l*, which is the size of the heterodimer. As a result, the lateral alpha-to-alpha or beta-to-beta contact between adjacent proto-filaments is disrupted at the contact between the first and the 13th proto-filament, and the alpha-to-beta contact is formed. This type of contact formed between the 1st and the 13th filaments is called seam



Microtubule

7.6 Microtubule 117

each other, forming a linear chain called protofilament. Thus like actin, microtubule has a structural polarity; beta tubulin lines at one end and alpha tubulin at the other end. At the end of a protofilament exposing alpha tubulin, a beta subunit of a heterodimer binds, whereas at the opposite end exposing beta tubulin, to which alpha subunit in the heterodimer binds. The number of protofilament in a microtubule varies between 10 and 15, but in the cell that is 14. When microtubule is grown in vitro from a nucleus (a natural seed for polymerization, which is isolated from protozoa such as *Chlamidomonas*), the number is 13 (see [59] for details).

In the microtubule consisted of 13 protofilament, 3-start, left-handed helices can be recognized, as shown in Fig. 7.16b (shaded parallelogram). A tubulin in one protofilament makes a contact with the tubulin of the same type (ie., alpha with alpha or beta with beta) in the adjacent protofilament. However, since the rise of the 3-start helix per turn is 1.5 times the length of the dimer, *l*, the alpha and beta tubulin in the 13<sup>th</sup> protofilament each makes contact with different type of tubulin (ie., beta and alpha) in the first protofilament. The contact thus formed along the microtubule is called seam. In the case of 13 protofilaments, each protofilament is straight so that the organelles transported by motor proteins walk on the same side of the microtubule [60].

### 7.6.2 Microtubule Polymerization and Depolymerization

#### 7.6.2.1 Basic Properties

A study on the polymerization of tubulin heterodimer has demonstrated that the polymerization needs rather high temperature (37 °C; [61, 62]); at 0 °C it depolymerizes [63]. Actin polymerization does not exhibit such a strong dependence on temperature. The degree of polymerization has been estimated from the amount of tubulin that is pelleted by centrifugation (the plot of the amount of the pelleted protein vs. total protein will provide empirical *Cc* value as the amount of protein below which no pelleted polymer exist [64]). For the kinetic measurement of polymerization, direct observation of individual microtubules by light microscopy (differential-interference or dark-field) has been employed (see Sect. 7.6.3).

The critical concentration of tubulin heterodimer varies with the solution condition, especially with the temperature in the case of microtubule as mentioned above. Typical values have been measured at 37 °C to be ~5  $\mu$ M for both ends [65]. The existence of critical concentration suggests existence of energetically unfavorable step in the polymerization. Electron microscopic study of polymerizing microtubules revealed that the protofilaments at the end of microtubule are aligned as in a microtubule, but making an open, sheet-like structure with outward curvature. This is thought to reflect the structural feature of the heterodimer [59, 66]. Polymerization would have to proceed with the closure of the sheet, but this requires transition of the sheet with outward curvature to more straight form that fits the microtubule cylinder. It is likely that between these two conformations exists an

energetic barrier [67]. After the polymerization the microtubule stores the curvature elastic energy, which seems to be utilized in the depolymeization process accompanying the restoration of the curved protofilaments [61] and also in the chromosomal movement [67–69]. One would expect that the seam plays some special role in the initiation of the depolymerization, but this point remains to be studied [57].

#### 7.6.2.2 The Role of GTP in Microtubule Polymerization

Each tubulin binds one GTP molecule. As shown in Fig. 7.16, the GTP molecule bound to alpha tubulin is "covered" by the beta tubulin, and remains bound to the same site as GTP. Thus, the GTP binding site of alpha tubulin is called N (non-exchangeable)-site. On the other hand, the GTP bound to the beta tubulin is hydrolyzed to GDP by catalytic action of the side chain of Glu254 of alpha tubulin in the adjacent heterodimer in the same protofilament. The GDP thus formed exchanges with the solution GTP after the heterodimer dissociates from the microtubule. Thus, the GTP binding site on beta tubulin is called E (exchangeable)-site.

In vivo, the energy liberated by the hydrolysis of GTP is ~30 kJ/mol [59]. But the polymerization does not require hydrolysis of GTP, because heterodimer binding non-hydrolyzable GTP analog, GMP-CPP, can polymerize [67]; if the beta tubulin binds GDP at E-site, the heterodimer is not polymerizable. The GTP hydrolysis in microtubule dynamics has been related to the change in the intrinsic curvature of a tubulin heterodimer. As a result of hydrolysis at the E-site, majority of heterodimers in a microtubule bind GDP at the inter-heterodimer interface. Thus, the outward curvature of the protofilament becomes apparent during the depolymerization (the protofilaments exhibiting outward curvature before they fall apart [61]). This curvature should stem from structural features of the heterodimer; it may reflect the intrinsic curvature of heterodimer binding GDP, or may be specific to the heterodimer without interaction with adjacent heterodimers in the microtubule lattice. A study has shown that the latter is the case [69]. The mode of the interaction between heterodimers seems to be essential for the curvature of the protofilament. A polymerized microtubule stores an elastic energy.

Upon polymerization of a heterodimer, GTP bound to the E-site is hydrolyzed, as described above. Like actin polymerization, when the heterodimer concentration is low, GTP hydrolysis occurs at the same rate as the polymerization of heterodimer, but when the heterodimer concentration is high, GTP hydrolysis lags behind the polymerization. As a result, the end of microtubule is occupied by a GTP-cap, the accumulation of heterodimers binding GTP on beta subunit. It has been suggested that the length of the cap can be as small as one layer of heterodimer [66]. The GTP cap plays a central role in the dynamics of polymerization/depolymerization (see Sect. 7.6.4). A study using antibodies against the tubulin that binds GTP has demonstrated that majority of the antibodies binds to the growing end of microtubules [70].

7.6 Microtubule 119

# 7.6.3 Dynamic Instability: Different Behavior of Plus and Minus Ends in Polymerization/Depolymerization Episode of Microtubule

Observation of microtubules that grew from isolated centrosomes (serving as nuclei for polymerization) demonstrated that those microtubules are divided into growing and shortening populations, in the *same* solution [71]. Thus, although as a whole, microtubules are either in a growing or a shortening phase, individual microtubules independently grow or shorten. This remarkable phenomenon has been called dynamic instability [72].

The dynamic instability results from the fact that the two ends of a microtubule are not equivalent as in the case of actin. The two ends behave independently during a polymerization/depolymerization episode. This was confirmed by the observation of the polymerization/depolymerization events at each end simultaneously. The nuclei prepared by binding dynein to microtubules, or a protein complex called axoneme that had been isolated from sea urchin sperm were used. By dark field microscopy [73] or differential interference contrast microscopy [65], researchers could confirm the independent nature of the dynamics of the two ends of a single microtubule.

Comparison of the elongation and shortening events at each end has shown that the rate of elongation was several times slower than the rate of shortening. As described above, this is because the shortening is accelerated by the elastic energy stored in the microtubule. The association and dissociation rate constants at two ends of microtubule as estimated by direct observations [65, 71, 74] and it has been demonstrated that at one end the elongation occurs faster and over a longer distance than the opposite end. The off-rate constant of the faster-growing end is smaller than that of the slow-growing end. This makes the former end look much more active than the opposite end; the more active end has been called "plus" end and the opposite end "minus" end.

# 7.6.4 Catastrophe and Rescue

As described above, in the dynamic instability, an elongation phase is followed by a shortening phase and vise-versa. The switch from the elongation to the shortening phase is called "catastrophe", and the switch from the shortening to the elongation phase is called "rescue". The catastrophe is thought to occur as a result of GTP hydrolysis: once GTP in each tubulin is hydrolyzed, the inter-protofilament interaction becomes weakened and the microtubule lattice destabilized by the outward curvature of protofilaments (see the previous section), leading to the catastrophe. The frequencies of catastrophe and rescue at plus ends are on the order of  $10^{-3}$ /sec at  $15-16~\mu$ M heterodimer [65, 74]; the catastrophe rate decreases and the rescue rate increases with the increase in tubulin concentration as one would expect.

The polymerization and depolymerization rates are modified greatly by the binding of microtubule associated proteins (MAPs). For example, the presence of MAP-2 stabilizes the polymer by decreasing the frequency of disassembly [75]. Dark-field microscopy combined with epi-fluorescence microscopy of microtubules that was decorated with fluorescently labeled MAP-2 demonstrated that at a low concentration of MAP-2 formed discrete clusters along the microtubule; based on this characteristic distribution of bound MAP-2, it has been suggested the rescue probability significantly increases at the positions of MAP-2 clusters [76]. Thus, the clusters will decrease the shortening length. The GTP-bound tubulin specifically labeled with the antibody demonstrated that GTP-tubulin exists not only at the plus end but also in the middle of microtubule. It has been hypothesized that the GTP-bound tubulins in the middle of microtubule participate in the rescue event [70].

### 7.7 Cell Motility

The movement of the cell has been a central theme in cell biology. Cell movement is important for all living organisms. For example, amoeba cells move in the soil to search for food; nerve cell extends a long process called axon during the formation of neuronal network; wound such as a cut in a skin will be repaired by the migration of cells of the skin to fill the wound. Cells move in a controlled manner during the development of multicellular organisms; the uncontrolled movements (e.g., loss of contact inhibition) of cancer cells are the essence of metastasis. In vitro, cells adhere to surfaces of culture dish or microscope slide and crawl on these substrates. How cells crawl can be easily observed from the top by light microscopy (Fig. 7.17a). The observation of the side view of amoeba cells crawling on the surface of glass rod has demonstrated that in the crawling movement the front edge is first extended and then, it adheres to the surface. This is followed by the retraction of the rear of the cell as a result of the contraction of cell body while the front part remains attached. The cell moves forward by repeating these three steps (Fig. 7.17b; [77]).

The speed of the movement of the cell varies from < 1  $\mu$ m/h to a millimeter per hour, depending on the cell type [78, 79]. Fibroblast usually moves slowly and the event of extension and that of the rear retraction occur with different timings, whereas in fast moving fish keratocyte the three activities is probably coordinated so that the cell moves without appreciable change in its shape [79]. However, as shown in Fig. 7.17a, even fibroblast moves over a short period of time with little change in the shape. In this case, the coordinated movements of the protrusion and the retraction can occur.

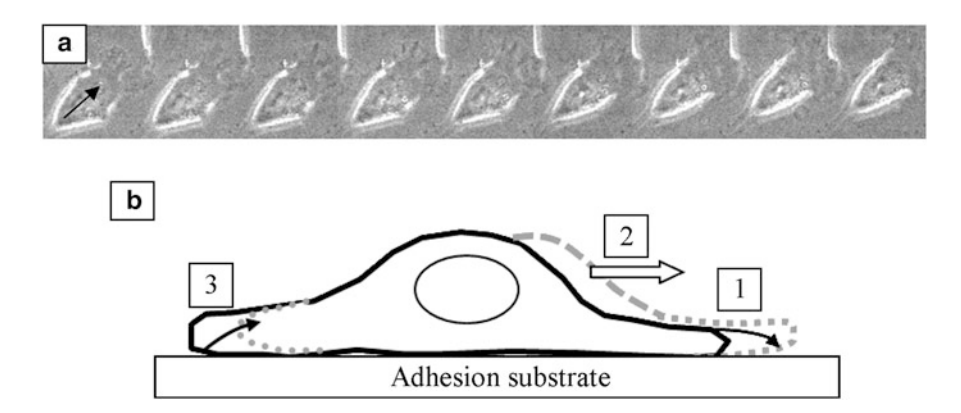


Fig. 7.17 An example of a moving cell and three basic steps of cell motility. Panel a, a fibroblast crawling in the direction shown by the black arrow in the leftmost panel. In this example, the cell moved at fairly constant speed of ~0.2  $\mu$ m/min. Panel b, three steps in the crawling motion of the adherent cell; step 1, extension of the cell front (lamellipodiun) followed by its adhesion to the adhesion substrate; step 2, contraction of the cell body while the front edge is firmly attached to the adhesion substrate by the cell adhesion molecules; step 3, retraction of the rear of the cell. These steps are repeated and the cell moves toward right. (Panel a: phase contrast micrographs taken by Sogo Khomoto, Department of Physics, Tohoku University)

### 7.8 Extracelluar Matrix and Its Connection to Cytoskeleton

Cells produce and secrete proteins that form an extracellular network structure called extracellular matrix (ECM; [80]). The ECM serves as the basis for the adhesion of the cell to the surrounding cells or tissues, or structures such as the surface of a culture dish. The binding of the cell to ECM is mediated by integrin, a family of transmembrane protein. Integrin is a heterodimer of alpha- and beta-integrins. There are many different alpha and beta integrins, and hence, there are a number of combinations of alpha and beta-integrins. There are also many types of ECMs; for example, fibronectin, collagen and laminin. The combination of alpha- and beta-integrin basically determines the partner ECM, for example alpha-5 beta-1 integrin heterodimer binds to fibronectin [81]. Interestingly, specific combination of alpha- and beta-integrins determines the partner cytoplasmic proteins that interact with the integrin heterodimer [82]. Thus, the integrin heterodimer bidirectionally transmit the information of the extracelluar binding event and the intracellular events [83, 84]. The ECM-cytoskeleton connection plays an essential role when the cell attaches its front part to substrate to pull the rear part by contraction.

#### 7.9 Cell Membrane and Membrane Skeleton

As described in Chap. 4, the basis of the cell membrane is a lipid bilayer. The lipid bilayer itself is a highly flexible entity: its bending rigidity is on the order of  $10^{-19}$  J, allowing thermal fluctuations [85]. It should be noted that the tensile strength of the

lipid bilayer membrane is on the order of 10<sup>-3</sup> N/m with maximum extensibility of a few percent. Thus, the lipid bilayer is rather like a cloth than a rubber sheet. The cell membrane is lined by a network structure called membrane skeleton. For example, red blood cell membrane is lined by a highly regular network made of a protein called spectrin [86]. Interestingly, the mechanical measurement has revealed that the bending rigidity of the red blood cell membrane is similar to that of pure lipid membrane [87]. This may be because the spectrin network is a highly flexible entity ([88]; see below).

The spectrin network is composed of spectrin and short actin filaments. Spectrin is a heterodimer of alpha- and beta-subunit [89]. An alpha (a beta)-subunit in one heterodimer binds to a beta (an alpha)-subunit of another heterodimer, and hence, two heterodimers make a spectrin tetramer. The spectrin tetramer assembly is then tied to the membrane by binding to a protein called ankyrin, which is then bound to a transmembrane anion exchanger protein (band 3). Several heterodimers bind to a short actin filament and a protein called band 4.1 to form spectrin/band 4.1/actin junction. This protein complex is then tied to the cell membrane through a number of transmembrane proteins. Thus, to the cytoplasmic side of the membrane of a red blood cell, the spectrin-based network structure is firmly attached. The network is most clearly seen in the plasma membrane isolated from red blood cell, which is literally a net when it is viewed under the electron microscopy [86, 90].

In animal cells, actin filaments make another type of membrane skeleton [91]; this skeleton is closely (~10 nm) attached to the whole plasma membrane, sandwiching the spectrin membrane skeleton [92]. It has been demonstrated that two populations of actin filaments exist in the membrane skeleton, which are distinguished by their length. The growth of the longer filaments was induced by an actin-nucleating protein called formin, while the shorter filaments were induced by a protein complex called arp2/3 that also is an actin nucleating protein (see Sect. 7.15). The longer filaments seem to provide the plasma membrane with more mechanical strength than arp2/3-nucleated actin filements [93].

With the lining, the lipid membrane is expected to become stronger against mechanical deformation. However, as mentioned above, the bending rigidity of the red blood cell membrane is not very much higher than the pure lipid bilayer membrane [87]. This may be because of the highly compliant nature of the spectrin network, as revealed by direct pulling of the isolated spectrin network [88]. In addition, the coupling of the spectrin network to the lipid bilayer may be weak in the plane of the membrane, and the two structures may respond to the external force almost independently. If this is the case, the bending rigidity may not be much greater the sum of the rigidity of the two structures. Since red blood cells must pass through narrow capillary vessels, their membrane structure might result from the compromise between the deformability and mechanical strength.

# 7.10 Lamllipodia and Filopodia: Protrusive Membranous Structures of the Cell

The cell suspended in solution and not attached to a surface is spherical, because of the lateral tension in the plasma membrane [94], but the adhered cell spreads on the surface attaining flat morphology. In the initial stage of the spreading, the cell assumes isotropic, round shape. Later, cell shape becomes more polarized (Fig. 7.18a, b). Early in this process the cell produces a number of thin membranous protrusions (lamellipodium), which appear along the whole cell edge. Lamellipodium is a thin veil-like protrusion formed along almost entire cell periphery (Fig. 7.18a). Its typical dimension is: 100-200 nm thick, several to 10 microns wide and a few microns deep. It contains a crisscrossed meshwork of actin filaments, in which actin filaments are crosslinked by actin-crosslinking proteins such as ABP280, filamin and alpha-actinin [90, 95]. In a fibroblast cell lamellipodium extends from any location of cell periphery at a velocity of ~1 µm/min over 1 min. It often retracts. This protrusion/retraction activity is especially prominent during the cell spreading process. Amoeba or neutrophils, which move around considerably faster than fibroblasts, extend another type of protrusion called pseudopods towards the chemoattractant molecules [96]. The pseudopod is much thicker than lamellipodium but also contains actin filament network. Another membranous protrusive structure is a filopodium. Filopodium is a finger-like protrusion and is ~100 nm thick, a few microns long. It contains a bundle of actin filaments (Fig. 7.19,

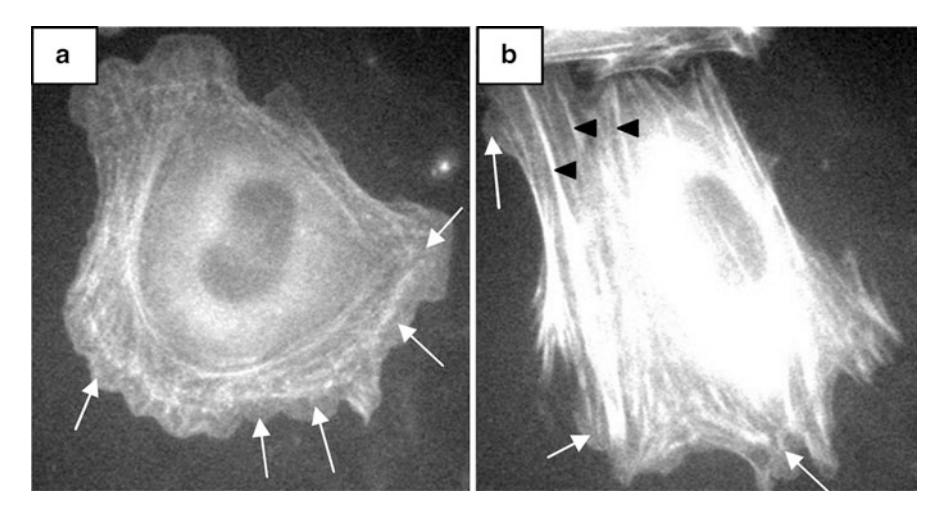
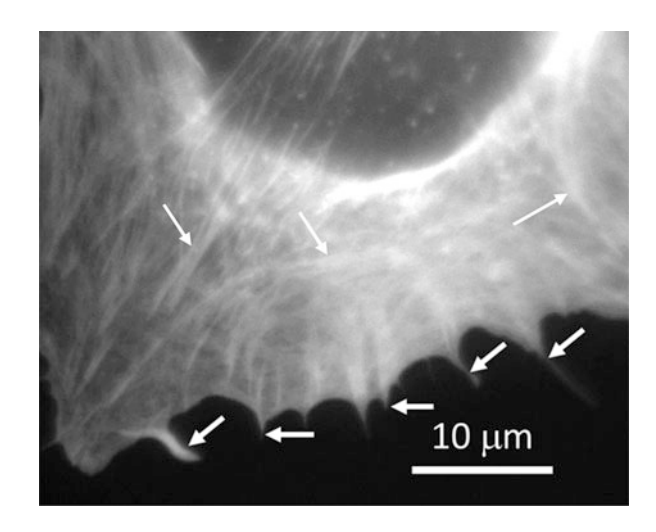


**Fig. 7.18** Spreading and polarization of a fibroblast cell. Panel a, a Swiss 3 T3 fibroblast 1 h after the adhesion to a glass surface. Bar, 20 µm. Panel b, the same cell after 5 h. Initially, the cell formed a numerous lamellipodia, thin, veil-like structures protruded toward every direction (white arrows). Later, the cell became polarized with most lamellipodia residing in upper left and lower right of the cell (arrows); a number of stress fibers (black arrowheads) were formed. (Fluorescence micrographs by Yosuke Senju, Department of Physics, Tohoku University)

Fig. 7.19 Fluorescence micrographs of actin filaments along the periphery of a Swiss 3 T3 fibroblast cell. Actin filaments were stained with rhodamine-conjugated phalloidin, Filopodia penetrating a lemellipodium are indicated with arrows. Filament bundles are indicated with thin arrows. (Fluorescence micrographs by Daisuke Nobezawa, Department of Physics, Tohoku University)



white arrows). As in lamellipodium, the barbed ends of individual filaments are facing toward the tip of filopodium. Like lamellipodium, filopodium also dynamically extends and retracts from the cell edge. The rate of filopodium extension has been measured to be  $\sim 1 \mu m/min$  [97].

Lamellipodia and filopodia seem to cooperate with each other during the movement of the cell. For example, in the neuronal cell, the growth cone resides at the front end of a neurite, a long process extending out of the cell body [90]. The growth cone has a fan-like lamellipodium and drives the extension of the neurite. The growth cone is penetrated by a number of long filopodia [98]. Similar feature also observed with fibroblasts. During the neurite extension, filopodia play a significant role of pathfinding through the search for signaling molecule and attachment to the substrate [99, 100]. Filopodia serves as a pathfinder it first extends and attaches to the surface. If myosin moving on the actin bundle is bound to the cell membrane, this movement will drive the extension of lalmellipdium [101]. This mechanism has also been a candidate for the mechanism of the extension of lamellipodia (Sect. 7.16).

#### 7.11 Actin Stress Fiber and Focal Adhesion

In non-muscle cells actin filament bundles are formed by actin bundling proteins such as alpha-actinin. Alpha-actinin bundles actin filaments in anti-parallel fashion [102]. Upon interaction with bipolar myosin II filaments, the actin bundles form a muscle-like, inter-digitated structure. This structure is called stress fiber (Fig. 7.18b, black arrowheads; Fig. 7.20 for schematic representation). They are so called because they are contractile and generate a tension. In the stress fiber, actin filaments are bound by tropomyosin [103]. Tropomyosin does not play a regulatory role, but increases the stability of the filament against depolymerization. The contractile

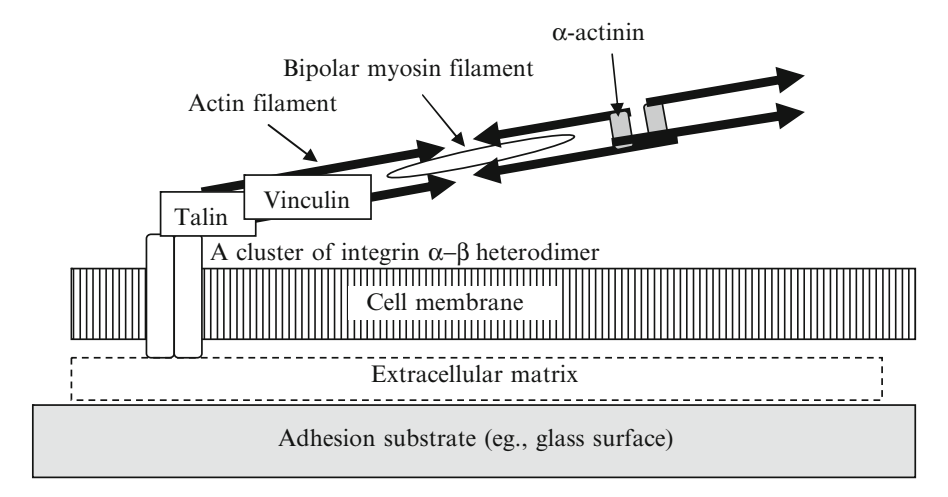


**Fig. 7.20** A highly schematic representation stress fiber and a focal adhesion. One end of the stress fiber is attached the focal adhesion from which actin polymerization and hence, the growth of the stress fiber occurs. The detail of the growth has not been elucidated, but two major processes have been proposed (Hotulainen and Lappaleinen [103], see text). The resultant actin filament is represented with arrows, which also indicates the direction of the contraction upon the generation of the contractile force by myosin filament, as in muscle contraction

forces generated by the stress fiber are utilized in many processes such as cell adhesion (development of the adhesion) or crawling (contraction of the cell body). The similarity among the constituents between muscle and the contractile nature of the stress fiber has suggested that the stress fiber is a prototype of muscle [105].

Within the cell, stress fibers are linked to the cluster of integrin heterodimers. The integrin cluster plays a central role in forming a specialized structure called focal adhesion. As described before, the extracellular partner of the integrin heterodimer varies according to the combination of alpha- and beta-integrin. For example, alpha-5- beta-1-integrin binds to an extracellular matrix protein, fibronectin. The binding alters the conformation of integrin and as a result, the intracellular signaling pathways are activated [83, 84]. This leads to the formation of stress fibers [105].

The cytoplasmic domain of integrin is linked to stress fiber through a protein called talin (see next paragraph). Other proteins residing at the focal adhesion include kindlin, vinculin and focal adhesion kinase, to name a few ([105–107]). The growth of the actin filament from the focal adhesion is promoted by the actin-nucleating protein, formin, which is activated by a small GTPase, cdc42 (Sect. 7.15) and nucleates the polymerization at the barbed end [108]. This activity of formin localizes to the site of polymerization at the barbed end. As a result, the filament grows from the focal adhesion toward the pointed end (the bold arrow in Fig. 7.20 schematically represents an actin filament with the direction from the barbed to the pointed end). This filament is bridged by the bipolar myosin filament to another actin filament that grows in the opposite direction from another focal adhesion The resultant structure allows the contraction of the stress fiber. The stress fiber is also

formed by bridging the actomyosin bundle grown from the focal adhesion to the actin bundles formed beneath the upper surface of the cell [104, 109, 110]. Formation of the bundle structure of filaments with opposing orientation is achieved by alphaactinin.

The focal adhesion bears the tension generated by the stress fiber. Interestingly, this tension is necessary for the maintenance of the stress fiber itself [111]. This interesting property has led to a suggestion that the contractile force acting within the actin network gathers actin filaments [112]. In a number of studies (eg., [113]), application of a uni-axial force to the cell aligns actin filaments along the force axis to generate a fibrous bundle-like actin structure. The decreased ATPase activity (corresponding to the contractile force) of myosin II by inhibitors resulted in the loss of fibrous structure, whereas removal of inhibitors resulted in the re-appearance of the fibrous structures. Thus, the external force plays important roles in the stress fiber maintenance and formation. In particular, it enhances the linkage of actin filament to integrin cluster; talin, an actin-crosslinking protein, makes a weak bond with actin filament, but under the external force, it undergoes a conformational change and becomes able to bind to another protein, vinculin, that also binds to actin filament, establishing more stable contact between the actin filament and the integrin cluster ([114] and references therein). Second, the external force recruits another protein, zyxin, to focal adhesion and in the middle of the stress fiber [115]. It is hypothesized that zyxin is activated by the external force and then recruits a protein, Ena/VASP, to the focal adhesion and to the middle of stress fiber. Ena/VASP mediates the extracellular signal to nucleation of actin polymerization by binding to both receptor and the nucleator for the polymerization [116]. For the sensing of the external force, mechano-sensing protein(s) has been postulated to localize to stress fiber and focal adhesion to which zyxin is bound [115].

Contraction-competent stress fiber has been isolated [104], indicating that the stress fiber is an independent entity. On the other hand, it has been shown that fluorescently labeled actin is rapidly incorporated into pre-existing stress fiber [117] and that fluorescently-labeled alpha-actinin constantly exchanged [118]. The rapid turnover of actin in stress fiber and the stability of the stress fiber seem to be difficult to reconcile, but the latter may be because of the use of low ionic strength buffer devoid of ATP, under which actin-myosin interaction is strong and stabilized the isolated bundle structure.

# 7.12 Actin Filaments in Lamellipodium and Lamella

Fluorescent staining of cellular actin demonstrated that there are two major staining patterns in the cell: uniform staining that is prominent in lamellipodia and streaks penetrating through the uniform staining (Fig. 7.19 and 7.21a). The former is thought to represent an actin filament network in lamellipodium and the latter the stress fiber/bundle continuing to the filopodium. Intracellular myosin II visualized by immunofluorescence microscopy, as shown in Fig. 7.21b, is found to distribute in

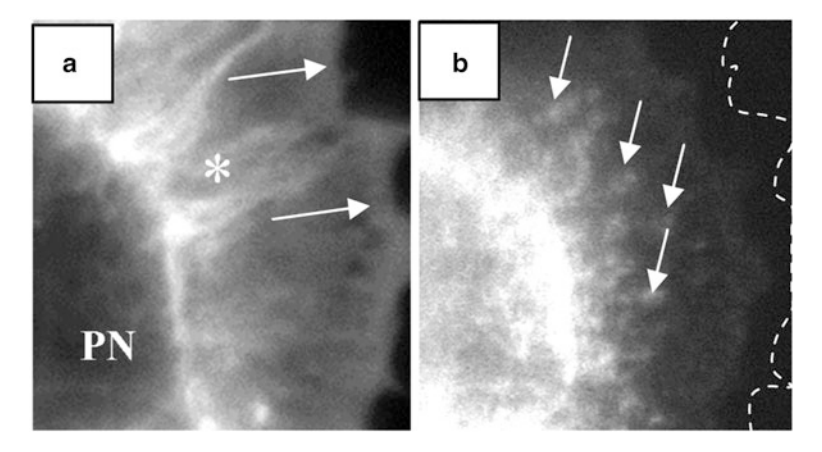


**Fig. 7.21** Comparison of the distribution of actin and myosin in the same mouse fibroblast. Panel a, A fluorescence micrograph of a fibroblast cell fluorescently stained for actin filaments with rhodamine-conjugated phalloidin. White arrows indicate lamellipodia region. The asterisk indicates the lamella region. "PN" indicates the perinuclear region. Panel b, The same region of the cell, but stained for myosin: the spots (arrows) probably represent myosin filaments. The boundary of the lamellipodium is indicated with a white dashed line. It is apparent that the staining pattern of myosin is different from actin: the myosin does not appear in lamellipodia, but colocalize to the lamella region with actin filaments

dot-like patterns in the region behind the lamellipodium. This region is called lamella [95, 119, 120]. As mentioned above, myosin II forms a bipolar filament and almost exclusively resides in lamella region [95, 119]. The meshwork of actin filaments in lamellipodium is thought to be formed by crosslinking activity of a protein called ABP (actin binding protein) and filamin. These proteins are consisted of two flexible subunits and crosslinks two actin filaments in diagonal fashion [121]. The absence or scarce distribution of myosin II in lamellipodia is consistent with a notion that if the myosin II-based contraction occurs in lamellipodia, the protrusion will be hampered. Hence, the contraction of actin-myosin II system does not seem to serve as the mechanism of the protrusion of lamellipodia. Nevertheless, a mechanism involving contractile activity has been proposed (see below).

# 7.13 Actin Polymerization and Lamellipodial/Filopodial Protrusion

In a lamellipodium actin filaments are oriented with their barbed ends facing toward the lamellipodial edge. The consensus is that the actin network grows toward the lamellipodial edge [122–124], which is the same as the direction of the extension of lamellipodia. Growth of actin filaments occurs immediately beneath lamellipodial edge, suggesting that the lamellipodial extension is driven by a local polymerization event. This notion is supported by the observation that the protrusion of lamellipodia

is halted when the growth of actin filaments is inhibited by cytochalasin, a mold toxin that binds to the barbed end of actin filament and blocks the turnover of actin there [125, 126]. Based on this observation and the absence of the myosin II in lamellipodium, it has been postulated that the growing actin filaments push out the membrane. The flexible nature of individual actin filaments seems to be impossible to be reconciled with this notion, but the mechanical weakness is probably compensated by the existence of the large number of the cross-linked filaments immediately beneath the lamellipodial edge as schematically shown in Fig. 7.22a [124, 127].

In the case of filopodium, the extension occurs at the structure called tip complex that resides at the tip of filopodium. In the tip complex, nucleation of actin polymerization at the barbed end is promoted by the actin-nucleating protein, formin that enables the pre-existing filament incorporating actin monomer albeit the presence of an acitn-sequestering protein. The activity of formin is under the control of a small GTPase called cdc42 [128].

### 7.14 Actin Turnover in Lamellipodium

In fast-moving cell like keratocyte, the protrusive growth of lamellipodia should be fast, if the protrusion is intimately coupled to the growth of the actin filament. For example, if a keratocyte moves at ~20  $\mu$ m/min [129], the rate of protrusion is the same, because in keratocyte moving without changing its shape, the velocity of protrusion is the same as that of the tail retraction. Assuming that the protrusion is driven by actin polymerization, the rate of the elongation of actin filaments along the direction of the extension of the lamellipodial edge is also the same as the moving velocity. Then, the rate of the addition of monomer to individual filament should be ~100 monomer/s (individual filaments are impinging on the edge at angles around 50 degrees; modal value measured in fibroblast; [130], but this will not quantitatively change the conclusion here).

In this situation, the actin monomer concentration should be high in the vicinity of the cell edge. Synthesis of actin is probably too slow to achieve the high concentration [131]. Thus, the supply of actin monomer must come from the actin network. It is known that the actin filaments in the network depolymerize at the rear of the network. Therefore, the actin monomer generated by depolymerization is likely to contribute to the supply of actin monomer. Still, the intrinsic rate of depolymerization in the intracellular ionic condition is too slow (7.6 monomer per second; [42]). Cell utilizes two strategies to circumvent this problem. One is to accelerate the depolymerization at the pointed end. This is achieved by a combination of the severing of actin filaments by weakening the inter-protomer binding in the filament (see below) at the back of the network and the capping of some barbed ends by a capping protein in the vicinity of lamellipodial edge. The severing will increase the number of pointed ends, and hence, increase the number of the dissociating monomer. The dissociated monomer is sequestered by monomer sequestering proteins such as thymosin beta-4 and profilin to prevent the re-polymerization. The capping

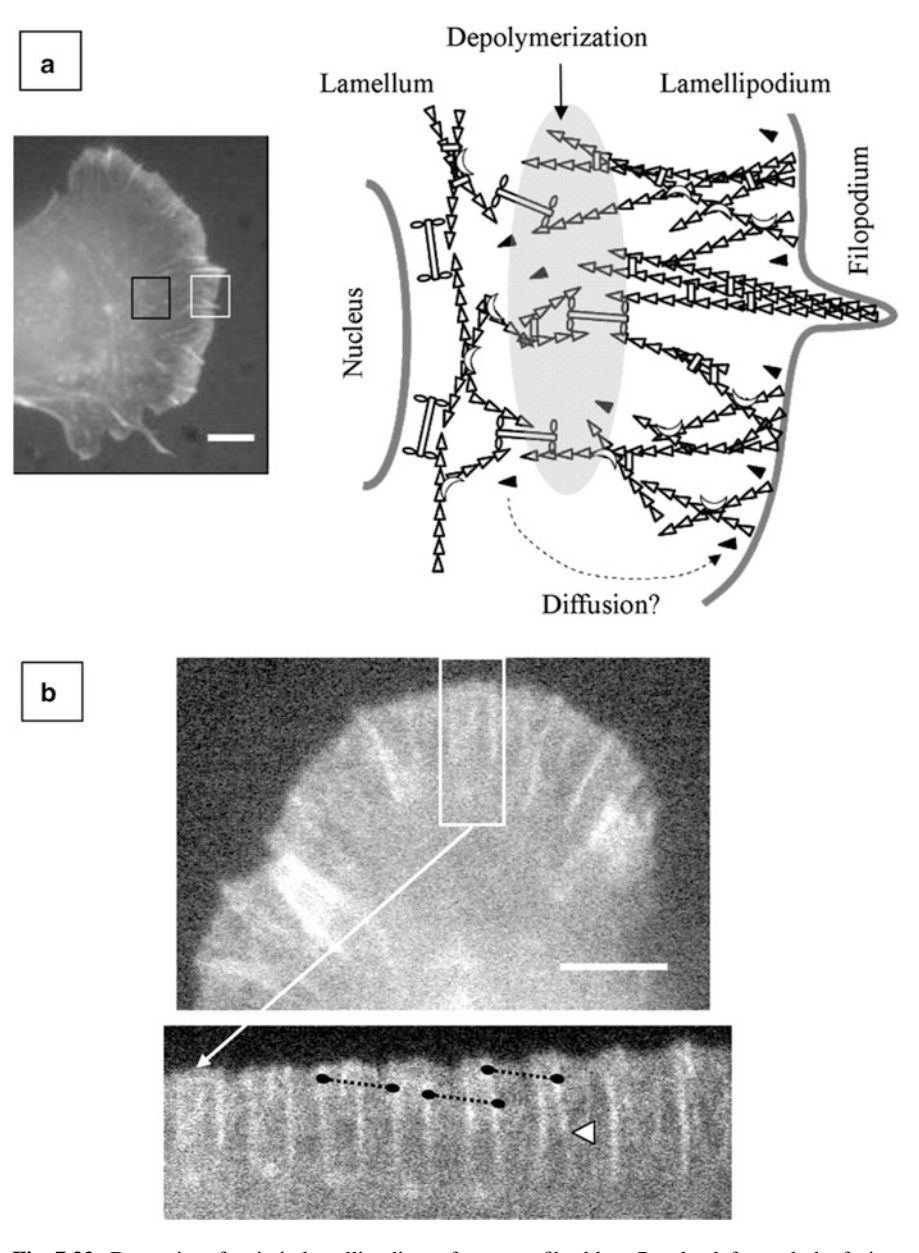


Fig. 7.22 Dynamics of actin in lamellipodium of a mouse fibroblast. Panel a, left panel: the fusion protein of red-fluorescent protein and actin in another lamellipodium of Swiss3T3 fibroblast. The white box indicates the part of lamellipodium; the black box indicates a part of lamellum, which resides behind the lamellipodium. Bar  $= 5 \mu m$ . Right panel: a skematic representation of the arrangement of actin and myosin filaments in lamellipodium and lamellum (after [95]). Triangle: actin monomer with the shortest side indicating the barbed end; H-shaped structure, bipolar myosin filament; crescent, an actin cross-linking protein; rectangle, an actin-bundling protein. Actin

at barbed ends will decrease the number of growth competent filaments but will increase the length of the growth per filament, because the monomer per filament available for the polymerization increases. This will reduce the protrusive force, but if the external force is not very large, the faster protrusion will be possible. This is called funneling effect [132].

The depolymerization of the actin filaments at the back of lamellipodium occurs after the filaments are transported by the backward motion of the actin network. This backward motion is called retrograde flow as shown in Fig. 7.22b; [120, 133]. Myosin II is assumed to participate in this process. Quite interestingly, it has been suggested that the retrograde flow contributes to the facilitation of severing of actin filament by the contractile force [134]. The involvement of myosin may depend on the cell system because in one type of fibroblast cell, the velocity of the retrograde flow was little affected by the inhibitors of myosin II activity [120].

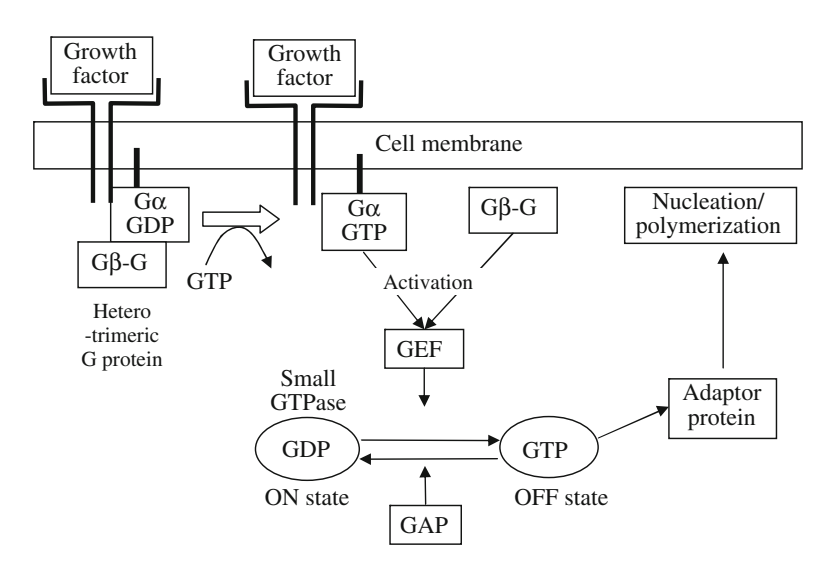
Since the intracellular ionic environment (ie., ~0.1 M K<sup>+</sup> and/or 1 mM Mg<sup>2+</sup>) is not suitable for depolymerization of actin, actin depolymerizing factor (ADF)/cofilin plays the central role in the accelerated depolymerization [132, 135–137], as mentioned above. The crystal structure of the actin monomer complexed with a fragment of an actin depolymerizing factor called twinfilin has been solved [138]. This protein has an actin interacting domain that is common among ADF, and its binding to actin filament was found to cause the weakening of the interaction among protomers, suggesting the facilitation of the depolymerization. As mentioned above, the actin monomer thus formed is bound by actin-sequestering proteins, thymosin beta-4 and profilin, which suppress spontaneous polymerization. Actin is then transported from the rear to the cell edge. The passive diffusion alone may be too slow for the monomer supply and it has been suggested that some facilitating transport mechanism is involved [139].

Fig. 7.22 (continued) monomers polymerize to the barbed ends of actin filaments, which are facing toward the lamellipodial edge. On the other hand, after the network is transported backward, the filaments in the network are severed by a protein, ADF/cofilin (not shown) and individual monomers coming off the pointed ends are sequestered by proteins, thymosin beata-4 and profilin (not shown). The actin monomers complexed with thymosin beta-4 or profilin are unpolymerizable and are transported to the front edge of lamellipodium (dashed arrow; after [127, 128]). This is the turnover of actin in lamellipodium. The contractile force exerted on actin filaments by myosin II may facilitate depolymerization as well as the retrograde flow. Panel b, an example of the retrograde flow of actin bundles in lamellipodium. Actin is fused to red-fluorescent protein and visualized by epi-fluorescence microscopy. Shown in the upper panel is the lamellipodium; many white streaks represent actin bundles. The lower panel shows time-lapse images of the area in the box indicated in the upper panel. Each tile was extracted every 6 s. Black dotted lines connect the positions of the bright fluorescent clusters probably formed by chance at different locations on the bundles. Because the actin bundles grow immediately beneath the lamellipodial edge and transported backward along with the retrograde flow of the actin network in the lamellipodium, those fluorescent spots moved at the same rate toward the back of lamellipodium. As a result, slopes of the three dotted lines, which represent the velocities of individual spots, are almost the same. Another remarkable feature is the actin bundles become obscure at the back of lamellipodium as indicated with the white triangle due to depolymerizaton of actin. Bar =  $10 \mu m$ 

# 7.15 Extracellular Signaling and Regulation of Actin Polymerization

As mentioned previously, actin polymerization is regulated by small GTPases: there are three types of Rho family proteins (RhoA, Rac 1 and cdc42). RhoA is involved in the formation of stress fibers, Rac1 is involved in the formation of actin network in lamellipodium, and cdc42 is involved in the formation of bundle in filopodium [140]. The function of small GTPase is regulated by the extracellular signals such as thrombin or various growth factors. These molecules bind to transmembrane receptors, and those receptors activate a heterotrimeric G protein (a complex of alpha-, beta- and gamma-subunits). As a result of the activation, the alpha-subunit dissociate from the beta-gamma subunits. The former and the latter subunits are respectively involved in the activation of small GTPases [140-143]. In the absence of the extracellular signals, the small GTPase binds GDP and remains inert (OFF state); the OFF state is stabilized by a protein called GDI that inhibits the dissociation of the bound GDP. In the activation, the bound GDP is exchanged with GTP by a protein called guanine nucleotide exchange factor (GEF). GEF is activated by the alpha- or beta-gamma-subunit of the heterotrimeric G protein and facilitates the dissociation of GDP from the small GTPase. The small GTPase thus is brought to the GTP-bound (ON) state (Fig. 7.23). The small GTPase binds to adaptor proteins that transmit the signal so that the process of nucleation of actin polymerization is activated. The activation of a small GTPase is thus under a multiple regulation. This is natural because as mentioned above, in the cell, without regulation actin would polymerize at any location.

The transduction of the signal from small GTPases to the localized actin polymerization depends on another group of proteins that promote the nucleation of actin polymerization and are localized to the cell membrane. To take a lamellipodium as an example, the factor that promotes the nucleation of actin is Arp2/3 protein complex that allows the branched growth of the actin filament from the barbed end [144]. A nucleator, arp2/3 is bound to and activated by WASP (Wiskott-Aldrich syndrome protein) family proteins (WASP, N-WASP and WAVE; [145]). These proteins are localized to the cell membrane and targets of the activated small GTPases; in the case of lamellipodium, the small GTPase is Rac, which has a hydrocarbon chain attached by the posttranslational modification, and hence, is localized to the cell membrane. Rac interacts with WAVE and activates the nucleating activity of arp2/3. Likewise, Cdc42 and arp2/3 interact with N-WASP in the formation of filopodium. Hence, the extracellular signal is translated into actin dynamics through the activation of the actin-nucleating proteins.



**Fig. 7.23** Conversion of an extracellular signal to intracellular process (here, actin dynamics). The binding of external stimuli such as growth factor to the receptor starts the signaling cascade. The heterotrimeric G-protein (a complex of alpha, beta and gamma subunits; the alpha-subunit binds and hydrolyzes GTP) is activated by the stimulus-bound receptor: the GDP bound to the alpha subunit is exchanged to GTP. The beta-gamma subunits remain associated and may be involved in the downstream activation process. The GTP will be hydrolyzed after some time and the trimer is formed again, leading to the de-activation. In the activated state, the subunits bind to GEF and activate it. The activated GEF then stimulates the exchange of GDP that is bound to a small GTPase (Rho, Rac or cdc 42) to GTP. This turns on the small GTPase and then activates the adaptor proteins such as N-WASP or WAVE at the cell membrane. The adaptor proteins then activate the nucleator of actin polymerization such as Arp2/3 or formin. Arp 2/3 is activated by Rac and participates in the formation of actin network in lamellipodia, while formin is activated by Rho or cdc42 and participates in the formation of filopodia or stress fibers

# 7.16 Actin-Based Biological Movements: Protrusion of Lamellipodium

As describbed above, lamellipodium protrudes as a result of the growth of the underlying actin network. Because individual actin filaments grow toward the cell edge, they eventually hit the cell membrane. One would expect that the growing actin filaments will push the lamellipodal membrane. This idea led to a theoretical proposal that the growth of actin filament or shrinkage of microtubule is capable of producing mechanical work [146]. The possibility of the force generation by the growing or shrinking biopolymers has been analyzed on the basis of irreversible thermodynamics (see Sect. 7.21, [147]).

Actually, polymerization has to occur at the interface between the cell membrane and the tip of individual actin filaments and this will not be possible, unless the gap opens between the barbed end of the filament and the cell membrane to allow a monomer to polymerize onto the barbed end. One possible mechanism to create the

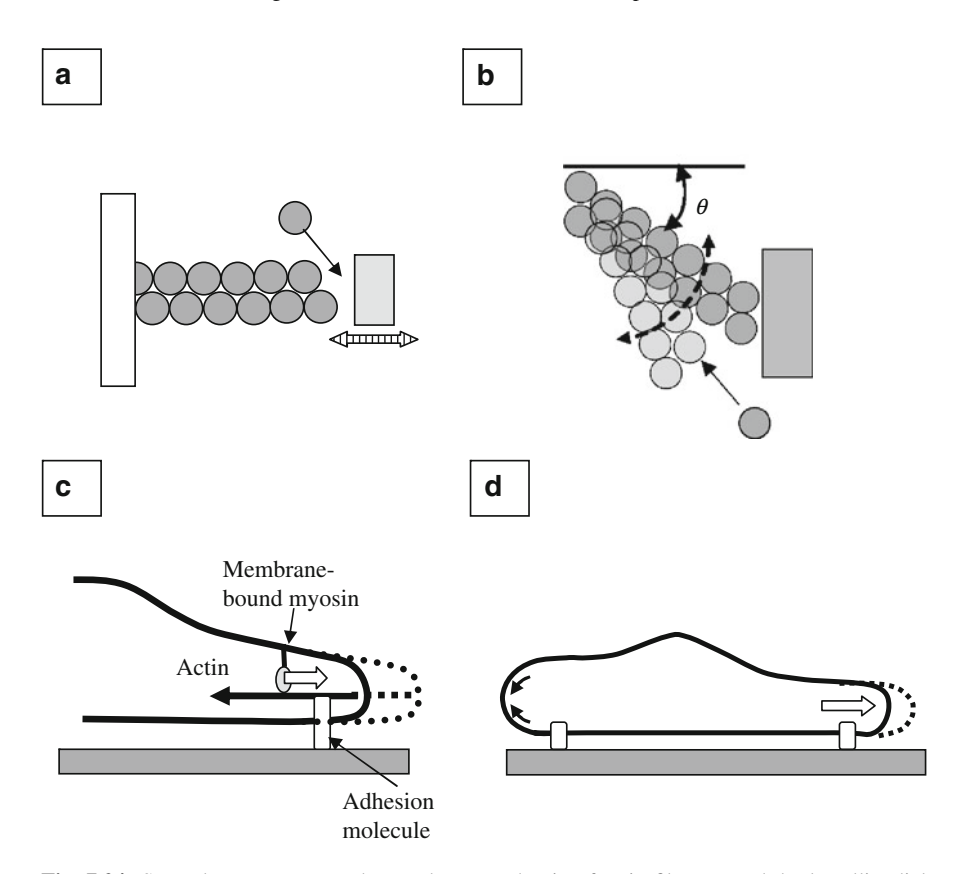


**Fig. 7.24** Several ways to create the gap between the tip of actin filament and the lamellipodial membrane. Panel a, thermal fluctuation of the cell membrane creates a gap; Panel b, thermally activated bending of an actin filament; in this case the elongated filament elastically push the membrane, when it bends back; Panel c, pulling of the membrane above the lamellipodial actin network driven by a membrane-bound myosin, such as myosin-I; Panel d, bleb-driven protrusive formation (see text)

gap is thermal fluctuation of cell membrane and/or actin filament abutting the membrane (Fig. 7.24a, b; [148]). The fluctuation models yield relationships between the stall force (the force that halts the elongation of the filament) and the monomer concentration in the solution. Another mechanism involves membrane-bound single-headed myosin (eg., myosin I in *Acahthamoeba Castellani* and *Dictyostelium discoideum*; [149, 150]). The membrane bound myosin I moves on the actin filament toward the barbed end (ie., toward the cell front) of an actin filament, which is fixed to the substrate (Fig. 7.24c). Then, as mentioned before, the membrane that is linked to the myosin I will be pulled forward, creating a gap between the tip of the actin filament and the membrane [151]. It is noted that in highly motile cells such as amoeba and cancer cells, the protrusion of the front edge has been shown to occur through the phenomenon called blebbing. The bleb is a hemispherical dome of lipid membrane which has been dissociated from the cell cortex (= membrane + actin

membrane skeleton + membrane-bound myosin; [152]). The bleb is created by the increase in the intracellular pressure due to the contraction of the cell cortex (Fig. 7.24d represents the contraction of the tail of the cell). In this case, polymerizing actin will fill the space in the bleb to form a protrusion (pseudopod in ameba; [153, 154]). The blebbing-based protrusive growth seems to be suitable for quick determination of the direction of the cell in response to the change in the distribution of extracellular signaling molecules.

It seems that living organisms have achieved the protrusive activity by utilizing every possible mechanism that probably had been explored in the process of evolution.

### 7.17 Other Motility Based on Actin Polymerization

The motility depending on the actin polymerization is often called "actin-based motility". There seem to be a number of modifications in coupling of actin polymerization to the biological work. Acrosomal reaction, in which the elongation of the structure called acrosomal process from the head of the sperm of sea cucumber, Thyone, in the initial stage of fertilization, is thought to be an example of the polymerization-coupled force generation [155, 156]. At the base of the future acrosomal process in the sperm head, actin is complexed with an actin binding protein that prevents the polymerization of monomer and hence is stored as a non-polymerized form. In the acrosomal reaction, the tip of the head comes into contact with the jelly coat layer of the egg, and actin is freed from the binding protein that had prohibited the polymerization. Like in lamellipodium, the freed actin rapidly polymerizes toward the tip to form the acrosomal process filled with actin bundle; there is no myosin II in the acrsosomal process. The rate of elongation, ~10 μm/s, seemed to be unable to be caught up by diffusion of actin from the base of the acrosome [155], but later, the discrepancy has been interpreted as the increased rate of actin transport by decrease in the volume of the actin reservoir and the increase in the chemical potential of actin monomer due to the high actin concentration [156]. This model has suggested that the speed of the extension is limited by the rate of delivery; the mechanism of the generation of the work may be the same as what is operating in lamellipodia, although it was not specified in the acrosomal study.

Another example of the actin-based motility is the propulsion of bacteria such as *Listeria* and *Shigella* in cytoplasm [90]. These bacteria enter the cell through phagocytosis (ingestion of small particles by invagination of the cell membrane). After entering the cell it moves around in the cytoplasm at 1 to 10 µm/s, depending on bacteria species, evading the host defense mechanism. At the end of the intracellular stage of its life cycle, the bacterium pushes the cell membrane and a long process is formed. This membranous process is phagocytosed by the surrounding cells and the bacteria further spread. Electron microscopy demonstrated that the intracellular trail of the moving bacterium (called comet due to the morphological similarity) contains actin of the host cell [157], and that the barbed end of each

filament was facing to the bacterial surface [158]. Since the complex is enriched in the rear region of the bacterial body, and neither myosin II nor non-muscle myosin has been found in that region, polymerization of actin was likely to push the bacterium forward.

Listeria possesses a membrane protein ActA on its surface to utilize the host cell actin. It has been demonstrated [159] that Act A allows the polymerization of actin at or near the bacterial surface. This protein contains domains that bind arp2/3, actin and VASP. With ActA, Listeria utilizes the cellular machinery to nucleate the actin polymerization in the vicinity of bacterial surface and convert the polymerization into a mechanical work to penetrate the crowded cytoplasm. In case of another bacterium, Shigella, IcsA, like cdc42, promotes actin polymerization by activating N-WASP (Neural Wiscott-Aldrich Syndrome Protein), the activator of Arp2/3 complex.

The actin polymerization-based, comet-type motility seems to be quite general, because it is not limited to the motility of micro-organisms. The actin polymerization has been observed in the transport of a membrane vesicle called endosome that are formed in the process of endocytosis (invagination and subsequent closure of the cell membrane [24]). The vesicle binds N-WASP, forming a comet tail at its back [160]. Thus, the bacteria and endosomes seem to utilize the regulatory machinery that induces actin polymerization on the cell membranes. As described earlier, the membrane vesicles are transported on actin filament or microtubule by appropriate motor proteins (myosin I, V, VI, kinesin, and cytoplasmic dynein [161, 162]). Thus, the intracellular transport of endosomes seems to be supported by the two very different mechanisms.

Another remarkable example is that of the sperm of a nematode, *Ascaris*. Like animal cells, *Ascaris* sperm crawls on the surface by extending lamellipodium at the front, followed by the retraction of the tail [163]. In the lamellipodium, neither actin nor myosin is present, but a dimer of major sperm protein (MSP) is structured into the filamentous network in the front edge; the MSP dissociates at the back of the lamellipodium.

# 7.18 Polymerization Force Developed by Lamellipodium

# 7.18.1 Keratocyte: Measurement with Atomic Force Microscope

Protrusive force developed by the lamellipodia of keratocyte has been measured by atomic force microscopy [164]. In this study the force was measured by the deflection of an AFM cantilever, which had been placed vertically with its back pushed against the lamellipodial edge. Forces on the order of nanonewton were developed by the lamellipodial edge; this was apparent from a considerable indentation of the cell edge around the cantilever. The result demonstrates that a large

force was developed by the lamellipodium and the lamellipodium was compliant (the elastic constant of lamellipodia of fibroblast has been measured to be ~0.5 kPa; [165]). A previous study using a glass microneedle found the forces on the similar magnitude required to stall the locomotion of keratocyte ( $\approx$  protrusive force; [166]). What was remarkable in the AFM study was that the measured force-velocity curve was similar to what has been predicted from the elastic ratchet mechanism. Thus, the velocity slowly decreased in the small force regime, but it decreased sharply when the force reached ~1 nanonewton; the relation was qualitatively different from the prediction of the thermal ratchet mechanism, which showed a concave dependence of the velocity on the force. The magnitude of the force on the order of nanonewton is indeed expected from the thermodynamically determined force developed by polymerizing actin filament (~a few piconewton) and the number density of the filaments estimated for the edge of fibroblast (roughly 150/µm cell edge; [127, 167] and the width of ~5 microns for the region of the lamellipodium of keratocyte, which pushes the AFM cantilever). Thus, the elastic ratchet model can explain both qualitatively and quantitatively the protrusion of keratocyte lamellipodia.

# 7.18.2 Fibroblasts: Measurement with Optical Trapping Technique

However, in some cases, much lower forces have been shown to affect the lamellipodial protrusion. For exmaple, lamellipodium extending from a fibroblast cell has been shown to be halted by the water flow from a glass capillary with a micron-sized opening [168]. Hydrodynamic calculation indicated that the force exerted on the lamellipodium is a few piconewtons/µm of the front edge. The experiment has shown that the hydrodynamic force immediately halted the protrusion. The interference contrast microscopy has suggested that this was due to the dissociation of the cell edge, which would have resulted in the incomplete adhesion of the extended lamellipodium, not the counterforce against the polymerization force. This result demonstrates that the lamellipodial protrusion is a complex process in which not only the magnitude of the force, but also the conversion of the protrusive motion to the advancement of the cell edge through the attachment is important.

In another case, the optical trapping technique was used to exert piconewton forces on extending lamellipodium (Fig. 7.25; [169]). In this experiment, a micronsized polystyrene bead (probe-bead) was held by the optical trap that was created by focusing an infra-red laser beam of up to a few mW. As described in Sect. 3.7.2, the trap is characterized by a spring constant trap stiffness, k. With this technique, lamellipodial activity of fibroblast cells was measured. The cell was observed by phase-contrast video microscopy and a bead held in the trap (the k value ranged from 0.01 pN/nm to 0.1 pN/nm) was contacted the edge of a lamellipodium to probe the movement of the lamellipodium.

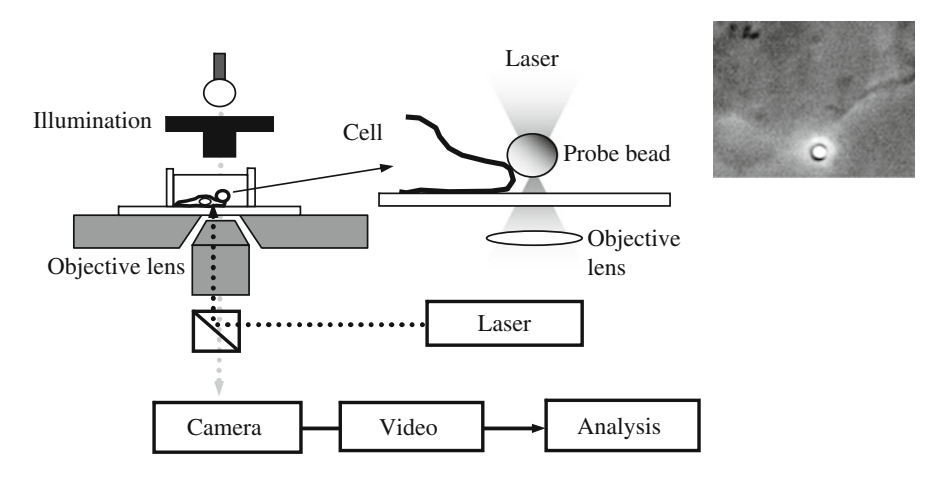
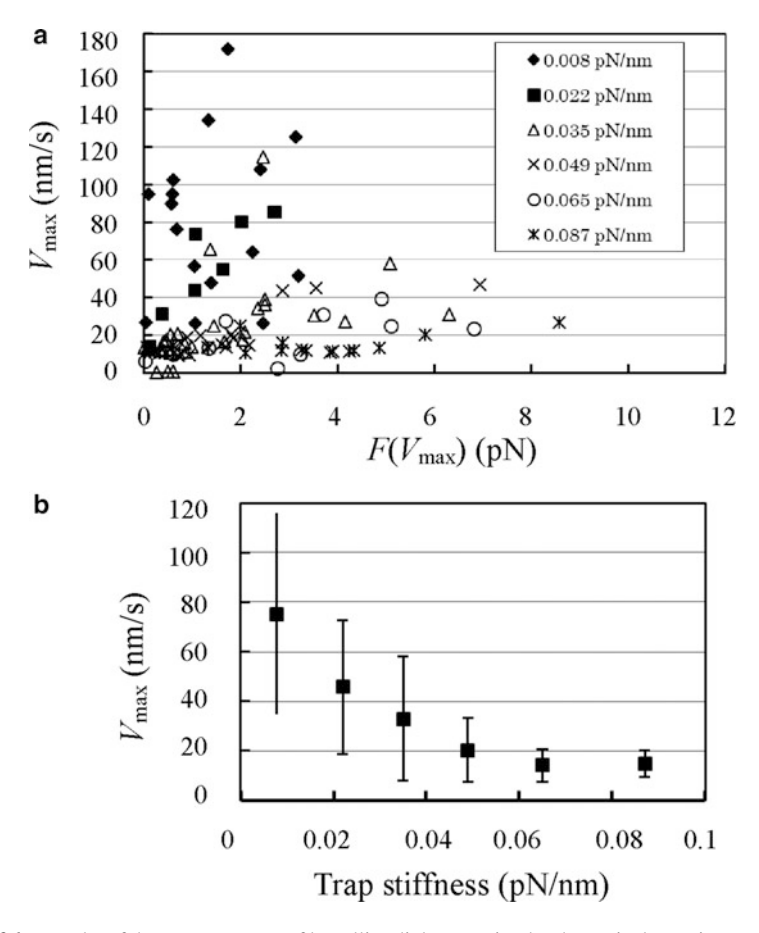


Fig. 7.25 Measurement of lamellipodial dynamics by optical trapping technique. An optical trap implemented in a phase contrast microscope: an infra-red laser beam was focused with an objective lens (numerical aperture =1.3) to create the optical trap at the focal point. A 1  $\mu$ m plastic bead was trapped and was contacted with the lamellipodium; the phase-contrast micrograph on the right exhibits an example of the contact during the experiment. The actual displacement was so minute that it could not be discerned by eye

It was found that the velocity of the probe-bead increased and reached a maximal value,  $V_{\rm max}$ , then decreased to zero. The decrease was somewhat unexpected, because the cell edge on the both sides of the probe bead seemed to continuously advance at the same time. The decrease may be a phenomenon similar to that observed with the lamellipodia under the water flow; the continuous protrusion of the lamellipodium around the bead suggests that the bead affected the lamellipodial motion rather locally (microscopic observation implied that the movement of the edge was not affected when the edge was ~1  $\mu$ m away from the bead).

During the protrusive phase, correlation existed between the  $V_{\rm max}$  and the velocity of the bead estimated from kymograph of the bead, as one might expect. One would also expect that the  $V_{\rm max}$  value decreased when a few pN forces was applied and the  $V_{\rm max}$  values decreased with the trap force,  $F_{\rm max}$ , which was calculated by  $k \times X_{\rm max}$ , where  $X_{\rm max}$  corresponds to the displacement at which the velocity was  $V_{\rm max}$ . However, as shown in Fig. 7.26a, even at the same  $F_{\rm max}$ , the  $V_{\rm max}$  scattered over a wide range indicating no dependence of  $V_{\rm max}$  on the trap force.

It seemed that the result simply reflected a scattering of data. Actually, the ensemble-averaged  $V_{\rm max}$  monotonically decreased with the trap stiffness (Fig. 7.26b), making the scatter unlikely to be due to an experimental error. This plot implies that the more restricted movement of the probe-bead was in the stiffer trap was reflected in the velocity. One would argue that this is not surprising, because the probe held by a "weak spring" will move with smaller forces. However, the analysis or the degree of fluctuation suggested that this view had to be modified. The size of the fluctuation of the probe-bead was calculated from the square-root of the accumulated power spectral density of the fluctuation [169]. It was maximally



**Fig. 7.26** Results of the measurement of lamellipodial protrusion by the optical trapping technique. Panel a, the relation between the  $V_{\rm max}$  and  $F(V_{\rm max})$ . The  $F(V_{\rm max})$  values were calculated by multiplying the trap stiffness and the distance at which the  $V_{\rm max}$  value was obtained; a simple decreasing tendency was expected for the collection of these plots, but there was no such correlation. Panel b, the relation between  $V_{\rm max}$  and trap stiffness; the  $V_{\rm max}$  values decreased with the trap stiffness, implying that the movement could be related to the fluctuation of the bead contacting the lamellipodial edge

~20 nm at the lowest trap stiffness and decreased with the trap stiffness. The size of the fluctuation also decreased with the trap stiffness for the bead that did not contact with the cell edge, executing only a Brownian motion in the trap (non-contacting bead). However, the size of the fluctuation of the probe-bead was significantly larger than that of the non-contacting bead. Thus, the fluctuation seemed to arise not only from Brownian motion but from some additional, active mechanism. It has been suggested that the excess fluctuation of the probe-bead was specific to the live cell, and its size exhibited a positive correlation with the protrusive velocity [169]. Thus, at least in the fibroblast cell, the excess fluctuation was produced in the protrusive

process of lamellipodium. The source of the fluctuation has not been elucidated in that study. Inhibition of the polymerization by cytochalasin or by depletion of ATP significantly lowered the degree of fluctuation. These results are consistent with the energy-requiring actin turnover is involved in the protrusive process, but it may simply indicate the requirement of the intact network structure.

Cell is a multi-scale entity and fluctuations must occur on a wide range of spatial and temporal scales. This is indeed the case, because fluctuations measured by optical microscopy exhibit various spectral characteristics [170–172]. Some fluctuations that have been revealed in other studies is an order of magnitude lower than that observed with the optical trapping technique, but the fluctuation detected on the apical (top) surface of the cell in one study [171] seems to have similar frequency range (a few Hz). Thus, although the location of the fluctuation was different between two studies, these fluctuations may share a common mechanism.

#### 7.18.3 What Fluctuates?

One may attribute the difference between the results obtained with AFM technique trapping technique to the different cell type (ie., optical keratocyte vs. fibroblast). But the commonality of the basic construction of lamellipodia of these cells (actin network wrapped in the cell membrane) and necessity of actin polymerization for the protrusion make this notion unlikely. Suppose the fluctuation-aided lamellipdial protrusion did occur, it will be natural to assume that both the fluctuation of lipid membrane and the fluctuation of actin filament were involved in the protrusive process. The lipid bilayer membrane is highly flexible: its out-of-plane amplitude of thermal fluctuation [85, 173] is estimated to be  $\sim$ 7 nm for 1  $\mu$ m  $\times$  1  $\mu$ m membrane ( $\sim$ size of the probe-bead used in the optical trapping measurement) in the presence of a lateral membrane tension (0.01 pN/nm; [174]). Hence, the thermal fluctuation of the membrane will create the gap sufficiently large for the insertion of an actin monomer. However, since the membrane tension is on the same or only slightly higher than the trap stiffness, the membrane fluctuation will be readily suppressed by the bead in a stiffer trap (k is up to 0.1 pN/nm).

On the other hand, the cantilever of the atomic force microscope is much stiffer (10–100 pN/nm). Thus, the membrane will be unable to fluctuate under the AFM cantilever. In this case, however, the fluctuation of actin filament will allow the growth of the actin filament as has been proposed. If a single 30 nm actin filament bends, the stiffness will be 0.01 pN/nm [175, 176]. The bending creates the ~1.8 nm gap between the filament tip and the cell membrane (assumed to be flat). This is comparable to the gap created by the fluctuating membrane. Of course, the stiffness of the cantilever is much larger than that of a single actin filament, but as mentioned earlier, the load can be borne by many filaments ( $\approx$  100 filaments per  $\mu$ m edge of lamellipodium [95, 127]. Hence, the growth of the will be possible. This notion is consistent with the result of an experiment using purified actin and ActA [177].

In in vivo situation, the imbalance in the osmotic pressure will inflate the cell resulting in the increased membrane tension, and also various other loads will be exerted against the protrusion. For example, immune cells must crawl through the cells constituting the blood vessel wall. Penetrating the membrane protrusion into the space between cells will impose a considerable resistance against the protrusion. The co-existence of the fluctuation of the cell membrane and actin filaments will be advantageous under these circumstances.

#### 7.19 Reconstituted Systems to Study the Polymerization-Based Phenomena

#### 7.19.1 Actin-Liposome System

In this section, mimicking the growth of the protrusions of the cell edge by using an actin-encapsulating liposome is described. Two studies appeared in the early stage of the research. In one study [178], micron-sized liposomes containing actin monomer were formed by swelling the lipid film in a solution containing actin monomer. The actin-encapsulating liposomes were observed under light microscope. The actin monomer in liposomes was polymerized by K<sup>+</sup> ions that were introduced using an ionophore. Polymerization of encapsulated actin was confirmed by fluorescence photo-bleaching recovery (FPR; Sect. 3.6.2) of the actin that had been fluorescently labeled with rhodamine. As a result of polymerization, the liposome assumed irregular shapes. Actin crosslinking protein filamin altered the final shape of the liposome to less irregular shapes suggesting that the lipid membranes could be sculpted by the structures formed by the combination of actin filaments and actin crosslinking proteins.

Another study [36] also observed actin-containing liposomes, but showing the process of morphological changes. Actin was allowed to slowly polymerize with a low concentration of Ca<sup>2+</sup> ions that had been co-encapsulated on ice with actin monomers. Polymerization was initiated by raising temperature from 5 °C to 30 °C. With the progress of the polymerization, the shape of the liposome changed from spherical to a disk- or a racket-like shape. In both types of liposomes, birefringence was observed along the contour of the deformed liposomes, which was interpreted as an alignment of actin filaments along the liposome contour. The shape change occurred slowly over several tens of minutes concomitant with the actin polymerization (the actin polymerization was separately confirmed by an increase in the light scattering of the actin solution).

The time scale of the above experiment was much longer than the time scale of the dynamics of lamellipodia (several tens of seconds in amoeba cell and in mammalian cells). Therefore, a method was developed that allowed faster polymerization [179]. To accelerate polymerization, polymerization nuclei (fragments of actin filaments) were incorporated with actin monomer. But most importantly,

polymerization was driven by K<sup>+</sup> ions introduced by the technique called electroporation. In the electroporation process, electric pulses were applied to actincontaining liposomes to transiently increase the permeability of the membrane to ions [180], which would allow a inward flow of K<sup>+</sup> ions, which had been included in the external solution. Indeed, after the application of electric pulse, liposomes changed their shape over ~1 min; it finally assumed ellipsoidal shape. The polymerization was confirmed by the diminished Brownian motion of 1 µm polystyrene beads that had been co-encapsulated with actin. Some liposomes even developed large protrusions on the similar time scale. Protrusions thus developed lasted for at least 10 min without notable change in their length or thickness suggesting the structural stability of the protrusion. The observation of fluorescently labeled actin monomer revealed that actin (probably in the filamentous form) filled the protrusion. These observations collectively led to a suggestion that the protrusive growth was a result of actin polymerization. The difference in the shape of liposomes between two studies might be due to the different time scales on which the polymerization occurred.

Fluorescently-labeled actin filaments have been shown to execute vigorous thermal fluctuation indicating the highly flexible nature of then filament [181]. Lipid membrane is also highly flexible, as mentioned earlier [85, 173]. Therefore, the development of the stable protrusions especially a long protrusion, could be possible, only if many filaments are oriented in the same direction and grew simultaneously; the maintenance of the protrusion would be only possible when the protrusion was filled with actin filaments, as actually observed. In a later study fascin that bundles actin filaments in the same polarity [182], or alpha-actinin, which bundles actin filaments in opposite directions both developed thin, but highly rigid protrusions [183]. This must have been a result of the mechanical strength of the bundled actin filaments [184, 185].

In the case of the slow polymerization with Ca<sup>2+</sup> ions [36], alignment of actin filaments could be a result of steric interaction between the lipid membrane and growing actin filaments. On the other hand, the fast protrusive growth occurred after the electroporation might be initiated by the localized but large mechanical deformation (budding) of the lipid membrane caused by the electroporation; that the growing filaments might have turned the initial small protrusions into large, long protrusions. In the latter case, the lipid membrane exhibited little fluctuation after the growth of protrusions, and the shape of the liposome with protrusions were stable over tens of minutes. The tensed membrane seems to have resulted from the force exerted by the growing filament. Thus, some mechanical work was done by the growing filaments.

# 7.19.2 Change in Liposome Shape Accompanying Severing of Actin Filaments

There are shape changes of liposomes, which is driven by a different mechanism [186]. As described above, liposome assumed disk-like shape as a result of slow polymerization, which remained unchanged over a long period (at least 20 min after the final shapes were reached). However, when cytochalasin was administered to the disk-shaped liposome, further shape change occurred: the liposome transformed to a rugby ball-like shape. This was accompanied by a re-arrangement of actin filaments from the original circular distribution to a rather uniform alignment along the longer axis of the rugby ball. The change in the alignment was deduced by the polarization microscopy of the encapsulated actin labeled with acrylodan [40]. Cytochalasin inhibits the actin polymerization, but it also severs the actin filaments. Since cytochalasin is membrane-permeable, it probably entered the liposome and severed the encapsulated filaments. Perhaps, this altered the force balance between the actin filaments and the lipid membrane, leading to the transformation. This is another example of sculpting of the lipid membrane by the structure of actin filaments, rather than polymerization force. To summarize, actin has an ability to mold the shape of lipid membranes, and actin cross-linking and bundling proteins should strongly enhance this ability by stabilizing various types of actin-based structures.

### 7.19.3 Liposomes Encapsulating Tubulin

The polymerization-coupled force has been demonstrated with liposomes containing tubulin, not actin [187, 188]. Tubulin dimer was encapsulated in liposomes on ice and was allowed to polymerize at 37 °C. The shape change of the tubulin-containing liposome follows considerably different path than the actin-containing liposome. Thus in the former case, small projections first appear at the two opposite ends of a liposome, altering the liposome shape to a lemon-like shape. The protrusions further grew in the opposite directions, and the main part of the liposome again became spherical. The remarkable difference from the case of actin is likely to stem from the large difference in the rigidity of two polymer systems; a single microtubule is about one hundred times higher than that of a single actin filament [189]. Hence, even a single microtubule was sufficient for the generation of membrane projection.

It has been shown that a thin tube (tether) grows by simply pulling glass bead that had been attached to the membrane of a liposome [87] or a red blood cell [190]. In another study, the end-to-end distance of the lemon-shaped liposome has been measured as a function of the axial force [191]. Micron-sized plastic beads were encapsulated in a giant liposome and were manipulated by the double-optical trap system: two beads were captured in each trap and were brought apart by deflection of the laser beam. As a result, the beads exerted forces on the lipid membrane at the opposite locations. An increase in the inter-bead distance first induced a lemon-shape and

abruptly small bud appeared. Further increase in the beads separation resulted in the growth of tether. Since the force could be estimated by knowing the trap stiffness and the shift in the bead center, authors could generate the relation between the inter-bead distance and the force. The analysis suggested that the axial force monotonously increased to about 10 pN until a certain inter-bead distance was reached; the force abruptly dropped to < 5 pN beyond that distance. This drop corresponded to the growth of a thin tube from the liposome accompanied by the change of the liposome shape from lemon to a sphere; further growth of the thin tube occurred at the lower forces. Shape changes of liposome under axial forces have been treated theoretically [eg., 192, 193]. The change in the shape of the body of liposome from the lemon to spherical shape has been interpreted as a phase transition phenomenon. In an early study, the shape of the liposome that had been deformed by growing microtubule has been theoretically analyzed based on a curvature elastic theory of a lipid membrane and the developing force has been estimated [194]. In that study the shape of the liposome was assumed to have a rotational symmetry and was regarded as a combination of straight lines and circular arcs. The resultant relation between the force and the end-to-end distance of liposome indicated that the force monotonically increased to ~3 pN until the end-to-end distance of  $\sim 15 \,\mu\text{m}$ , but the force did not drop upon the extension of the protrusion.

### 7.20 Mimicking Bacteria Propulsion with Various Reconstituted Systems

The velocity of *Listeria* has been shown to be equal to the rate of elongation of actin filament [195]. As described earlier, *Listeria* expresses a membrane protein, ActA, to promote the actin polymerization on the bacterial surface, which pushes the bacterial body. The validity of this notion has been examined with various reconstituted systems. In one study [196], the reconstituted system with *E-coli* artificially expressing IcsA, an actin-nucleating protein of *Shigella*, is driven by the actin polymerization. The genetically engineered *E-coli* have been shown to move with a comet tail in the cytoplasm of the egg of *Xenopus laevis* at a velocity similar to that of the polymerization-driven bacteria.

The role of factors involved in the propulsion of *E-coli* expressing IcsA and *Listeria* expressing ActA has been analyzed by measuring the velocity of the polymerization-driven movements. Three factors, Arp2/3 (actin-nucleating protein), ADF/cofilin (depolymerizing factor) and a capping protein (barbed-end capper), were necessary [197]. The combination of purified proteins and plastic beads instead of bacteria has been used to further investigate the role of the bacterial protein: plastic beads that had been coated with ActA moved at a velocity comparable to that of *Listeria* in the *Xenopus* extract supplemented with exogenous actin [198]. The bead started moving with the cloud of actin filaments that had been formed around the bead; apparently, no asymmetric distribution of ActA is necessary for the movement. In another study, bead was replaced with a liposome of a few microns

diameter [199]. Like bacteria, the comet tail grew from the surface and extended to the back of the liposome. The actin filaments were bound to the liposome through ActA. An advantage of using liposome was that the forces exerted on the moved object could be visualized. Thus, the liposome coated by ActA, moving with a comet tail, was pulled back at the central part of the rear and was pushed forward along its side. These observations suggested that some actin filaments were bound to the liposome by ActA around the rearmost region, whereas other filaments obliquely pushed the side of the liposome. Similar force distribution has been demonstrated using oil droplet [200]. The spontaneous breakage of the symmetric distribution of actin filaments around the bead is postulated to be the key to the directed motion [201, 202]. An elastic energy of the gel made of actin filaments around the bead has been assumed to be released through fracture of the gel [198]: this might propel the objects. In another study, the force exerted by the actin polymerization on the surface of the cantilever of atomic force microscope has been measured. The cantilever was coated with ActA and actin filaments were allowed to grow at the lower surface of the cantilever in a *Xenopus* egg. The cantilever was pushed up demonstrating > 100 nN force was produced [177]. Another study utilizing an N-WASP-coated plastic bead has shown to generate a few nN force when actin was allowed to polymerized from the bead surface in the presence of Arp2/3, gelsolin (a barbedend capping protein), ADF/cofilin, profilin and actin [203].

The reconstituted system has been also used to study the motility of the *Ascaris* sperm, which, as mentioned above, does not depend on actin-myosin system. Addition of ATP to the sperm extract showed a formation of a fibrous structure that bound a plasma membrane vesicle and had an arrangement of the filaments similar to that made of MSP (major sperm protein) in vivo. The growth of the fibrous structure, which occurred at the interface of the fiber and the plasma membrane of the vesicle, seemed to propel the membrane vesicle [204]. The movement realized in this intriguing system has been treated theoretically [205].

#### 7.21 Polymerization Force: Theoretical Studies

#### 7.21.1 Hill's Theory

As mentioned in Sect. 7.16, Hill [147] developed the theory based on irreversible thermodynamics to explain the polymerization-based force development. There are several assumptions: (1) The monomer and polymer coexist in the solution; (2) One end of the polymer is fixed and the other end is touching an obstacle, which is pushed against the polymer end by an external force F; (3) The polymer was assumed to be a linear chain of monomer and infinitely rigid. As before, we call the monomer incorporated in the polymer "protomer" to distinguish it from the monomer in solution. The chemical potential of a monomer in solution is designated as  $\mu$  and that of protomer,  $\mu_{\text{pro}}$ . Hill assumed that the value of  $\mu_{\text{pro}}$  does not depend on the position of the protomer (monomer in the polymer); this is a simplification, because

the protomers at the filament end possess different conformation than those within the filament. In the equilibrium state at F=0, incorporation of a monomer (solution concentration =  $C_{\rm eq}$ , where "eq" represents the equilibrium) into the polymer is balanced by the dissociation of a protomer from the polymer. If the chemical potential of the solution monomer and the protomer in the polymer is represented with symbols,  $\mu_{\rm s}$  and  $\mu_{\rm pro}$ ,  $\mu_{\rm s}=\mu_{\rm pro}$  at the equilibrium. The  $\mu_{\rm s}$  is written with the concentration of monomer, C:

$$\mu_s = \mu_0 + k_B T \ln C.$$

Hence, at the equilibrium, the relation,

$$\mu_0 + k_B T \ln C_{eq} = \mu_{pro},$$

holds, where  $C_{eq}$  is the equilibrium concentration (C) of the monomer.

When  $F \neq 0$ , a mechanical work ( $\equiv w$ ) is required to move the obstacle to allow a monomer to polymerize at the end of the polymer. If the length of polymer increases as a result of the polymerization by the monomer length, d, w = -Fd. Here, F is positive, if the direction of the force is parallel to that of the elongation of the polymer (the extension force), whereas F is negative in the reverse case (compressing force). If the concentration and the chemical potential of the solution monomer in the presence of F are designated as  $C_{\rm eq}$ ' and  $\mu_{\rm s}$ ', respectively, the following relation will hold at the equilibrium:

$${\mu_{\rm s}}' = {\mu_0} + k_B T \ln {C_{eq}}'.$$

The work for the elongation is equal to the decrease in the chemical potential of the monomer in the solution. Thus,  $-Fd = \mu_s' - \mu_s$ . Hence, at the equilibrium,

$$-Fd = k_B T \ln \left(\frac{C'_{eq}}{C_{eq}}\right),\,$$

or

$$C'_{eq} = C_{eq} \exp\left(-\frac{Fd}{k_B T}\right).$$

Thus with the external compressive force (F < 0), the equilibrium concentration  $C_{\rm eq}$ ' is higher than  $C_{\rm eq}$ , because the compressive force makes polymerization less favorable and more monomer will remain unpolymerized. The  $C_{\rm eq}$ ' value increases rapidly with the magnitude of the force; for example, if we assume d = 2.7 nm (the elongation of the actin filament upon polymerization of one terminal subunit), 300 K for T and 5 pN for F, then, the factor,  $-Fd/k_{\rm B}T \approx 3.6$ , and hence, the  $C_{\rm eq}$ '  $\approx 36C_{\rm eq}$ .

Hill discussed the kinetic aspect of the effect of external force on the rate of actin polymerization. From the detailed balance, the  $C_{\rm eq}$  for free polymerization (F=0) is related to the off rate of protomer,  $k_{\rm off}$  and the on rate of monomer,  $k_{\rm on}$  in the

following manner,  $C_{\rm eq} = k_{\rm off}/k_{\rm on}$ . In the presence of the compressive force F,  $C_{\rm eq}$ ' will be related to the on and off rates:  $C_{\rm eq}$ ' =  $k_{\rm off}$ '/ $k_{\rm on}$ ', where  $k_{\rm off}$ ' and  $k_{\rm on}$ ' represent the rate of the depolymerization and polymerization in the presence of F. In a simple case where it is assumed that the off rate constant is not affected by the external force ( $k_{\rm off}$ ' =  $k_{\rm off}$ ), then,

$$k_{on} = k_{on} \exp(Fd/k_BT).$$

The  $k_{\rm on}$  may be regarded as a probability per unit time for opening of the gap with a size d in the presence of the force F. We then consider the rate of elongation of the length of the polymer, dL/dt, in the presence of the external force, following Hill's treatment. When F=0

$$dL/dt = d \{k_{on} \times C - k_{off}\}.$$

Likewise, when  $F \neq 0$ ,

$$dL/dt = d \left\{ k_{on} C - k_{off} \right\} = d \left\{ k_{on} C \exp \left( \frac{Fd}{k_B T} \right) - k_{off} \right\}.$$

When *F* is equal to the "stall force",

$$F_{stall} = (k_B T/d) \ln (k_{on} C/k_{off}),$$

 $\mathrm{d}L/\mathrm{d}t=0$  and the elongation stops. Thus, the stall force depends on the temperature, size of monomer, the on rate and the off rate and the solution concentration of monomer. Under the constant solution condition,  $F_{\mathrm{stall}}$  depends logarithmically on C.

Hill has proposed that the filament elongation rate, dL/dt, can be written in a more general form:

$$dL/dt = d \left[ k_{on}C \exp\left(\frac{tFd}{k_B T}\right) - k_{off} \exp\left\{\frac{(t-1)Fd}{k_B T}\right\} \right]$$

where t ( $0 \le t \le 1$ ) is a parameter introduced to distribute the exponential term over on and off rates. Physically, t represents the relative significance of the effect of the force on  $k_{\rm on}$  and  $k_{\rm off}$ . Here, the external force is assumed to affect the dissociation of the protomer (this was not considered in the above discussion); note that the stall force is still  $(k_{\rm B}T/d) \times \ln(k_{\rm off}/k_{\rm on}C)$ . Hill assumes that at large compressive force (IFI >> 0),  $t \to 1/2$ , whereas at large extending force (IFI >> 0),  $t \to 1/2$ . The latter condition, the  $k_{\rm off}$  value will approach that for the free end.

If one adopts 116 (s<sup>-1</sup>), 1.1 (s<sup>-1</sup>), 300 (K) and 2.7 nm as numerical values for  $k_{\rm on}C$ ,  $k_{\rm off}$ , T and d [25, 206],

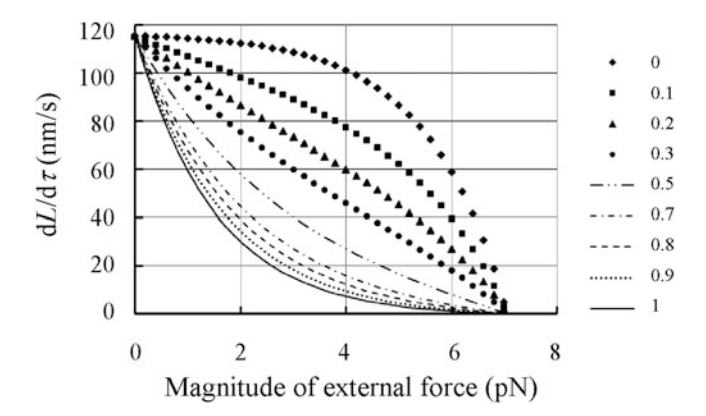


Fig. 7.27 Plots of the rate of elongation of actin filament in the presence of compressive forces. The rate of elongation, dL/dt, was calculated according to the model of Hill [148] with the parameter, t, representing the distribution of the external force on the on-rate and off-rate. The parameter values are indicated to the right

$$\frac{dL}{dt} = 2.7 \times [116 \exp(0.66tF) - 1.1 \exp\{0.66(1-t)F\}].$$

The graph of  $\mathrm{d}L/\mathrm{d}t$  against |F|, the magnitude of compressive force F, is shown in Fig. 7.27. Here, no dependence of t on F is assumed. At |F| = 0, all  $\mathrm{d}L/\mathrm{d}t$  naturally converges to a single value; as mentioned above, the  $F_{\mathrm{stall}}$  is independent of t. The curve corresponding to t = 0 simply serves as a reference, because it is physically unlikely that the compressive force does not affect the process of binding of a monomer to the polymer end. Nevertheless, this simple model demonstrates that the convex nature of the curve appears to depend on the choice of t, as well as that of  $k_{\mathrm{on}}$  and  $k_{\mathrm{off}}$ .

#### 7.21.2 Thermal Ratchet Model of Polymerization Force

As mentioned in the Sect. 7.19, the growth of actin filaments needs the insertion of the incoming monomer between the filament tip and the cell membrane. Hill suggested [147] the usage of the elasticity of the actin filament for the insertion, but the detailed mechanism was not presented. As mentioned previously, Peskin et al. [207] proposed a model, in which a gap is assumed to open between the filament tip and the membrane as a result of the fluctuation of the cell membrane. The position of the membrane is biased by the elongation of the filament that occurs by the binding of a monomer to the tip of the filament. In the formulation of this

"Thermal ratchet" model, it has been assumed that the x axis is parallel to the direction of the polymer, actin filament is straight; no bending is considered, and that the membrane was replaced with a disk with a diffusion coefficient, D. The external force, F, causes the constant drift of the disk: the velocity of which,  $V_{\text{drift}}$ , is related to the D value and F by the Einstein's relation;  $V_{\text{drift}} = F (D/k_{\text{B}}T)$ . The quantity in the parentheses is equal to the inverse of the frictional coefficient of the disk. Based on the structure of the reconstituted actin filament, a simplified model of the protomer addition to the tip was adopted. Thus, because of the stagger between two protofilaments in an actin filament, the actin filament was assumed to elongate by half the protomer length, d along the filament axis. Peshkin et al. derived a diffusion-reaction equation for the ratcheting action of the fluctuating and drifting obstacle (the disk). They considered an ensemble of the filament tip and obtained a function for the probability of the distribution of the filament tip, g(x), x being the distance of the tip from the obstacle. The expression of g(x) was derived by solving a system of differential equations, and they obtained the ensemble average of the velocity of the obstacle,  $\langle V \rangle$ , as follows:

$$< V> = d \left[ \left( k_{on} C \int_{d}^{\infty} g(x) dx - k_{off} \int_{0}^{\infty} g(x) dx \right) / \int_{0}^{\infty} g(x) dx \right].$$

In the above expression the denominator  $\int_0^\infty g(x) dx$  represents the normalization factor. The first term in the numerator represents the on rate of the monomer weighted by the population of tips at the distance from the obstacle, which is equal to or larger than d; the second term represents the off rate weighted by g(x).

They made an assumption that the process of polymerization and depolymerization "velocities",  $k_{\rm on}C d$  and  $k_{\rm off} d$  are much slower than the "ratchet velocity", which is determined by an equation, 2D/d, and they arrived at an expression,

$$V = d \left[ k_{on} C \exp(-Fd/k_B T) - k_{off} \right].$$

This is the same expression as Hill's theory (for t=1). Thus, the stall force,  $F_{\rm stall}$ , is represented with the same equation as that derived from the thermodynamic argument in the preceding section. Peshkin et al. claimed that their mechanistic treatment should reach the same conclusion as that reached by thermodynamic argument, which is supported by this result.

Mogilner and Oster [175] proposed a model that assumes fluctuation of both actin filament and the membrane. This is more realistic when one considers that the both actin filament and the lipid membrane can thermally fluctuate. They modified the expression of the diffusion-reaction equation by incorporating bending motion of the polymer. The polymer is assumed to be abutting the flat membrane with an angle  $\pi/2$  -  $\theta$ , where  $\theta$  represents the incident angle of the filament with respect to the normal of the membrane surface. The gap opens when the polymer tip bends away from the obstacle by thermal fluctuation. They arrived at an expression of the elongation velocity:

$$V = d[k_{on}Cp(\theta, y_0) - k_{off}].$$

Here,  $k_{\rm on}$ ,  $k_{\rm off}$ , d and C have the same meaning as above. The  $y_0$  represents the average distance between the filament tip and the obstacle. The function,  $p(\theta, y_0)$  depends on the tip-to-membrane distance and the incident angle of the filament with respect to the membrane normal. The  $y_0$  value strongly depends on the length of the filament tip that is capable of thermally fluctuatiing; shorter tip bends less frequently but when it is bent and elongated by polymerization, it can exert larger force on the membrane than the longer filament. The incident angle also affects the protrusion, because when it is near 0, the pushing force from the returning tip would be small, whereas when it is ~90 degrees angle, the pushing force in the protrusve direction would be zero. Thus, there is an optimum value of  $\theta$ . Mogilner and Oster have derived the velocities of the protrusion under various conditions at individual optimal  $\theta$  values.

### 7.22 The Force Measured in the Keratocyte and a Reconstituted System

As described in the Sect. 7.21.1., the protrusive force of the lamellipodium of a keratocyte has been measured by the AFM technique [164]. In this example, the force on the order of nano-newton has been needed to stall the protrusion. The velocity of the protrusion decreased with the cantilever force in a similar fashion as predicted by the elastic ratchet model. Thus, the curve was bell-shaped with the convex portion around zero force. On the other hand, with the reconstituted system [203], a convex shape of the force-velocity relation has been obtained. The curve has similarity to what was predicted by the thermal ratchet model, but actually the bacterial body is connected to the actin filaments, the researchers have explained this result with a model based on the elasticity of actin gel that simultaneously pushes and hinders the movement of the bead [208].

#### 7.23 The ATPase Activity of Actin

The ATPase activity of actin is not necessary for the polymerization, because ADP-binding actin monomer can polymerize. As pointed out by Hill [147], it does not contribute the generation of the work. However, this property is important for maintenance of the lamellipodial actin network that is dynamically turning over. The difference in the critical concentration of the barbed and the pointed ends enable the elongation at the former end and shrinkage at the latter end, resulting in the constant network width. When the cell is advancing, the network should be constantly renewed at its front edge. On the other hand, the rear part should be disassembled,

because this part is no longer needed for the movement. The key is the different critical concentration of the barbed and pointed ends. ATPase activity of actin is essential to maintain the kinetic difference between the two ends. A detailed theoretical analysis [209] was performed including relevant biochemical processes. Those are the sequestration of actin monomer by thymosin beta-4, the exchange of ADP bound to actin monomer with solution ATP by profilin, binding of profilin-ATP-bound actin monomer complex to the barbed and pointed ends and severing of actin filament. The study has considered a steady state of the amount of actin filament in the network. It was found that if the part of the barbed ends is incompetent of polymerization due to the capping, the uncapped filaments grow faster than the shrinkage of the pointed ends to maintain the steady state of the network. This is because actin monomers polymerize at the limited number of the barbed ends that are uncapped (funneling effect; [132]). To compensate for the depletion of polymerization-competent monomer, actin filaments in the network are severed at the back of the network by the severing protein (ADF/cofilin); depolymerization of actin occurs predominantly at the pointed end due to the higher critical concentration at this end than the barbed end, since the actin protomer near the filament end is in the ADP-bound form. The newly exposed barbed end is thought to be capped to block futile polymerization (not producing mechanical work). The actin monomer generated by the depolymerization binds ADP and will be sequestered by thymosinbeta 4. Profilin also binds the ADP-bound actin monomer, but the bound ADP is rapidly exchanged to ATP. The ATPase activity of actin thus maintains the directionality in an individual actin filament. The slow release of Pi might enhance the vectorial nature; the distinction of the kinetic properties between the ADP-Pi bound protomer and ADP-bound protomer will only occur some distance from the barbed end due to the delayed release of Pi form the protomer.

# 7.24 The Experimental Evidence of the Polymerization Force by a Single Actin Filament

The theoretical treatment of the force accompanying the polymerization should be applicable to general cases, but the experiment with a single actin filament to confirm the force-velocity relation is difficult, because of an intrinsic flexibility of a single actin filament. An attempt has been made to measure the force by tethering an actin filament to the glass surface with chemically modified myosin that are unable to hydrolyze ATP, but binds actin strongly; the barbed end is bound by formin that had been also bound to the surface [210]. With the growth of an actin filament by the nucleating activity of formin at the barbed end, the filament started buckling. The shape of the buckled filament was analyzed by the elastic rod theory. The buckling force depended on the conditions for the attachment of the filaments to two proteins was between 1-10 pN, depending on the attachment condition (freely pivoting around the tethered point or direction of the filament fixed). It also strongly depended

on the distance between the attachments. The growth will occur between the barbed end and the bound formin, but the detail of how the end of the growing filament was pushed remains to be clarified. Nevertheless, the magnitude of the forces are consistent with the theoretically predicted values.

### 7.25 Generation of the Polymerization Force by Microtubule

Microtubule is much more suitable for the direct measurement of the polymerization force, because, as described previously, it is far more rigid than an actin filament. Dogterom and Yurke [211] measured the force exerted by a single polymerizing microtubule: they allowed microtubule to polymerize in a micro-fabricated narrow glass chamber (30  $\mu$ m long and 1  $\mu$ m wide). They attached polymerization nuclei at the floor of the chamber to fasten the microtubule and observed the growth by differential interference contrast microscopy. After two ends of the growing microtubule hit the wall of the chamber, the microtubule started bending, suggesting that the elongating microtubule pushed against the wall of the chamber and was bent by the reaction force from the wall. The mechanical properties of microtubule have been measured [212], and the force exerted on the growing microtubule could be calculated from the arc-shape of the microtubule. They also estimated the velocity of elongation from the optical micrograph of an individual microtubule and found that the elongation velocity monotonously decreased with the increase in the force.

To obtain the stall force from the force-velocity curve, Dogterom and Yurke attempted the curve-fitting for two limiting cases with the equation shown in the last paragraph in Sect. 7.21.1. In one case, the parameter, t, was set to be zero, which yielded rather unrealistic  $k_+$ ,  $k_-$  values and almost linear decrease of velocity with increasing force was obtained, which could not reproduce the experimental result. In the other case, the parameter, t, was set to be unity, which resulted in more realistic the  $k_+$  value, but the  $k_-$  value turned out to be negative, and hence, they could not estimate the stall force; the actual growth velocity rapidly approached zero around 4 pN force [213].

In a subsequent study van Doorn et al. [214] attempted to estimate  $F_{\text{stall}}$ . From thermodynamic argument; they derived an expression for  $F_{\text{stall}}$ :  $F_{\text{stall}} = N(k_{\text{B}}T/d)\ln(k_{\text{+}}/k_{\text{-}})$ , where N represents the number of protofilaments in a microtubule (= 13), which bear the load. Physically, this means that the work needed to displace the load, Fd, is distributed over N protofilaments. With a discrete version of the thermal ratchet model [208], they obtained the stall force between 9.2 pN and 18.5 pN, depending to the choice of  $k_{+}$  and  $k_{-}$  values.

Kolomeisky and Fisher [213] pointed out that the number of protofilament, over which the load is distributed, may not be 13 and argued that the work of displacing the load, F, is F < z - d >, where z represents the shortest distance of the tip from the obstacle, d, the size of heterodimer and d > d enotes the ensemble average. Because

of the averaging, < d - z > can be larger than d/N (= 8/13 nm). They considered the case of N=1, ie., only the longest protofilament supports the obstacle, and they obtained a satisfactory fit to the data and the stall force of 4.2 pN with t=0.22. The estimated value of the stall force was close to the value that had been inferred from the velocity-force curve by Dogterome and Yurke [211]. The total number of protofilaments, N, appearing in the thermodynamic treatment by van Doorn et al. did not appear in the treatment by Kolomeisky and Fisher. Kolomeisky and Fisher argued that the N implicitly affected the result through the interaction of heterodimer with surrounding protofilaments. Based on these results, it is highly likely that the fluctuation-driven polymerization occurred and the magnitude of the generated force could be explained as a result of thermal fluctuation-based mechanism.

In a later study, Kerssemakers et al. [215] applied the calibrated forces by the optical trapping technique to measure the polymerization force by microtubule. They found that the microtubule exhibited a stepwise growth. The step size exhibited a distribution with a peak around 25 nm on the average, suggesting that a few heterodimers polymerized within the time resolution of the system (40 ms). A protein XMAP215, which has been known to increase the rate of the elongation of microtubule was found to shift the distribution of the step size toward larger values. This has been interpreted that XMAP25 complexed with several heterodimers binds to a pre-existing protofilament or XMAP25 first binds to a protofilament and serves as a scaffold for the binding of heterodimers.

### 7.26 The Force Exerted by Depolymerization of Microtubule

It has been pointed out that a polymer can shorten (depolymerize) against an extending force. In the cell, depolymerizing microtubule develops a force on the attached chromosomes in the process of segregation of chromosomes during the cell division [216]. A system mimicking this motion has been reconstituted [217]. The plus end of microtubules was capped by rhodamine-labeled tubulin and the minus end was attached to a structure called pellicle (derived from lysed *Tetrahymena*). Tubulin residing in the middle of microtubule was chemically linked to biotin. Then, a bead coated with avidin was attached to the side of the microtubule through strong affinity of biotin to avidin. The rhodamine-labeled tubulin cap was destroyed by a strong laser beam and the microtubule started depolymerizing. The bead often simply came off the microtubule, as one might expect, but occasionally, the bead was pulled away from the trap center, indicating that the force was exerted on the bead toward the minus end direction. The force was estimated to be ~0.3 pN. It was presumed that the force arose from the curved (ie., depolymerizing) part of one or two protofilaments. The geometrical consideration has suggested that the force directed toward the surface of the bead was ~5 pN. Thus, if some mechanism of References 153

dynamic connection between the bead and the protofilaments existed, the force along the microtubule can be stronger.

#### References

- 1. R.C. Woledge, N.A. Curtin, E. Homsher, *Energetic Aspects of Muscle Contraction*, Monographs of Physiological Society (Academic Press, London, 1985)
- 2. M.C. Maw, A.J. Rowe, Nature 286, 412–414 (1980)
- 3. J.S. Davis, Ann. Rev. Biophys. Biophys. Chem. 17, 217–239 (1988)
- I. Rayment, W.R. Rypniewski, K. Schmidt-Base, R. Smith, D.R. Tomchick, M.M. Benning, D.A. Winkelmann, G. Wesenberg, H.M. Holden, Science 261, 50–58 (1993)
- J.M. Berg, J.L. Tymoczko, L. Stryer, Chap. 10: Regulatory Strategies: Enzymes and Hemoglobin, in *Biochemistry*, 5th edn., (WH Freeman and Co, New York, 1999)
- 6. N. Suzuki, H. Miyata, S.-I. Ishiwata, K. Kinosita Jr., Biophys. J. 70, 401–408 (1996)
- H. Miyata, H. Hakozaki, H. Yoshikawa, N. Suzuki, K. Kinosita Jr., T. Nishizaka, S.-i. Ishiwata, J. Biochem. 115, 644–647 (1994)
- 8. H. Miyata, H. Yoshikawa, H. Hakozaki, N. Suzuki, T. Furuno, A. Ikegami, K. Kinosita Jr., T. Nishizaka, S.-I. Ishiwata, Biophys. J. 68, 286s–290s (1995)
- 9. J. Finer, R.M. Simmons, J.A. Spudich, Nature **368**, 113–119 (1994)
- 10. P.A. Coulomb, P. Wong, Nat. Cell Biol. 6, 699–706 (2004)
- 11. B. Geiger, S.J. Singer, Proc. Natl. Acad. Sci. U.S.A 77, 4769–4773 (1981)
- R.D. Goldman, S. Khuon, Y.H. Chou, P. Opal, P.M. Steinert, J. Cell Biol. 134, 971–983 (1996)
- 13. H. Herrmann, S.V. Strelkov, BMC Biol 9, 16-1-5 (2011)
- R.D. Goldman, M.M. Cleland, S.N. Murthy, S. Mahammad, E.R. Kuczmarski, J. Struct. Biol. 177, 14–23 (2012)
- 15. T.D. Pollard, E.D. Korn, J. Biol. Chem. 248, 4682–4690 (1973)
- 16. T. Soldati, E.C. Schwarz, H. Geissler, Protoplasma 209, 28–37 (1999)
- 17. E.J. Ezratty, M.A. Partridge, G.G. Gundersen, Nature Cell Biol. 7, 581–590 (2005)
- J.M. Durán, F. Valderrama, S. Castel, J. Magdalena, M. Tomás, H. Hosoya, J. Renau-Piqueras, V. Malhotra, G. Egea, Mol. Biol.Cell. 14, 445

  –449 (2003)
- R. Nambiar, R.E. McConnell, M.J. Tyska, Proc. Natl. Acad. Sci. U.S.A 106, 11972–11977 (2009)
- C. Kural, H. Kim, S. Syed, G. Goshima, V.I. Gelfand, P.R. Selvin, Science 308, 1469–1472 (2005)
- 21. V.I. Rodinov, A.J. Hope, T.M. Svitkina, G.G. Borisy, Curr. Biol. 8, 165–168 (1998)
- 22. X. Wu, B. Bowers, K. Rao, Q. Wei, J.A. Hammer, III, J. Cell Biol. 143, 1899-1918 (1998)
- 23. B.M. Slepchenko, I. Semenova, I. Zaliapin, V. Rodionov, J. Cell Biol. 179, 635–641 (2007)
- 24. C.J. Merrifield, S.E. Moss, C. Ballestrem, B. Imhof, G. Giese, I. Wunderlich, W. Almers, Nature Cell Biol. 1, 72–74 (1999)
- 25. E.D. Korn, Physiol. Rev. **62**, 672–737 (1982)
- 26. W. Kabsch, H.G. Mannherz, D. Suck, E.F. Pai, K.C. Holmes, Nature 347, 37–44 (1990)
- J.E. Estes, L.A. Selden, H.J. Kinosian, L.C. Gershman, J. Muscle Res. Cell Motil. 13, 272–284 (1992)
- 28. W. Kabsch, J. Vandekerchkhove, Ann. Rev. Biophys. Biomol. Struct. 21, 49–76 (1992)
- 29. J. Hanson, J. Lowy, J. Mol. Biol. 6, 46–60 (1963)
- 30. E.D. Korn, M.-F. Carlier, D. Pantaloni, Science 238, 638-644 (1987)
- 31. K.C. Holmes, D. Popp, W. Gebhard, W. Kabsch, Nature **347**, 44–49 (1990)
- 32. H. Huxley, J. Mol. Biol. 7, 281-308 (1963)
- 33. A. Narita, T. Oda, Y. Maeda, EMBO J. 30, 1230–1237 (2011)

- 34. Y. Nakaoka, M. Kasai, J. Mol. Biol. 44, 319-332 (1969)
- 35. A. Wegner, P. Savko, Biochemistry 21, 1909–1913 (1982)
- 36. H. Miyata, H. Hotani, Proc. Natl. Acad. Sci. U.S.A 89, 11547-11551 (1992)
- 37. S. Asakura, Biochim. Biophys. Acta **52**, 65–75 (1961)
- 38. T. Kouyama, K. Mihashi, Eur. J. Biochem. 114, 33 (1981)
- 39. J.F. Tait, C. Frieden, Arch. Biochem. Biophys. 216, 133 (1982)
- 40. G. Marriott, K. Zechel, T.M. Jovin, Biochemistry 27, 6214–6220 (1988)
- 41. H. Kondo, S.-i. Ishiwata, J. Biochem. **79**, 159–171 (1976)
- 42. T.D. Pollard, J. Cell Biol. 103, 2747–2754 (1986)
- 43. I. Fujiwara, D. Vavylonis, T.D. Pollard, Proc. Natl. Acad. Sci. U.S.A 104, 8827–8832 (2007)
- 44. M.-F. Carlier, D. Pantaloni, Biochemistry 25, 7789–7792 (1986)
- 45. L. Blanchoin, T.D. Pollard, Biochemistry 41, 597–602 (2002)
- 46. M. Kasai, E. Nakano, F. Oosawa, Biochim. Biophys. Acta 94, 494–503 (1965)
- 47. E.M. De La Cruz, T.D. Pollard, Biochemistry 34, 5452-5461 (1995)
- 48. M.-F. Carlier, D. Pantaloni, E.D. Korn, J. Biol. Chem. 259, 9983-9986 (1984)
- 49. M.-F. Carlier, D. Pantaloni, Biochemistry **25**, 7789–7792 (1986)
- 50. M.-F. Carlier, D. Pantaloni, J. Biol. Chem. 263, 817-825 (1988)
- 51. J.E. Rickart, P. Sheterline, J. Mol. Biol. 191, 273–280 (1986)
- 52. F. Oosawa, M. Kasai, J. Mol. Biol. 4, 10-21 (1962)
- 53. L.S. Tobacman, E.D. Korn, J. Biol. Chem. 258, 3207–3214 (1983)
- 54. A. Wegner, J. Engel, Biophys. Chem. **3**, 215–225 (1975)
- 55. A. Wegner, J. Mol. Biol. 108, 139–150 (1976)
- 56. U. Pieper, A. Wegner, Biochemistry 35, 4396–4402 (1996)
- 57. E. Nogales, Annu. Rev. Biophys. Biomol. Struct. **30**, 397–420 (2001)
- 58. E. Nogales, M. Whittaker, R. Milligan, K.H. Downing, Cell 96, 79–88 (1999)
- 59. A. Desai, T.J. Mitchson, Annu. Rev. Cell Dev. Biol. 13, 83-117 (1997)
- J.M. Kollman, A. Merdes, L. Mourey, D.A. Agard, Nature Rev. Mol. Cell. Biol. 12, 709–721 (2011)
- 61. E.-M. Mandelkow, E. Mandelkow, R.A. Milligan, J. Cell Biol. 114, 977-991 (1991)
- 62. T.J. Itoh, H. Hotani, Cell Struct. Funct. 19, 279-290 (1994)
- 63. R. Melki, M.-F. Carlier, D. Pantaloni, S.N. Timasheff, Biochemistry 28, 9143–9152 (1989)
- 64. T. Mitchison, M. Kirschner, Nature 312, 237–242 (1984)
- R.A. Walker, E.T. O'Brien, N.K. Pryer, M.F. Soboeiro, W.A. Voter, H.P. Erickson, E.D. Salmon, J. Cell Biol. 107, 1437–1448 (1988)
- 66. H.W. Wang, E. Nogales, Nature 435, 911-915 (2005)
- 67. L. Mahadevan, T.J. Mitchison, Nature 435, 895–896 (2005)
- 68. E. Nogales, H.-W. Wang, Curr. Opin. Cell Biol. 18, 179–184 (2006)
- 69. L.M. Rice, E.A. Montabana, D.A. Agard, Proc. Natl. Acad. Sci. U.S.A 105, 5378-5383 (2008)
- A. Dimitrov, M. Quesnoit, S. Moutel, I. Cantaloub, C. Pous, F. Perez, Science 322, 1353–1356 (2008)
- 71. T.J. Mitchson, M. Kirschner, Nature **312**, 232–237 (1984)
- L. Wardman, T.J. Mitchison, in *Microtubules*, ed. by J. S. Hyams, C. W. Lloyd (Eds), (Wiley-Liss, Inc, New York, 1994), pp. 287–301
- 73. T. Horio, H. Hotani, Nature **321**, 605–607 (1986)
- T.J. Itoh, S. Hisanaga, T. Hosoi, T. Kishimoto, H. Hotani, Biochemistry 36, 12574–12582 (1997)
- 75. R.J. Kowalski, R.C. Williams Jr., J. Biol. Chem. 268, 9847–9855 (1993)
- 76. T.J. Itoh, H. Hotani, Cell Struct. Funct. **19**, 279–290 (1994)
- 77. D.A. Lauffenburger, A.F. Horwitz, Cell **84**, 359–369 (1996)
- 78. T.P. Stossel, Sci. Am. **271**, 54–63 (1994)
- 79. J. Lee, A. Ishihara, J.A. Theriot, K. Jacobson, Nature **362**, 167–171 (1993)

References 155

80. H. Lodish, A. Berk, S.L. Zipursky, P. Matsudaira, D. Baltimore, J. Darnell, Chap. 22: Integrating Cells into Tissues, in *Molecular Cell Biology*, 4th edn., (W.H. Freeman and Company, New York, 2000)

- 81. R.O. Hynes, Cell **69**, 11–25 (1992)
- 82. F.G. Giancotti, Nat. Cell Biol. 2, E13–E14 (2000)
- 83. M.J. Humphries, AP. Mould, Science. **301**, 1720–1725 (2003)
- 84. M. Kim, C.V. Carman, T.A. Springer, Science **301**, 1720–1725 (2003)
- 85. R.M. Servuss, W. Harbich, W. Helfrich, Biochim. Biophys. Acta 436, 900-903 (1976)
- 86. L. Stryer, Chap. 11, in *Biochemistry*, 4th edn., (W.H. Freeman and Co, New York, 1995)
- 87. L. Bo, R.E. Wauch, Biophys. J. 55, 509–517 (1989)
- 88. K. Svoboda, C.F. Schmidt, D. Branton, S.M. Block, Biophys. J. 63, 784–793 (1992)
- 89. A.J. Baines, Biochem. Soc. Trans. 37, 796-803 (2009)
- 90. H. Lodish, A. Berk, S.L. Zipursky, P. Matsudaira, D. Baltimore, J. Darnell, Chap. 18, in *Molecular Cell Biology*, 4th edn., (W.H. Freeman and Company, New York, 2000)
- N. Morone, T. Fujiwara, K. Murase, R.S. Kasai, H. Ike, S. Yuasa, J. Usukura, A. Kusumi, J. Cell Biol. 174, 851–862 (2006)
- 92. N. Parasain, T. Stevens, Microvasc. Res. 77, 53-63 (2009)
- 93. M. Fritzsche, C. Erlenkämper, E. Moeendarbary, G. Charras, K. Kruse, Sci. Adv. 2, e1501337 (2016)
- 94. O.Z.A. Diz-Mun, D.A. Fletcher, O.D. Weiner, Trends Cell Biol. 23, 47–53 (2013)
- S.A. Koestler, S. Auinger, M. Vinzenz, K. Rottner, J.V. Small, Nat. Cell Biol. 10, 306–313 (2008)
- 96. C.A. Parent, P.N. Devreotes, Science **284**, 765–770 (1999)
- 97. M.P. Sheetz, D.B. Wayne, A.L. Pearlman, Cytoskeleton 22, 160–169 (1992)
- 98. S.J. Smith, Science 242, 708-715 (1988)
- 99. T.J. Mitchison, M. Kirschner, Neuron 1, 761–772 (1988)
- 100. R.W. Davenport, P. Dou, V. Rehder, S.B. Kater, Nature **361**, 721–724 (1993)
- 101. L.P. Cramer, T.J. Mitchison, J. Cell Biol. 131, 179–189 (1995)
- 102. R.K. Meyer, U. Aebi, J. Cell Biol. 110, 2013–2024 (1990)
- 103. K. Mochitate, P. Pawelek, F. Grinnel, Exp. Cell Res. 193, 198–207 (1991)
- 104. G. Langanger, M. Moeremans, G. Daneels, A. Sobieszek, M. De Brabander, J. De Mey, J. Cell Biol. 102, 200–209 (1986)
- 105. F.G. Giancotti, E. Rouslahti, Science **285**, 1028–1032 (1999)
- 106. X. Wei, X. Wang, J. Zhan, Y. Chen, W. Fang, L. Zhang, H. Zhang, J. Cell Biol. **216**, 1455. https://doi.org/10.1083/jcb.201609073
- 107. K. Burridge, K. Fath, K. Kelly, G. Nuckolls, C. Turner, Annu. Rev. Cell Biol. 4, 487–525 (1988)
- 108. M. Evangelista, S. Zigmond, C. Boone, J. Cell Sci. 116, 2603–2611 (2003)
- 109. K. Katoh, Y. Kano, M. Masuda, H. Onishi, K. Fujiwara, Mol. Biol. Cell 9, 1919–1938 (1998)
- J.V. Small, K. Rottner, I. Kaverina, K.I. Anderson, Biochim. Biophys. Acta 1404, 271–281 (1998)
- 111. P. Hotulainen, P. Lappaleinen, J. Cell Biol. **173**, 383–394 (2006)
- 112. J. Bereiter-Hahn, in *Cytomechanics*, ed. by J. Bereiter-Hahn, O. R. Anderson, W.-E. Reif (Eds), vol. 3, (Springer-Verlag, Berlin/Heidelberg, 1987), p. 273
- 113. H. Hirata, H. Tatsumi, M. Sokabe, Biochim. Biophys. Acta 1770, 1115–1127 (2007)
- 114. H. Hirata, H. Tatsumi, C.T. Lim, M. Sokabe, Am. J. Physiol. Cell Physiol. **306**, C607–C620 (2014)
- 115. H. Hirata, H. Tatsumi, M. Sokabe, Commun. Integr. Biol. 1, 1–4 (2007)
- 116. K.E. Prehoda, D.J. Lee, W.A. Lim, Cell **97**, 471–480 (1999)
- 117. Y.-L. Wang, J. Cell Biol. 99, 1478-1485 (1984)
- 118. F. Hasebe-Kishi, Y. Shimada, J. Muscle Res. Cell Motil. 21, 717–724 (2000)
- 119. A.B. Verkhovsky, T.M. Svitkina, G.G. Borisy, J. Cell Biol. 131, 989–1002 (1995)

 D. Nobezawa, S. Ikeda, E. Wada, T. Nagano, H. Miyata, BioMed. Res. Int. 2017, 7804251-1-14 (2017)

- 121. T.P. Stossel, Science 260, 1086-1094 (1993)
- 122. J.V. Small, G. Isenberg, J.E. Celis, Nature **272**, 638–639 (1978)
- 123. J.V. Small, T. Stradal, E. Vignal, K. Rottner, Trends Cell Biol. 12, 112–110 (2002)
- 124. A. Narita, J. Mueller, E. Urban, M. Vinzenz, J.V. Small, Y. Maeda, J. Mol. Biol. 419, 359–368 (2012)
- 125. J.A. Cooper, J. Cell Biol. 105, 1473–1478 (1987)
- 126. P. Sampath, T.D. Pollard, Biochemistry 30, 1973–1980 (1991)
- 127. J. Heath, B.F. Holifield, Symp. Soc. Exp. Biol. 47, 35–56 (1993)
- 128. C. Le Clainche, M.-F. Carlier, Physiol. Rev. 88, 489–513 (2008)
- 129. V.C. Abraham, V. Krishnamurthi, D.L. Taylor, F. Lanni, Biophys. J. 77, 1721-1732 (1999)
- 130. S.-T. Sit, E. Manser, J. Cell Sci. 124, 679-683 (2011)
- 131. J. Lee, A. Ishihara, J.A. Theriot, K. Jacobson, Nature **362**, 167–171 (1993)
- 132. J.E. Bear, S.T.M. vitkina, M. Krause, D.A. Schafer, J.J. Loureiro, G.A. Strasser, I.V. Maly, O.Y. Chaga, J.A. Cooper, G.G. Borisy, F.B. Gertler, Cell 109, 509–521 (2002)
- 133. J.P. Trinkaus, Exp. Biol. Med. 10, 130–173 (1985)
- 134. D. Pantaloni, C. Le Clainche, M.-F. Carlier, Science **292**, 1502–1506 (2001)
- 135. N.A. Medeiros, D.T. Burnette, P. Forscher, Nature Cell Biol. 8, 215–226 (2006)
- 136. T.D. Pollard, G.G. Borisy, Cell **112**, 453–465 (2003)
- 137. B. Xue, R.C. Robinson, Eur. J. Cell Biol. 92, 316-332 (2013)
- 138. V.O. Paavilainen, E. Oksanen, A. Goldman, P. Lappalainen, J. Cell Biol. 182, 51-59 (2008)
- D. Zicha, I.M. Dobbie, M.R. Holt, J. Monypenny, D.Y.H. Soong, C. Gray, G.A. Dunn, Science 300, 142–145 (2003)
- 140. A.J. Ridley, Chap. 4, in *GTPases*, ed. by A. Hall (Ed), (Oxford University Press, Oxford, 2000)
- 141. A.B. Jaffe, A. Hall, Annu. Rev. Cell Dev. Biol. 21, 247–269 (2005)
- 142. K. Kaibuchi, S. Kuroda, M. Amano, Annu. Rev. Biochem. 68, 459-486 (1999)
- 143. D.J.G. Mackay, A. Hall, J. Biol. Chem. 273, 20685–20688 (1998)
- 144. R.C. Robinson, K. Turbedsky, D.A. Kaiser, J.-B. Marchand, H.N. Higgs, S. Chow, T.D. Pollard, Science 294, 1679–1684 (2001)
- 145. T. Takenawa, H. Miki, J. Cell Sci. 114, 1801–1809 (2001)
- 146. S. Inoue, H. Ritter, in *Molecules and Cell Movement*, ed. by S. Inoue, R. E. Stephens (Eds), (Ravenn Press, New York, 1975), p. 3
- 147. T.L. Hill, Proc. Natl. Acad. Sci. U.S.A 78, 5613–5617 (1981)
- 148. A. Mogilner, Curr. Opin. Cell Biol. 18, 32-39 (2006)
- 149. R.J. Adams, T.D. Pollard, Cell Motil. Cytoskeleton 14, 178–182 (1989)
- 150. H. Miyata, B. Bowers, E.D. Korn, J. Cell Biol. 109, 1519–1528 (1989)
- 151. T.J. Mitchison, L.P. Cramer, Cell 84, 371–379 (1996)
- 152. Z.H. Price, Exp. Cell Res. 48, 82-92 (1967)
- 153. J. Condeelis, Cell Motil. Cytoskeleton 22, 1-6 (1992)
- 154. E. Zatulovskiy, R. Tyson, T. Bretschneider, R.R. Kay, J. Cell Biol. 204, 1027–1044 (2014)
- 155. G.F. Oster, A.S. Perelson, J. Cell Sci. Suppl. **8**, 35–54 (1987)
- 156. D.J. Olbris, J. Herzfeld, Biophys. J. 77, 3407–3423 (1999)
- 157. L.G. Tilney, D.A. Portnoy, J. Cell Biol. 109, 1597–1608 (1989)
- 158. L.G. Tilney, D.J. DeRosier, A. Weber, M.S. Tilney, J. Cell Biol. 118, 83–93 (1992)
- 159. P. Cossart, Curr. Biol. 7, 94–101 (1995)
- J. Taunton, B.A. Rowning, M.L. Coughlin, M. Wu, R.T. Moon, T.J. Mitchison, C.A. Larabell,
   J. Cell Biol. 148, 519–530 (2000)
- 161. H.V. Goodson, C. Valetti, T. Kreis, Curr. Opin. Cell Biol. 9, 18–28 (1997)
- 162. J. Lane, V. Allan, Biochim. Biophys. Acta 1376, 27–55 (1998)
- 163. K.L. King, M. Stewart, T.M. Roberts, M. Seavy, J. Cell Sci. 101, 847-857 (1992)
- 164. M. Prass, K. Jacobson, A. Mogilner, M. Radmacher, J. Cell Biol. 174, 767–772 (2006)

References 157

- 165. S. Park, D. Koch, R. Cardenas, J. Kas, C.K. Shih, Biophys. J. 89, 4330–4342 (2005)
- 166. T. Oliver, M. Dembo, K. Jacobson, Cell Motil. Cytoskeleton 31, 225–240 (1995)
- E. Urban, S. Jacob, M. Nemethova, G.P. Resch, J.V. Small, Nature Cell Biol. 12, 429–436 (2010)
- 168. S. Bohnet, R. Ananthakrishnan, A. Mogilner, J.J. Meister, A.B. Verkhovsky, Biophys. J. 90, 1810–1820 (2006)
- K. Sakai, S. Kohmoto, D. Nobezawa, S. Ikeda, H. Miyata, J. Phys. Soc. Japan 84, 024802-1-7 (2015)
- 170. J.C. Neto, U. Agero, R.T. Gazzinelli, O.N. Mesquita, Biophys. J. 91, 1108–1115 (2006)
- B. Szabo, D. Selmeczi, Z. Kornyei, E. Madarasz, N. Rozlosnik, Phys. Rev. E 65, 041910-1-6 (2002)
- 172. C. Rotsch, K. Jakobson, M. Radmacher, Proc. Natl. Acad. Sci. U.S.A 96, 921-926 (1999)
- 173. W. Helfrich, Chap. 6, in *Perspectectives in Supramolecular Chemistry, Giant Vesicles*, ed. by P. Luigi Luisi, P. Walde (Eds), (Wiley, Chichester, 2000)
- 174. C.E. Morris, U. Homann, J. Memb. Biol. 179, 79-102 (2001)
- 175. A. Mogilner, G. Oster, Biophys. J. 71, 3030–3045 (1996)
- 176. R.B. Dickinson, L. Caro, D. Purich, Biophys. J. 87, 2838–2854 (2004)
- 177. S.H. Parekh, O. Chaudhuri, J.A. Theriot, D.A. Fletcher, Nature Cell Biol. 7, 1219–1223 (2005)
- 178. J.D. Cortese, B. Schwab III, C. Frieden, E.L. Elson, Proc. Natl. Acad. Sci. U.S.A 86, 5773–5777 (1989)
- H. Miyata, S. Nishiyama, K.-I. Akashi, K. Kinosita Jr., Proc. Natl. Acad. Sci. U.S.A 96, 2048–2053 (1996)
- M. Hibino, H. Shigemori, H. Itoh, K. Nagayama, K. Kinosita Jr., Biophys. J. 59, 209–220 (1991)
- 181. T. Yanagida, M. Nakase, K. Nishiyama, F. Oosawa, Nature 307, 58-60 (1984)
- 182. J.R. Bartles, Curr. Opin. Cell Biol. 12, 72–78 (2000)
- 183. M. Honda, K. Takiguchi, S. Ishikawa, H. Hotani, J. Mol. Biol. 287, 293–300 (1999)
- 184. J.H. Shin, L. Mahadevan, P.T. So, P. Matsudaira, J. Mol. Biol. 337, 255-261 (2004)
- 185. M. Bathe, C. Heussinger, M.M.A.E. Claessens, A.R. Bausch, E. Frey, Biophys. J. 94, 2955–2964 (2008)
- 186. H. Miyata, K. Kinosita Jr., Biophys. J. 67, 922-928 (1994)
- 187. H. Hotani, H. Miyamoto, Adv. Biophys. 26, 135–156 (1990)
- 188. T. Kaneko, T.J. Itoh, H. Hotani, J. Mol. Biol. 284, 1671–1681 (1998)
- 189. E. Egelman, Muscle Res. Cell Motil. 6, 129–151 (1985)
- 190. R.M. Hochmuth, E.A. Evans, Biophys. J. **39**, 71–81 (1982)
- T. Inaba, A. Ishijima, M. Honda, F. Nomura, K. Takiguchi, H. Hotani, J. Mol. Biol. 348, 325–333 (2005)
- 192. V. Heinrich, B. Bozic, S. Svetina, B. Zeks, Biophys. J. 76, 2056–2071 (1999)
- 193. I. Derenyi, F. Julicher, J. Prost, Phys. Rev. Lett. 88, 238101-1-4 (2002)
- 194. D.K. Fygenson, J.F. Marko, A. Libchaber, Phys. Rev. Lett. 79, 4497–4500 (1997)
- 195. J.A. Theriot, T.J. Mitchison, L.G. Tilney, D.A. Portnoy, Nature 357, 257–260 (1992)
- 196. M.B. Goldberg, J.A. Theriot, Proc. Natl. Acad. Sci. U.S.A 92, 6572–6576 (1995)
- 197. T.P. Loisel, R. Boujemaa, D. Pantaloni, M.-F. Carlier, Nature 401, 613-616 (1999)
- L.A. Cameron, M.J. Footer, A. van Oudenaaden, J.A. Theriot, Proc. Natl. Acad. Sci. U.S.A 96, 4908–4913 (1999)
- A. Upadhyaya, J.R. Chabot, A. Andreeva, A. Samadani, A. van Oudenaarden, Proc. Natl. Acad. Sci. U.S.A 100, 4521–4526 (2003)
- 200. H. Boukellal, O. Campas, J.-F. Joanny, J. Prost, C. Sykes, Phys. Rev. E 69, 061906-1-4 (2004)
- 201. A. Van Oudenaarden, J.A. Theriot, Nature Cell Biol. **1**, 493–499 (1999)
- 202. J. Van der Gucht, E. Paluch, J. Plastino, C. Sykes, Proc. Natl. Acad. Sci. U.S.A 102, 7847–7852 (2005)

 Y. Marcy, J. Prost, M.-F. Carlier, C. Sykes, Proc. Natl. Acad. Sci. U.S.A 101, 5992–5997 (2004)

- 204. J.E. Italiano, T.M. Roberts, M. Stewart, C.A. Fontana, Cell 84, 105-114 (1998)
- E. Demekhin, N. Haugen, B. Ibanez, J. Lederman, K. Murphy, D. Verzi, D. Witczak, Cell Motil Cytoskel. 66, 317–327 (2009)
- D. Vavylonis, Q. Yang, B. O'Shaughnessy, Proc. Natl. Acad. Sci. U.S.A 102, 8543–8548 (2005)
- 207. C. Peskin, G. Odell, G. Oster, Biophys. J. 65, 316-324 (1993)
- 208. A. Mogilner, G. Oster, Eur. Biophys. J. 28, 235-242 (1999)
- 209. P.A. Dufort, C.J. Lumsden, Cell Motil. Cytoskeleton 35, 309–330 (1996)
- J. Berro, A. Michelot, L. Blanchoin, D.R. Kovar, J.-L. Martiel, Biophys. J. 92, 2546–2558 (2007)
- 211. M. Dogterom, B. Yurke, Science **278**, 856–860 (1997)
- 212. F. Gittes, E. Meyhofer, S. Baek, J. Howard, Biophys. J. 70, 418-429 (1996)
- 213. A.B. Kolomeisky, M.E. Fisher, Biophys. J. 80, 149–154 (2001)
- 214. G.S. van Doorn, C. Tanase, B.M. Mulder, M. Dogterom, Eur. Biophys. J. 29, 2–6 (2000)
- J.W.J. Kerssemakers, E.L. Munteanu, L. Laan, T.L. Noetzel, M.E. Janson, M. Dogterom, Nature 442, 709–712 (2006)
- 216. D.E. Koshland, T.J. Mitchison, M.W. Kirschner, Nature 331, 499–504 (1988)
- E.L. Grishcuk, M.I. Molodtsov, F.I. Ataullakhanov, J.R. McIntosh, Nature 438, 384–388 (2005)

# **Chapter 8 Global Environment and Biophysics**



**Abstract** Living organisms were born on the earth and have made evolution through long history of the earth, and recorded genetic information corresponding to each global environment. And corresponding gene is switched on for adaptation to their environment. Temperature change is major factor of environment. And metabolic change for membrane lipid synthesis alters physical property of membrane fluidity through change of phase transition temperature of lipid bilayer.

#### 8.1 Living Organisms on the Earth

Living organisms on the earth were born in closely related with existence of the third planet in the solar system. Materials and some energy sources on the earth were used for creation of the living organisms. Interaction between the global environment and living organisms is important factor in long history of evolution, and existence of living organisms have changed global environment. Oxygen content, 21% in the present atmosphere is result of global evolution changed by living organisms, in particular, by plants. Nowadays, social activities of human beings raise concentration of carbon dioxide up to 400 ppm, and induce global warming and climate change. Averaged concentration of carbon dioxide was 278 ppm in 1750 (before the industrial revolution). And some abnormal changes are found in ecological system. Living organisms on the earth have adapted to mild change of the environment and the adaptation mechanisms to survive in the changed environment have been stored in genetic information on DNA during their evolution. In diurnal temperature variations and annual temperature variation in particular decrease of temperature, living organisms such as amphibian cannot control body temperature. And low body temperature results in lowering rate of chemical reactions in the body and induces slow movement. On the other hand, homeotherms maintain body temperature constant in variable external temperature to keep proper rate of chemical reactions in their metabolism. When cells derived from a tissue of homeotherms, the cells show adaptation to temperature of culture. The adaptation indicates that cells of homeotherms have acquired genetic information of mechanism to adapt change of environmental temperature in long history of evolution and preserve it in DNA. Both single cell and multi-cells organisms live in surrounding environment, and they maintains constant state to survive in variable environment (='homeostasis'). Their direct environment is water molecules, and water molecules mediate interaction between cells. Each cell uses genetic information on DNA correspondent to external stimulus and responds to that. Temperature of environment is an important factor and physical property has temperature dependency. Therefore biological functions are greater or lesser extent affected by temperature. Homeotherms have been born as living organisms whose enzyme activities unaffected by change of external temperature in evolution. All animals and plants are under environment of variable temperature and are affected by temperature directly or indirectly. And these living organisms provide mechanisms to adapt temperature change at level of cell. And the mechanism to adapt to temperature change is observed in cultured cells derived from homeotherms such as rat or chines hamster. This mechanism is response of the cell itself to temperature change, and the mechanism has been preserved in evolution process. The mechanisms of adapting to environment at level of gene are called 'stress-induced gene expression'. Temperature acclimation of cell is one of them. Living organisms provide mechanism responding to change of environment at gene level essentially and becomes possible to maintain their life.

### 8.2 Mechanism of Adaptation to Environment on Gene Level

Living organisms respond to change of external environment; the mechanism of response exists on level of an individual and a cell. And this is called 'response to stress'. The response to stress has been acquired in process of evolution, and it is essential for living organisms on the earth. Environmental factors such as temperature, pressure, radiation, ultraviolet light, metal ions, oxygen and various compounds are candidates of stress. When a cell is exposed to a stress, protein synthesis at normal state is lowered and some species of protein are newly synthesized instead of them. Typical stress is heat shock and proteins synthesized in this state are called 'heat shock proteins'. When a cells or individuals are exposed to temperature higher than physiological temperature by a few degrees, heat shock response is observed in every level from cell to individual. This response is observed in deep-sea fish living in below zero temperature and thermophilic bacteria living in hot spring. The maximum response of heat shock is observed at 5~10 degrees higher than physiological temperature. Ritossa first observed three new puffs in chromatin of drosophila larva exposed to high temperature [1].

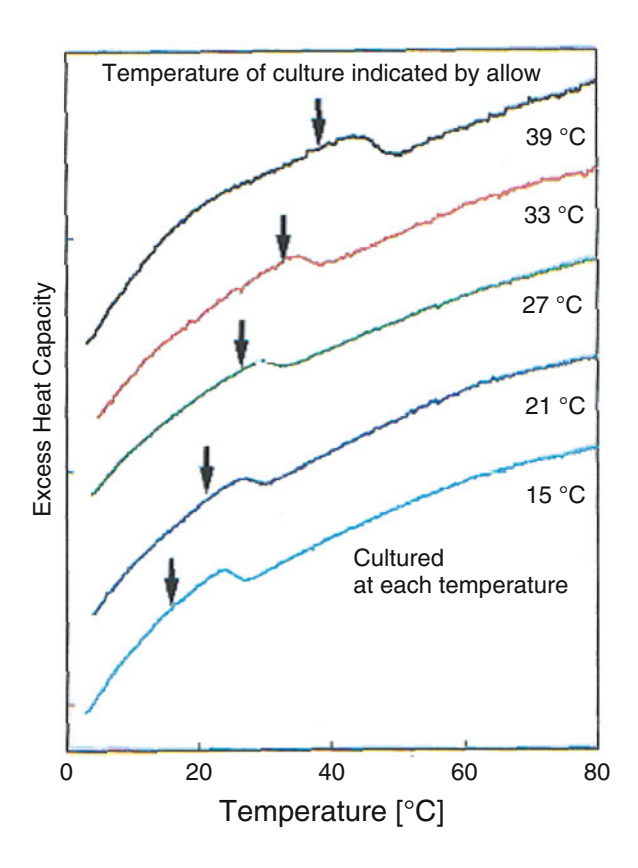
# 8.3 Temperature Acclimation of Cells and Physical Properties of Membranes

As a cell is an essential unit of life and important biological functions are located on biomembranes, influence of change in external temperature on biomembranes is focused in particular on statistical physical properties of lipid bilayer membranes such as phase transition and phase separation. In addition, membrane fluidity is an expression of lateral diffusion and rotational diffusion of molecules composed in lipid bilayer membranes. Physical properties of biomembranes depend on molecular composition of the biomembranes. Lipid composition of biomembranes is modified during temperature acclimation by enzymatic metabolism. Metabolic conversion of lipid composition is also important in signal transduction mechanism of cell. Both adaptation of cell to external environment and signal transduction of a cell include development and division of a cell, which are essential parts of regulation of cellular function. And these responses to external stimuli are supposed to be originated from common origin.

# 8.4 Temperature Acclimation of Cells Observed by Phase Transition and Membrane Fluidity

R.N. McElhaney and K.A. Souza found temperature acclimation of cell appeared on phase transition in Bacillus subtilis by use of DSC. When Bacillus subtilis cells were cultured at 42, 58 and 62 °C, phase transition temperature of each culture of cells were shown at temperature 10 degrees below temperature of the culture in wild type cells. However, phase transition appeared around 30 °C for mutant unable to live above 60 °C when the mutant cells were cultured at 42, 52 and 58 °C [2]. Phenomenon that phase transition temperature shifted corresponding to culture temperature was not observed in this mutant. And the result indicates that mechanism of temperature acclimation is coded on gene. Bacillus subtilis is a prokaryote that does not have any organelle such as nucleus, mitochondria endoplasmic reticulum and Golgi apparatus. On the other hand, the authors observed similar temperature acclimation in an eukaryote, Tetrahymena having organelle as intracellular membrane structures. Tetrahymena cells cultured at different temperatures were measured by DSC in the first heating scan and the second heating scan. At the first scan large peak from protein denaturation appeared on DSC thermograph. Figure 8.1 shows the second scan and phase transition from lipid membranes of Tetrahymena cells. Phase transition is accompanied with structural change, and transition of the membrane structure depends on culture temperature of Tetrahymena cell, which is observed by X-ray diffraction [3, 4]. Lipids of biomembranes are composed of various species of lipid molecules. Phase transition temperature of each lipid is

Fig. 8.1 Phase transition temperature of *Tetrahymena* cells cultured at different temperatures *Tetrahymena* cells were cultured at different temperatures. DSC thermographs of the second scans are shown because the first scan included denaturation of proteins



determined by its molecular structure. Membrane fluidity increases with transition from solid phase to fluid phase as temperature is raised. Membrane fluidity of lipid bilayer membranes composed of various lipid molecules is measured as order parameter by ESR using lipid spin probe. Change of membrane fluidity in various lipid molecules with phase transition is shown in Fig. 8.2. Phase transition of each molecular species of phosphatidylcholine appears on change of order parameter and decrease of order parameter indicates increase of membrane fluidity with phase transition from gel phase to fluid phase by raising temperature. Sinensky has found that *Escherichia coli* has ability to maintain constant viscosity of biomembranes and lipid membranes formed by extracted lipids even in change of culture temperature. This biological phenomenon is called 'homeoviscous adaptation' [5]. In the experiment, viscosity was measured by RSR using fatty acid spin probe. Viscosity of *E.coli* biomembranes cultured at 43 °C showed 2 poise measured at 43 °C. However, the viscosity increased to 15 poise when the viscosity was

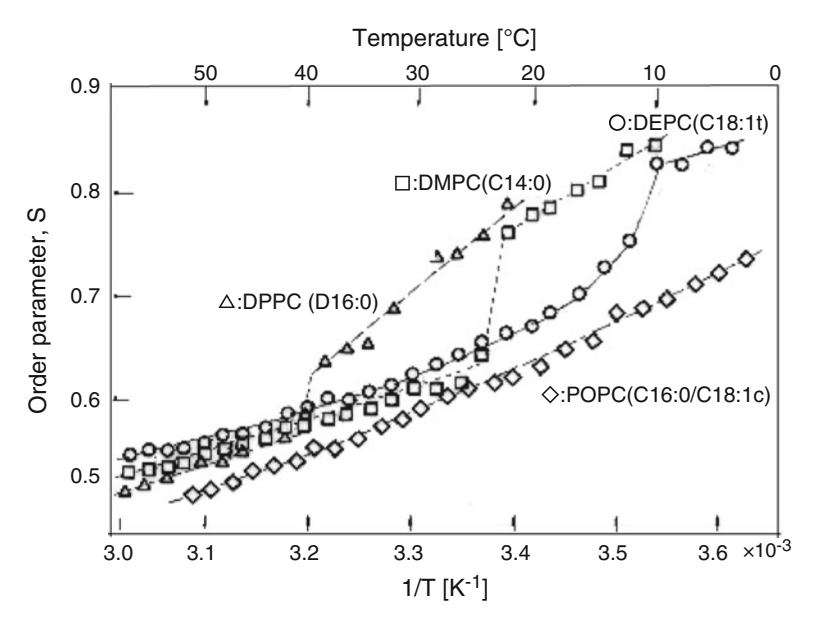


**Fig. 8.2** Change of membrane fluidity with phase transition Liposomes of various phospholipids were prepared by voltexing method. And membrane fluidity of the liposomes were measured by ESR using stearate spin probe at different temperatures. Order parameter S was obtained from ESR spectrum

measured at 15 °C. On the other hand, when E. coli cells were cultured at different temperatures such as 37 °C, 30 °C and 15 °C, viscosity measured at the cultured temperature ranged in  $1.9 \pm 0.1$  poise. The results indicate that adaptation mechanism is operated to keep viscosity constant even in change of culture temperature. Viscosity of biomembranes is strongly correlated with composition of lipid molecules. A mechanism synthesizing cis-vaccenic acid with cis-double bond at higher temperature was found in E. coli. In Tetrahymena cells, desaturases introducing double bond into fatty acyl chains of phospholipids are sequentially activated when culture temperature is lowered from 39.5 °C to 15 °C as shown in Figs. 8.3 and 8.4 shows temporal change of fatty acid composition of Tetrahymena cells during temperature change from 39.5 °C to 15 °C. The result indicates that change of culture temperature induces activation of fatty acid desaturases to convert the membrane lipids to those of lower phase transition temperature by introducing double bonds. In order to prove this adaptation mechanism, an experiment of knock outing desaturase genes was performed in cyanobacteria [6]. Phase transition profiles of wild type cyanobacteria and knockouted desaturases are shown in Fig. 8.5. Cyanobacteria cells are grown by photosynthesis using solar energy. When cyanobacteria cells were cultured at 35 °C, both wild type cells and

Fig. 8.3 Activation of various desaturases by lowering temperature of culture
Temporal changes of fatty acid desaturases were measured after lowering temperature of *Tetrahymena* cells from 39.5 °C to 15 °C

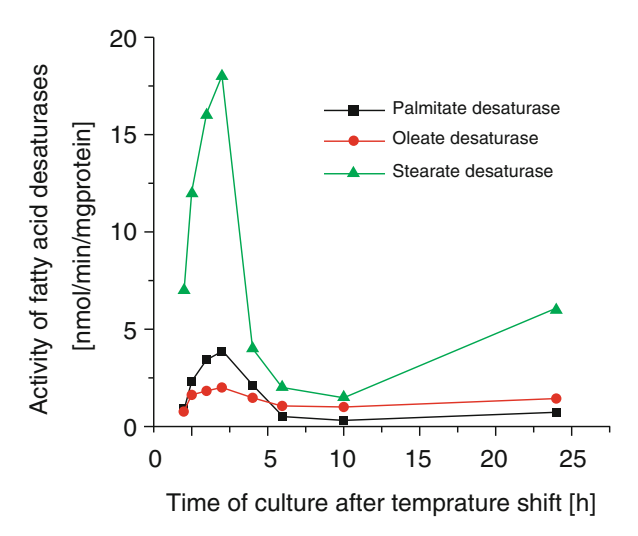
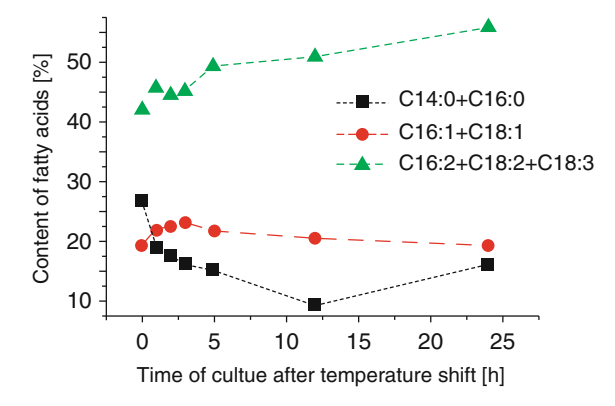
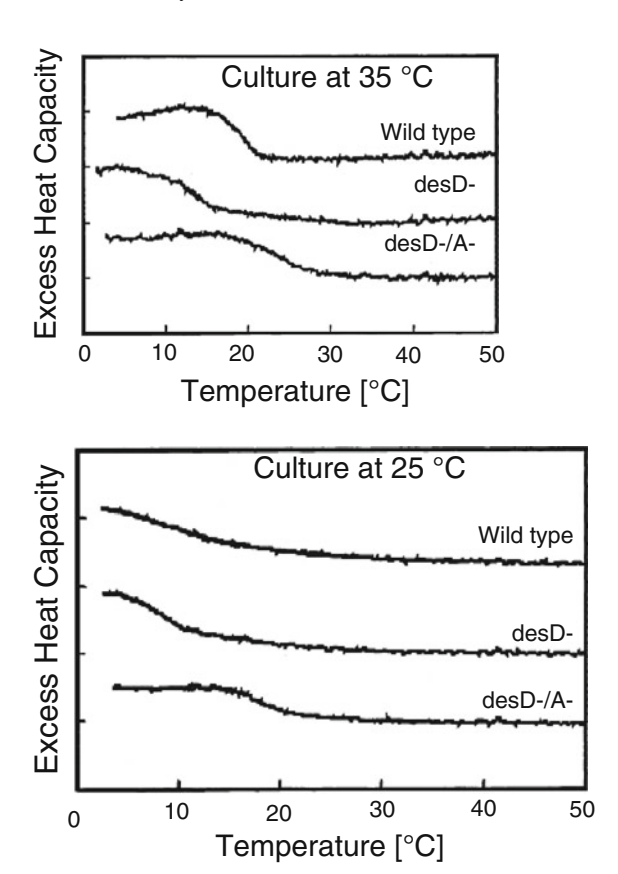


Fig. 8.4 Change of fatty acid composition in *Tetrahymena* cells by lowering culture temperature Culture-temperature of *Tetrahymena* cells was lowered from 39.5 °C to 15 °C and the culture was continued. Lipids were extracted from the cells and temporal change of fatty acid composition was obtained from GLC measurements



desaturase-knockout cells showed phase transition temperature measured by DSC around 20 °C. When temperature of culture was lowered to 25 °C, phase transition temperature of wild type cells was lowered but effect of lowering phase transition temperature was reduced in the desaturase-knockout cells. The result indicates desaturases directly alters phase transition temperature of biomembranes. Change of phase transition temperature caused by desaturase also induces phase separation in biomembranes as shown in Fig. 8.6. Phase separation is observed as smooth area

Fig. 8.5 Disappearance of temperature acclimation by knockout of fatty acid desaturase genes in cyanobacteria Wild type of cyanobacteria with normal gene of desaturase showed temperature acclimation by lowering phase transition temperature when culture temperature was shifted from 35 °C to 25 °C. However, cyanobacteria with knockouted desaturase gene showed smaller effect of lowering phase transition temperature when temperature of culture was shifted from 35 °C to 25 °C



without proteins and rough area with protein particles in endoplasmic reticulum of *Tetrahymena* fed with palmitic acid and cooled to 15 °C. For analysis of lipid composition in each area, rough and smooth endoplasmic fractions were separated by density gradient centrifugation after homogenizing the cells. Saturated fatty acids are rich in the smooth area and unsaturated fatty acids are rich in rough area of *Tetrahymena* endoplasmic reticulum [7].

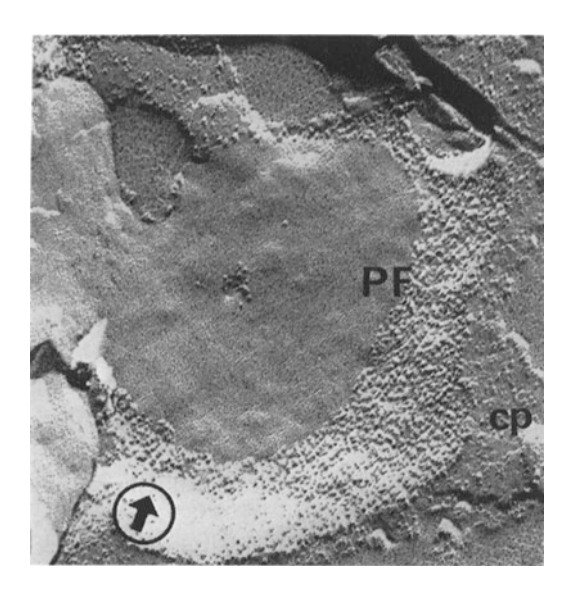


Fig. 8.6 Phase separation observed by freeze-fractured electron microscope in *Tetrahymena* microsome

Tetrahymena cells were cultured in medium containing palmitic acid (C16:0) at 39 °C. After lowering culture temperature to 4 °C, these cells were destroyed and microsomal fraction was isolated by ultra- centrifugations. The microsome were observed by freeze-fractured electron microscope. Region of integral protein particles and smooth area were observed. Unsaturated fatty acids were rich in the particle region and saturated fatty acids were rich in the smooth area from fatty acid analysis

#### References

- 1. F. Ritossa, Experimentia **18**, 571 (1962)
- 2. R.N. McElhaney, K.A. Souza, Biochim. Biophys. Acta 443, 348 (1976)
- 3. H. Nakayama, M. Goto, K. Ohki, M. Mitsui, Y. Nozawa, Biochim. Biophys. Acta 730, 17 (1983)
- 4. H. Nakayama, K. Ohki, T. Mitsui, Y. Nozawa, Biochim. Biophys. Acta 769, 311 (1984)
- 5. M. Sinensky, Proc. Natl. Acad. Sci. USA 71, 522 (1974)
- 6. Y. Tasaka, Z. Gombos, Y. Nishiyama, T. Ohba, K. Ohki, N. Murata, EMBO J. 15, 641 (1996)
- 7. Y. Kameyama, K. Ohki, Y. Nozawa, J. Biochem. 88, 1291 (1980)

### **Index**

© Springer Japan KK, part of Springer Nature 2018 K. Ohki, H. Miyata, *Physical Principles of Biomembranes and Cells*, Biological and Medical Physics, Biomedical Engineering, https://doi.org/10.1007/978-4-431-56841-4

Crystal phase, 61	Filamin, 127, 140
Cyclic AMP (cAMP), 82	Flip-flop, 59
β-Cyclodextrin, 84	Fluctuation, 14, 15
Cytochalasin, 128, 142	Fluid phase, 61, 65
	Fluorescence, 23
	Fluorescence lifetime, 45, 46
D	Fluorescence microscope, 44, 59
Diacylglycerol, 85, 90	Fluorescence photo-bleaching recovery (FPR)
Differential scanning, 23	46, 47, 81
Differential scanning calorimetry (DSC), 32,	Fluorescence polarization anisotropy, 45
33, 59, 61, 77, 78, 161, 164	Flux, 15
Diffraction pattern, 30	Focal adhesion, 124–126
Diffusion, 81	Force, 15
Diffusion constant, 41, 81	Formaldehyde, 3
Diffusion-controlled process, 82	Formin, 122, 128
Diffusion potential, 26	Free energies, 21, 77, 85
Dilatometer, 33, 61	Freeze-fractured, 59, 61, 90
Dimyristoylphosphatidylcholine, 78	Freeze-structured, 88
Dissipative structures, 14, 15	Funneling effect, 150
DNA, 30	
Donnan equilibrium potential, 26	
Donor, 48	G
Dynamic instability, 119	G-actin, 96
	Gel phase, 61, 65
	Generalized polarization (GP), 48
E	Genetic information, 23, 159
E (exchangeable)-site, 118	Geometrical factor, 42
Effector protein, 82	g-factor, 35, 36
Einstein's relationship, 46	Gibb's equation, 17
Electron beam diffraction, 71	Gibbs free energy, 4, 11, 12, 61, 65
Electron density, 31	Global environment, 159
Electron magnetic resonance (ESR), 42-44,	Global warming, 159
162	Glycine, 3
Electron microscope, 23, 61	Glycolipids, 19
Electron transfer system, 90	Glycolysis, 82
Electron transport, 77	G-protein, 82, 85
Electro static interaction, 60, 76, 77	g-tensor, 36
Encounter frequency, 40	
Entropy, 13, 14	
Enzymes, 11, 20, 23, 71, 160	Н
Epi-fluorescence illumination, 53	Hamiltonian, 35
Equilibrium constant, 9, 11	Heat shock proteins, 160
Equilibrium state, 1, 3, 11, 13, 73	Heavy atom replacement, 31
Escherichia coli, 162	Heavy meromyosin, 108
Evanescent-wave illumination, 50, 53	Heterodimer, 116
Evolution, 159	Heterotrimeric G protein, 131
Exchange narrowing, 40	Hexagonal II phase, 61, 87, 89
External system, 14	Hormone, 25
Extracellular matrix (ECM), 121	Hydrogen cyanide, 3
	Hydrophobic effect, 59
	Hydrophobic interaction, 21, 60, 76, 77
F	Hydrothermal deposits, 8
Fast-growing and the slow-growing ends, 111	Hydrothermal vent, 3
Fatty acid desaturases, 163	Hyperfine interaction, 36
Feedback inhibition, 75	Hyperfine splitting, 38

Index 169

I Imaging, 48 Imaging microscopic, 84 Immune response, 23 Information processing, 24 Inhibitor, 72, 76 Integral proteins, 76 Integrin, 121 Intermediate complex, 74, 75 Inverted micelle, 90 Ionic intensity, 59 Ionic strength, 76 Isolated system, 11, 13, 73	Microtubule associated proteins (MAPs), 120 Minus end, 119 Mitochondria, 9 Molecular concentration, 73 Molecular dynamics, 57 Molecular recognition, 29 Molecular structure, 71 Motor domain, 99 Muscle contraction, 96–99 Myosin, 96 Myosin-I, 103 Myosin II, 103 Myosin head, 99
K Keratocyte, 54, 128 Kinetic energy, 73	N NADPH, 8 Nernst equation, 26 Neuro transmitter, 25 Nitroxide radicals, 36
L Lamella, 126–127 Lamellipodia, 53 Lamllipodia and filopodia, 123–124 Lateral diffusion, 40, 59, 82 Laurdan, 48, 84 Le Chaterier.'s principle, 16 Lever-arm, 99 Ligand, 82 Lipid assembly, 20 Lipid bilayer membranes, 19, 22, 23, 61, 78	N (non-exchangeable)-site, 118 Non-bilayer structures, 87, 90 Non-equilibrium state, 12 Non-equilibrium thermodynamics, 15 Non-muscle myosins, 103–106 Nuclear fusion, 1 Nuclear magnetic resonance (NMR), 42, 43, 72, 83 Nuclear spin quantum number, 42
Lipid bilayers, 36, 90 Lipid rafts, 83 Lipids, 19 Liposome, 23 Liquid-ordered phase, 83, 84 <i>Listeria</i> , 134 Living organisms, 6, 14, 71, 84, 159 Local equilibrium, 15, 16	Open system, 13, 14 Operon theory, 75 Optical isomers, 72 Optical microscope, 30 Optical tweezers, 54 Overhauser effect, 42
M Magnetic resonance imaging (MRI), 42–44 Mechanochemical coupling, 99 Mechano-enzyme, 96–99 Melittin, 78, 88 Membrane fluidity, 34, 162 Membrane fusion, 40, 88 Membrane potential, 25, 26 Membrane skeleton, 121–122 Membrane traffic, 77 Metabolic pathway, 72, 75 Metabolic system, 8 Michaelis constant, 11 Microtubule, 105, 116–120	Packing parameter, 22 Pair annihilation, 54 Partition coefficient, 83 Patch clamp, 26 Peptide synthesis, 71 Peripheral proteins, 76 Perrin-Weber equation, 46 PET imaging, 54 Phase diagram, 65 Phase equilibrium, 65 Phase separation, 40, 82, 85, 164 Phase transition temperature, 61, 77 Phase transitions, 59, 61, 82, 161 Phenomenological equation, 15

Phosphatidic acids, 87	SNARE, 88
Phosphatidylcholine (PC), 85	Solar energy, 8
Phosphatidylethanolamine (PE), 85	Spectrin, 122
Phosphatidylinositol (PI), 85	Sphingolipids, 83
Phosphatidylserine (PS), 85, 87	Spin labeling, 23, 34
Phospholipase, 90	Spin-lattice relaxation time, 43
Phospholipids C, 85 Phospholipids, 19, 22	Spin-pin exchange interaction, 40 Spin probe, 38, 76
± ± · · · · · · · · · · · · · · · · · ·	
Phosphorylation, 85	Spin-spin relaxation time, 43
Photosynthetic bacteria, 8	Stall force, 133, 151
Physical properties, 48, 85, 160, 161	Stationary state, 14, 75
Plus end, 119	Statistical independency, 16
Polarized light, 45	Sterols, 19
Polymerase chain reaction, 5	Stress-induced gene expression, 160
Positron, 54	Subdomains, 106
Power stroke, 99	Substrate specificity, 72
Promoter, 75	Sulfur bacteria, 7, 8
Proteases, 75	Supernova explosion, 1
Protein kinase, 75	Surface pressures, 86
Protein kinase C, 85, 86	
Proteins, 4, 19, 23	
Protofilament, 117	T
Protrusive force, 57	Talin, 125
	Temperature acclimation, 82, 160, 161
	Temperature dependency, 160
Q	TEMPO parameter, 39
Quantum yield, 45	Tetrahymena, 161, 163
	Thermal polymer, 4
	Thermodynamics, 20
R	Transition state, 11
Rate constants, 73, 81	Transition state theory, 73
Rate of entropy production, 17	Transmission electron microscope (TEM), 31
Reaction velocity, 74	Treadmilling, 115
Receptor, 25, 82, 84	Tropomyosin, 124
Relaxation process, 43	T-tensor, 36
Retrograde flow, 130	Tubulin, 142–143
RhoA, Rac 1 and cdc42, 131	Tubulin dimers, 103
Ripple phase, 61	
Rotational correlation time, 38, 46	
Rotational diffusion, 82	U
,,,,	Unit lattice, 30
S	
Scanning electron microscope (SEM), 31	V
Scattering factor, 30	Viscosity, 38, 45, 46, 82, 162
Seam, 117	Voltage clamp, 26
Second messenger, 85	tomge emily, 20
Signaling, 23, 83–85	
Signaling system, 82	X
Signal peptidase, 78	X-ray crystallography, 30, 72
Signal peptide, 77	X-ray diffraction, 23, 30, 59, 71, 77, 88, 90
Signal transduction, 24, 161	21 ray diffraction, 25, 50, 57, 71, 77, 60, 90
Single-molecule measurement, 101–102	
Small GTPases, 131	Z
Smolucowski equation, 81	Zeeman energy, 35